Progress Towards Ultrasound-mediated Targeted Drug Delivery in the Small Intestine

Mihnea Vlad Turcanu

School of Engineering
College of Science and Engineering
University of Glasgow

Submitted in fulfilment of the requirements for the degree of
Doctor of Philosophy (PhD)

February 2022

Thesis Abstract

The intestinal mucosa acts as a selective barrier to permeation of material. Small molecules can usually pass the barrier provided they fulfil specific physicochemical requirements, but many macromolecular biotherapeutics cannot cross it. This restricts the delivery of biologics to injections, which can be associated with administration-related injuries and often require administration by a healthcare professional. However, the oral route is the drug administration route best accepted by patients. Ultrasound (US) and microbubbles (MBs) may allow this route to be used in future for biotherapeutics. Hence, an ingestible capsule incorporating an US transducer has the potential to offer a method for oral delivery of drugs to the small intestine. This capsule could both protect the drug payload against the destructive action of low stomach pH and facilitate delivery of a drug once it reaches the intestine.

The thesis describes the development and testing of a proof of concept tethered therapeutic capsule for delivering medication to the small intestine. The first experimental chapters present *in vitro* work, progressing to *ex vivo* tests on porcine tissue and *in vivo* tests in pigs. Preliminary studies suggested how to increase the relevance of *in vitro* tests for *in vivo* systems, in order to help reduce the number of animals used for research. To this end, classical *in vitro* systems for testing US-mediated drug delivery were refined to include stem cell-derived cell layers. US combined with either MBs or nanodroplets decreased the barrier function of these improved cell layers to different extents. The *in vitro* pathway also identified suitable transducer types and US parameters to facilitate the delivery of compounds across relevant cell layers. It was found that the effect of focused single-element transducers was surpassed by unfocused single-element and phased array transducers, with the latter allowing most control over barrier permeation. Array transducers were therefore integrated into test capsules. The US parameters tested *in vitro* were frequency, cycle number, pulse repetition frequency, duty cycle, mechanical index and surface area insonated. A decrease in barrier function was associated with lower

frequencies, more cycles, more pulses, a higher duty cycle, a higher mechanical index and insonating a larger surface area.

The results obtained determined the insonation parameters for the *in vivo* test with capsules able to deliver insulin, MBs and fluorescent quantum dots (qDots). One control pig was administered insulin and qDots alone and two test pigs were administered insulin and qDots, with US and MBs. Blood glucose tests showed that the two test pigs displayed a smaller increase in glucose levels than the control pig, suggesting that more insulin reached the systemic circulation. This early result suggests US combined with MBs can facilitate drug delivery through the small intestine.

Table of Contents

List of Figures

List of Tables

Acknowledgements

A.M.D.G.

I offer my sincerest gratitude to my main supervisor, Professor Sandy Cochran, who guided me with wisdom and patience throughout my PhD project. I owe particular thanks to my other supervisors, Professor Inke Näthke and Dr Maya Thanou for continuous support and advice.

Throughout the journey, I was inspired by the courage and determination of everyone in C-MIU at the University of Glasgow. I would like to acknowledge Dr Alexandru Moldovan for working together, for developing capsules and protocols and for his friendship.

I am indebted to Dr Driton Vllasaliu and everyone in his and Dr Maya Thanou's team for pharmacology related advice and help, especially while working in their laboratory at King's College London.

A debt of gratitude is owed to Professor Eddie Clutton and everyone at LARIF, the University of Edinburgh, for making the *in vivo* trial possible.

I would like to thank Dr Jeff Moore and everyone at Curileum Discovery Ltd. for supervising me during my secondment at St Marks Hospital, Harrow, London.

I wish to extend my appreciation to Dr Manlio Tassieri and his colleagues for collaborating on the rheology component of my work.

Many thanks to Dr Ben Cox and Mr Ian Newton for the odd banter during my secondment at the University of Dundee. To everyone at the Dundee Imaging Facility for help with histology and imaging work.

I am thankful to Dr Helen Mulvana for acting as a co-supervisor over the first two years of my PhD.

Furthermore, I acknowledge the BBSRC and the EPSRC for providing the necessary funding to conduct the project.

Due to the interdisciplinary nature of the work presented in this thesis, I was required to spend time at the institutions mentioned over the paragraphs above. This required me to relocate often, leading to living in 11 different places throughout my PhD. I would like to thank all flatmates I had throughout the journey, especially Marius, Larissa, Shishir, Matthew, Giuseppe and Matheus for putting up with my working schedule and for making life enjoyable despite the Covid pandemic.

I am grateful to my girlfriend Annemie for her kind patience and for forgiving me on the numerous occasions when I was devoid of energy and socially inept, especially during the write-up phase of the project.

Finally, it is to my family and especially my parents that I owe the most, in this as in so much else.

Declaration

I hereby declare that except where specific reference is made to the work of others, the contents of this doctoral thesis are original and have not been submitted in whole (or in part) for consideration for any other degree or qualification in this (or any other) university.

This doctoral thesis is the result of my own work, under the supervision of Prof Sandy Cochran (University of Glasgow), Prof Inke Näthke (University of Dundee) and Dr Maya Thanou (King's College London). Nothing included is the outcome of work done in collaboration, except where specifically indicated within the text.

Permission to copy without fee all or part of this doctoral thesis is granted, provided that copies are not made or distributed for commercial purposes and that the name of the author, the title of the thesis and date of submission are clearly visible on the copy.

Signature 

Mihnea Vlad Turcanu

Leuven, Belgium

19/02/2022

Abbreviations and Symbols

This table covers all engineering, biology and physics abbreviations and symbols used throughout this thesis.

ATCC	American Type Culture Collection
BSA	Bovine serum albumin
CAs	Cavitation agents, either MB or ND
DAPI	4'-6-Diamidino-2-phenylindole
Ø	Diameter
DMSO	Dimethyl sulfoxide
DMEM	Dulbecco's Modified Eagle Medium
DIF	Dundee Imaging Facility
DC	Duty cycle
Em	Emission wavelength
EDTA	Ethylenediaminetetraacetic acid
Ex	Excitation wavelength
ECM	Extracellular matrix
F-actin	Filamentous actin
FITC	Fluorescein isothiocyanate

FD3	Fluorescein isothiocyanate-dextran 3 kilodalton
FD4	Fluorescein isothiocyanate-dextran 4 kilodalton
FACS	Fluorescence activated cell sorting
FDx	Fluorescent dextran, either FD3 or FD4
FUS	Focused ultrasound surgery
FBS	Foetal bovine serum
FDA	Food and Drug Administration
OGMH	Full organoid media
GI	Gastrointestinal
G-actin	Globular monomeric actin
HBSS	Hank’s Balanced Salt Solution
HIFU	High intensity focused ultrasound
Caco-2	Human colorectal adenocarcinoma cells
IgG	Immunoglobulin G
IBD	Inflammatory bowel disease
ID	Inner diameter
PZT	Lead Zirconate Titanate
LGR5	Leucine Rich Repeat Containing G Protein-Coupled Receptor 5
MG	Matrigel
MB	Microbubble
MTT	3-(4,5-dimethylthiazol-2-yl)-2,5-diphenyltetrazolium bromide
MW	Molecular weight
MUC	Mucin protein

NDs	Nanodroplets
NADH	Nicotinamide adenine dinucleotide (reduced)
NADPH	Nicotinamide adenine dinucleotide phosphate (reduced)
NEAA	Non-essential amino acid
OG	Organoid
OGM	Organoid media
OD	Outer diameter
ON	Overnight
PFA	Paraformaldehyde
P/S	Penicillin streptomycin
PBS	Phosphate-buffered saline
PE	Phycoerythrin
PAM	Polyacrylamide
PRF	Pulse repetition frequency
qDots	Quantum dots
RT	Room temperature
AIM V	Serum-free media
TEER	Transepithelial electrical resistance
US	Ultrasound
UV	Ultraviolet
UofD	University of Dundee
UofE	University of Edinburgh
UofG	University of Glasgow

USmTDD	US-mediated targeted drug delivery

Chapter 1
Introduction

This chapter introduces the concepts of ultrasound (US) – mediated targeted drug delivery (USmTDD), describes the motivation and objectives of the thesis, lists the contributions to knowledge, explains the thesis structure, and provides a record of the publications resulting from the work described here.

1.1 Ultrasound-mediated Targeted Drug Delivery

As a primary part of the pathway by which a human gains nutrition, the intestinal mucosa acts as a selective barrier to permeation of material. Molecules smaller than 900 Da, termed *small molecules* in pharmacology, can usually cross the intestinal mucosa, provided they fulfil certain physicochemical requirements, but macromolecular biotherapeutics cannot (Moroz *et al.*, 2016). This limits the delivery of large molecules to injections, which can be associated with administration-related injuries and often require delivery by a healthcare professional. However, the oral route is the drug administration route best accepted by patients (Cyriac and James, 2014; Homayun *et al.*, 2019).

US is under active research as a means for enhancing local tissue permeability to medication (Castle *et al.*, 2013). US technology uses non-ionising radiation, is generally safe, non-invasive and a socially and culturally accepted medical technique, providing a basis for adoption by clinicians and patients. An ingestible capsule, termed a smart capsule, incorporating an US transducer has the potential to offer a method for oral delivery of drugs to the small intestine (Turcanu *et al.*, 2018). The capsule could both protect the drug payload against the destructive action of low stomach pH and microbiota and facilitate delivery of a drug once it reaches the intestine.

US may also transiently modulate the permeability of the epithelium and promote the passage of the drugs into the mucosa (Helfield *et al.*, 2016; McLaughlan *et al.*, 2013). This targeted approach has the potential to translate into reduced side effects since the amount of drug required would be much smaller than the regular dose administered systemically and the drug will be delivered locally. An US capsule could also reduce dependence on needle injections, increasing patient treatment adherence.

1.2 Motivation and Objectives

The aim of my project was to use US in a capsule to deliver drugs in the intestine and record systemic effects.

Previous work conducted within the UK EPSRC Sonopill Programme (EP/K034537/1) indicated US has the potential to decrease the barrier function of the intestinal mucosa *in vitro* (Stewart *et al.*, 2018) and to mark tissue *in vivo* (Turcanu *et al.*, 2018; Stewart *et al.*, 2021). The compounds delivered were immobilised in the mucus layer covering the intestinal mucosa. The present thesis describes further investigations into how US can deliver compounds through the intestinal mucosa *in vitro* and *in vivo*. Previous work made use of focused single-element transducers; the current work explored unfocused single-element and phased array transducers to increase the insonated area.

The hypothesis of this project is that US and cavitation agents (CAs) can be employed to deliver drugs in useful quantities through the mucosa of the small intestine *in vitro* and *in vivo*. *In vivo*, this would rely on opening the mucosal barrier to allow the absorption of therapeutics into the portal circulation.

1.3 Contributions to Knowledge

The present thesis has contributed to knowledge in six specific areas:

1. Demonstration that tissue barrier function was decreased with phased array transducers *in vitro* and *in vivo*.

    a. *In vitro*, a decrease in barrier function was associated with the application of a lower US frequency, higher intensity, higher number of cycles, a higher number of pulses and a larger insonation area.

b. *In vivo*, US, CAs and insulin delivery to the small intestine of live pigs correlated with lower glucose values than those recorded in a control pig. This was the first proof-of-concept experiment on therapeutic US applied to the small intestine where a systemic effect was recorded.

2. Demonstration of the degree of barrier function decrease with focused and unfocused single-element and phased array US transducers (Turcanu *et al.*, 2018; Turcanu *et al.*, 2021). It was shown that phased array transducers can insonate a larger surface area than an unfocused single-element, which can insonate a larger area than a focused single-element. As expected, the level of efficiency in decreasing the barrier function can be described as phased array transducer > unfocused transducer > focused transducer.

3. Demonstration that the intestinal mucus can represent a barrier to US drug delivery. I have also contributed to developing and testing an artificial mucus rheologically similar to the porcine intestinal mucus.

4. Demonstration that US combined with MBs and US combined with NDs can transiently decrease the barrier function of an organoid (OG)-derived cell layer (Turcanu *et al.*, 2020). Porcine rectum OG-derived cell layers cycle between confluent and detached until reaching a plateau**.**

5. Demonstration that a glucometer, which relies on test strips with blood samples, is less reliable than intradermal sensors or laboratory plasma analysis methods for assessing blood glucose levels.

1.4 Thesis Structure

Chapter 2 is a literature review that describes the gastrointestinal tract, detailing the small intestine, therapy in the small intestine, and capsule based therapy. The chapter then introduces US, therapeutic US, contrast agents and sonoporation.

Chapter 3 presents tests conducted to characterise the intestinal mucus, showing that it can represent a barrier to US-mediated targeted drug delivery. qDots delivered in the presence of US and MBs have lodged in the murine intestinal mucus. The chapter also describes a recipe for artificial mucus rheologically similar to porcine *ex vivo* mucus, which could be used for preliminary tests on mucus.

Chapter 4 builds on the previous chapter by investigating transducers alternative to those used previously which can promote compounds to be delivered to or through the intestinal mucosa. Focused and unfocused single-elements and phased array transducers are used in conjunction with MBs to decrease the barrier function of a human colorectal adenocarcinoma cell (Caco-2) monolayer and deliver fluorescent dextran across it.

Chapter 5 describes insonation of cell layers derived from OGs. Due to the presence of stem cells, such layers should better resemble *in vivo* intestinal tissue compared to a conventional Caco-2 cell layer. The chapter also compares the efficiency of using US in conjunction with MBs and NDs to decrease the barrier function of such an OG-derived layer and promote insulin transfer across the layer.

Chapter 6 builds on the *in vitro* work in previous chapters by presenting how a tethered capsule with a phased array transducer delivered MBs and insulin to the small intestine of live pigs and decreased the glucose levels. The chapter briefly describes the design and fabrication process of the capsule and compares three different methods to assess glucose levels of pigs administered insulin.

Chapter 7 contains conclusions and future work. The latter describes alternative *in vitro* systems for studying the effects of insonation on compounds delivery. This includes a method to microinject OGs or grow them with either the apical or basal cellular side towards the exterior, depending on the experiment conducted.

1.5 List of Publications Resulting from this Thesis

Peer Reviewed Journal Articles

F. Stewart, G. Cummins, **M. Turcanu**, B.F. Cox, A. Prescott, E. Clutton, I.P. Newton, M.P.Y. Desmulliez, M. Thanou, H. Mulvana, S. Cochran, I. Näthke, *Ultrasound Mediated Delivery of Quantum Dots from a Capsule Endoscope to the Gastrointestinal Wall*. Scientific Reports vol. 11, pp. 2584, 2021, doi: https://doi.org/10.1038/s41598-021-82240-1

H.S. Lay, G. Cummins, F.B. Cox, Y. Qiu, **M. Turcanu**, R. McPhillips, C. Connor, R. Gregson, E. Clutton, M.P.Y. Desmulliez, S. Cochran, *In-Vivo Evaluation of Microultrasound and Thermometric Capsule Endoscopes*, IEEE Transactions on

Biomedical Engineering, vol. 66, no. 3, pp. 632-639, March 2019, https://doi.org/10.1109/TBME.2018.2852715

J. Beeley, G. Melino, M. Al-Rawahani, **M. Turcanu**, F.S. Stewart, S. Cochran, D. Cumming, *Imaging Fluorophore-Labelled Intestinal Tissue via Fluorescence Endoscope Capsule*. 2018. Proceedings, vol. 2(13), pp.766, http://dx.doi.org/10.3390/proceedings2130766.

Book Chapters

P. Cressey, W. Zhang, **M. Turcanu**, S. Cochran, M. Thanou, 2019, Design of Nanoparticles for Focused Ultrasound Drug Delivery. In: Kumar C. *Nanotechnology Characterization Tools for Tissue Engineering and Medical Therapy*. Springer, Berlin, Heidelberg. https://doi.org/10.1007/978-3-662-59596-1_5

A. Moldovan, **M. Turcanu** and S. Cochran, 2022, Ultrasound Technology for Capsule Endoscopy. In: Manfredi L. *Endorobotics: Design, R&D and Future Trends.* Elsevier. https://doi.org/10.1016/C2019-0-04341-5

Conference Papers

M. Turcanu, A. Moldovan, , M. Thanou, I. Näthke, S. Cochran, *Manipulating the Barrier Function of a Cell Monolayer using a High-power Miniature Ultrasonic Transducer*, 2021 IEEE International Ultrasonics Symposium (IUS), China, 2021, pp. 1-3, In Press. Doi: https://doi.org/10.1109/IUS52206.2021.9593741

M. Turcanu, A. Moldovan, S. Vlatakis, D. Vllasaliu, M. Thanou, I. Näthke, S. Cochran, *An Organoid-derived Cell Layer as an in vitro Model to Measure US-mediated Drug Delivery across the Intestinal Wall, 2020 IEEE International Ultrasonics Symposium (IUS)*, Las Vegas, 2020, pp. 1-4, doi: https://doi.org/10.1109/IUS46767.2020.9251401

M. Turcanu, F.R. Stewart, B.F. Cox, R.E. Clutton. H. Mulvana, D. Vllasaliu, M. Thanou, I. Näthke, S. Cochran, *Ultrasound and Microbubbles Promote the Retention of Fluorescent Compounds in the Small Intestine, 2018 IEEE International Ultrasonics Symposium (IUS)*, Kobe, 2018, pp. 1-4, https://doi.org/10.1109/ULTSYM.2018.8580036

H. S. Lay, C. Connor, G. Cummins, V. Seetohul, B.F. Cox, **M. Turcanu**, Y. Qiu, R. McPhilips, M.P.Y Desmulliez, E. Clutton, S. Cochran, *Translational trial outcomes for capsule endoscopy test devices*, *2017 IEEE International Ultrasonics Symposium (IUS)*, Washington, DC, 2017, pp. 1-4, https://doi.org/10.1109/ULTSYM.2017.8091826

Conference Presentations

IEEE International Ultrasonics Symposium, Las Vegas USA. **Poster Presentation** entitled *An Organoid-Derived Cell Layer as an in Vitro Model for US-Mediated Drug Delivery Studies.* 2020.

IEEE International Ultrasonics Symposium, Kobe Japan. **Oral Presentation** entitiled *Ultrasound and Microbubbles Promote the Retention of Fluorescent Compounds in the Small Intestine*. 2018.

International Society for Therapeutic Ultrasound, Nashville Tennessee USA. **Poster Presentation** entitled *Ultrasound and Microbubbles Promote the Retention of Fluorescent Compounds in the Small Intestine.* 2018.

Ultrasound Microbubble Symposium, Leeds UK. **Poster Presentation** entitled *Ultrasound and Microbubbles Promote the Retention of Fluorescent Compounds in the Small Intestine*. 2018.

Other Presentations

Image-Guided Therapies Network+, Kent UK. **Oral Presentation** entitled *Drug Delivery and Imaging for Enhanced Uptake in the GI Tract.* 2018.

Megameet, Edinburgh UK. **Oral Presentation** entitled *Ultrasound-mediated Targeted Drug Delivery in the Small Intestine: Translational Research*. 2017.

Scottish Ultrasound Group, Edinburgh 2017. **Poster Presentation** entitled *Investigation of LAMP-1 expression in cells treated with ultrasound and microbubbles as an indicator of cell membrane repair.*

Image-Guided Therapies Network+, London UK. **Poster Presentation** *Acoustic Sensing and Ultrasonic Drug Delivery in Multimodal Theranostic Capsule Endoscopy*. 2017.

Therapeutic Ultrasound Winter School, Les Houches France. **Oral Presentation** entitled *Ultrasound-mediated Targeted Drug Delivery in the Small Intestine*. 2017.

1.6 References

Castle, J., Butts, M., Healey, A., Kent, K., Marino, M., Feinstein, S.B., 2013. Ultrasound-mediated targeted drug delivery: recent success and remaining challenges. American Journal of Physiology-Heart and Circulatory Physiology 304, H350–H357. https://doi.org/10.1152/ajpheart.00265.2012

Cyriac, J.M., James, E., 2014. Switch over from intravenous to oral therapy: A concise overview. J Pharmacol Pharmacother 5, 83–87. https://doi.org/10.4103/0976-500X.130042

Helfield, B., Chen, X., Watkins, S.C., Villanueva, F.S., 2016. Biophysical insight into mechanisms of sonoporation. Proc Natl Acad Sci USA 113, 9983–9988. https://doi.org/10.1073/pnas.1606915113

Homayun, B., Lin, X., Choi, H.-J., 2019. Challenges and Recent Progress in Oral Drug Delivery Systems for Biopharmaceuticals. Pharmaceutics 11, E129. https://doi.org/10.3390/pharmaceutics11030129

McLaughlan, J., Ingram, N., Smith, P.R., Harput, S., Coletta, P.L., Evans, S., Freear, S., 2013. Increasing the sonoporation efficiency of targeted polydisperse microbubble populations using chirp excitation. IEEE Trans Ultrason Ferroelectr Freq Control 60, 2511–2520. https://doi.org/10.1109/TUFFC.2013.2850

Moroz, E., Matoori, S., Leroux, J.-C., 2016. Oral delivery of macromolecular drugs: Where we are after almost 100 years of attempts. Adv. Drug Deliv. Rev. 101, 108–121. https://doi.org/10.1016/j.addr.2016.01.010

Stewart, F., Verbeni, A., Qiu, Y., Cox, B.F., Vorstius, J., Newton, I.P., Huang, Z., Menciassi, A., Näthke, I., Cochran, S., 2018. A Prototype Therapeutic Capsule Endoscope for Ultrasound-Mediated Targeted Drug Delivery. J. Med. Robot. Res. 03, 1840001. https://doi.org/10.1142/S2424905X18400019

Chapter 2
Background: Therapy in the Small Intestine

This chapter introduces the gastrointestinal (GI) tract, local and systemic therapy in the GI tract, the benefits of oral drug delivery over injected drugs and how this can be achieved using capsules. The chapter then introduces the concepts of US and CAs and how these can facilitate capsule-based therapy by producing pores in the small intestine.

2.1 The Gastrointestinal Tract

The GI tract comprises the organs through which food and liquids pass in order to be swallowed, absorbed, digested and eliminated from the body. The GI tract is nine metres long at autopsy. It comprises the mouth, pharynx, oesophagus, stomach, small intestine, large intestine, rectum and anus (Marieb and Hoehn, 2010). The major location for absorption of drugs and nutrients from food is the small intestine and it forms the anatomical focus for this thesis.

The small intestine is divided into three parts: duodenum, jejunum and ileum (Drake *et al.*, 2005, pp. 312). The duodenum attaches to the distal end of the stomach; it is C-shaped and about 22 cm in length. Secretions from the duodenum neutralize the acidic gastric chyme that exits the stomach (Lopez *et al.*, 2021). The jejunum is the middle section between the duodenum and the ileum. It is about 2.5 m in length and contains circular folds and villi. These two structures increase its surface area, maximising nutrient absorption. The ileum is about 3 m long and it connects the small intestine to the large intestine. Its anatomical features are similar to those of the jejunum. The small intestine is anchored to the abdominal wall by the mesentery, a thin layer of tissue that contains blood vessels, nerves and lymphatic vessels (Stallard *et al.*, 1994).

The wall of the small intestine comprises multiple layers: the serosa, muscularis, submucosa and mucosa, Figure 2-1, from the outside in. The serosa is the outside layer of

the small intestine. It is a protective slippery membrane involved in regulating the inflammation response and tissue repair (Mutsaers, 2002). The muscularis is composed of two smooth muscle layers: a thin outer longitudinal layer and a thick inner circular layer. There are nerves between these two layers that promote peristalsis, a sequence of coordinated muscle contractions. These contractions have two roles: (1) they maximise exposure of compounds from the lumen to the wall of the intestine to enhance absorption and (2) promote luminal compounds to move forward the in GI tract (Huizinga and Lammers, 2009). The following layer is the submucosa, which consists of connective tissue with blood vessels, nerves and lymphatic vessels.

The layer that is exposed to the lumen is the mucosa, which is composed of four layers: muscularis mucosa, lamina propria, basement membrane and epithelium. The muscularis mucosa is a thin layer of muscle situated between the lamina propria and the submucosa. The lamina propria is a thin layer of connective tissue situated underneath the basement membrane. The basement membrane is a thin layer of extracellular matrix (Li, 2003). The basement membrane, lamina propria and the muscularis mucosa support the epithelium layer. The epithelium has a simple columnar nature and it plays a role in both absorption of compounds from the lumen and restriction of pathogens crossing the intestinal wall.

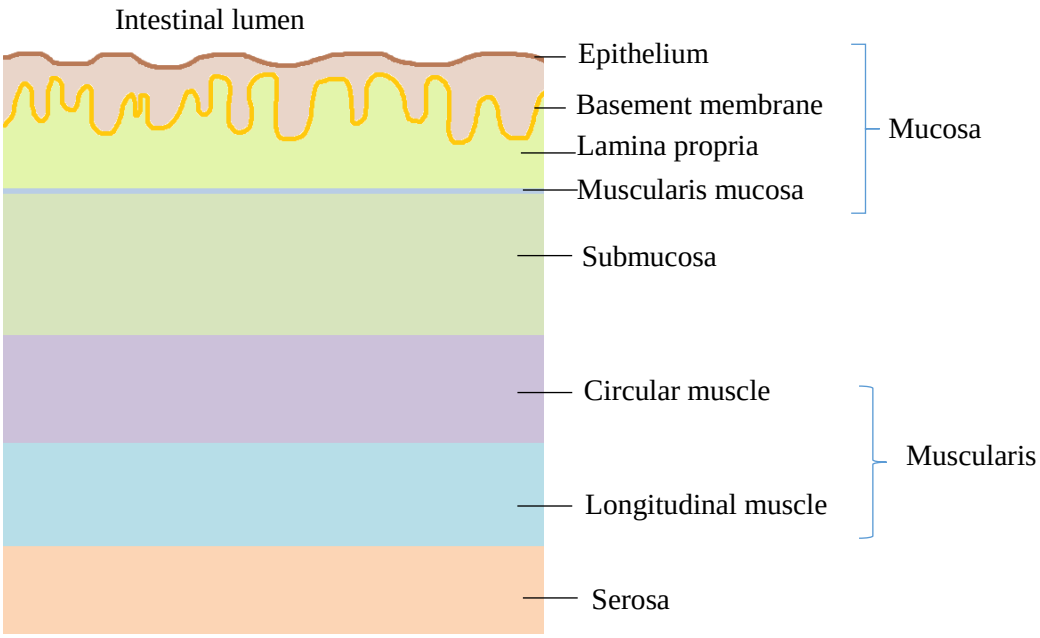

Figure 2-1 Layers of the intestine. *The role of the small intestine is realised by its component layers: serosa, muscularis, submucosa and mucosa. The muscularis is composed of circular and longitudinal muscles. The submucosa is composed of epithelium, basement membrane, lamina propria and muscularis mucosa. According to Carmel et al. (2010), the total thickness of these layers varies in humans from 2.1 mm in the duodenum to 1.8 mm in the terminal ileum. Blood vessels span all layers underneath the epithelium as depicted in Figure 2-3.*

Epithelial cells are protected by two layers of mucus, Figure 2-2 (Hansson, 2012). Mucus is produced by goblet cells and it is composed mainly of water and mucin proteins (MUC) (Forstner, 1978). Mucus has multiple roles: (1) it impedes pathogen interaction with the epithelium, (2) it lubricates the intestine during peristalsis, (3) it helps transport chyme from the gut to the colon, and (4) it protects the cell lining against the acidity in the lumen (Johansson *et al.*, 2014). Intestinal mucus contains high levels of antibacterial peptides and proteins secreted by both Paneth cells and enterocytes (Hansson, 2012). Chloride is released into mucus via cystic fibrosis transmembrane conductance regulator (CFTR) channels and promote the movement of loose mucus and its bound bacteria distally into the large intestine, rendering the small intestine low in microbial content (Johansson *et al.*, 2014).

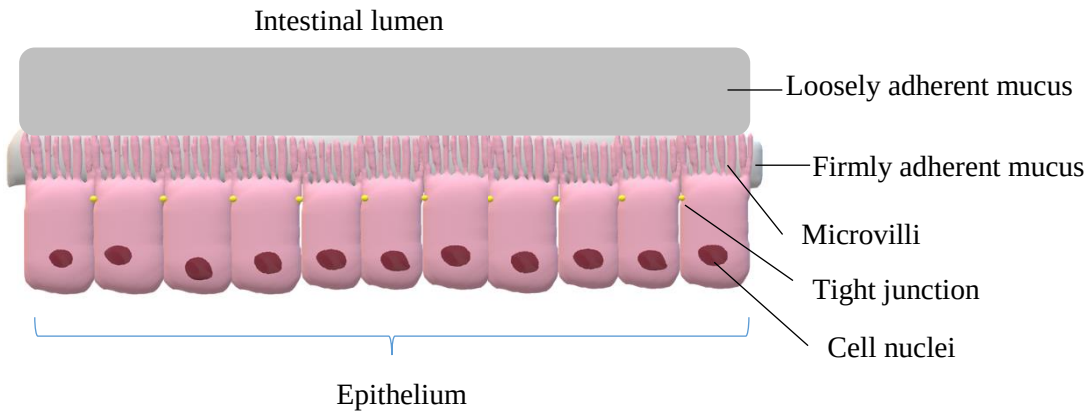

Figure 2-2 Epithelium protected by mucus layers. *In the intestinal lumen, there are two mucus layers: one layer is firmly adherent to the epithelium and another layer is loosely adherent to it. The epithelium consists of simple columnar cells, held together by tight junctions. Microvilli increase the surface area of cells, maximising absorption ability.*

2.1.1 Therapy in the Small Intestine

The GI tract has evolved as a place for food breakdown and pathogen destruction: the highly acidic pH of the stomach induces protein protonation, hence unfolding proteins and inducing the exhibition of more motifs that are to be bound by protein-degrading enzymes (Fuhrmann and Leroux, 2014). The enzymes present in the stomach, such as pepsin, and the ones present in the small intestine, such as chymotripsin, aminopeptidases, RNases and DNases, further disrupt the structure of protein and nucleic acids. These compounds are further cleaved in the colon under the activity of the enzymatic fermentation processes (Fuhrmann and Lerous, 2014). Orally administered pharmacological agents are exposed to the same processes, hence being largely inactive by the time they reach the small intestine (Goldber and Gomez-Orellana, 2003). The mucosal barrier is a multicomponent biological barrier comprising a mucus 'blanket' ~200 μm thick, epithelial cells and the basement membrane directly beneath the epithelium (Kim and Ho, 2010). These barriers need to be overcome in order to deliver an active biomacromolecule. The biomacromolecules can have either a local or a systemic effect.

2.1.1.1 Local Therapy

Local therapy can be applied for intestinal tumours or for inflammatory bowel disease (IBD). IBD describes a group of idiopathic disorders that cause chronic inflammation of the digestive tract. IBD can be either Crohn's disease or ulcerative colitis. Crohn's disease mainly affects the small intestine, whereas ulcerative colitis affects the rectum and the

colon. IBD affects patients' social and psychological wellbeing and increases the risk of developing colorectal cancer (Fakhoury *et al.,* 2014).

During normal conditions, the intestinal epithelium is fully covered with mucous, protecting the cells from luminal antigens and bacteria. Goblet cells produce the mucous, Paneth cells produce the antimicrobial peptides, leucocytes search the area for antigens, mitochondria produce ATP, antioxidants negate reactive oxygen species (ROS) and the tight junctions restrict translocation of luminal compounds into the lamina propria. In contrast, the ability of inflamed goblet cells to produce mucous is greatly reduced, rendering the epithelial cells exposed to antigens and intestinal bacteria; the number of antioxidants is decreased, leading to high amounts of ROS; mitochondria shrink and their ATP production is downregulated; and tight junctions cannot restrict the passing of bacteria and antigens into the lamina propria, triggering the infiltration of immune cells, hence further increasing the amount of ROS (Novak and Mollen, 2015).

Current treatment strategies often include steroids and immunosuppressive drugs that can lead to unwanted systemic effects (Fakhoury *et al.*, 2014). These side effects could potentially be minimised and disease remission could be achieved with a targeted drug delivery system, which could deliver medication only to the site of inflammation. This would minimise side effects, as the amount of medication reaching the systemic circulation would be reduced. The total amount of medication required would also be greatly reduced (Thanou *et al.,* 2018, pp. 198). A suitable targeted drug delivery system is presented after the following section on systemic therapy.

2.1.1.2 Systemic Therapy

A type of therapy in the small intestine different to local therapy is systemic therapy.

In order to reach the systemic circulation, a pharmacological agent needs to diffuse through the mucous layer protecting the intestinal wall. Intestinal epithelial cells are connected through tight junctions, enabling the paracellular passage of molecules only up to 500 Da (Menard *et al.*, 2010). Transcytotic transport can be (1) passive transport following a concentration gradient, (2) active transport using ATP to transport molecules against a concentration gradient, or (3) endocytosis, whereby biomacromolecules can bind to receptors such as transferrin and be transported across the cell, from the intestinal lumen into the portal circulation (der Rieux *et al.,* 2013, Misra *et al.,* 2011). A similar transcytotic

passage system is controlled by the phagocytotic M-cells of Peyer's patches, which can transport intestinal antigens to lymphoid follicles to trigger an immune response (Jepson *et al.*, 2004).

Compounds that cross the epithelial barrier can be absorbed from villi through capillaries or lacteals, Figure 2-3. While capillaries are part of the circulatory system, lacteals are part of the lymphatic system. Fatty acids pass into lacteals, while other compounds pass into capillary beds. These compounds are taken via the hepatic vein into the liver, where metabolism takes place. This is also the location of first pass effect for many compounds (Pond and Tozer, 1984). The first pass effect is the process whereby the concentration of a drug is greatly reduced before entering the systemic circulation. For certain drugs, such as insulin, the first pass effect takes place in the small intestine when administered orally and the drug spends a considerable amount of time in the gut. Once a drug leaves the liver, it enters the systemic circulation. The blood returns to the liver for filtration, so drug bioavailability is further reduced every time it passes though the liver.

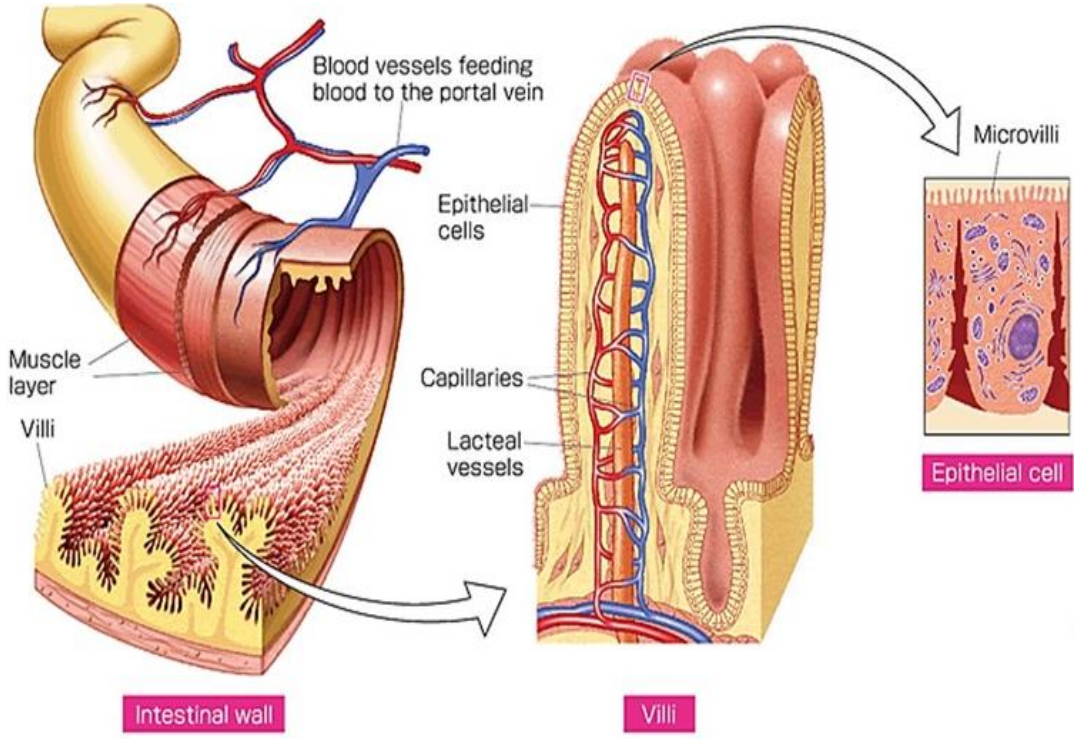

Figure 2-3 Absorption from the intestine. *Blood vessels facilitate the transport of compounds between lacteals in the villi and the liver. Pharmaceutical compounds and nutrients from the intestine need to cross the epithelial cell layer of the villi, enter capillaries or lacteals and access the hepatic portal circulation in order to reach the liver. (Kim & Ho, 2010).*

Orally administered insulin has poor bioavailability due to its inability to permeate the intestinal epithelium and many oral insulin formulations have been suspended or discontinued. These include nanoparticles coated with B12 (Apollo Lifesciences, San Francisco, CA, USA), liposomes (Endorex, Lake Bluff, IL, USA), insulin encapsulated in dextran matrix (Bow Pharmaceuticals, Zug, Switzerland), nanosized insulin (Diasome, Cleveland, OH, USA) and other formulations developed by AutoImmune with Eli Lilly and Provalis with Cortecs (Smart *et al.,* 2014). A sublingual formulation was developed by Biodel (CN, USA), but it was also discontinued.

Furthermore, 60% of diabetes patients treated with subcutaneously administered insulin fail to achieve long term glycaemic control (Fonte *et al.,* 2013). Potential reasons for this include poor patient compliance due to use of needles, the complexity of the insulin treatment regimen, fear of hypoglycaemia episodes, and weight gain (Heinemann and Jacques, 2009).

Another class of drugs generally administered subcutaneously is vaccines. They often require administration by trained medical staff and come with the potential issue of needle compliance and administration in a medical centre (Lin and Wang, 2008).

Advanced drug delivery approaches represent systems that target drugs to specific locations and enable drug release in a therapeutically effective manner. The types of triggers proposed for releasing drugs from delivery systems have included pH (Ishida *et al.,* 2006), temperature (Needham *et al.,* 2000), light (Zhang *et al.,* 2002) and enzymes (Ghadiali and Stevens, 2008).

2.1.1.3 Capsule Endoscopy for Targeted Drug Delivery

Therapeutic ingestible smart capsules are devices that can shield medication from degradative enzymes and increase the diffusion rate of medication through the GI mucosa. These devices can reduce dependence on needle injections, increase patient treatment adherence and reduce needle-associated drawbacks (Caffarel-Salvador *et al.,* 2017). There are two main problems that smart capsules address. The first one is that biologics (molecules >1000 Da) degrade in the GI space and do not easily permeate biological barriers. The second one is that hypodermic needle injections require training, cause pain, lead to needle injuries and present risk of infectious transmitted diseases. Furthermore,

10% of the population suffer from needle-phobia, leading to low prescription rates, especially in children (Hamilton, 1995)

There are at least four therapeutic capsules under development that have their effect in the small intestine. These are RaniPill™, which inflates in the intestine and injects its content into the intestinal wall (Hashim *et al.*, 2019), MucoJet, which creates a high-pressure liquid jet to deliver a vaccine (Munangandu *et al.*, 2018), LUMI, which injects biodegradable needles with drugs in the mucosa (Abramson *et al.*, 2019), and DGIST, a magnetically actuated microneedle capsule (Lee *et al.*, 2020).

It has also been postulated that US can be employed as an external effect to deliver molecules across the intestines, while enabling the control of drug release location and profile, as well as circumventing the need for complex pharmacological formulations and coating development (Kinoshita *et al.*, 2006; O'Neil and Li, 2008). The absorption step is enhanced by the ability of low frequency US to transiently permeabilize and push therapeutic molecules into tissue. To achieve good acoustic coupling, the intestine needs to be collapsed on the device with the transducer and an acoustically conductive medium, such as a fluid, needs to exist between the face of the transducer and the intestinal wall.

2.2 Therapeutic Ultrasound

In recent decades, the potential of US for therapeutic purposes has started to be researched substantially. One of the emerging topics it has been employed in is US-mediated targeted drug delivery, or USmTDD. The technology is based on US applied to drugs packaged in nanoparticles. US can place drugs close to the treatment site via effects such as acoustic streaming and acoustic radiation (Shung, 2015), release drugs from the nanoparticles and enhance drug absorption by increasing tissue permeability (Pitt *et al.*, 2004). Accurate and efficient delivery of drugs to specific areas of the GI tract represents one of the major unmet pharmacological needs. US technology uses non-ionising radiation, which is safe, non-invasive and a socially and culturally accepted medical technique, providing a basis for adoption by clinicians and patients (Miller *et al.*, 2012).

2.2.1 Introduction to Ultrasound

US is mechanical energy, most often comprising waves that are longitudinal and always requiring a supporting medium to propagate through. US propagates via vibrations of

molecules (i.e. they disturb the air particles), creating alternating regions of increased and decreased pressure in the medium.

US vibrations are sound waves with frequencies too high to excite the human eardrum and be perceived as sound by the human brain (Cracknell, 1980). The upper frequency limit of human hearing ranges between 10 kHz and 18 kHz, whereas US frequencies are above 20 kHz (Cracknell, 1980).

US is produced by the conversion of electrical energy into mechanical energy (Kinsler, 2000). This conversion is usually performed by a material with electromechanical properties, such as piezoelectric crystals. When an electric field is applied to the material, it deforms, producing vibrations. This is called the piezoelectric effect. The reverse of the phenomenon works too: upon application of mechanical forcing to piezoelectric crystals, they deform and can thus convert mechanical energy into electrical energy. The piezoelectric effect underpins the usage of US in medical diagnostics (Lee and Roh, 2017).

Diagnostic US is based on the ability to interpret the return of a transmitted US wave as an echo image of the surface. The typical frequencies employed range between 2 and 20 MHz. Blood and perfused tissue are anechogenic, so contrast agents are often used to image them (Cobbold, 2006). As the US waves emitted by piezoelectric crystals encounter tissues with different characteristics and densities, they reflect echoes back to the piezoelectric crystals (more than 1000 times/second). Returning echoes are converted to electric signals, which computers convert into points corresponding to the anatomic position and the strength of the reflecting echoes (Cobbold, 2006).

A medical transducer contains a large array of crystals which allow to make a series of image lines, that together make a complete image frame, called a sonogram. In addition, all the crystals are repeatedly activated many times, in such a way that a complete image frame is formed around 20 times/second or more, so that real time motion can be displayed as a series of US images (Cobbold, 2006). A lower US frequency offers images with greater penetration depth but lower resolution, whereas a higher frequency enables acquisition of images with lower penetration depth but higher resolution. In order for an US device to be approved by the United States Food and Drug Administration (FDA, Silver Spring, MD, USA), its maximum overall intensity, the spatial-peak temporal-average intensity needs to be less than 720 mW/cm^2 (FDA, 2019).

The conversion of electrical energy into mechanical energy underpins the usage of US for therapeutic applications.

2.2.2 Ultrasound-mediated Targeted Drug Delivery

Therapeutic US is successfully employed in phacoemulsification (cataract surgery), dental treatments, physical therapy (ligament, muscle strain, join inflammation), lithotripsy (destruction of liver/gallbladder/kidney stones) and high intensity focused US (HIFU), also called focused ultrasound surgery (FUS). FUS is a non-invasive technique that employs heating of the tissue to the level of necrosis (ablation, 55 – 70°C). The range of frequencies used is lower than the one used for diagnostic purposes, 0.25 – 12 MHz, because the targets in therapy are larger than in imaging (Miller *et al.*, 2012). The tissue in which US propagates should not be affected as the whole beam converges to a focal point; only the focal zone heats up to a temperature high enough to damage cells (Gourevich, 2013).

2.2.2.1 Bioeffects Produced by Therapeutic Ultrasound

Bioeffects occur at sufficiently high-pressure levels and intensities, with the most important ones being heating, wave distortion, cavitation and radiation force.

Heat can be generated through conversion of US (kinetic) energy as it propagates through tissue or another medium. At low US intensities, there is no risk of reaching dangerous temperatures, but as intensity increases, temperature increases as well. Adverse effects may occur when the temperature is over 38.5°C. The ALARA (as low a power level as reasonably achievable) principle is employed in patient scanning to prevent thermal adverse reactions (Cobbold, 2006). A thermal index lower than 1 is considered safe and does not need to be displayed by the device (Shung, 2015).

Wave distortion can take place when a wave of high enough amplitude travels through a medium, leading to nonlinear propagation (Hamilton and Blackstock, 1989, pp 55-57). The wave displaces particles in the medium it travels through, producing regions of high density with positive pressure and regions of low density with negative pressure. Higher pressure correlates with higher temperatures; because the speed of sound increases locally while propagating through regions of high temperature, the peaks of the pressure wave travel faster than the troughs, distorting the wave. The resulting saw tooth waveform transfers energy to higher harmonics of the wave, resulting in higher energy absorption (Shung, 2015).

Radiation force is an effect in which US waves, by absorption, can transfer momentum to the medium. Acoustic streaming and direct transfer of momentum can then push objects such as microbubbles or solid particles in the direction of the sound wave. Acoustic streaming can also lead to shear stress (Shung, 2015).

Cavitation describes the effect of US on pre-existing, injected or newly formed bubbles; it represents the oscillation or collapse of gas bubbles in a liquid in response to pressure fluctuations in the liquid (Rayleigh, 1917). Under very low pressure, formation of bubbles filled with gas or vapour takes place. Such bubbles can then undergo stable or inertial cavitation.

Stable cavitation is described as small amplitude oscillations in the size and shape of a bubble about its equilibrium, without collapsing (Flynn, 1967; Brennen, 1995). There is gas influx during the expansion phase and gas efflux during the compression phase. The oscillations exert pressure, producing flow around the bubble, or microstreaming (Elder, 1959). If this phenomenon take place near cells, they will experience shear stress and their membrane may be disrupted (Wu, 2002).

In contrast, inertial cavitation, formerly known as transient cavitation, is described as the collapse of a bubble, producing shock waves and sometimes microjets (Cobbold, 2006). The bubble normally has a relatively low internal gas pressure; a high enough pressure in the medium surrounding a bubble, or applied acoustic pressure, can cause the bubble to firstly grow in size and subsequently implode rapidly due to the inertia of the inrushing fluid.

During inertial cavitation, the internal bubble pressure can increase up to 80 000 atm and the temperature can exceed 9 000°C. Such high temperatures can decompose water into chemically active acidic compounds, leading to damaging biological effects. The process also results in free radical formation, which generates light – a phenomenon known as sonoluminescence (Riesz *et al.,* 1985). The gas inside the bubble dissolves in the surrounding liquid.

Inertial cavitation was described by Lord Rayleigh at the beginning of the 20th century (Rayleigh, 1917). It was suggested to be the reason behind the damage to ship propellers: under low enough pressure in the liquid surrounding rapidly rotating propellers, a rupture in the liquid leads to the formation of a cavity, or spherical void. Vapour and gases from

the surrounding medium fill the void, forming a low-pressure gas bubble. Bubbles are then isothermically enlarged and rapidly collapse to small fractions of their initial size, applying strain on the propellers' tips. The resulting smaller bubbles can act as new cavitation nuclei, grow in size, and subsequently collapse again (Liang *et al.*, 2010).

The likelihood of an inertial cavitation event taking place is quantified using a unitless measure termed mechanical index (MI), Equation 2-1 (Apfel and Holland, 1991, Church *et al.*, 2005).

$$MI = \frac{PNP}{P_{t,n}\sqrt{f_c}} \qquad \textbf{Equation 2-1}$$

where *PNP* is the peak negative pressure measured in MPa, $P_{t,n}$ is the threshold for inertial cavitation, which accounts for pulse length, and f_c is the centre frequency measured in MHz. The lower the frequency, the higher the likelihood of inducing cavitation; the higher the pressure and threshold for inertial cavitation, the higher the likelihood of inducing cavitation (Anderson and Hampton, 1980). The FDA MI limit for diagnostic devices is 1.9, above which the clinician must use discretion (Sen *et al.*, 2015).

Intensity affects the MI too.

$$I = \frac{\Delta p^2}{2\rho \times c} \qquad \textbf{Equation 2-2}$$

where *I* is the intensity measured in W, Δp is the pressure measured in MPa, ρ is the density calculated as mass / volume and measured in kgm^{-3}, and *c* is the speed of sound calculated as distance / time and measured in ms^{-1} (Postema and Attenborough, 2011, p.68). As intensity and pressure are proportional, but pressure and frequency are inversely proportional, Equation 2-1, an increase in frequency requires an increase in intensity to reach cavitation.

The intensity of the US field that will induce cavitation depends on the properties of the liquid and its impurity. For frequencies less than 1 MHz, an acoustic pressure of 0.2 MPa is enough to induce transient cavitation in aqueous solutions and in blood (Apfel and Holland, 1991). Cavitation likelihood can be suppressed by degassing the liquid, increasing its viscosity or reducing the static pressure. Cavitation results in broadband noise, which can be recorded by hydrophones (Cobbold, 2006).

2.2.2.2 Cavitation Agents

CAs used can be microbubbles (MBs) or volatile liquid-cored nanodroplets (NDs). MBs act as focused cavitation sites for the energy in the US wave. In the stable mode, the MBs oscillate locally, causing enhanced mechanical effects from fluid flow and other local effects. In the transient mode, they collapse.

MBs have a gas core and a shell that may be composed of lipids, proteins, polymers, surfactants or a combination of these. They often have a diameter ranging from 0.5 to 10 µm (Sirsi and Borden, 2009). The MBs clinically approved within the EU and the UK are SonoVue (Bracco, UK) and Optison (GE Healthcare, USA), whereas the ones approved and used mainly in the USA are Definity (Lantheus Medical Imaging, MA, USA). NDs are liquid-filled compounds stabilised by a surfactant shell. They are often custom made in small batches. Under the effect of acoustic radiation they can undergo vaporisation, a phase shift whereby they become MBs (Reznik *et al.*, 2011). MBs have short half-lives *in vivo* (minutes) (Mullin *et al.*, 2011). In contrast, NDs are generally more stable and have longer half-lives *in vivo* (Moyer *et al.*, 2015).

MBs are usually employed as contrast agents for imaging but can sometimes be employed to enhance drug delivery. Under the action of US, MBs oscillate, vibrate, scatter US waves and can reradiate energy from US waves. According to their diameter, bubbles often resonate around 1 – 4 MHz and can then radiate US in all directions (Doinikov *et al.*, 2009).

2.2.2.3 Sonoporation

Preliminary data has suggested that cavitation can facilitate the passage of large molecules through the GI epithelium (Stewart *et al.*, 2018). There are three main mechanisms by which US and CAs allow this: (i) transcellularly i.e. through cells; (ii) paracellularly i.e. through intercellular spaces; and/or (iii) by sonoporation i.e. through formation of pores in cell membranes (Hersh *et al.*, 2016), as illustrated in Figure 2-4.

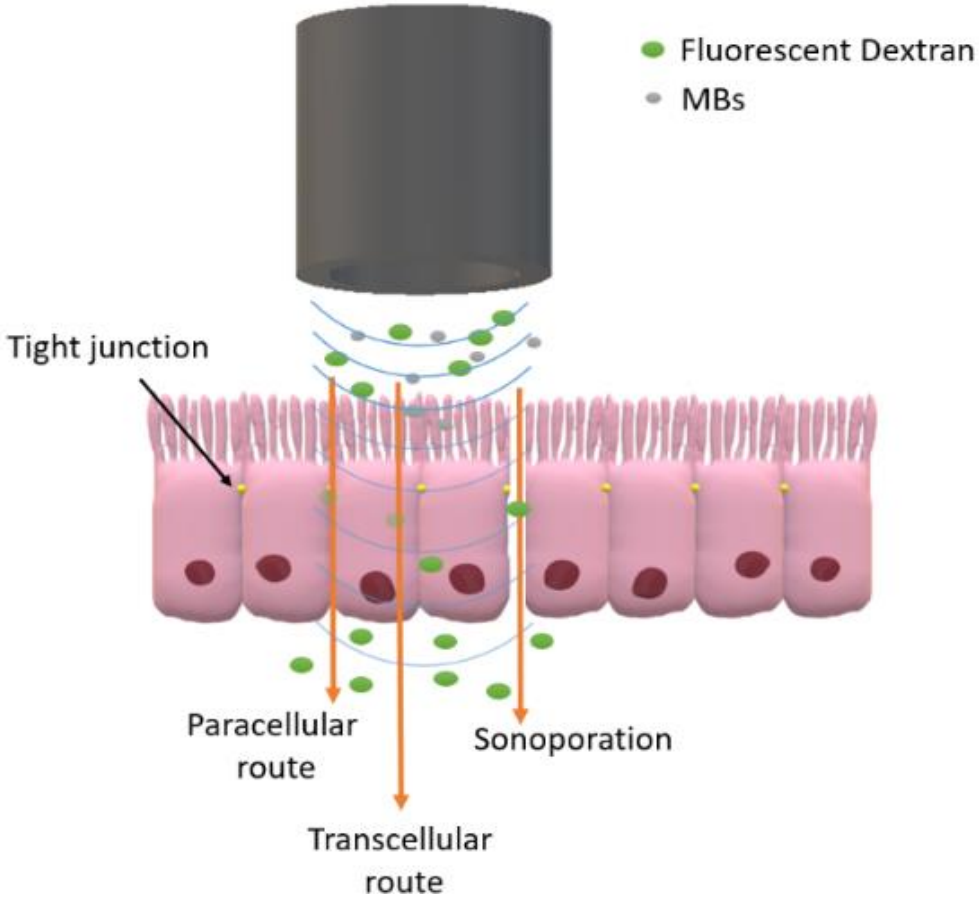

Figure 2-4 The effect of US and MBs on the epithelium lining the small intestine. *Under the effect of US and MBs, drug molecules are considered to cross the intestinal wall by means of one or a combination of the following routes: transcellular, paracellular or through sonoporation (Stewart et al., 2018). Fluorescent dextran is depicted in green and is present above and below the cell layer and MBs are depicted in grey only above the cell layer. MBs can cavitate and produce pores in the cell layer (sonoporation).*

When bubbles undergo stable cavitation, part of the energy can be absorbed, resulting in acoustic streaming and displacement of the bubble in the direction of the US beam (Dayton *et al.*, 2002). Stable cavitation can then generate shear stress on a nearby cell membrane, promoting pore formation. The bubble could even be pushed through the cell membrane to enter the cell (Wu *et al.*, 2002).

In contrast, inertial cavitation can promote sonoporation via shockwaves or microjetting. When a spherical bubble collapses near a surface such as a cell membrane, the bubble can transform into a toroidal shape and a liquid microjet is generated starting from the side of the bubble furthest from the cell membrane (Zhang *et al.*, 1993). The tip of the jet is always directed towards the membrane, travelling at high speed. A high-pressure region is generated around the penetration interface, leading to cell extravasation. This can

permeabilize cells by perforating cell membranes and producing pores (Tomizawa *et al.,* 2013; Tachibana and Tachibana, 1991). The effect is normally transient and can promote the permeation of large molecules through membranes, or the "injection" of bubble components into the cell. Agents larger than 154 kDa were reported to be too large to be delivered to the cell via these pores (Meijering *et al.,* 2009). These compounds are delivered via endocytosis, as a result of Ca^{2+} ions influx into the cell following pore formation.

Sonoporation can have short term and long-term effects. Short term effects (< 2 h) mentioned in the literature include Ca^{2+} mediated membrane resealing (Hassan *et al.,* 2010, Zhou *et al.,* 2008), compromised viability (Guzman *et al.,* 2001, Lai *et al.,* 2006), free radical formation (Juffermans *et al.,* 2006), cell size reduction (Chen *et al.,* 2013) and membrane blebbing (Schlicher *et al.,* 2010, Leow *et al.,* 2015). Long term effects (> 2 h) include apoptosis (Millar and Dou 2009, Honda et al 2002), cell cycle arrest (Zhong *et al.,* 2011), clonogenicity and regulation of signalling proteins (Zhong *et al.,* 2011, Tang *et al.,* 2008).

Sonoporation is an extremely important effect in the context of this thesis as it was previously suggested to be the main phenomenon for the passage of drugs through the epithelium as a result of cavitation (Wamel *et al.,* 2006; Meijering *et al.,* 2009; Kooiman *et al.,* 2011).

Few cavitation nuclei are normally found in blood and tissue, so introducing MBs or NDs can increase the probability of cavitation and sonoporation and also reduce the cavitation threshold. Intracellular delivery of propidium iodide to epithelial cells was successfully achieved at an MI between 0.2 and 0.4 (Wang *et al.,* 2018). However, sonoporation was reported across a wider MI range, between 0.08 and 0.5, when using a 1 MHz single element focused transducer (Kooiman *et al.,* 2011; van Rooij *et al.,* 2016).

2.2.2.4 Approaches to Ultrasound-mediated Targeted Drug Delivery

In 2013, Kotopoulis and his team published a clinical case study where US, MBs and gemcitabine were employed to treat human pancreatic cancer (Kotopoulis *et al.,* 2013). Following gemcitabine standard treatment, the patients were injected with SonoVue MBs and US was applied using a customised clinical US scanner. Compared to the 80 patients who underwent gemcitabine chemotherapy alone, the five patients who received the US

treatment exhibited hindered tumour expansion or tumour reduction to about 75% of the original size, hence suggesting the therapy has potential.

Another approach involves the administration of drugs enclosed in liposomes, lipid bilayer spheres that release the drug upon low frequency US treatment (Schroeder *et al.*, 2009). Acoustic cavitation is suggested to be facilitated by the addition of molecules that absorb US energy, such as highly hydrated PEG-lipopolymers, as well as by the presence of molecules which destabilise the lipid bilayer, such as amphiphiles, phospholipids with unsaturated acyl chains.

Thermodox® is an example of the loading of MBs, in this case with doxorubicin, a drug which stabilises topoisomerase II, preventing the DNA double helix from being resealed (Swenson *et al.*, 2015). Thermodox® was employed to treat breast tumours and liver tumours: FUS was employed to kill the cells present in the middle of the tumour, whereas the doxorubicin in MBs was used to kill efficiently the remaining tumorous cells found on the edge of the tumour due to the high temperature present in the tumour site. In a clinical trial on 10 patients, for seven of them the treatment resulted in an increase of 3.7 times in intratumoral drug concentration after application of FUS. The treatment was deemed clinically safe and effective at enhancing intratumoral drug concentration (Lyon *et al.*, 2018).

In 2014, Sinnecker *et al.,* showed that the isolated perfused rat small intestine can effectively restrict nanoparticles from uptake, using fluorescence as a marker. Fluorescence measurements of luminal, vascular, lymphatic and mucous samples showed that 95% of the nanoparticles resided in the luminal samples and the mucous. No heightened fluorescence was present in the vascular and lymphatic compartments. The nanoparticles used had diameters of 20 and 200 nm. These are much larger than the pharmaceutical agents absorbed from the intestine. Even macromolecules, such as insulin dimmers (5800 Da), which are poorly absorbed from the intestines, have a diameter of only 2 – 3 nm (Shorten *et al.*, 2007). In comparison, a bicellular tight junction has a diameter of 2 – 4 nm, while a tricellular junction can be up to 10 nm in diameter (Hou, 2019). However, many drugs have transcytosis receptor biomimetics and are transported across cells.

Sinnecker's work was taken a step further by Stewart *et al.,* 2016, exploring nanoparticle delivery through the gut wall was using US treatment. 14 murine small bowel samples

were employed in 23 sonication and control experiments to suggest that US was effective in passing 6 nm fluorescent nanoparticles through the gut wall in 80% of cases. These findings further support the potential of combining US and MBs for delivering pharmaceutical agents through the gut wall.

Extracorporeal therapeutic US was studied for different applications, but intracorporeal therapeutic US for treating the small intestine is more challenging and was explored to a much lesser degree. The issues associated with extracorporeal treatment are patient movement and tissue obstruction; the advantage of an intracorporeal transducer is that it should address these issues. However, the capsule would need to be miniaturised to ensure patients, especially elderly ones, find it easier to take it orally. Additional issues to consider are that the capsule can become lodged in the intestine and as it cannot be retrieved once administered, widespread use may be considered unsustainable without incorporation of appropriate materials and consideration for the sustainability of disposal.

In a proof of concept paper (Stewart *et al.*, 2021), it was shown that US and MBs can promote the delivery of fluorescent compounds into the gut mucosa of live pigs. The aim of the work described in this thesis was to explore the use of US in a capsule to deliver drugs effectively through the intestinal wall.

2.3 Conclusion

The chapter briefly introduced the topics of therapy in the small intestine, therapeutic US and therapeutic capsules. The remainder of this thesis will describe proof of concept studies relating to the effectiveness of therapeutic US based on targeted drug delivery to the small intestine using an intracorporeal capsule.

2.4 References

Abramson, A., Caffarel-Salvador, E., Khang, M., Dellal, D., Silverstein, D., Gao, Y., Frederiksen, M.R., Vegge, A., Hubálek, F., Water, J.J., Friderichsen, A.V., Fels, J., Kirk, R.K., Cleveland, C., Collins, J., Tamang, S., Hayward, A., Landh, T., Buckley, S.T., Roxhed, N., Rahbek, U., Langer, R., Traverso, G., 2019. An ingestible self-orienting system for oral delivery of macromolecules. Science 363, 611–615. https://doi.org/10.1126/science.aau2277

Anderson, A.L., Hampton, L.D., 1980. Acoustics of gas-bearing sediments I. Background. The Journal of the Acoustical Society of America 67, 1865–1889. https://doi.org/10.1121/1.384453

Apfel, R.E., Holland, C.K., 1991. Gauging the likelihood of cavitation from short-pulse, low-duty cycle diagnostic ultrasound. Ultrasound in Medicine & Biology 17, 179–185. https://doi.org/10.1016/0301-5629(91)90125-G

Brennen, C.E., 1995. Cavitation and bubble dynamics, Oxford engineering science series. Oxford University Press, New York.

Caffarel-Salvador, E., Abramson, A., Langer, R., Traverso, G., 2017. Oral delivery of biologics using drug-device combinations. Curr Opin Pharmacol 36, 8–13. https://doi.org/10.1016/j.coph.2017.07.003

Chen, X., Leow, R.S., Hu, Y., Wan, J.M.F., Yu, A.C.H., 2014. Single-site sonoporation disrupts actin cytoskeleton organization. J. R. Soc. Interface. 11, 20140071. https://doi.org/10.1098/rsif.2014.0071

Church, C.C., 2005. Frequency, pulse length, and the mechanical index. Acoustics Research Letters Online 6, 162–168. https://doi.org/10.1121/1.1901757

Cobbold, R.S.C., 2007. Foundations of biomedical ultrasound. Oxford University Press, Oxford ; New York.

Cracknell, A.P., 1980. Ultrasonics, The Wykeham science series. Crane, Russak, New York.

Cronin, C.G., Delappe, E., Lohan, D.G., Roche, C., Murphy, J.M., 2010. Normal small bowel wall characteristics on MR enterography. European Journal of Radiology 75, 207–211. https://doi.org/10.1016/j.ejrad.2009.04.066

Dayton, P.A., Allen, J.S., Ferrara, K.W., 2002. The magnitude of radiation force on ultrasound contrast agents. The Journal of the Acoustical Society of America 112, 2183–2192. https://doi.org/10.1121/1.1509428

des Rieux, A., Pourcelle, V., Cani, P.D., Marchand-Brynaert, J., Préat, V., 2013. Targeted nanoparticles with novel non-peptidic ligands for oral delivery. Advanced Drug Delivery Reviews 65, 833–844. https://doi.org/10.1016/j.addr.2013.01.002

Doinikov, A.A., Haac, J.F., Dayton, P.A., 2009. Resonance frequencies of lipid-shelled microbubbles in the regime of nonlinear oscillations. Ultrasonics 49, 263–268. https://doi.org/10.1016/j.ultras.2008.09.006

Drake, R.L., Vogl, W., Mitchell, A.W.M., Gray, H., Tibbitts, R.M., 2005. Gray's anatomy for students: online access + interactive extras ; studentconsult.com. Elsevier, Churchill Livingstone, Philadelphia, Pa.

Elder, S.A., 1959. Cavitation microstreaming. The Journal of the Acoustical Society of America, 31(1), pp.54-64.

Fakhoury, M., Negrulj, R., Mooranian, A., Al-Salami, H., 2014. Inflammatory bowel disease: clinical aspects and treatments. J Inflamm Res 7, 113–120. https://doi.org/10.2147/JIR.S65979

FDA, U.S.D. of H. and H.S.F. and D.A.C. for D. and R.H., 2019. Marketing Clearance of Diagnostic Ultrasound Systems and Transducers Guidance for Industry and Food and Drug Administration Staff.

Flynn H.G., 1964. Physics of acoustic cavitation in liquids. In: Mason WP, editor. Physical Acoustics. New York: Academic; pp. 58–172. vol I-B.

Fonte, P., Araújo, F., Reis, S., Sarmento, B., 2013. Oral Insulin Delivery: How Far are We? J Diabetes Sci Technol 7, 520–531. https://doi.org/10.1177/193229681300700228

Forstner, J.F., 1978. Intestinal Mucins in Health and Disease. Digestion 17, 234–263. https://doi.org/10.1159/000198115

Fuhrmann, G., Leroux, J.-C., 2014. Improving the Stability and Activity of Oral Therapeutic Enzymes—Recent Advances and Perspectives. Pharm Res 31, 1099–1105. https://doi.org/10.1007/s11095-013-1233-y

Ghadiali, J.E., Stevens, M.M., 2008. Enzyme-Responsive Nanoparticle Systems. Adv. Mater. 20, 4359–4363. https://doi.org/10.1002/adma.200703158

Goldberg, M., Gomez-Orellana, I., 2003. Challenges for the oral delivery of macromolecules. Nat Rev Drug Discov 2, 289–295. https://doi.org/10.1038/nrd1067

Gourevich, D., Dogadkin, O., Volovick, A., Wang, L., Gnaim, J., Cochran, S., Melzer, A., 2013. Ultrasound-mediated targeted drug delivery with a novel cyclodextrin-based drug carrier by mechanical and thermal mechanisms. Journal of Controlled Release 170, 316–324. https://doi.org/10.1016/j.jconrel.2013.05.038

Guzmán, H.R., Nguyen, D.X., Khan, S., Prausnitz, M.R., 2001. Ultrasound-mediated disruption of cell membranes. II. Heterogeneous effects on cells. J Acoust Soc Am 110, 597–606. https://doi.org/10.1121/1.1376130

Hamilton, J.G., 1995. Needle phobia: a neglected diagnosis. J Fam Pract 41, 169–175.

Hamilton, M.F., Blackstock, D.T. (Eds.), 1998. Nonlinear acoustics. Academic Press, San Diego, CA.

Hansson, G.C., 2012. Role of mucus layers in gut infection and inflammation. Current Opinion in Microbiology 15, 57–62. https://doi.org/10.1016/j.mib.2011.11.002

Hashim, M., Korupolu, R., Syed, B., Horlen, K., Beraki, S., Karamchedu, P., Dhalla, A.K., Ruffy, R., Imran, M., 2019. Jejunal wall delivery of insulin via an ingestible capsule in anesthetized swine—A pharmacokinetic and pharmacodynamic study. Pharmacol Res Perspect 7. https://doi.org/10.1002/prp2.522

Hassan, M.A., Campbell, P., Kondo, T., 2010. The role of Ca(2+) in ultrasound-elicited bioeffects: progress, perspectives and prospects. Drug Discov Today 15, 892–906. https://doi.org/10.1016/j.drudis.2010.08.005

Heinemann, L., Jacques, Y., 2009. Oral Insulin and Buccal Insulin: A Critical Reappraisal. J Diabetes Sci Technol 3, 568–584. https://doi.org/10.1177/193229680900300323

Hersh, D.S., Nguyen, B.A., Dancy, J.G., Adapa, A.R., Winkles, J.A., Woodworth, G.F., Kim, A.J., Frenkel, V., 2016. Pulsed ultrasound expands the extracellular and perivascular

spaces of the brain. Brain Res 1646, 543–550. https://doi.org/10.1016/j.brainres.2016.06.040

Hou, J., 2019. The paracellular channel: biology, physiology, and disease. Academic Press is an imprint of Elsevier, London ; San Diego, CA.

Huizinga, J.D., Lammers, W.J.E.P., 2009. Gut peristalsis is governed by a multitude of cooperating mechanisms. American Journal of Physiology-Gastrointestinal and Liver Physiology 296, G1–G8. https://doi.org/10.1152/ajpgi.90380.2008

Ishida, T., Okada, Y., Kobayashi, T., Kiwada, H., 2006. Development of pH-sensitive liposomes that efficiently retain encapsulated doxorubicin (DXR) in blood. International Journal of Pharmaceutics 309, 94–100. https://doi.org/10.1016/j.ijpharm.2005.11.010

Jepson, M.A., Clark, M.A., Hirst, B.H., 2004. M cell targeting by lectins: a strategy for mucosal vaccination and drug delivery. Advanced Drug Delivery Reviews 56, 511–525. https://doi.org/10.1016/j.addr.2003.10.018

Johnston, K., Tapia-Siles, C., Gerold, B., Postema, M., Cochran, S., Cuschieri, A., Prentice, P., 2014. Periodic shock-emission from acoustically driven cavitation clouds: A source of the subharmonic signal. Ultrasonics 54, 2151–2158. https://doi.org/10.1016/j.ultras.2014.06.011

Juffermans, L.J.M., Dijkmans, P.A., Musters, R.J.P., Visser, C.A., Kamp, O., 2006. Transient permeabilization of cell membranes by ultrasound-exposed microbubbles is related to formation of hydrogen peroxide. Am J Physiol Heart Circ Physiol 291, H1595-1601. https://doi.org/10.1152/ajpheart.01120.2005

Kim, Y.S., Ho, S.B., 2010. Intestinal Goblet Cells and Mucins in Health and Disease: Recent Insights and Progress. Curr Gastroenterol Rep 12, 319–330. https://doi.org/10.1007/s11894-010-0131-2

Kinoshita, M., McDannold, N., Jolesz, F.A., Hynynen, K., 2006. Noninvasive localized delivery of Herceptin to the mouse brain by MRI-guided focused ultrasound-induced blood–brain barrier disruption. Proc Natl Acad Sci USA 103, 11719. https://doi.org/10.1073/pnas.0604318103

Kinsler, L.E. (Ed.), 2000. Fundamentals of acoustics, 4th ed. ed. Wiley, New York.

Kooiman, K., Foppen-Harteveld, M., der Steen, A.F.W. van, de Jong, N., 2011. Sonoporation of endothelial cells by vibrating targeted microbubbles. Journal of Controlled Release 154, 35–41. https://doi.org/10.1016/j.jconrel.2011.04.008

Kotopoulis, S., Dimcevski, G., Helge Gilja, O., Hoem, D., Postema, M., 2013. Treatment of human pancreatic cancer using combined ultrasound, microbubbles, and gemcitabine: A clinical case study: Clinical sonoporation setup for human pancreatic cancer. Med. Phys. 40, 072902. https://doi.org/10.1118/1.4808149

Lai, C.-Y., Wu, C.-H., Chen, C.-C., Li, P.-C., 2006. Quantitative relations of acoustic inertial cavitation with sonoporation and cell viability. Ultrasound Med Biol 32, 1931–1941. https://doi.org/10.1016/j.ultrasmedbio.2006.06.020

Lee, J., Lee, H., Kwon, S., Park, S., 2020. Active delivery of multi-layer drug-loaded microneedle patches using magnetically driven capsule. Medical Engineering & Physics 85, 87–96. https://doi.org/10.1016/j.medengphy.2020.09.012

Lee, W., Roh, Y., 2017. Ultrasonic transducers for medical diagnostic imaging. Biomed. Eng. Lett. 7, 91–97. https://doi.org/10.1007/s13534-017-0021-8

Leow, R.S., Wan, J.M.F., Yu, A.C.H., 2015. Membrane blebbing as a recovery manoeuvre in site-specific sonoporation mediated by targeted microbubbles. J R Soc Interface 12, 20150029. https://doi.org/10.1098/rsif.2015.0029

Li, A.C.Y., 2003. Basement membrane components. Journal of Clinical Pathology 56, 885–887. https://doi.org/10.1136/jcp.56.12.885

Liang, H.-D., Tang, J., Halliwell, M., 2010. Sonoporation, drug delivery, and gene therapy. Proc Inst Mech Eng H 224, 343–361. https://doi.org/10.1243/09544119JEIM565

Lin, J.-C., Wang, T., 2008. Criminal Liability Research in Vaccine Administration by Public Health Nurse: A Case Study of the Nantou Vaccine Administration Case. Journal of Nursing Research 16, 1–7. https://doi.org/10.1097/01.JNR.0000387284.45935.c7

Lopez, P.P., Gogna, S., Khorasani-Zadeh, A., 2021. Anatomy, Abdomen and Pelvis, Duodenum, in: StatPearls. StatPearls Publishing, Treasure Island (FL).

Lyon, P.C., Gray, M.D., Mannaris, C., Folkes, L.K., Stratford, M., Campo, L., Chung, D.Y.F., Scott, S., Anderson, M., Goldin, R., Carlisle, R., Wu, F., Middleton, M.R., Gleeson, F.V., Coussios, C.C., 2018. Safety and feasibility of ultrasound-triggered targeted drug delivery of doxorubicin from thermosensitive liposomes in liver tumours (TARDOX): a single-centre, open-label, phase 1 trial. The Lancet Oncology 19, 1027–1039. https://doi.org/10.1016/S1470-2045(18)30332-2

Marieb, E.N., Hoehn, K., 2010. Human anatomy & physiology, 8th ed. ed. Benjamin Cummings, San Francisco.

Meijering, B.D.M., Juffermans, L.J.M., van Wamel, A., Henning, R.H., Zuhorn, I.S., Emmer, M., Versteilen, A.M.G., Paulus, W.J., van Gilst, W.H., Kooiman, K., de Jong, N., Musters, R.J.P., Deelman, L.E., Kamp, O., 2009. Ultrasound and Microbubble-Targeted Delivery of Macromolecules Is Regulated by Induction of Endocytosis and Pore Formation. Circulation Research 104, 679–687. https://doi.org/10.1161/CIRCRESAHA.108.183806

Ménard, S., Cerf-Bensussan, N., Heyman, M., 2010. Multiple facets of intestinal permeability and epithelial handling of dietary antigens. Mucosal Immunol 3, 247–259. https://doi.org/10.1038/mi.2010.5

Miller, D.L., Dou, C., 2009. Induction of apoptosis in sonoporation and ultrasonic gene transfer. Ultrasound Med Biol 35, 144–154. https://doi.org/10.1016/j.ultrasmedbio.2008.06.007

Miller, D.L., Smith, N.B., Bailey, M.R., Czarnota, G.J., Hynynen, K., Makin, I.R.S., Bioeffects Committee of the American Institute of Ultrasound in Medicine, 2012. Overview of therapeutic ultrasound applications and safety considerations. J Ultrasound Med 31, 623–634. https://doi.org/10.7863/jum.2012.31.4.623

Misra, A., 2011. Challenges in delivery of therapeutic genomics and proteomics, 1st ed. ed, Elsevier insights. Elsevier, Amsterdam Boston.

Moyer, L., Timbie, K., Sheeran, P., Price, R., Miller, W., Dayton, P., 2015. Direct nanodroplet and microbubble comparison for high intensity focused ultrasound ablation enhancement and safety. J Ther Ultrasound 3, O67. https://doi.org/10.1186/2050-5736-3-S1-O67

Mullin, L., Gessner, R., Kwan, J., Kaya, M., Borden, M.A., Dayton, P.A., 2011. Effect of anesthesia carrier gas on in vivo circulation times of ultrasound microbubble contrast agents in rats. Contrast Media Mol Imaging 6, 126–131. https://doi.org/10.1002/cmmi.414

Munang'andu, H.M., 2018. MucoJet: a novel noninvasive buccal mucosa immunization strategy. Ann. Transl. Med. 6, 64–64. https://doi.org/10.21037/atm.2018.01.11

Mutsaers, S.E., 2002. Mesothelial cells: Their structure, function and role in serosal repair. Respirology 7, 171–191. https://doi.org/10.1046/j.1440-1843.2002.00404.x

Needham, D., Anyarambhatla, G., Kong, G., Dewhirst, M.W., 2000. A new temperature-sensitive liposome for use with mild hyperthermia: characterization and testing in a human tumor xenograft model. Cancer Res 60, 1197–1201.

Novak, E.A., Mollen, K.P., 2015. Mitochondrial dysfunction in inflammatory bowel disease. Front. Cell Dev. Biol. 3. https://doi.org/10.3389/fcell.2015.00062

O'Neill, B.E., Li, K.C.P., 2008. Augmentation of targeted delivery with pulsed high intensity focused ultrasound. International Journal of Hyperthermia 24, 506–520. https://doi.org/10.1080/02656730802093661

Pitt, W.G., Husseini, G.A., Staples, B.J., 2004. Ultrasonic drug delivery – a general review. Expert Opinion on Drug Delivery 1, 37–56. https://doi.org/10.1517/17425247.1.1.37

Pond, S.M., Tozer, T.N., 1984. First-Pass Elimination: Basic Concepts and Clinical Consequences. Clinical Pharmacokinetics 9, 1–25. https://doi.org/10.2165/00003088-198409010-00001

Postema, M., Attenborough, K., 2011. Fundamentals of medical ultrasonics. Spon Press, Milton Park, Abingdon, Oxon ; New York. https://doi.org/10.1201/9781482266641

Rayleigh, Lord, 1917. VIII. On the pressure developed in a liquid during the collapse of a spherical cavity. The London, Edinburgh, and Dublin Philosophical Magazine and Journal of Science 34, 94–98. https://doi.org/10.1080/14786440808635681

Reznik, N., Williams, R., Burns, P.N., 2011. Investigation of Vaporized Submicron Perfluorocarbon Droplets as an Ultrasound Contrast Agent. Ultrasound in Medicine & Biology 37, 1271–1279. https://doi.org/10.1016/j.ultrasmedbio.2011.05.001

Riesz, P., Berdahl, D., Christman, C.L., 1985. Free radical generation by ultrasound in aqueous and nonaqueous solutions. Environ Health Perspect 64, 233–252. https://doi.org/10.1289/ehp.8564233

Schlicher, R.K., Hutcheson, J.D., Radhakrishna, H., Apkarian, R.P., Prausnitz, M.R., 2010. Changes in Cell Morphology Due to Plasma Membrane Wounding by Acoustic Cavitation. Ultrasound in Medicine & Biology 36, 677–692. https://doi.org/10.1016/j.ultrasmedbio.2010.01.010

Schroeder, A., Kost, J., Barenholz, Y., 2009. Ultrasound, liposomes, and drug delivery: principles for using ultrasound to control the release of drugs from liposomes. Chemistry and Physics of Lipids 162, 1–16. https://doi.org/10.1016/j.chemphyslip.2009.08.003

Sen, T., Tufekcioglu, O., Koza, Y., 2015. Mechanical index. Anatol J Cardiol 15, 334–336. https://doi.org/10.5152/akd.2015.6061

Shorten, P.R., McMahon, C.D., Soboleva, T.K., 2007. Insulin Transport within Skeletal Muscle Transverse Tubule Networks. Biophysical Journal 93, 3001–3007. https://doi.org/10.1529/biophysj.107.107888

Shung, K.K., 2015. Diagnostic Ultrasound: Imaging and Blood Flow Measurements, Second Edition, 0 ed. CRC Press. https://doi.org/10.1201/b18323

Sinnecker, H., Krause, T., Koelling, S., Lautenschläger, I., Frey, A., 2014. The gut wall provides an effective barrier against nanoparticle uptake. Beilstein J. Nanotechnol. 5, 2092–2101. https://doi.org/10.3762/bjnano.5.218

Sirsi, S., Borden, M., 2009. Microbubble Compositions, Properties and Biomedical Applications. Bubble Sci Eng Technol 1, 3–17. https://doi.org/10.1179/175889709X446507

Smart, A.L., Gaisford, S., Basit, A.W., 2014. Oral peptide and protein delivery: intestinal obstacles and commercial prospects. Expert Opinion on Drug Delivery 11, 1323–1335. https://doi.org/10.1517/17425247.2014.917077

Stallard, D.J., Tu, R.K., Gould, M.J., Pozniak, M.A., Pettersen, J.C., 1994. Minor vascular anatomy of the abdomen and pelvis: a CT atlas. RadioGraphics 14, 493–513. https://doi.org/10.1148/radiographics.14.3.8066265

Stewart, F., Cummins, G., Turcanu, M.V., Cox, B.F., Prescott, A., Clutton, E., Newton, I.P., Desmulliez, M.P.Y., Thanou, M., Mulvana, H., Cochran, S., Näthke, I., 2021. Ultrasound mediated delivery of quantum dots from a proof of concept capsule endoscope to the gastrointestinal wall. Sci Rep 11, 2584. https://doi.org/10.1038/s41598-021-82240-1

Stewart, F., Verbeni, A., Qiu, Y., Cox, B.F., Vorstius, J., Newton, I.P., Huang, Z., Menciassi, A., Näthke, I., Cochran, S., 2018. A Prototype Therapeutic Capsule Endoscope for Ultrasound-Mediated Targeted Drug Delivery. J. Med. Robot. Res. 03, 1840001. https://doi.org/10.1142/S2424905X18400019

Stewart, F.R., Qiu, Y., Lay, H.S., Newton, I.P., Cox, B.F., Al-Rawhani, M.A., Beeley, J., Liu, Y., Huang, Z., Cumming, D.R.S., Näthke, I., Cochran, S., 2017. Acoustic Sensing and Ultrasonic Drug Delivery in Multimodal Theranostic Capsule Endoscopy. Sensors (Basel) 17. https://doi.org/10.3390/s17071553

Swenson, C.E., Haemmerich, D., Maul, D.H., Knox, B., Ehrhart, N., Reed, R.A., 2015. Increased Duration of Heating Boosts Local Drug Deposition during Radiofrequency Ablation in Combination with Thermally Sensitive Liposomes (ThermoDox) in a Porcine Model. PLoS ONE 10, e0139752. https://doi.org/10.1371/journal.pone.0139752

Tachibana, K., Tachibana, S., 1991. Transdermal delivery of insulin by ultrasonic vibration. J Pharm Pharmacol 43, 270–271. https://doi.org/10.1111/j.2042-7158.1991.tb06681.x

Thanou, M., Royal Society of Chemistry (Great Britain) (Eds.), 2018. Theranostics and image guided drug delivery, RSC drug discovery series. Royal Society of Chemistry, London. https://doi.org/10.1039/9781788010597-00182

Tomizawa, M., Shinozaki, F., Motoyoshi, Y., Sugiyama, T., Yamamoto, S., Sueishi, M., 2013. Sonoporation: Gene transfer using ultrasound. World J Methodol 3, 39–44. https://doi.org/10.5662/wjm.v3.i4.39

van Rooij, T., Skachkov, I., Beekers, I., Lattwein, K.R., Voorneveld, J.D., Kokhuis, T.J.A., Bera, D., Luan, Y., van der Steen, A.F.W., de Jong, N., Kooiman, K., 2016. Viability of endothelial cells after ultrasound-mediated sonoporation: Influence of targeting, oscillation, and displacement of microbubbles. Journal of Controlled Release 238, 197–211. https://doi.org/10.1016/j.jconrel.2016.07.037

van Wamel, A., Kooiman, K., Harteveld, M., Emmer, M., ten Cate, F.J., Versluis, M., de Jong, N., 2006. Vibrating microbubbles poking individual cells: Drug transfer into cells via sonoporation. Journal of Controlled Release 112, 149–155. https://doi.org/10.1016/j.jconrel.2006.02.007

Wang, M., Zhang, Y., Cai, C., Tu, J., Guo, X., Zhang, D., 2018. Sonoporation-induced cell membrane permeabilization and cytoskeleton disassembly at varied acoustic and microbubble-cell parameters. Sci Rep 8, 3885. https://doi.org/10.1038/s41598-018-22056-8

Wu, J., 2002. Theoretical study on shear stress generated by microstreaming surrounding contrast agents attached to living cells. Ultrasound in Medicine & Biology 28, 125–129. https://doi.org/10.1016/S0301-5629(01)00497-5

Zhang, S., Duncan, J.H., Chahine, G.L., 1993. The final stage of the collapse of a cavitation bubble near a rigid wall. J. Fluid Mech. 257, 147. https://doi.org/10.1017/S0022112093003027

Zhang, Z.-Y., Shum, P., Yates, M., Messersmith, P.B., Thompson, D.H., 2002. Formation of Fibrinogen-Based Hydrogels Using Phototriggerable Diplasmalogen Liposomes. Bioconjugate Chem. 13, 640–646. https://doi.org/10.1021/bc015580j

Zhong, W., Sit, W.H., Wan, J.M.F., Yu, A.C.H., 2011. Sonoporation induces apoptosis and cell cycle arrest in human promyelocytic leukemia cells. Ultrasound Med Biol 37, 2149–2159. https://doi.org/10.1016/j.ultrasmedbio.2011.09.012

Zhou, Y., Shi, J., Cui, J., Deng, C.X., 2008. Effects of extracellular calcium on cell membrane resealing in sonoporation. J Control Release 126, 34–43. https://doi.org/10.1016/j.jconrel.2007.11.007

Chapter 3
The Intestinal Mucus Layer May Represent a Barrier for USmTDD

The intestinal lumen is lined with a layer of mucus. In order to understand whether mucus represents a barrier to USmTDD, exploratory work was conducted to:

- characterise the intestinal mucus by determining its pH, dry substance content and rheological properties,
- develop an artificial mucus recipe with similar rheological properties to the *ex-vivo* mucus,
- test whether the artificial mucus has detrimental effects on cells,
- identify its acoustic transparency and
- test whether US + MBs facilitate quantum dots (qDots) to lodge in the mucus or the cell layer beneath.

3.1 Chapter Introduction and Motivation

In the human intestine, mucus lines the luminal surface (Kim and Ho, 2010). Medical devices and drugs in the intestine must therefore first interact with the mucus layer before interacting with the mucosa. Hence, understanding mucus can help predict the fate of devices and drugs in the lumen.

The mucus barrier works at three different levels (Lieleg *et al.*, 2010). Firstly, it is dynamic, with mucus continuously secreted and shed. Secondly, it is steric, acting as a molecular sieve with a molecular mass cut off within the range of 600 – 700 Da (Matthes *et al.*, 1992). Absorption of substances with higher molecular mass remains at a low level.

Thirdly, it is interactive, allowing hydrophobic interactions to form between the core of the MUCs and the diffusing compounds (drugs, toxins, other molecules) (Lieleg *et al.*, 2010).

In the large intestine, there are two layers of mucus: a loosely adherent one, which can be scraped off, and a firmly adherent one, which cannot be easily removed (Ermund *et al.*, 2013). The thickness of the two mucus layers differs throughout the intestine. In the small intestine, most literature suggests there is just one loosely adherent layer of mucus in humans (Figure 3-1, Ermund *et al.*, 2013). The literature suggests that because the lumen of the small intestine is sterile (except the distal ileum), there is no need for a further adherent mucus layer to protect the mucosa against pathogens.

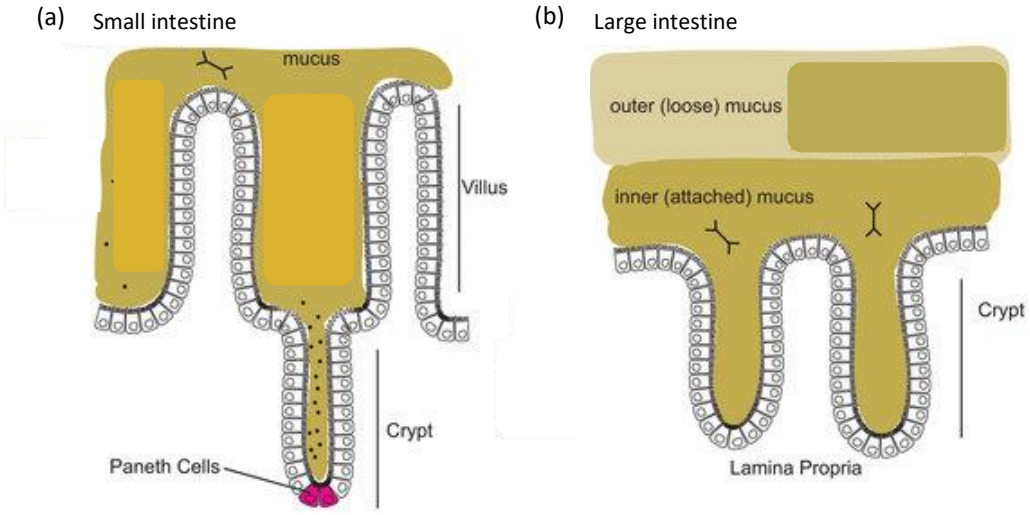

Figure 3-1 Mucus lines the wall of the intestine. *In the small intestine (a), mucus consists of one firmly adherent layer that penetrates the space between villi and crypts and attaches to the mucosa. In contrast, in the large intestine (b), it consists of a firmly adherent layer and a loose (outer) layer (adapted from Donaldson et al., 2015).*

Mucus thickness varies along the GI tract and from species to species. Table 3-1 presents these differences in humans, pigs and mice. Notably, the mucus in the human small and large intestine varies in thickness between 10 and 200 µm.

Table 3-1 Thickness of the mucus layer (in µm) in humans, pigs and mice (Garcia-Diez *et al.*, 2017). *In pigs and humans, the thickness ranges from 10 to 200 µm, whereas in mice it ranges from 10 to 450 µm.*

Species	*Stomach*	*Small Intestine*	*Large intestine*	*Rectum*
Human	106 - 175	10 - 162	9 - 218	88 - 155
Pig	51 - 222	25 - 53	14 - 56	40 - 58
Mouse	100 - 140	200 - 450	10 - 150	n/a

Mucus is secreted by goblet cells and consists primarily of water and MUCs ("mucins"). Mucins are linear, elongated, rod-like polymers (Philippe *et al.*, 2017). Their C-terminals form dimers via disulphide (S-S) bridges, while their N-terminals form trimers via S-S linkages. Mucus is therefore a network cross-linked covalently via S-S bridges, Figure 3-2. Mucoadhesion is due to the many different interactions present in mucus. Besides covalent and S-S bonds, there are also electrostatic (van der Walls), hydrophobic and H-bonding interactions. Glycosylated regions of mucins are rich in sugars (oligosaccharides), which are suggested to be responsible for the water-holding capacity of mucus and the resistance to proteolysis, which might help in maintaining the mucosal barrier.

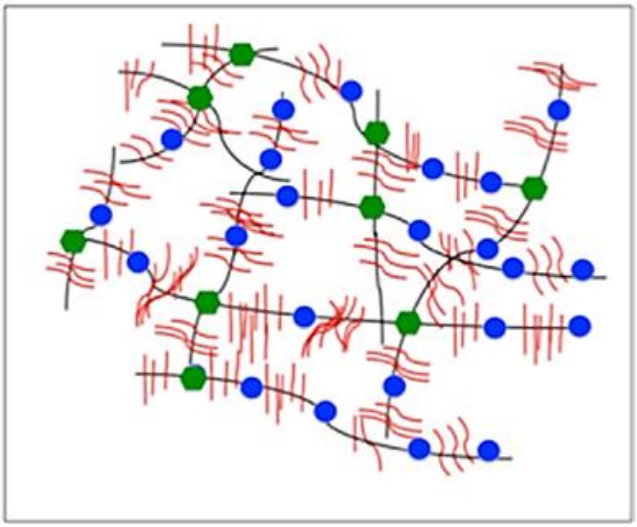

Figure 3-2 Mucin gel structure. *Mucus is a cross-linked network of polymers consisting of mucins bound mainly through S-S bridges (green dots). Mucins consist of domains that are glycosylated (sugar-rich, depicted as black strands with red brushes) or non-glycosylated (sugar-free, depicted as blue dots) (Bansil et al., 2013).*

Mucus is a non-Newtonian fluid (Lai *et al.*, 2009). Hence, its viscosity cannot be described as a constant coefficient; instead, its properties can be defined by means of rheological measurements such as oscillatory shear and extensional flow. These properties are studied mostly by using rheometers. Mucus' viscoelastic behaviour depends on pH, ionic strength, temperature and degree of hydration.

At high pH values, polymers such as mucins release protons and become negatively charged (Bhaskar *et al.*, 1991). Because like-charged parts of the polymer repel each other, the polymer swells. Conversely, at low pH values and sufficiently high mucin concentration, there is a solution to gel transition. This is due to the interplay between electrostatic and hydrophobic interactions. As the pH is reduced towards low values, the mucus flows slower, until reaching pH 2, when a gel forms and it stops flowing.

To summarise, when predicting compound permeability through mucus, one needs to take into account (1) compound characteristics, such as size, net charge, lipophilicity and spatial distribution of charged and hydrophobic groups, and (2) mucus characteristics such as rheology and shedding.

3.2 pH of Harvested Porcine Mucus

This section presents how mucus was harvested from pigs and its pH tested to ensure experiments were conducted on relevant samples. This was important as pH affects rheological properties, as described in Section 3.1.

3.2.1 Source and Method of Harvesting Porcine Mucus

Landrace x pigs aged 3 – 6 months old were ethically sacrificed using an overdose of anaesthetic according to the UK Home Office regulations (Project Licence PPL 70/8812) at Dryden Farm, University of Edinburgh (UofE). The pigs were fasted for 15 h prior to culling. *Post mortem*, the intestine and stomach were isolated and cut longitudinally and the mucus was gently scraped from the luminal side using a cell scraper (179693PK, ThermoFisher, UK). Parts of the gastric tissue contained chyme. Where such debris was noticed, the gastric tissue was rinsed gently with phosphate-buffered saline (PBS) at room temperature (RT). The intestinal tissue did not require rinsing. The mucus was collected in 20 ml Falcon tubes, stored at 3 – 7°C and transported to the University of Glasgow (UofG) for tests.

3.2.2 Method

The pH of the mucus was measured 3 – 5 h post-harvesting with a research grade bench pH meter (HI-5221, Hanna Instruments, UK). The probe was calibrated and cleaned before measurements on each sample. Samples were obtained from the small intestines of four pigs and the stomachs of three pigs.

3.2.3 Results

As seen in Table 3-2, pH results are overall consistent with the available literature (Merchant *et al.*, 2011). Pigs 1 and 3 presented a slightly higher gastric mucus pH compared to that suggested by Merchant and colleagues (2011). This could be due to the rinsing of chyme with PBS, as mentioned in Section 3.2.1. Since PBS has a neutral pH, it could be expected to have slightly increased the acidic pH of mucus.

Table 3-2 pH results of porcine GI mucus are consistent with the literature. *The slightly higher values recorded for Pigs 1 and 3 can be due to the rinsing step conducted to remove chyme. Literature values obtained from (Merchant et al., 2011).*

Location	*Literature*	*Pig 1*	*Pig 2*	*Pig 3*	*Pig 4*
Gastric pH	4.5 – 1.5	5.4	3.5	4.7	N/A
Intestinal pH	6.4 – 6.6	6.7	6	6.3	6.4

3.3 Mucus Dry Substance Content

3.3.1 Method

Mucus samples (0.5 – 3 g) were transferred to glass vials. The glass vials were weighted prior to and post mucus addition to calculate the weight of the mucus samples. The experiment was conducted twice. For the first trial, the glass vials were heated to 150°C on a hotplate stirrer (Stuart, UC152, UK) for 5 h. At the end of the 5 h, there was no more boiling noticed and the surface of the samples appeared cracked, suggestive of dehydration. The samples were weighed and discarded. For the second trial, after the boiling and weighing steps, the samples were allowed to further dry at RT for two weeks prior to weighting again. The weight of the mucus sample post heating was subtracted from the weight prior to heating. The resulting value was considered the wet substance in the mucus. Aspects of these methods, including references to literature, are mentioned in the first paragraph of the discussion section.

3.3.2 Results

Figure 3-3 suggests that boiling the samples until they appear dry (5 h) did not promote the evaporation of the entire liquid content. A further drying period of two weeks at RT decreased the dry substance percentage in samples by ~50%, although statistically insignificant. After 5 h of boiling and two weeks of drying at RT, the gastric mucus samples presented ~8% dry substance.

Recent literature (Johansson *et al.*, 2013; Lai *et al.*, 2009; Philippe *et al.*, 2017) references two original papers (Allen and Garner, 1980; Mantle and Allen, 1981) and notes that mucus consists of ~95% H_2O and ~5% dry substance. The study is based on porcine biochemically-purified mucus, scraped from the intestine. The study described here shows intestinal mucus consisting of 40 – 80% dry substance, depending on the analysis method. The difference might lie in the additional mucus purification that were conducted by Allen and Garner (1980) and Mantle and Allen (1981).

Although the pigs have fasted prior to mucus harvesting in the present study, it is possible that a thin layer of chyme was present on the intestine and so the tested sample contained molecules of ingested products, increasing the dry substance content. However, if this had been rinsed off, the water content of the sample would no longer have been reliable.

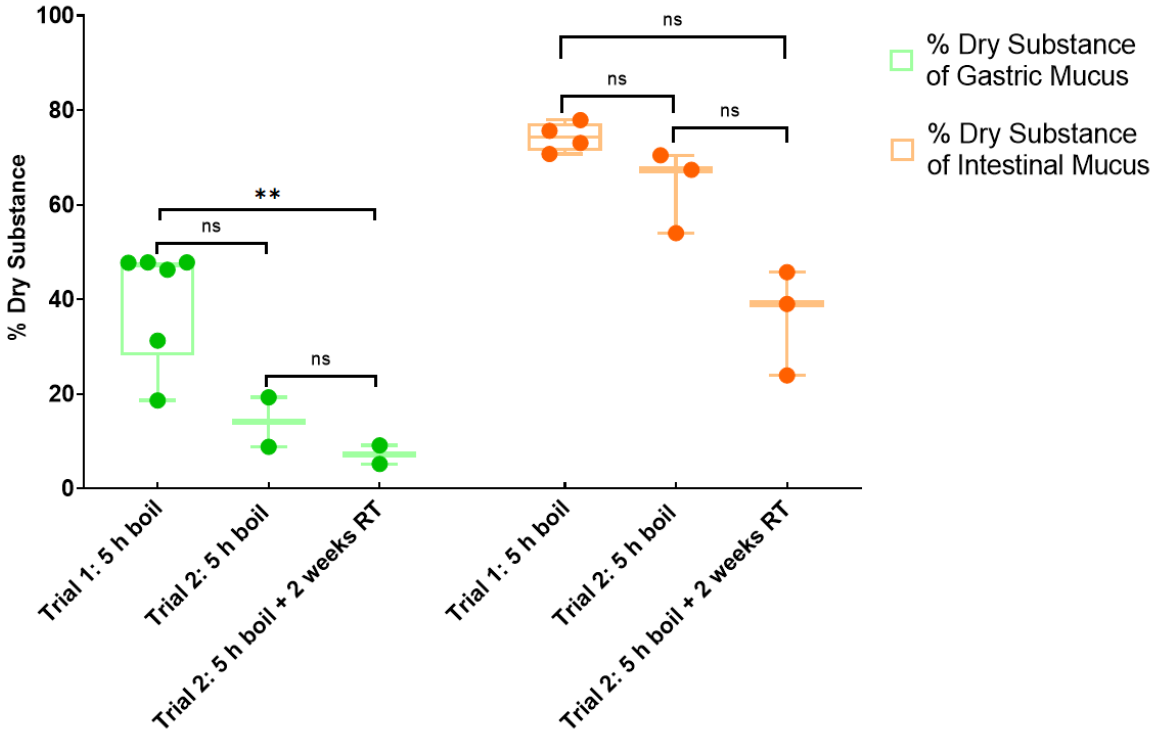

Figure 3-3 Difference between gastric and intestinal mucus dry substance. *Intestinal mucus dry substance appears to be greater than the gastric mucus dry substance, likely due to the washing step the stomach required before mucus harvesting. Brown-Forsythe and Welch ANOVA multiple comparisons showed the difference between the groups indicated are non-significant with the exception of* Gastric Trial 1: 5 h boil *versus* Gastric Trial 2: 5 h boil + 2 weeks RT *($p = 0.0045$). More samples are necessary to decrease the variability and increase the significance of the results. $n \geq 2$.*

3.4 Rheology of Porcine Intestinal Mucus Compared to Literature on Human and Porcine Mucus

A fluid's complex viscosity influences sound attenuation through it (Stokes, 2009, pp. 75-129). Given that the wall of the intestine is covered in mucus and US might need to propagate through it, it was important to ensure that the artificial recipe developed had the correct rheology, thus ensuring the relevance of experiments on the artificial mucus for native mucus. Furthermore, from a pharmacological point of view, viscosity also influences a compound's ability to cross a layer. The higher the viscosity, generally the lower amount of passive diffusion through it (Lai *et al.*, 2009). This section describes how the rheology of native mucus was studied and how it compares to the literature.

3.4.1 Method

Following harvesting, the mucus was stored at 4°C overnight (ON). Rheological measurements were carried out by using a stress-controlled rotational rheometer

(MCR302, Anton Paar, Austria) by Dr Manlio Tassieri, a collaborator at UofG. Measurements were performed at a temperature of 37°C with a cone and plate geometry (CP50-1) of 50 mm diameter and 1° angle. In order to stop evaporation of water near the edges of the plate, potentially leading to an overestimation of the actual mucus' viscoelastic properties, low viscous mineral oil was added to the rims.

The porcine mucus was harvested using the same method as described in Section 3.2.1. As a result, the mucus might have been combined with chyme. Given that chyme is still present on the wall of the intestine 12 h post fasting, this is what a drug or US device would encounter when reaching the intestine 12 h post fasting. Hence, rheological measurements were not conducted on pure mucus, but on what the compound or US would encounter in the intestine.

3.4.2 Results

Average complex velocities (η*) at low angular frequencies (10^{-1} rad/s) describe the macrorheology of a substance, or the activity between molecules. Conversely, measurements at high angular frequencies (10^{-2} rad/s) describe the microrheology of a substance, or the activity within a molecule. When comparing the rheological properties of different substances according to a plot, the slope describes the type of non-Newtonian behaviour. If the viscosity of substances decreases with an increase in shear stress, it can be suggestive of thixotropic behaviour (Ghica *et al.*, 2016).

Figure 3-4 shows the average values of the frequency-dependent η* of mucus harvested from five porcine small intestines. At relatively low angular frequencies (10^{-1} rad/s) the complex velocity has values as high as ~400 Pas; whereas, at relatively high angular frequencies (10^{2} rad/s) η* drops by more than two orders of magnitude down to ~2 Pas. This is a typical non-Newtonian behaviour (i.e., $\eta^* \neq$ constant), with viscosity scaling with frequency as a power law, suggestive of thixotropic materials. Available literature describes intestinal mucus as a thixotropic material too (Lai *et al.*, 2009; Sellers *et al.*, 1991).

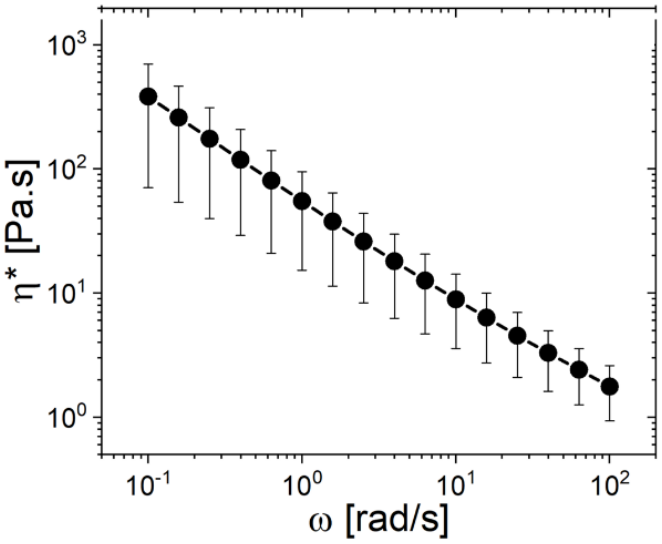

Figure 3-4 Rheology of mucus harvested from the porcine small intestine. *A stress-controlled rotational rheometer was used to obtain rheological measurements. The complex velocity starts at 400 Pas at angular frequencies of 10^{-1} rad/s and decreases to 2 Pas at angular frequencies of 10^2 rad/s. The slope describes the type of non-Newtonian behaviour. In the present case, complex viscosity decreases with an increase in angular frequency, suggestive of thixotropic behaviour. n = 5. Error bars are standard deviation.*

3.5 Rheology of Artificial Mucus Compared to Native Porcine Mucus

It was important to study the propagation of US through the media and through mucus because it was considered that CAs might cross the mucus layer and come into contact with the cell layer. In order to promote cavitation and sonoporation there, it is necessary to ensure that US can propagate though the mucus, reach the CAs and promote cavitation.

Harvesting sufficient quantities of porcine mucus to establish reliable results would be labour intensive and require the culling of many animals. Hence, an artificial mucus compound similar to natural material would be helpful for preliminary experiments. This section describes recipes for producing artificial mucus, with rheological properties similar to those of native porcine mucus.

3.5.1 Method

Two mucus recipes were explored, one suggested by a manufacturer (Sigma-Merck) and the other developed at UofG. The one suggested by Sigma-Merck consisted of mucin (Mucin Type II, M2378-100G, Merck, UK) concentrations between 4 – 400 % (w/w) prepared in 1M NaOH by stirring on a magnetic stir plate for up to 50 h. The pH of the

samples was then adjusted with either HCl or NaOH and tested with a bench pH meter (HI-5221, Hanna Instruments, UK). The second recipe was developed at UofG by Louise Mason, Lee Jia Xin and Manlio Tassieri. It consisted of 3.1% w/w polyacrylamide (PAM, Polysciences Inc, PA, USA) and 3.7% w/w mucin (as above) in Dulbecco's Modified Eagle's Medium F12 (DMEM F12, Thermo Fisher Scientific, Waltham, MA, USA) + 10% foetal bovine serum (FBS, GE Life Sciences, Chicago, IL, USA) + 1% penicillin streptomycin (P/S, Thermo Fisher Scientific, Waltham, MA, USA). Hereafter, this recipe is referred to as the *PAM mucus*. This recipe was developed because the *mucin only* recipe did not present appropriate rheology and our collaborators suggested to incorporate polyacrylamide in the recipe.

3.5.2 Results

The rheology of harvested mucus and of mucin-only mucus adjusted to different pH values are presented in Figure 3-5 (a). Only at relatively high frequency was it possible to find an agreement between the complex viscosity values of the harvested mucus and of the mucin-only mucus at different pH values. In contrast, at relatively low frequencies, the agreement was poor, with differences in the measured complex viscosities of at least an order of magnitude. Notice that only the rheology of samples at 400% (w/w) mucin are shown, as these were most similar to the porcine mucus.

In contrast, the *PAM mucus*, Figure 3-5 (b), displayed complex viscosity that matched almost perfectly the one of the harvested mucus at low angular frequencies, and diverged only slightly from it at relatively high frequencies, yet within the one standard deviation of the harvested mucus. However, *PAM mucus*, reveals to be the best substitute.

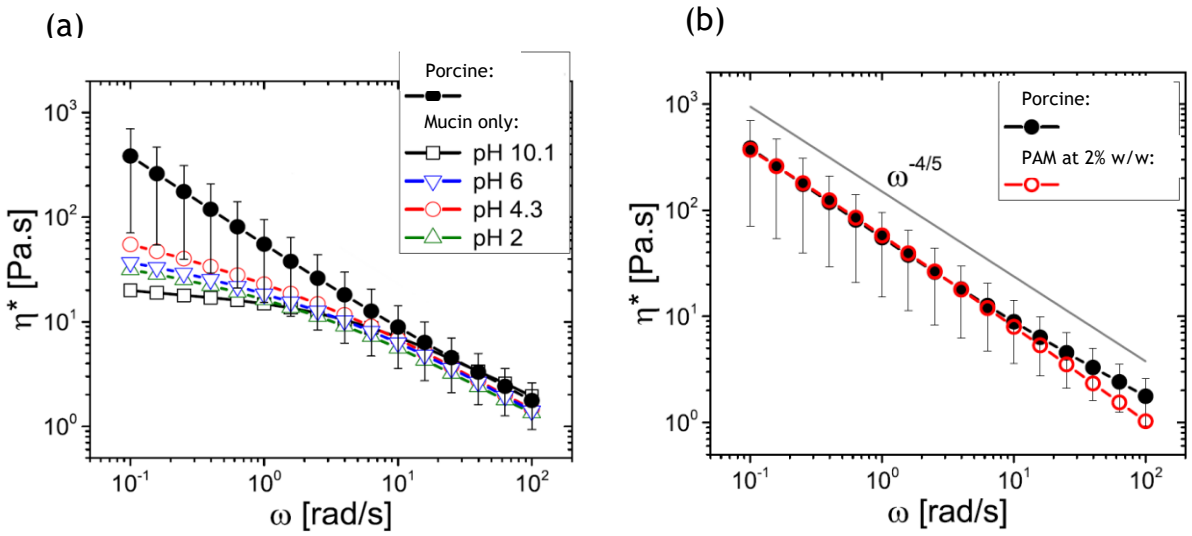

Figure 3-5 Bulk rheology measurements of porcine mucus and synthetic mucus compounds. *(a) At high angular frequencies, the artificial mucus and ex-vivo mucus have similar complex viscosities. In contrast, at low angular frequencies, the artificial samples prepared in NaOH show a decrease in viscosity with a decrease in pH. (b) There is good agreement between the averaged complex viscosity of native porcine intestinal mucus and that of a PAM mucus at 2% w/w. n = 4 for porcine mucus. n = 1 for artificial mucus.*

3.6 Suitability of MTT Assay for Testing the Cytotoxicity of Artificial Mucus

Once the rheological behaviour of *PAM mucus* was identified as similar to that of native mucus, it was explored whether *PAM mucus* had a detrimental effect on cell viability. The 3-[4,5-di-methylthiazol-2yl]-2,5-diphenyl-tetrazolium bromide (MTT) assay enables the quantification of reduction in cell viability because of cell apoptosis or necrosis. MTT is a yellow tetrazolium salt that is reduced by metabolically active cells, in part by the action of dehydrogenase enzymes, to generate reducing equivalents such as nicotinamide adenine dinucleotide (NADH) and nicotinamide adenine dinucleotide phosphate (NADPH). The resultant intracellular purple formazan can be solubilized and quantitated using a plate reader.

It was hypothesized that a decrease in indicated cell viability would correlate with a decrease in cell metabolism, less reduction of salts, less intracellular purple formazan formation and lower absorbance readings. Hence, exposing cells to *PAM mucus* and then conducting the MTT assay could allow detrimental effects of the *PAM mucus* to be determined. The next two subsections show how this assay is unsuitable for such an experiment and are included because of the general paucity of literature relating to intestinal mucus.

3.6.1 Cell culture

This experiment required the use of a cell line, which is described in this section prior to continuing with the method of cytotoxicity testing.

3.6.1.1 Cell line

The human colorectal adenocarcinoma cell line used, Caco-2, was sourced from the American Type Culture Collection (ATCC, Rockville, MD, US). It is commonly used as a model for the mucosa of human small intestine to study drug delivery *in vitro*. The cells were cultured to form a continuous polarised monolayer as a barrier for ions and molecules. A TEER above 600 Ω*cm^2 suggests the cells are confluent and polarised (Liu *et al.*, 2017). The model is approved by the FDA (CDER/FDA, 2015). The passage number of cells was in the range 20 – 60.

3.6.1.2 Defrosting Cells

Vials containing frozen cell suspension were removed from liquid nitrogen cold storage and defrosted in a 37°C water bath. The suspension was transferred to a Falcon tube and centrifuged at 200 rpm for 2 min. The supernatant was removed, the pellet was resuspended in growth medium and the suspension was then transferred to a tissue culture flask with warm growth medium.

3.6.1.3 Maintenance of Cells

Caco-2 cells were routinely maintained in Dulbecco's Modified Eagle's Medium (DMEM (Thermo Fisher Scientific, Waltham, MA, USA) with the following additions: 10% FBS (GE Life Sciences, Chicago, IL, USA), 1% P/S (Thermo Fisher Scientific, Waltham, MA, USA) and 1% non-essential amino acids (NEAA, Thermo Fisher Scientific, Waltham, MA, USA). The cells were kept at 37°C in a humidified atmosphere containing 5% CO_2. Cells were grown in 75 cm^2 flasks with 13 ml medium that was changed every 2 – 3 days.

3.6.1.4 Passaging Cells

When the cells became 80% confluent, they were split. The growth medium from the flask was removed and the cells were washed twice with PBS. This ensured dead cells and serum were removed. It was important to discard the serum because it inactivates trypsin. 1 x trypsin/EDTA (5 ml for a 75 cm^2 tissue culture flask) was added to the flask and

returned to the incubator for 10 min, until the cells detached from the wall of the flask. Growth medium was then added to the flask and the liquid was pipetted several times against the flask wall to remove the cells still attached to the wall. The suspension of cells, media and trypsin was then transferred to a centrifuge tube and centrifuged at 13,000 rpm for 3 min. The supernatant was removed and an appropriate amount of cells and media was added to a new tissue culture flask. For a T75 tissue culture flask, ~4 million cells were seeded in 13 ml of warm growth medium.

3.6.1.5 Cell Counting

Cells were counted using either an automated cell counter, Countess II (Applied Biosystems, Waltham, MA, USA), or a haemocytometer. 10 µl of cell suspension was diluted at a 1:1 ratio in Trypan Blue to distinguish between dead and live cells. The 20 µl suspension was pipetted between the haemocytometer and the cover slip. Cells were visualised using a bright field microscope. Five squares were counted and the number obtained was divided by 5, multiplied by 2 (to account for the dilution factor), and multiplied by 10,000 to obtain the number of cells per ml, as seen in Equation 3-1.

$$Total\ cells/ml = Total\ cells\ counted\ x\ \frac{Dilution\ factor}{Number\ of\ squares}\ x\ 10,000\ cells/ml \qquad \textbf{Equation 3-1}$$

3.6.1.6 Cryopreservation of Cells

Cells were grown to 80% confluency on T75 tissue culture flasks. The cells were washed twice with PBS, 5 ml of 1 x trypsin/Ethylenediaminetetraacetic acid (EDTA) were added to the flask and the cells were returned to the incubator for 10 min. Growth medium was added to the flask, and the suspension was transferred to a Falcon tube. The tube was centrifuged at 2000 rpm for 2 min. The supernatant was removed and the cells were resuspended in 1 ml freezing medium. Freezing medium consisted of 90% FBS and 10% dimethyl sulfoxide (DMSO, Sigma-Aldrich Corporation, St. Louis, MO, USA). 200 µl of the suspension were transferred to labelled cryogenic vials (Corning, New York, USA). The vials were placed in a freezing container ON at -80°C for a gradual and controlled temperature decrease. The vials were then transferred to a liquid nitrogen cell storage tank.

3.6.2 Method

Caco-2 cells were seeded into 96 well plates. Each well received 100 µl of 1 x 10^4 cells/ml in growth media. Cells were allowed to adhere to the substrate for 24 h. The *PAM mucus*

was sterilised by exposing it to ultraviolet (UV) light (250 nm) for 1 h. 20 µl of *PAM mucus* were applied to each well. Cells were exposed to *PAM mucus* for lengths of time between 10 min and 2 days. To conduct the MTT assay, the manufacturers protocol was followed (TACS® MTT Cell Proliferation Assays Cat# 4890-25-K, 2500 Tests.). Briefly, the cells were incubated with 2 µl MTT ON. 100 µl of the detergent provided in the kit was then also incubated ON to lyse the cells and enable the formazan crystals to exit the cell. Absorbance was measured at 540 – 570 nm using a microplate reader (SpectraMax i3x, USA). Cells were provided with fresh medium every two days, unless mucus had already been applied to them.

3.6.3 Results

Figure 3-6 displays the absorbance values of different conditions. Normally, the absorbance of the condition Mucus + MTT would be considered background absorbance. This value would be subtracted from the conditions with cells and then the condition Control: 10 min Cells + Mucus + MTT would be considered 100% viability. The other conditions would be expressed according to it. When cell viability decreases in a sample, it leads to less formazan formation, less absorption, and hence a lower absorption value. However, this was impossible to determine because the mucus and MTT combination masked the effect of mucus on cell viability. The absorbance of mucus alone was 1.27, of MTT was 0, but of Mucus + MTT was 2.16. This suggested that when combined, mucus and MTT might have reacted and obstructed more light than when separated. When the Mucus + MTT absorbance value was considered control and subtracted from the conditions Cells + Mucus + MTT, the resulting values were negative, preventing any conclusions being drawn on the effect of mucus on cell viability. Potentially, the *PAM mucus* had proteins similar to the dehydrogenase enzymes and reduced the tetrazolium salt into formazan.

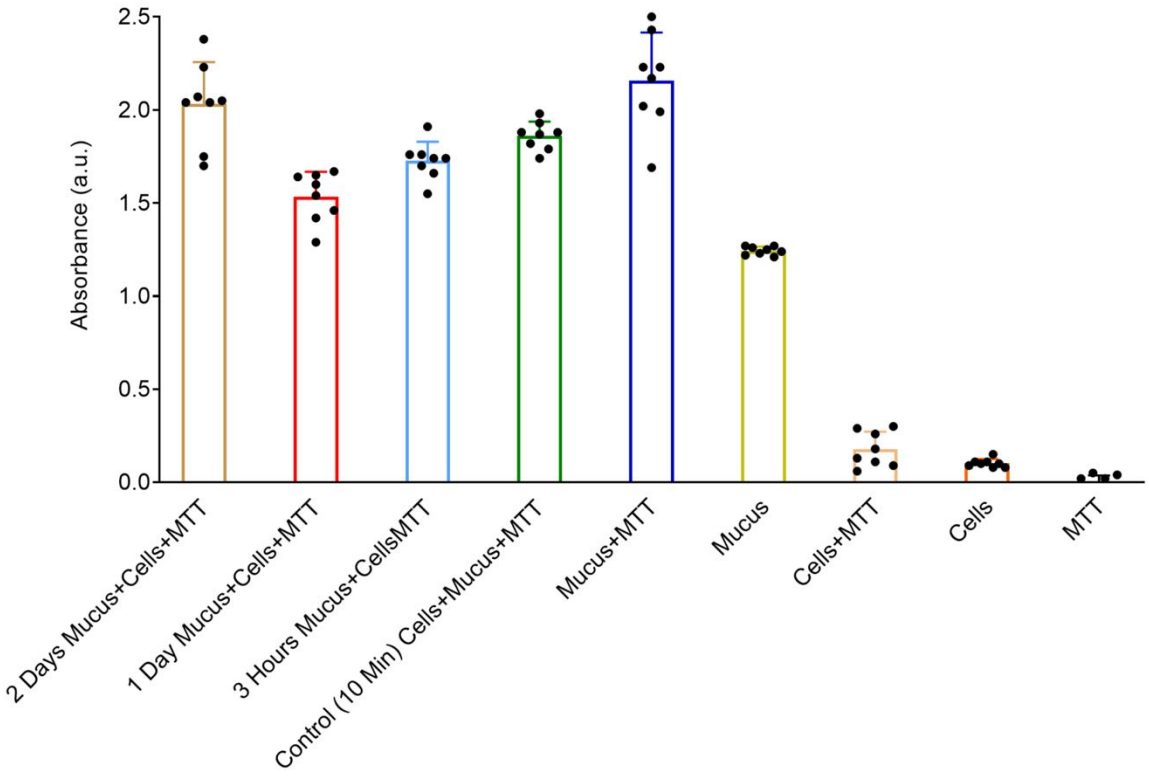

Figure 3-6 Absorbance values of mucus and related conditions. *The absorbance values are shown after subtracting the background absorbance recorded in wells containing only medium. Data cannot be represented as viability because the high absorbance of mucus + MTT masked the cellular viability. Mucus and MTT might have reacted and obstructed more light than when separated, preventing any conclusions being drawn on the effect of mucus on cell viability. All conditions included added detergent and medium, hence this is not mentioned on Y axis. All conditions that include MTT had the reagent applied at the same time. n = 8.*

3.7 US Attenuation through Artificial Mucus

It was important to study the propagation of US through the media and through mucus because CAs might cross the mucus layer and come into contact with the cell layer. In order to promote cavitation and sonoporation there, it is necessary to ensure that US can propagate though the mucus, reach the CAs and promote cavitation. This section describes the development of a system to determine the acoustic transparency of mucus.

3.7.1 Method

A ring-shaped holder was prototyped with SolidWorks 2016 (Dassault Systemes SE, France). The holder had an inner diameter, ID = 23 mm, outer diameter, OD = 31.5 mm, height = 7 mm (Fig. 4.7.A). It was 3D printed in VeroGrey Gloss with an Objet Eden 350. The holders were cleared of the coating material. Mylar membranes of varying thicknesses were tested to identify a suitable transparent acoustic window for the holder. The one

chosen was 6 µm thick (410-993-06, Goodfellow, UK). It was cleaned with IPA and cut into appropriate sizes. UV epoxy (4UV80HV, Permabond, UK) was applied to the sides of the holder and the membrane was placed over its edges and weighted in place. The epoxy was cured using a UV lamp (UVGL-58, UVP LLC, Upland, CA, USA) to expose it for 5 min. Excess membrane was trimmed off and the holder was then filled with 3 ml artificial mucus using a syringe. As seen in Figure 3-7 (a), the holder ring has two orifices of different diameters. Mucus was injected through the larger orifice and air bubbles exited through the smaller one. The orifices were then sealed with 3D printed plugs and epoxy. Figure 3-7 (b) shows a holder filled with mucus.

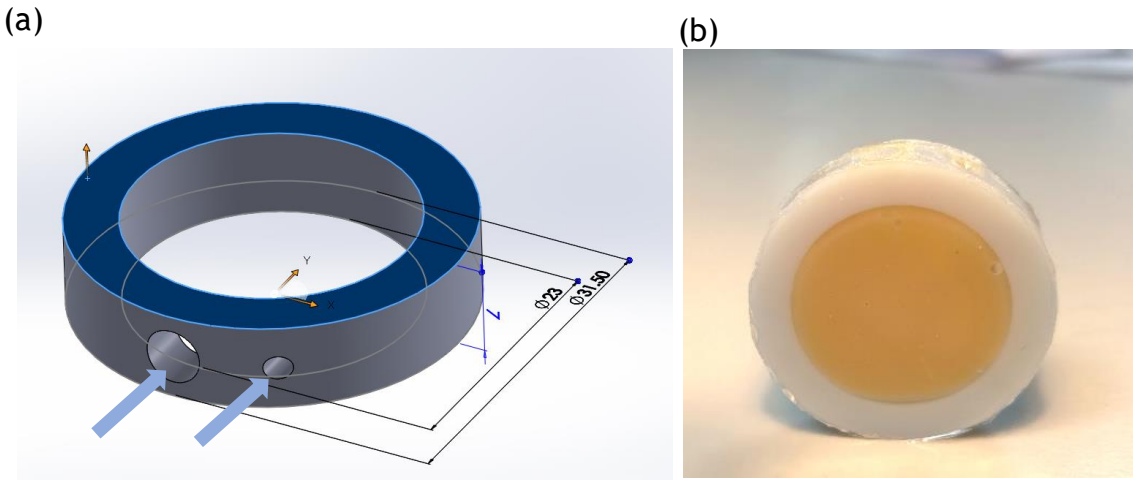

Figure 3-7 Mucus holder. *(a) Computer aided design prototype with dimensions in mm. Arrows point to two orifices, one for injecting mucus and one for enabling air bubbles to exit the construct. (b) Holder with acoustically transparent membranes filled with artificial mucus. ID = 23 mm OD = 31.5 mm.*

Rigid supporting structures were constructed with optical components (Newport, UK) to hold and align the mucus holder, the transducer (3.1 MHz, element size = 2.5 cm, designation 7.5 cm in PTF, spherical focus, V380, Olympus, UK) and the fibre-optical hydrophone (FOH, Precision Acoustics and UCL, UK), Figure 3-8.

The transducer was connected to a waveform generator (gated sine wave, 20 cycles, 10 ms bursts, 33250A, Agilent, USA) and a power amplifier (A075, E&I RF, USA) and the hydrophone was connected to an oscilloscope (DSO-X 3014, Agilent, USA) and a PC for data acquisition. Transducer calibration and field mapping were conducted (data not shown) to ensure the devices were working correctly and to identify the maximum signal which could be recorded. The water in the tank was degassed and allowed to reach RT. The oscilloscope displayed voltage after averaging 512 pulses. The voltage recorded was

transformed into pressure using the manufacturer's software for the FOH. The acoustic pressure recorded with the FOH ranged between 1.65 – 2 MPa when there was no holder between the transducer and the FOH, Figure 3-9 (a).

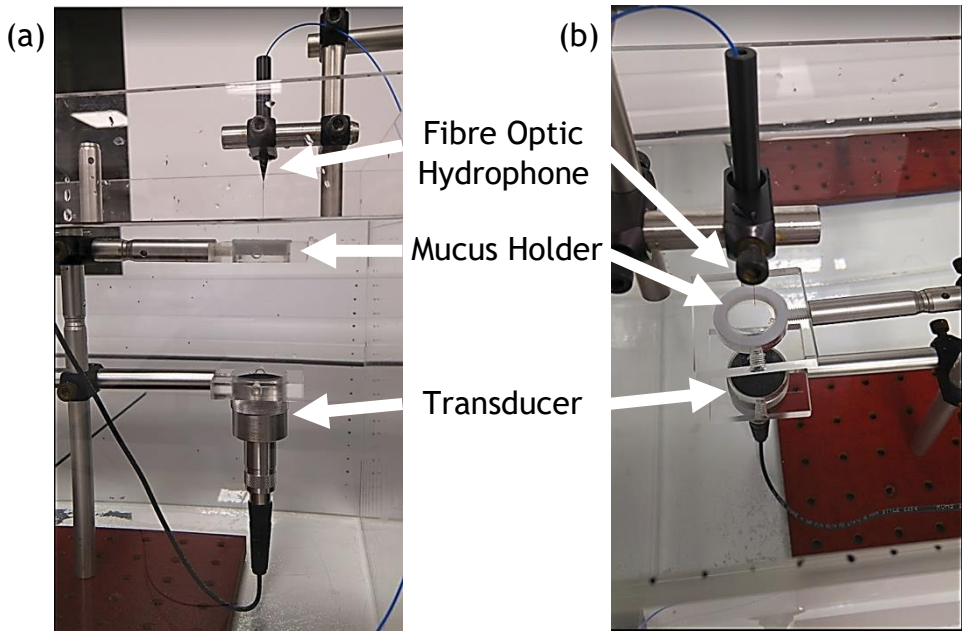

Figure 3-8 Setup for investigating the acoustic transparency of mucus. *(a) Side view. (b) Isometric view. The two supporting structures were constructed on two different breadboards: one immersed in the tank, holding the transducer and the mucus holder, and one external, holding the hydrophone. The structure with the hydrophone was attached to an xyz micropositioning stage for field mapping to ensure the maximum signal was recorded. The source transducer, mucus holder and hydrophone were fixed in optical holders using nylon screws.*

3.7.2 Results

As mentioned previously, an artificial mucus recipe was developed in order to replace the use of fresh mucus. The present experiment would have required 12 ml of fresh mucus harvested from substantial amounts of small intestine from freshly sacrificed pigs that had been fasted prior to culling. As this approach was not possible, artificial mucus was used instead.

According to Figure 3-9 (b), a 7 mm thick layer of artificial mucus caused an attenuation of 14% of the US signal. The mucus in the small intestine is in the thickness range 50 – 300 µm. If 7 mm of mucus reduced the signal by 14% and the thickness and US attenuation are considered directly proportional, then 50 – 300 µm will reduce the signal

by 0.1 – 0.6%. If this difference is deemed important, it can be accounted for by increasing the MI. The artificial mucus attenuated 0.93 ± 0.16 dB/cm of a 4 MHz US signal.

A broadband transducer could have been used to investigate simultaneously attenuation at a large range of frequencies. However, the use of broadband pulse could have increased the probability of error at each frequency, affecting the accuracy of the results.

As pH decreases, viscosity would increase (Bansil *et al.*, 2013). This would be expected to lead to a reduction in attenuation (Stokes, 2009, pp. 75-129). Conversely, an increase in pH would be expected to correlate with an increase in attenuation.

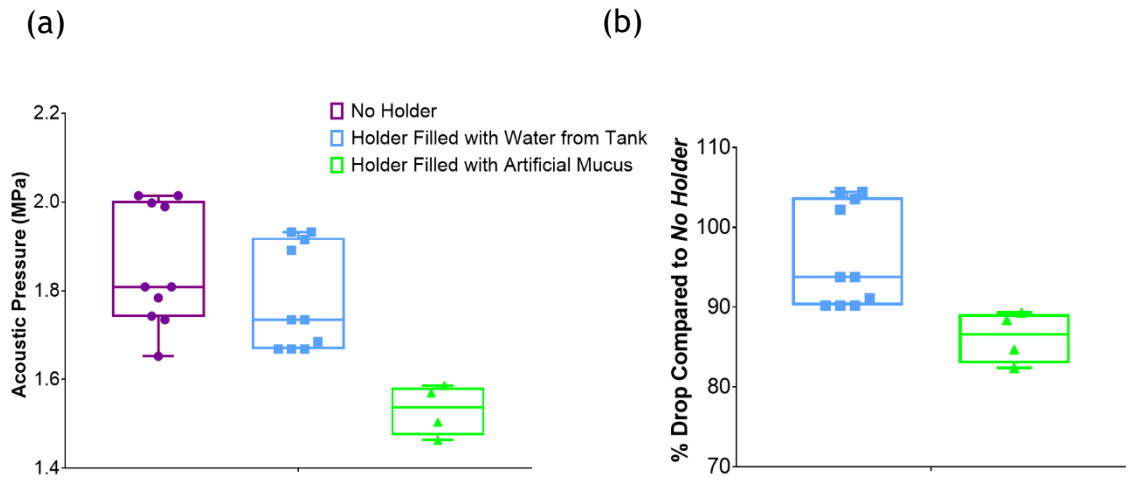

Figure 3-9 Acoustic transparency of artificial porcine mucus. *(a) The holder and the mucus caused attenuation of the US pressure; (b) When the mucus holder was filled with water from the tank, US pressure was reduced by ~7%. When the mucus holder was filled with artificial mucus, the US pressure was reduced by ~14%. $n \geq 4$.*

3.8 Ultrasound and Microbubbles can Lodge qDots into Murine *ex-vivo* Small Intestine

This section describes the method used to verify whether US + MBs + qDots facilitate qDots to lodge into the mice intestinal mucus or the mucosa. Mice were used for this experiment because intestinal mucus starts to disintegrate as soon as an animal is culled; hence, it was important to conduct the experiment in a building with access to live animals. It was not possible to transport the equipment and conduct the experiment in an abattoir with pigs, so the experiment was conducted on mice at the University of Dundee (UofD).

3.8.1 Method

Animal work was conducted in accordance with the Home Office guidelines and approved by the Home Office Licensing committee (Project license P3800598E). Three mice (CL57BL/6 wild type) were sacrificed by cervical dislocation by the animal technician, dissected and the small intestines were isolated. Each lumen was flushed with cold PBS via luminal syringe injection to clean the section. The small intestine was cut longitudinally and pinned to a sound absorber, with the mucosa facing upwards.

The tissue was immersed in a water tank filled with PBS at RT and insonated with a 4.18 MHz miniature focused US transducer (13 mm focal length, 1.79 mm^2 cross-sectional focal area, described in Stewart *et al.,* 2017) for 90 s (1 MPa PNP, MI = 0.5, continuous sine waves). A suspension of 5% CdSeS/ZnS qDots (6 nm average diameter, Sigma, UK) and 5% MBs (2 – 5 x 10^8 MBs/ml in saline, 2 – 8 µm average diameter, SonoVue, Bracco, UK) in PBS was delivered simultaneously with US application using a syringe pump (NE-1000, New Era Pump Systems Inc., USA). CdSeS/ZnS qDots were chosen because they were previously used in the research group where the work took place and the product was deemed suitable for this experiment too.

Following the experiment, the tissue was removed from PBS and rinsed with PBS at RT with a syringe, taking care not to damage the mucosa. It was illuminated with a UV lamp to check whether qDots marked the insonated tissue. Pictures were acquired with a phone camera (G4, LG, South Korea). The tissue was then fixed in either 4% paraformaldehyde (PFA) in PBS or Carnoy fixative and processed and imaged by the Dundee Imaging Facility (DIF) as follows: the samples were cryoprotected ON in a solution consisting of 30% sucrose in PBS. The tissue was sectioned and positioned in cryomolds and allowed to incubate for 30 min in mounting media for cryotomy (OCT, 361603E, VWR International, Radnor, PA, USA). The tissue was then frozen in a cryostat, mounted on microtome chucks with OCT and sectioned into 10 – 12 µm pieces and placed onto LEice X-tra slides (Leica Biosystems Nussloch 24 GmbH, Nußloch, Germany). It was allowed to air dry and freeze and the edges were blocked with PAP pen and rinsed in PBS.

The tissue was stained with Texas 2 Red conjugated WGA (10 µg/ml) and Hoechst (1 µg/ml) for 60 min and was mounted with anti-fade non-setting mounting agent (Vectashield). It was then imaged with a Zeiss LSM 710 or LSM 4 880 laser scanning confocal microscope (Carl Zeiss AG, Oberkochen, Germany).

3.8.2 Results

The insonated areas can be visualised during and after the treatment, Figure 3-10 (a-c). The treatment has damaged the mucosa of the murine colon and pieces of tissue have dislodged. This suggests the superficial mucosa was damaged. As a result, the mucus layer is very likely to have been displaced too.

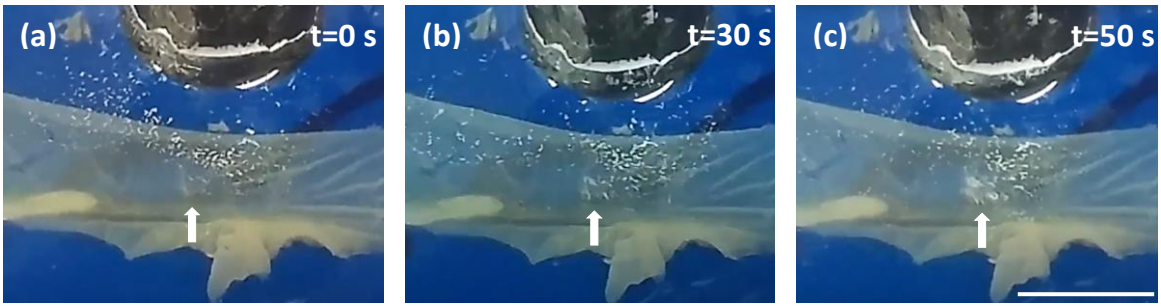

Figure 3-10 Insonation with MBs and qDots damaged the murine colon tissue. *Colon tissue was excised, cut longitudinally, pinned to a sound absorber immersed in PBS and was treated with US + MBs + qDots. Over a 50 s time span, the tissue displayed white marks suggestive of damage. White arrows point to the transducers' focal area, where white marks on tissue developed. The insonation treatment is considered responsible for these marks, which are assumed to correspond to damage to the tissue. The time between (a) and (b) is 30 s, and between (b) and (c) is 20 s. Scale bar = 1 cm for tissue width. NB: The transducer is closer to the camera lens than the tissue, hence the scale bar does not apply to it; transducer OD = 7 mm.*

Figure 3-11 shows that fluorescent qDots (green) have lodged in the sample as a result of the treatment. However, it is unclear if they have lodged in the mucus layer or in the underlying mucosa. Two-photon laser scanning microscopy, as seen in Figure 3-12 (a-c), showed that qDots (green) lodged in mucus (red), but not in the cell layer (blue). This agrees with previous work (Stewart *et al.*, 2021) which showed that qDots delivered without US + MBs did not mark the intestinal porcine mucosa *in vivo*.

This result appears to contradict Figure 3-10, where the mucosa is damaged. As this is likely to have removed the mucus layer as well, one may question if the two-photon microscopy study was conducted on the actual insonated / damaged area, or on a surrounding area, where qDots have only attached. Arrow (A) in Figure 3-11 points to an area with qDots that is approximately 80 mm^2, but the cross-sectional focal area of the transducer used is only 1.79 mm^2.

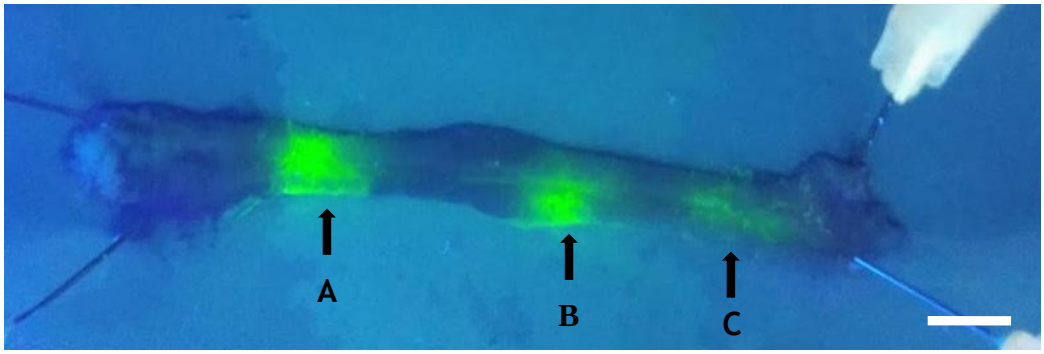

Figure 3-11 qDots mark the murine small intestine. *Tissue pinned to a sound absorber was illuminated with a UV lamp to identify whether qDots were present on the small intestine. Each area (A-C) was treated once with US + MBs + qDots. Black arrows point to treated areas. The marked areas indicated by arrows A and B are much larger than the 1.7 mm^2 focal area of the transducer. This suggests the qDots also attached to the tissue surrounding the focal area. Scale bar = 1 cm.*

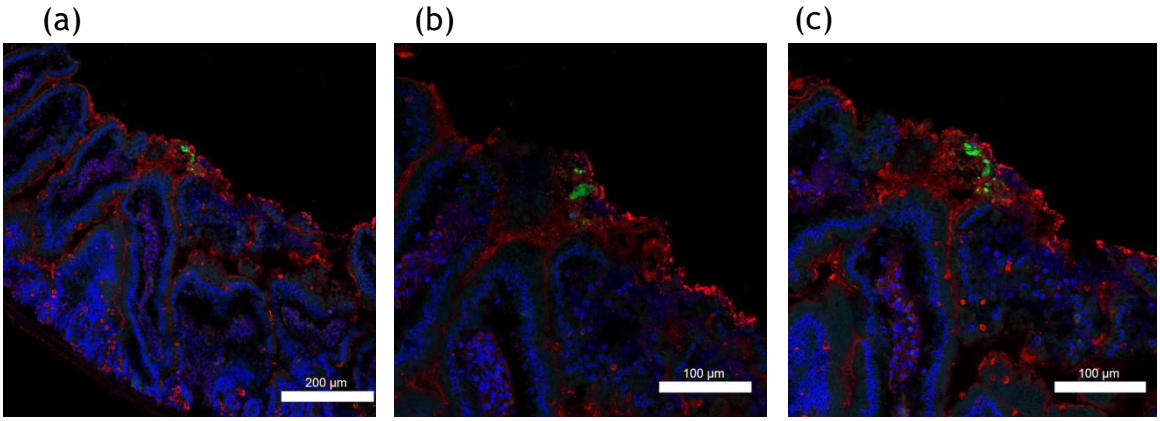

Figure 3-12 Cross-sections of murine small intestine after insonation with qDots and MBs. *Following treatment, the tissue was fixed with PFA, processed and imaged with laser scanning confocal microscopy. The images obtained showed qDots (green) lodged in the mucus (red, stained with WGA) after insonation and did not penetrate the underlying intestinal tissue (blue, cell nuclei stained Hoechst). Figure adapted from (Stewart et al., 2021).*

3.9 Discussion

After conducting the experiment on mucus dry matter, a desiccation assay published by the European Pharmacopoeia (Groo *et al.*, 2013) was identified. This protocol suggests a heating period of 4 h at 100°C and a cooling period of 45 min in a desiccator, then repeated cycles of 1 hour at 100°C followed by 45 min of cooling, until mass stabilization is achieved. Groo *et al.*, (2013) harvested porcine intestinal mucus using a similar method to the one described here and calculated the dry substance content using the protocol published by the European Phamacopoeia (Groo *et al.*, 2013). They conducted the

experiment twice and the dry substance in the samples was 9.2% ± 0.1% and 12.4% ± 0.1%, respectively. The slightly higher water content in their samples compared to the one discussed here could be because they rinsed the tissue twice with distilled water, which might have slightly hydrated the mucus. The gastric samples reported here, which were also rinsed, had a similar content of dry substance (8%).

Groo *et al.* (2013) used a similar method to harvest and analyse the rheology of porcine mucus but their results showed lower average complex viscosity. This could be because they rinsed the lumen twice with distilled water before harvesting. By combining the mucus with small amounts of water, their mucus more closely matches values associated with the rheology of water.

Different rheological properties were identified between the mucus harvested from porcine small intestine and that from human small intestine, found in the literature. This may be because of difficulties associated with sourcing mucus samples.

The reported rheological properties of human mucus differ in different papers (Cone *et al.*, 2005; Macierzanka *et al.,* 2014). Insufficient work on human mucus rheology has been conducted to reach a consensus on the methods of harvesting and analysis. This may be because of difficulties associated with sourcing mucus samples.

In order to harvest fresh mucus from the human small intestine, the patient needs to give consent and the researcher must collect it quickly post mortem. A patient whose time of death is reasonably predictable is likely to be ill and illness may affect food intake and the health of the GI tract. Therefore, the mucus may be dehydrated or affected in different ways. Such mucus samples will not be representative of the healthy human intestine, hence of little value. Although mucus could be scraped from resected small intestine tissue, this will often originate from diseased tissue and hence will be unrepresentative.

A further limitation on reliability of data is the additional mucus purification step conducted by some groups prior to rheological analysis. Furthermore, the intestine needs to be sectioned longitudinally, leading to slight bleeding. Particular care must be taken when harvesting mucus to ensure the mucus sample is not contaminated with blood that trickles along the lumen. Finally, relatively large amounts of mucus need to be harvested to conduct enough replicates to draw conclusive observations.

Limitations of testing the effect of *PAM mucus* on cells include (1) Sigma Type II mucin is not distributed sterile by the manufacturer and (2) difficulties associated with preparing the *PAM mucus* in sterile conditions. Exposure of mucus to UV for different lengths of time was not found effective (the *PAM mucus* still developed fungus), while UV is known to affect the chemical structure of the compounds in the *PAM mucus*, which in turn might affect its rheology.

There are other assays available for checking the effect of mucus on cell viability. A potentially suitable one is XTT, which is based on the same concept as MTT, but with the formazan crystals visible without lysis. This would enable an inverted microscope to visualise and quantify the formazan crystals present on the bottom of the well. Formazan is fluorescent and its intensity can be quantified and compared to a control condition.

Obtaining mucus for investigation from animals and humans is difficult. *In vitro* sources, which would be preferable, include cell lines, co-cultures and OGs. Cell lines such as Calu-3, human epithelial lung cancer cells, can secrete a thin layer of mucus on the apical surface when grown on a filter at the interface between air and medium. However, the amount of mucus secreted is too small for measurements with several repeats: after two weeks of culture, the thickness of the layer was found to be 30.6 ± 5.6 μm (Audry *et al.*, 2019). Other cellular models which secrete mucus are HT29-MTX, HT29-FU and HT29-GlucH, and co-cultures such as Caco-2/HT29-MTX, Caco-2/HT29-H and Caco-2/ HT29-M6 (Groo *et al.*, 2013). OGs grown from small intestinal stem cells also secrete mucus. If this could be harvested, its rheology could be studied. Such OGs could be used for preliminary experiments, similar to the 2D cultures mentioned above if the experimental setup is adequate.

Potential strategies to facilitate the passage of compounds through the mucus layer and into the mucosa include decreasing the frequency to decrease the attenuation, increasing the MI, increasing the quantity of MBs to promote more cavitation, and using mucolytics. The latter make mucus less thick and sticky, hence potentially easier to pass, but the treated area would still not be maximised. To increase that area, a flat or phased array transducer could be used. This approach is explored in subsequent chapters.

There is a paucity of available literature on the interaction between mucus and US. The work presented in this chapter represents progress towards better understanding how the mucus barrier can be manipulated to enable USmTDD in the small intestine.

3.10 Conclusions

pH results from harvested porcine mucus were consistent with the available literature, but dry substance measurements were inconsistent with the figures in the literature. This could be because the methods of harvesting and analysis differed. The rheology measurements of mucus from porcine small intestine made in the present work differed from the published measurements of mucus harvested from the human small intestine, though the latter was harvested using a different method.

In order to avoid culling pigs for further experiments, an artificial recipe with similar rheology was developed. The final recipe consisted of PAM and mucin prepared in DMEM F12 + FBS + P/S. It was not possible to study if the artificial mucus has a detrimental effect on cells as the MTT assay that was investigated gave inconclusive results due to the high light absorbance of mucus in a plate reader.

Understanding was sought as to whether mucus represents a barrier to drug permeation of the intestinal wall. The acoustic transparency of mucus was thus tested on an artificial recipe based on Mucin Type II. The mucus caused an attenuation of US signal between 0.1 % and 0.6 % at a frequency of 1 MHz when controlling for the thickness of the mucus layer in the *in vivo* small intestine. Although this experiment suggested that the artificial mucus was relatively acoustically transparent, it was also found that qDots lodged in the mucus layer, not in the mucosa, when delivered with US + MBs, suggesting that this transparency may be moot.

Aspects of interest emerged throughout the present proof of concept work on mucus, providing useful information for future studies. To promote the delivery of the model drug through the mucus layer over a larger surface area, the chapters which follow will make the case for exploring USmTDD for the GI tract with high power unfocused single-element and phased array transducers. Focused, unfocused high power single-element and phased array transducers will be tested in the next chapter.

3.11 References

Allen, A., Garner, A., 1980. Mucus and bicarbonate secretion in the stomach and their possible role in mucosal protection. Gut 21, 249–262. https://doi.org/10.1136/gut.21.3.249

Audry, M., Robbe-Masselot, C., Barnier, J.-P., Gachet, B., Saubaméa, B., Schmitt, A., Schönherr-Hellec, S., Léonard, R., Nassif, X., Coureuil, M., 2019. Airway Mucus Restricts Neisseria meningitidis Away from Nasopharyngeal Epithelial Cells and Protects the Mucosa from Inflammation. mSphere 4, e00494-19. https://doi.org/10.1128/mSphere.00494-19

Bansil, R., Celli, J.P., Hardcastle, J.M., Turner, B.S., 2013. The Influence of Mucus Microstructure and Rheology in Helicobacter pylori Infection. Front. Immunol. 4. https://doi.org/10.3389/fimmu.2013.00310

Bhaskar, K.R., Gong, D.H., Bansil, R., Pajevic, S., Hamilton, J.A., Turner, B.S., LaMont, J.T., 1991. Profound increase in viscosity and aggregation of pig gastric mucin at low pH. American Journal of Physiology-Gastrointestinal and Liver Physiology 261, G827–G832. https://doi.org/10.1152/ajpgi.1991.261.5.G827

CDER/FDA, 2015, Guidance for Industry, Waiver of in vivo bioavailability and bioequivalence studies for immediate release solid oral dosage forms based on a biopharmaceutics classification system, Center for Drug Evaluation and Research.

Cone, R.A., 2005. Chapter 4 - Mucus, in: Mestecky, J., Lamm, M.E., McGhee, J.R., Bienenstock, J., Mayer, L., Strober, W. (Eds.), Mucosal Immunology (Third Edition). Academic Press, Burlington, pp. 49–72. https://doi.org/10.1016/B978-012491543-5/50008-5

Donaldson, G.P., Lee, S.M., Mazmanian, S.K., 2016. Gut biogeography of the bacterial microbiota. Nat Rev Microbiol 14, 20–32. https://doi.org/10.1038/nrmicro3552

Ermund, A., Schütte, A., Johansson, M.E.V., Gustafsson, J.K., Hansson, G.C., 2013. Studies of mucus in mouse stomach, small intestine, and colon. I. Gastrointestinal mucus layers have different properties depending on location as well as over the Peyer's patches. American Journal of Physiology-Gastrointestinal and Liver Physiology 305, G341–G347. https://doi.org/10.1152/ajpgi.00046.2013

García-Díaz, M., Birch, D., Wan, F., Nielsen, H.M., 2018. The role of mucus as an invisible cloak to transepithelial drug delivery by nanoparticles. Advanced Drug Delivery Reviews, Technological strategies to overcome the mucus barrier in mucosal drug delivery 124, 107–124. https://doi.org/10.1016/j.addr.2017.11.002

Ghica, M.V., Hîrjău, M., Lupuleasa, D., Dinu-Pîrvu, C.-E., 2016. Flow and Thixotropic Parameters for Rheological Characterization of Hydrogels. Molecules 21, E786. https://doi.org/10.3390/molecules21060786

Groo, A.-C., Saulnier, P., Gimel, J.-C., Gravier, J., Ailhas, C., Benoit, J.-P., Lagarce, F., 2013. Fate of paclitaxel lipid nanocapsules in intestinal mucus in view of their oral delivery. IJN 4291. https://doi.org/10.2147/IJN.S51837

Johansson, M.E.V., Sjövall, H., Hansson, G.C., 2013. The gastrointestinal mucus system in health and disease. Nat Rev Gastroenterol Hepatol 10, 352–361. https://doi.org/10.1038/nrgastro.2013.35

Kim, Y.S., Ho, S.B., 2010. Intestinal Goblet Cells and Mucins in Health and Disease: Recent Insights and Progress. Curr Gastroenterol Rep 12, 319–330. https://doi.org/10.1007/s11894-010-0131-2

Lai, S.K., Wang, Y.-Y., Wirtz, D., Hanes, J., 2009. Micro- and macrorheology of mucus. Advanced Drug Delivery Reviews 61, 86–100. https://doi.org/10.1016/j.addr.2008.09.012

Lieleg, O., Vladescu, I., Ribbeck, K., 2010. Characterization of Particle Translocation through Mucin Hydrogels. Biophysical Journal 98, 1782–1789. https://doi.org/10.1016/j.bpj.2010.01.012

Macierzanka, A., Mackie, A.R., Bajka, B.H., Rigby, N.M., Nau, F., Dupont, D., 2014. Transport of Particles in Intestinal Mucus under Simulated Infant and Adult Physiological Conditions: Impact of Mucus Structure and Extracellular DNA. PLoS ONE 9, e95274. https://doi.org/10.1371/journal.pone.0095274

Mantle, M., Allen, A., 1981. Isolation and characterization of the native glycoprotein from pig small-intestinal mucus. Biochem J 195, 267–275. https://doi.org/10.1042/bj1950267

Matthes, I., Nimmerfall, F., Vonderscher, J., Sucker, H., 1992. [Mucus models for investigation of intestinal absorption mechanisms. 4. Comparison of mucus models with absorption models in vivo and in situ for prediction of intestinal drug absorption]. Pharmazie 47, 787–791.

Merchant, H.A., McConnell, E.L., Liu, F., Ramaswamy, C., Kulkarni, R.P., Basit, A.W., Murdan, S., 2011. Assessment of gastrointestinal pH, fluid and lymphoid tissue in the guinea pig, rabbit and pig, and implications for their use in drug development. European Journal of Pharmaceutical Sciences 42, 3–10. https://doi.org/10.1016/j.ejps.2010.09.019

Philippe, A.-M., Cipelletti, L., Larobina, D., 2017. Mucus as an Arrested Phase Separation Gel. Macromolecules 50, 8221–8230. https://doi.org/10.1021/acs.macromol.7b00842

Sellers, L.A., Allen, A., Morris, E.R., Ross-Murphy, S.B., 1991. The rheology of pig small intestinal and colonic mucus: weakening of gel structure by non-mucin components. Biochimica et Biophysica Acta (BBA) - General Subjects 1115, 174–179. https://doi.org/10.1016/0304-4165(91)90027-E

Stewart, F., Cummins, G., Turcanu, M.V., Cox, B.F., Prescott, A., Clutton, E., Newton, I.P., Desmulliez, M.P.Y., Thanou, M., Mulvana, H., Cochran, S., Näthke, I., 2021. Ultrasound mediated delivery of quantum dots from a proof of concept capsule endoscope to the gastrointestinal wall. Sci Rep 11, 2584. https://doi.org/10.1038/s41598-021-82240-1

Stokes, G.G., 2009 (first published in 1880). Mathematical and Physical Papers vol.1., On the Theories of the Internal Friction of Fluids in Motion, and of the Equilibrium and Motion of Elastic Solids, Cambridge University Press, Cambridge. https://doi.org/10.1017/CBO9780511702242

Chapter 4
Single-element Focused and Unfocused and Phased Array Transducers Demonstrate the Effect of US *in vitro*

The previous chapter dealt with the first barrier to drug delivery, the mucus layer. This chapter deals with the second barrier, the mucosa, which is the epithelial layer covering the surface of the intestinal tract, including villi. In the work described here, the potential of single-element focused and unfocused transducers and US phased arrays when used with MBs was demonstrated as a tool for delivery of macromolecular fluorescent agents across an epithelial layer. An overview of the parameters tested is shown in Figure 4-1. To do this, the ThinCert *in vitro* model of the gut lumen was used to obtain a readout of the decrease in barrier function of the epithelial layer. It was found that a drop in transepithelial electrical resistance (TEER) and delivery of fluorescently-tagged dextran through a cell monolayer *in vitro* were promoted to different degrees when the cell layer was exposed to MBs and US with different parameters.

Type of Transducer	Focused	Unfocused	Phased Array
Parameters Tested	*Proof of concept: US+MBs*	DC MI	f MI Cycles PRF Surface area

Figure 4-1 Overview of experiments presented in Chapter 4. *Three types of transducers, single-element focused and unfocused and phased array, were used to test parameters such as duty cycle (DC), mechanical index (MI), frequency (f), pulse repetition frequency (PRF), cycles and surface area.*

4.1 General methods

To investigate whether US and MBs facilitate compound delivery across a cell layer, Caco-2 cells, an FDA-approved *in vitro* model of the intestinal mucosa, was used for experiments in this chapter (CDER/FDA, 2015). Cell culture protocols are detailed in Section 3.6.1.

4.1.1 Cell Culture Using ThinCert Filters

ThinCert filters (Greiner Bio-One, Kremunster, Austria) are inserts placed into multiwell plates. The ThinCert filters have a PET porous membrane and are available with pores ranging from 0.4 to 8 µm, with suitable pore sizes identified in Section 4.3.2.1. Cells can adhere, polarise and form a continuous monolayer on the membrane, creating two chambers in the system: an apical chamber in the ThinCert and a basolateral chamber below the ThinCert, see Figure 4-2. The cells can be accessed from either the apical chamber, or the basolateral chamber.

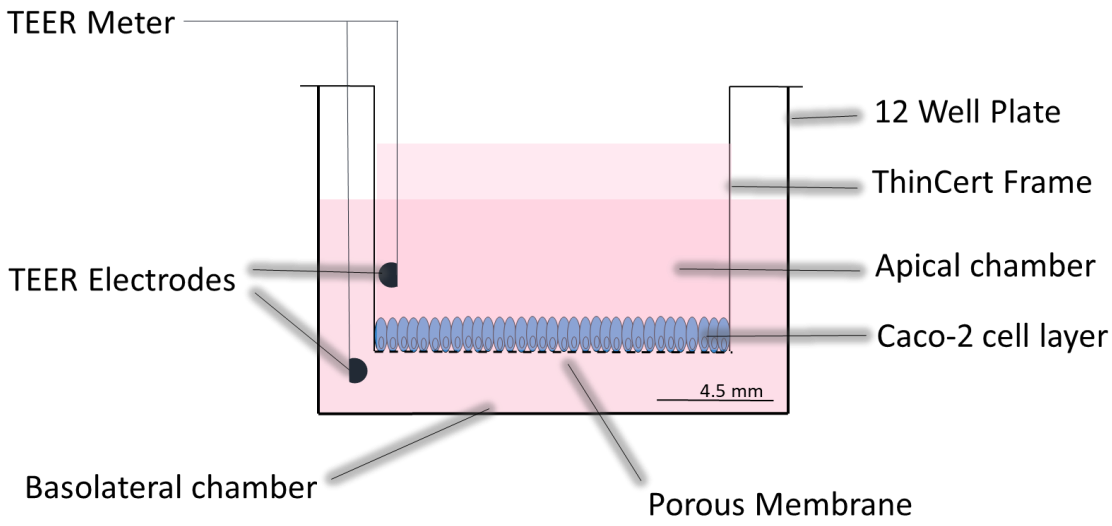

Figure 4-2 Setup for measuring the effect on the barrier function. *The cells were grown on a porous PET membrane (filter) that separated the system into an apical chamber (inside the ThinCert frame) and a basolateral chamber below the filter. One electrode was inserted in the apical chamber and the other one in the basolateral chamber. A confluent cell layer represents a barrier for electrons to travel between electrodes (Powell, 1981). A gap in the cell layer would enable electrons to travel easier and this change would be indicated through a drop in TEER. The porous membrane had a 13.8 mm diameter, suitable for 12 well plates. Larger well plates require ThinCerts with porous membranes with larger diameters. Scale bar applies only to well frame and ThinCert filter, not to the cell layer, and is approximate.*

Cells were seeded at a density of 150 000 cells/well on ThinCert filters in 12 well plates. The basolateral chamber received 1.5 ml of growth medium, whereas the apical chamber received 0.5 ml of growth medium. The media were aspirated and replaced with fresh media every two days.

4.1.2 Measurement of Transepithelial Electrical Resistance

The barrier function of a cell layer can be assessed by measuring its TEER. Such measurements require the placement of an electrode on each side of the epithelial cell layer, Figure 4-2 **Error! Reference source not found..** A continuous electrical current is passed through the epithelial cell layer, via both transcellular and paracellular routes. The apical and basolateral plasma membranes are responsible for the transcellular resistance, whereas cell-substrate and cell-cell contacts are responsible for paracellular resistance (Powell, 1981).

The TEER was measured with a Millipore Millicell ERS Volt-Ohm meter (Merckmillipore, MA, USA) in triplicate every three days. For Caco-2 cell layers, a TEER above 600 Ω*cm^2 suggests the cells are confluent and polarised (Liu *et al.*, 2017). Cell polarisation refers to the asymmetry present within cells, from the distribution of cellular organelles, determining a cell's organisation and shape to enable it to perform its functions (Rappel and Edelstein-Keshet, 2017). This is achieved in response to chemical, electrical, mechanical and physical stimuli. For example, as mentioned in Section 2.1, Caco-2 cells are simple columnar epithelial cells which express microvilli. Correct polarity will ensure the microvilli are expressed on the apical side, where they need to interact with the lumen, or the apical chamber in the present case. Conversely, the basal side expresses receptors that enable the cell to adhere to the substrate, or the ThinCert filter in the present case. The TEER was calculated using Equation 4-1

$$TEER = (R_{Measured} - R_{Blank})(\Omega) * Area_{Filter}\ (cm^2) \qquad \textbf{Equation 4-1}$$

where $R_{Measured}$ is the resistance measured with the TEER Meter, R_{Blank} is the resistance measured without cells on the filter and $Area_{Filter}$ is 113.1 mm^2, the surface area of the ThinCert for 12 well plates.

According to Meunier et al. (1995), Caco-2 cells undergo spontaneous enterocytic differentiation in culture, which starts as soon as the cells achieve monolayer density (i.e., 7 days) and is completed within 20 days. Differentiated Caco-2 cells have a well-defined brush border on the apical surface and tight cellular junctions. To investigate delivery across cell monolayers, Caco-2 cells were allowed to fully differentiate for a minimum of 3 weeks; this enabled the formation of a monolayer with cellular junctions and microvilli similar to small intestinal enterocytes (Meunier *et al.*, 1995). Monolayers were allowed to reach a TEER of 700 – 1700 Ω before being used for experiments. The passage number of cells was in the range 20 – 60.

Some method development was required and the set-ups used for the three different insonation experiments were updated accordingly to improve their reliability, efficiency and relevance. Chiefly, the focused single-element transducer had a central channel for delivering MBs and fluorescent compounds, whereas the unfocused single-element and phased array transducers required a suspension delivery tube inserted in the well to deliver MBs and fluorescent compounds.

Statistical analysis was performed using a paired parametric t-test. Statistical significance was defined as $P < 0.05$. The number of replicates (n) is provided in each relevant figure legend.

4.2 Effect of Focused Transducers and MBs on the Barrier Function of Caco-2 Monolayers

4.2.1 Methods

On the day of the experiment, cell medium was exchanged for Hank's Balanced Salt Solution (HBSS, Sigma-Aldrich Corporation, MO, USA) and the cells were placed in an incubator at 38°C for 30 min. The ThinCert's working volume was 1.2 ml and the well's working volume was 1.5 ml. The cells were incubated at RT for 1 h prior to starting the experiments to allow them to equilibrate to this temperature.

A suspension of 0.2 mg/ml 4 kDa dextran labelled with fluorescein isothiocyanate (FITC, Sigma-Aldrich Corporation, MO, USA) +/- 50% MBs (2 – 5 x 10^8 MBs/ml, 2 – 8 μm average diameter, SonoVue, Bracco, UK) prepared in HBSS was introduced into a multiwell plate containing ThinCerts with cells (Figure 4-3). Dextran and MBs were delivered with a syringe pump (NE-1000, New Era Pump Systems Inc., USA) through a channel in the centre of a miniature focused US transducer {f = 3.98 MHz, PNP = 1 MPa,

focal length = 13 mm, cross-sectional focal area at -6 dB = 1.79 mm^2}. The focused single-element transducers were fabricated by Stewart and their details, including characterisation, were presented elsewhere (Stewart, 2018, pp 83-84). US was delivered for 6 min, with the MB suspension delivered at 0.1 ml/min throughout the minutes 3 and 4. Fluid in both the apical and basolateral chamber was sampled and the amount of fluorescent dextran was measured with a plate reader.

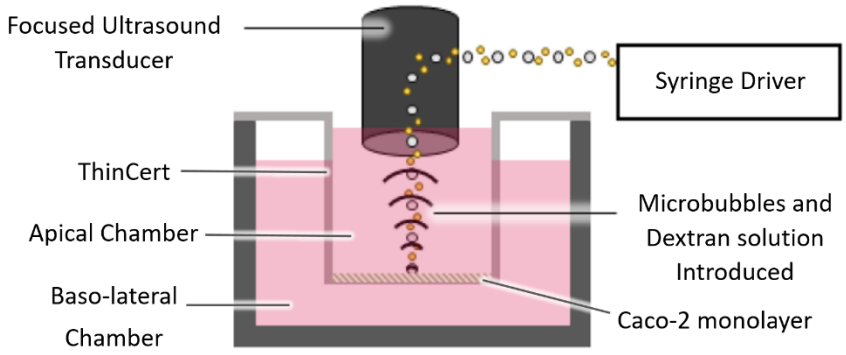

Figure 4-3 Focused US was applied to a cell monolayer using a bespoke ultrasonic transducer with a central delivery channel. *A syringe driver connected to the central delivery channel introduced microbubbles and fluorescent dextran in the apical chamber, or the ThinCert. The apical chamber's initial volume was 1.2 ml and the basolateral chamber's initial volume was 1.5 ml. Adapted from (Stewart, 2018).*

4.2.2 Results

Although the fluorescence intensity values in the medium in the basal chamber were low, insonation and MBs promoted delivery of fluorescent dextran across a Caco-2 monolayer in 5 out of 6 cases and did so more than when dextran was applied to the apical chamber without any US (0.007 and 0.005 µg/ml respectively, Figure 4-4). Although this trend is encouraging, the average difference between the control and experimental situation was small and not significant (paired parametric t-test comparing the effect of application of dextran alone to dextran with US and MBs (t = 2.2, df = 10, P = 0.067), Figure 4-4 (a).

The FD4 concentrations detected in the basolateral chamber were low compared to what was delivered to the apical chamber, so any conclusions on variations are limited.

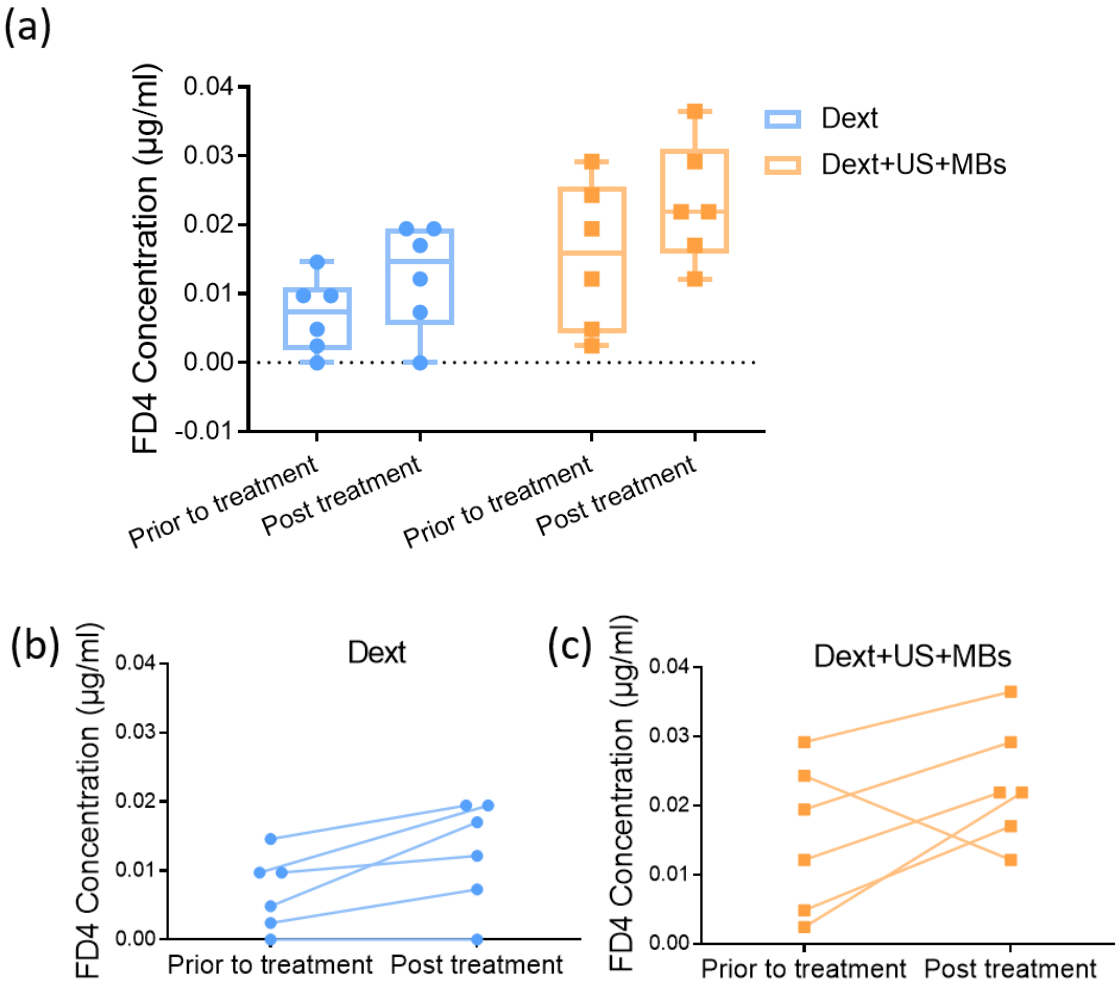

Figure 4-4 Focused transducers may slightly decrease the barrier function. *(a) US + MBs can facilitate delivery of small amounts of dextran through a Caco-2 monolayer (P = 0.067; two-tailed paired parametric t-test). Box-and-whisker plots show the median values (centre line), the 25-75th percentiles (box) and the minimum and maximum values (whiskers), for all data points. n = 6. (b,c) Interleaved bars show the increase in dextran concentration in each sample. Dext = Dextran. Post-treatment = after the US + MBs treatment. (Turcanu et al., 2018).*

4.2.3 Section Conclusion

This section reported preliminary results for use of US as a method for targeted drug delivery in the small intestine. The results suggest that focused US + MBs may enhance epithelial translocation of macromolecules *in vitro*, although the results were not statistically significant.

4.3 Effect of Unfocused Single-element Transducers and MBs on the Barrier Function of Caco-2 Monolayers

Data in the previous section suggested that US and MBs can promote the delivery of compounds across epithelial layers. However, *in vitro* experiments are often hindered by the limited proportion of large tissue areas that can be insonated, the difficulty of delivering buoyant CAs in proximity to cell layers, and adequately decreasing the barrier function to allow measuring transport. Experiments in this section aim to address these issues by adapting a cell culture system and using an unfocused single-element US transducer without a central delivery channel.

4.3.1 Unfocused transducer manufacturing and characterisation

Two unfocused transducers were fabricated from a composite made with a piezoelectrically soft ceramic, lead zirconate titanate (PZT)-5H by Dr A Moldovan. They were resonant at 1.0 MHz and had a Spatial-peak Temporal-average Intensity, I_{SPTA} = 4.9 W/cm^2, Spatial-average Temporal-peak, Intensity I_{SATP} = 2.8 W/cm^2, Spatial-average Temporal-average Intensity, I_{SATA} = 1.34 W/cm^2, total acoustic power, P_{total} = 0.5 W, with an US radiating area of 0.4 cm^2. The -3 dB pressure profile area was 4.9 mm^2 at 7 mm in front of the transducer. The transducers had an ID = 7.6 mm and were housed in cases with OD = 10 mm, which were designed in SolidWorks 2016 (SolidWorks Corp, MA, USA). They were printed in VeroGrey Gloss at UofG. The backing material consisted of Epofix filled with air-filled microballoons. The electrodes on the back and front faces of the transducer were applied as silver coatings (118-09A/B119-44, Creative Materials, MA, USA). The active element of one transducer was a regular octagon and the active element of the other was in an irregular octagon. The regular transducer was used for all experiments unless otherwise mentioned. The transducers were powered by a signal generator (RIGOL 4102, USA) and a power amplifier (RF Power Amplifier, Electronics and Innovation, UK) with a 50 dB gain.

A custom-built 3D scanning tank and a 0.2 mm needle hydrophone (Precision Acoustics, Dorchester, UK) were used to create a pressure map of the transducers' outputs and an impedance analyser (4395A, Agilent, CA, USA) was used to check their resonant frequencies.

4.3.2 Background experiments and specific experimental methodology

Preparatory experiments comprised (1) identification of ThinCert filters with suitable pore size, (2) measuring whether US enhances passage of dextran into the basolateral chamber, (3) determining the amount of dextran that adsorbs to the face of the transducer, (4) testing whether the presence of the transducer in the well has deleterious effects on cells, (5) measuring if the TEER is decreased by heat and the length of time required for it to return to its initial value, and (6) imaging of filters post-insonation to ensure the treatment did not displace cells from the filter.

4.3.2.1 Identification of filters with suitable pore diameter

The filter of the ThinCert offers support for growing a layer of cells that can then be used as a cell barrier. The filter itself does not constitute a barrier that is replicated *in vivo*; however, it might obstruct passage of model drugs if the pore diameter is small. This section describes how several pore diameters were tested to identify the most suitable one for my experiments.

Fluorescent dextrans are often used as model drugs in drug permeability experiments because they can mimic the size, shape, charge and certain chemical groups of drugs (Ahn *et al.*, 2020; Frost *et al.*, 2019). Furthermore, the fluorescent moiety enables the quantification of the compound via microfluorimetry. To determine how much of a given molecule can diffuse through the filter, the model drugs, fluorescein isothiocyanate-dextran 4 kDa (FD4, FITC, Excitation wavelength (Ex) 490 nm, Emission wavelength (Em) 535 nm, Sigma-Aldrich Corporation, MO, USA) and 3 kDa (FD3, Texas Red, Ex 590 nm, Em 625 nm, Life Technologies, UK), were delivered to the ThinCert in a well at a concentration of 100 µg/ml. The three types of filters used had pore diameters of 0.4 µm (665641, Greiner Bio-One, Kremunster, Austria), 1 µm (665610, Greiner Bio-One, Kremunster, Austria) and 3 µm (665630, Greiner Bio-One, Kremunster, Austria). At different time points, the ThinCert was removed from the well, the basolateral chamber was mixed 15 times with a P200 pipette, and a 100 µl sample was dispensed into a 96 well plate. The 96 well plate was read in a fluorescence plate reader (SpectraMax i3x, USA). Prior to the experiment, the basolateral chamber was also sampled to identify the initial FD4 concentration, which was zero.

Six minutes following dextran delivery to the ThinCert, no FD3 was detectable in the basolateral chamber for 0.4 and 1 µm pore diameter filters, Figure 4-5. Filters with 3 µm

pore diameters enabled FD3 to pass through, producing a basolateral chamber concentration of ~0.5 µg/ml dextran. After 30 min, FD3 had started to cross the 0.4, 1 and 3 µm pore diameter filters producing basolateral concentrations of ~0.1, ~0.5, and 2 µg/ml FD3, respectively. After 1 hour, the basolateral chamber below the 1 and 3 µm pore diameter filters reached concentrations of 1 and 4 µg/ml FD3, respectively. Similar trends were recorded for FD4, although the values were slightly higher. FD4 has a molecular weight larger than FD3; hence, it is counterintuitive that more FD4 diffused through the filter. However, the two compounds have different charges and were produced by different companies and this may account for the difference. Given these uncontrolled variables, any conclusions from this specific experiment are limited. In the recent literature, it was reported that charge affects absorption (Guo et al., 2021). A low-magnitude negative charge promoted transport of nanoparticles across the small intestinal mucus layer. Afterwards, positive surface charge helped nanoparticles cross the epithelial cell layer.

According to Figure 4-5, the filters with the largest pore diameter tested, 3 µm, permitted a larger amount of dextran to cross in the basolateral chamber and they were chosen for the subsequent experiments. Caco-2 cells cannot pass through the filter, as their diameter is ~ 20 µm when seeded and ~ 8 µm when in suspension (Guertin and Sabatini, 2006).

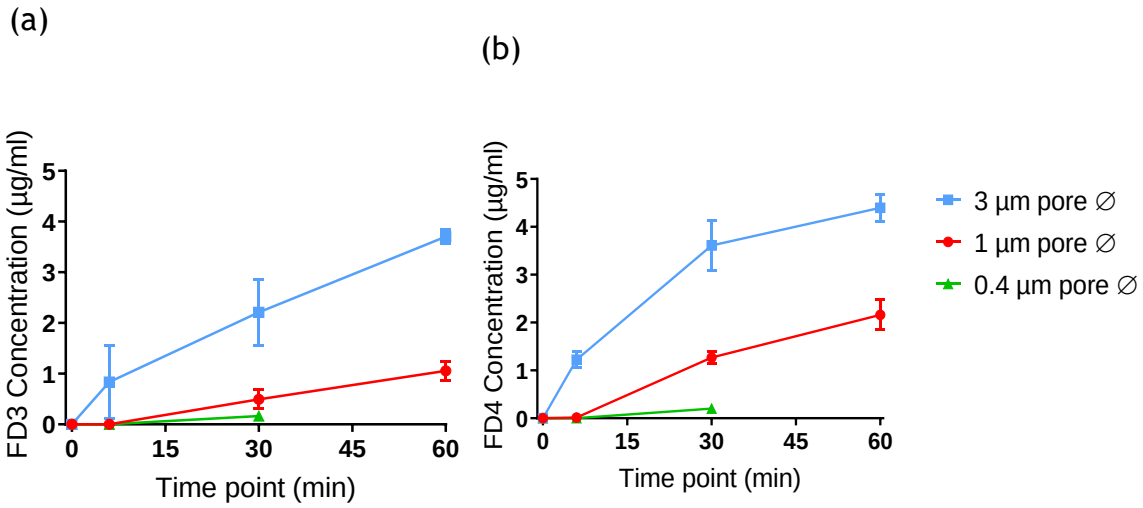

Figure 4-5 FD3 and FD4 diffusion through filters with different pore diameters. *ThinCert filters with pore diameters of 0.4 µm, 1 µm and 3 µm were used to test the amount of FD3 (a) and FD4 (b) that can cross into the basolateral chamber via passive diffusion. The time points recorded were 0, 15, 30 and 60 min. Filters with a 3 µm pore diameter enabled the largest amount of dextran to cross into the basolateral chamber for both FD3 and FD4. Diffusion via the 0.4 µm was followed only for 30 min. n = 3. Error bars are standard deviation.*

It was investigated whether TEER values were affected by the presence or absence of the ThinCert filter in the well, by the volume of fluid in the well while electrodes were fully immersed, or by the pore diameter of the ThinCert filter.

It was found that the presence of the ThinCert in the well correlates with larger TEER values, Figure 4-6**.** The volume of fluid in the well did not affect TEER values, but the size of filter pore diameters did. Smaller pore diameters in the ThinCert filter correlated with higher TEER values compared to larger pore diameters.

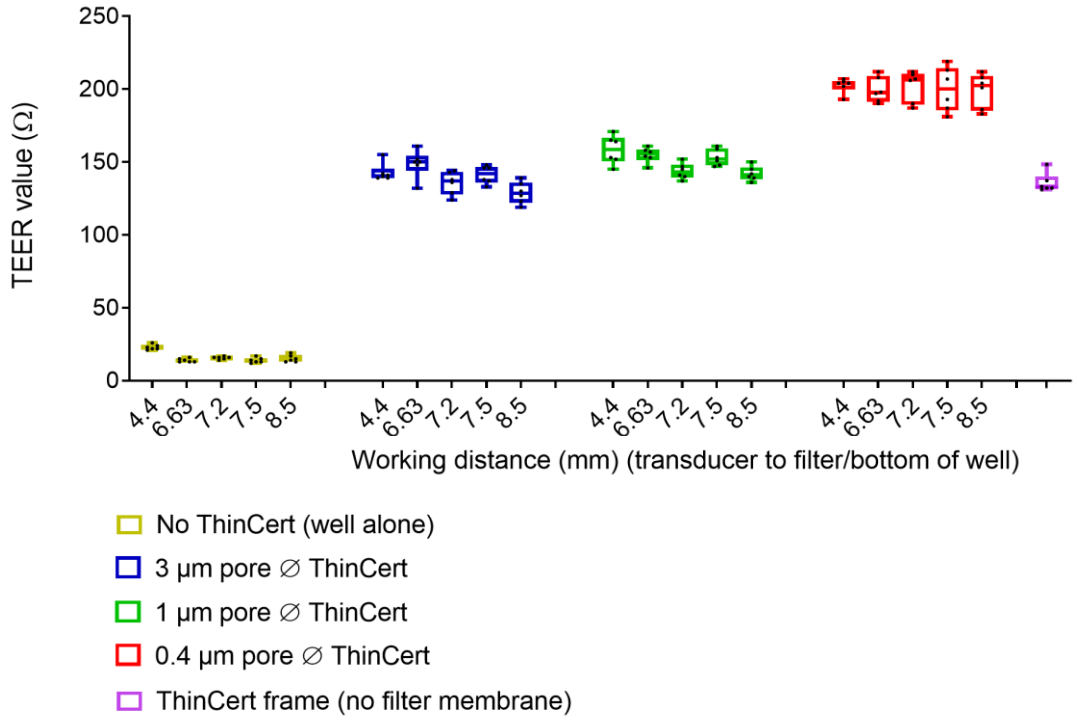

Figure 4-6 TEER background values in ThinCerts with different pore diameters. *In the absence of a filter, the TEER was 20 ± 10 Ω. In the presence of ThinCerts with pore diameters between 0.4 and 3 µm, the TEER was 170 ± 50 Ω. The filters used in subsequent experiments, with 3 µm pore diameters, have an average TEER background value of 130 ± 10 Ω when the liquid in the ThinCert has a height of 8.5 mm. The presence of the ThinCert frame without a filter membrane correlated with a TEER of 135 ± 5 Ω. n = 5.*

Other groups have used ThinCerts with 0.4 µm pore diameter filters for model drug permeability experiments (Stewart *et al.*, 2017). Using ThinCerts with larger pore diameters, such as 3 µm, was intended to reduce the contribution of the filter to compound diffusion through the cell layer, enabling more drug to pass through and therefore better representing *in vivo* conditions. Therefore, they were used for subsequent experiments.

This experiment enabled the identification of the background TEER value for ThinCert filters with 3 µm pore diameters, 130 ± 30 Ω. All TEER values reported hereafter have been applied Ohm's law, Equation 4-1. According to it, the TEER value should be representative for a surface area with the background value subtracted. From the raw TEER value, the background TEER value (130 Ω) was subtracted and the value was then multiplied by the surface area of the filter (1.13 cm^2).

4.3.2.2 Effect of US on dextran diffusion across the filter in the absence of cells

Using the method described in Section 4.3.2.1, I determined whether US could promote FD4 delivery across the filter in the absence of cells. The two concentrations in the apical chamber used were 100 and 200 µg/ml, Figure 4-7.

A larger concentration of FD4 measured in the basolateral chamber is obtained with larger MI and larger DC. Other factors that may affect FD4 diffusion through the filter include:

- dextran jamming in ThinCert pores, which is a random process (Guariguata et al., 2012),
- acoustic streaming (Shung, 2015),
- variability in dextran molecular weight. According to the manufacturer's specification sheet, FD4 is 4 kDa +/- 1 kDa (product code *FD4-100MG*, Sigma-Aldrich Corporation, MO, USA).

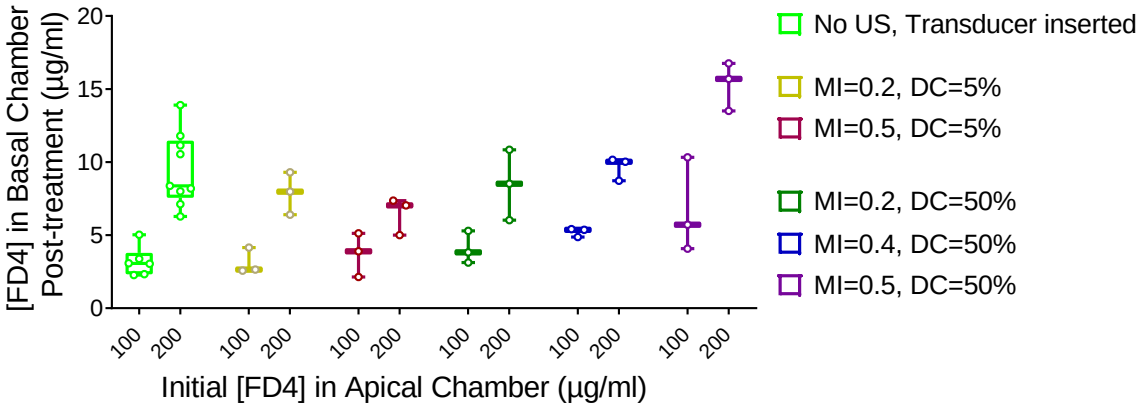

Figure 4-7 US alone does not promote FD4 diffusion through the filter alone. *When the transducer was inserted in the well, without delivering US, for FD4 initial concentrations in the apical chamber of 100 and 200 µg/ml, the concentrations recorded in the basolateral chambers were ~3 and ~8 µg/ml, respectively. When US was delivered at different MI and DC values, for the 100 and 200 µg/ml initial concentrations in the apical chamber, the concentrations recorded in the basolateral chamber were up to ~5 and ~14 µg/ml. $n \geq 3$.*

To further investigate whether heat produced by the transducer during operation might be responsible for the increase in diffusion noticed at higher MI and DC, and to account for FD4 adsorption to the face of the transducer, the experiment was repeated at 400 µg/ml initial FD4 concentration in the apical chamber, Figure 4-8. The results confirmed that US alone did not promote FD4 diffusion through the filter alone.

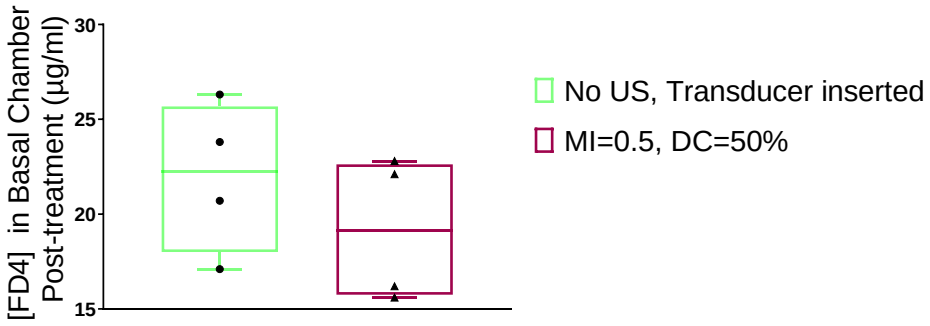

Figure 4-8 US alone does not promote FD4 diffusion through the filter alone. *When no US was delivered, the concentration in the basolateral chamber was ~22 µg/ml, whereas when US was delivered at the highest MI, MI = 0.5, and at the highest DC, DC = 50%, the amount of FD4 detected in the basolateral chamber was only ~20 µg/ml. n = 4.*

4.3.2.3 Adsorption of dextran to the face of the transducer

Dextran consists of condensed glucose, or glucan, which can adsorb to silver (Dahle *et al.*, 2013). To check whether the presence of the transducer in the well affected FD4 readings in the basal chamber by adsorption, FD4 was delivered to the apical chamber in the presence or in the absence of the transducer and the basal chamber was sampled after 20 min. The three apical chamber FD4 concentrations investigated were 100, 200 and 400 µg/ml, Figure 4-9.

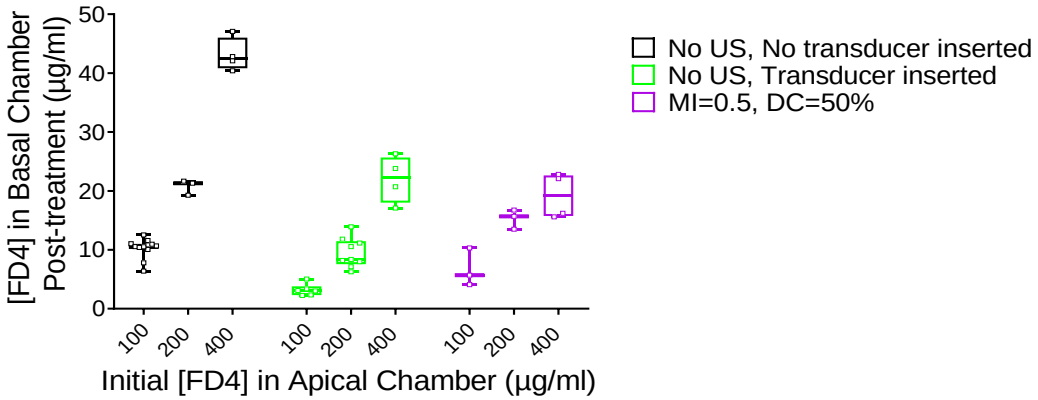

Figure 4-9 Absorption of FD4 to the face of the transducer. *When the transducer was inserted in the well, there was a lower FD4 concentration detected in the basal chamber compared to when there was no transducer inserted in the well. This suggested some of the FD4 adsorbed to the face of the transducer. When the transducer was inserted in the well, the FD4 concentrations detected in the basal chamber post-treatment were relatively similar, regardless of whether US was being delivered or not. While the values recorded at 200 µg/ml initial FD4 concentration in the apical chamber were larger when US was delivered, they were relatively similar at 400 µg/ml. $n \geq 3$.*

When no transducer was inserted in the apical chamber, concentrations of FD4 in the basal chamber reached about 10% of that in the apical chamber Figure 4-9. However, when the transducer was inserted, regardless of whether US was delivered or not, the concentration in the basal chamber was only 5% of that in the apical chamber. The trend was consistent at all concentration used, including 400 µg/ml, suggesting that adsorption was not saturated up to this concentration.

4.3.2.4 Effect of presence of the transducer in the well on TEER

To check whether the presence of the transducer, with its silver front face electrode, had deleterious effects on cells, the TEER was recorded for 30 min in the absence of the transducer, in the presence of the transducer and in the presence of the transducer covered

in cling film. When the transducer was present, it was kept in the ThinCert for only 15 min before it was removed.

As shown in Figure 4-10, TEER variation in the presence or absence of the transducer is similar, suggesting that the presence of the transducer in the well does not have deleterious effects recordable with TEER over a 30 min period.

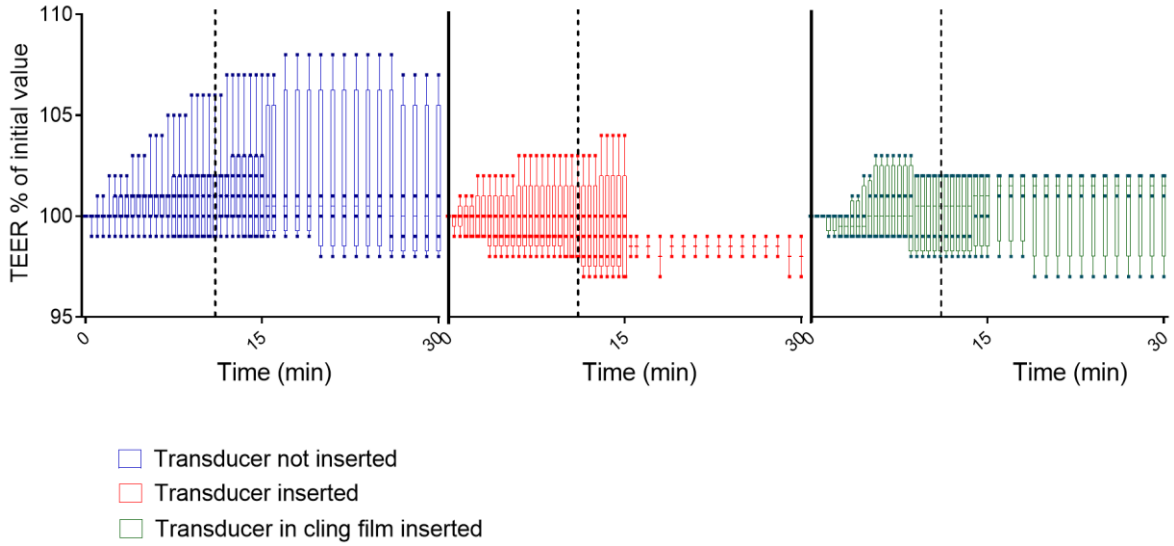

Figure 4-10 Effect of silver coating of active surface of transducer on cellular TEER. *(Note vertical scale does not start at zero.) The presence of the transducer in the well and its coating does not affect the TEER of cells. When no transducer was inserted, the TEER varied between 98 and 106% of the initial value. When the transducer was present, with its face covered or not covered by cling film, the TEER varied less, between 97% and 104%. $n \geq 4$.*

4.3.2.5 Effect of Heat on the TEER value of cells

The environmental chamber in Figure 4-11 was used to induce a heat increase similar to that produced by US to check whether heat induced a similar TEER change to US. The chamber was pre-heated to 41°C. ThinCerts with Caco-2 cells and 1.5 ml growth medium in the basolateral chamber and 0.96 ml growth medium in the apical chamber were allowed to acclimatize at RT for 20 min. They were then introduced into the environmental chamber and TEER and temperature readings were taken every minute. To be replicate conditions of the insonation experiments, the cells were kept in the environmental chamber for 11 min. Afterwards, the door of the environmental chamber was opened and the heating was switched off. The TEER and temperature of the medium with cells were recorded until the temperature fell to RT.

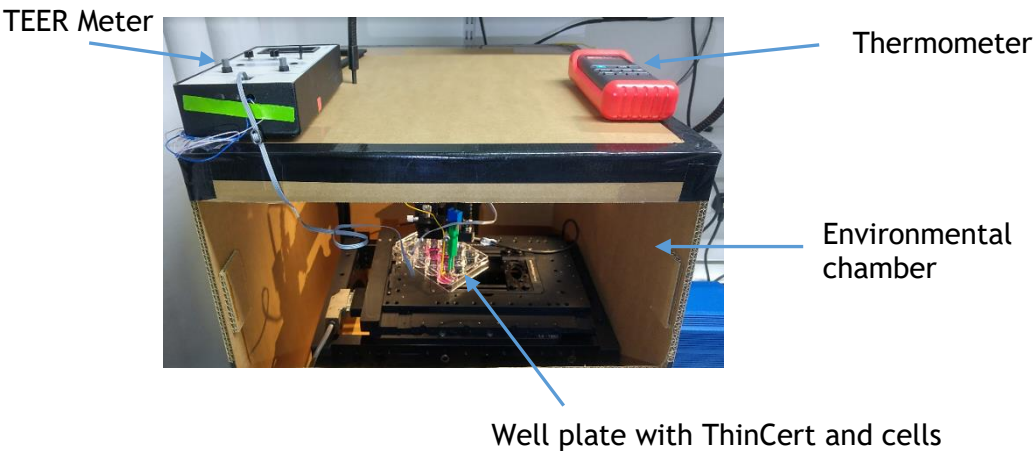

Figure 4-11 Environmental chamber used to mimic the heating bioeffect of US. *ThinCert filters with cells were placed inside the environmental chamber pre-heated to 41°C for 11 min. The TEER meter and thermometer were outside the environmental chamber and their probes were inside, enabling the recording of values both when the door was open and closed.*

As shown in Figure 4-12, there was an inversely proportional relationship between TEER and temperature: as the temperature increased, the TEER dropped. The fact that heat alone can affect the TEER, and hence the barrier properties, suggests that the effect of heat correlates with the effect of US.

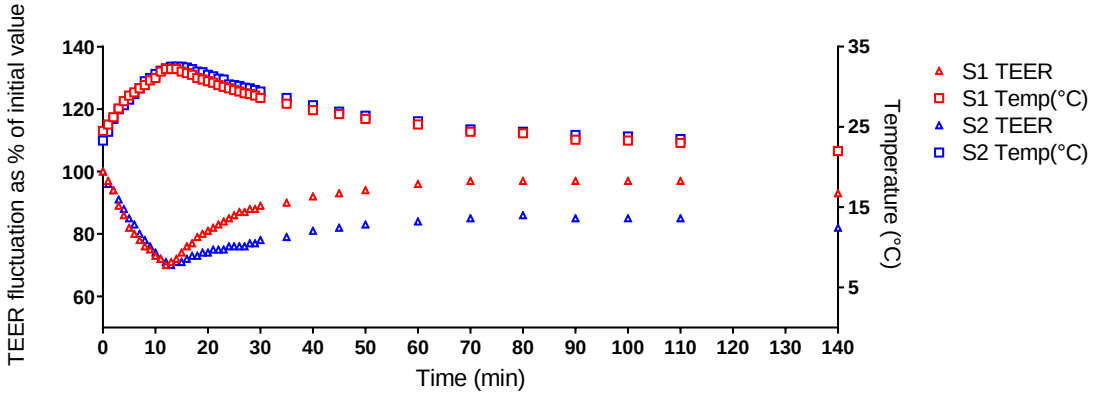

Figure 4-12 Heat alone decreases TEER. *Cell layers introduced in the environmental chamber were exposed to heat alone for 11 min. TEER measurements were recorded for 140 min. The barrier function of two samples, S1 and S2, displayed similar behaviour. An increase in temperature correlated with a drop in TEER. At the end of the 11 min heat exposure, a temperature increase of ~8 °C corresponded to a TEER drop of ~30% from the initial value. After the 11 min time point, once the temperature started to decrease, the TEER started to gradually increase. n = 2.*

Figure 4-13 presents on a single graph how TEER varied with changes in temperature induced by either US (including its heating bioeffect) or heat alone. The trend was similar, suggesting there is a correlation between TEER decrease and temperature increase, regardless of the source of heat. A further observation was that US, at an MI of 0.5 and duty cycle (DC) of 50%, produced a heat increase up to a temperature of 30°C, suggesting the temperature increase was not harmful to cells. Attaining a temperature above the physiological range (37°C) might induce deleterious effects on cells (LEBER *et al.*, 2012).

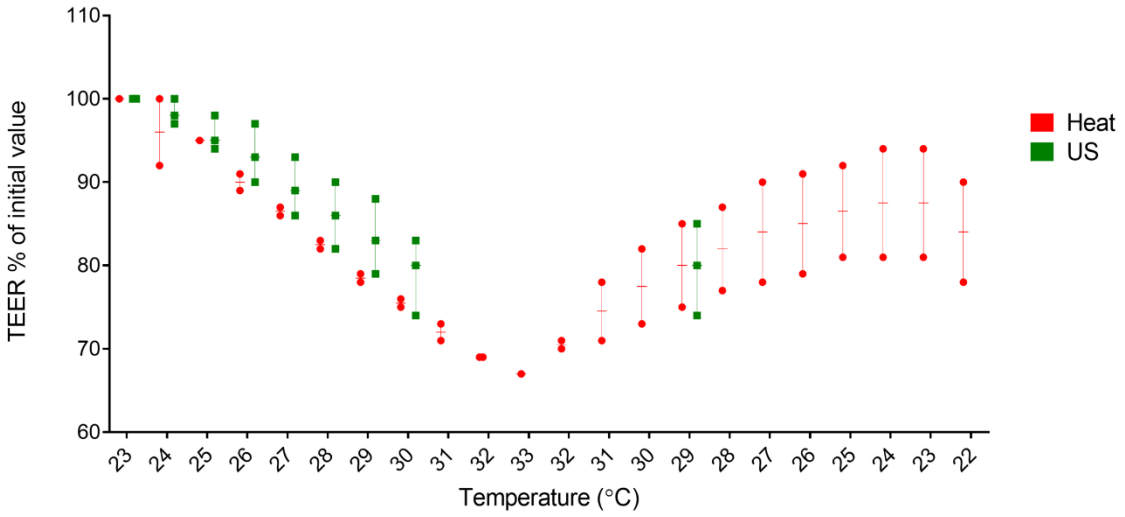

Figure 4-13 US alone and heat alone produced a similar drop in TEER values. *Cell layers were exposed to either heat alone or insonation alone and TEER measurements were recorded. The insonation treatment increased the temperature of the fluid in the apical chamber. Temperature values from heat alone or insonation alone were matched and it appeared that their corresponding TEER values were similar. A temperature increase from 23 to 32 °C corresponded to a 30% drop in TEER. $n \geq 2$.*

4.3.2.6 Effect of US alone on cells

Given that US bioeffects can have cellular effects, it was important to investigate whether insonation displaces cells from the ThinCert filter.

Following insonation (1 MHz, 100 cycles, 50% DC, MI = 0.5), cells were fixed with 4% PFA for 10 min. They were washed once in PBS and stained for 10 min with 1 µg/ml 4,6-diamidino-2-phenylindole (DAPI). They were rinsed with PBS and the filters with cells were removed and mounted on a microscope slide (Fisherbrand™ Frosted Microscope Slides, Thermo Fisher Scientific, Waltham, MA, USA) with mounting agent (ProLong™ Gold antifade mounting medium, Thermo Fisher Scientific, Waltham, MA, USA). A coverslip (no. 1.5, 22 x 22 mm^2, Agar Scientific Ltd, Stansted, UK) was placed on top and

nail varnish was used to seal the coverslip to the microscope slide. A CoolSnaps HQ^2 microscope (Photometrics, AZ, USA) was used to check whether the nuclei were still present. Five images of each slide were taken (one for each quadrant and one for the central area), as shown in Figure 4-14.

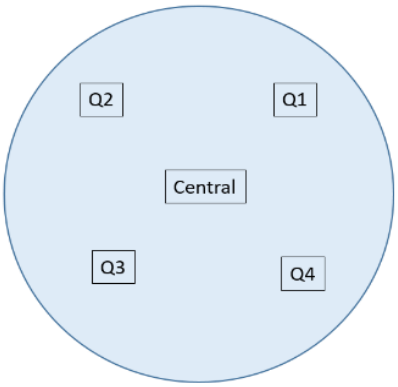

Figure 4-14 Regions of cell layers used for taking images. *One image of each quadrant and of the central area was taken to assess whether cells detached from the filter following insonation. Five images per ThinCert filter were taken.*

As shown in Figure 4-15, US treatment did not result in cellular detachment from the ThinCert filter.

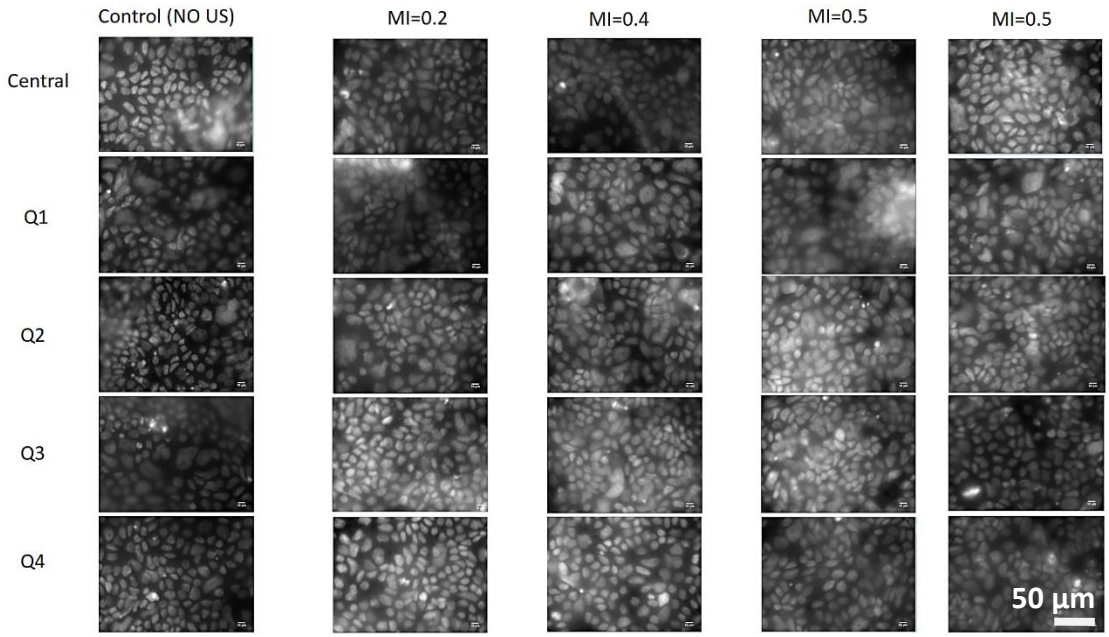

Figure 4-15 Insonation did not result in cellular detachment from the filter. *Following insonation at MI values ranging between 0.2 and 0.5 or in the absence of insonation (control), pictures of the ThinCert filters were taken to assess whether cells were still present on the filter. Cell nuclei were present on filters in all conditions studied, suggesting cells were also present.*

4.3.3 Experimental method

On the day of the experiment, each ThinCert was removed from the incubator, rinsed once with PBS and placed in another 12 well plate. The basolateral chambers each received 1.5 ml HBSS and the ThinCert received 0.96 ml HBSS. This produced a fluid height of 7 mm, which was the focal working distance of the transducer. Once the transducer came into contact with the fluid, the appropriate working distance was reached. The ThinCert was allowed to acclimatize at RT for 20 min prior to insonation.

A suspension of 0.1 mg/ml of FD3 or FD4 +/- 5% MBs ($2 – 5 \times 10^8$ MBs/ml, 2 – 8 µm average diameter, SonoVue, Bracco, UK) prepared in HBSS was introduced into a ThinCert inserted in a multiwell plate. Dextran and MBs were delivered with a syringe pump (NE-1000, New Era Pump Systems Inc., USA) through a pipette tip attached to the transducer in such a way as to project the suspension towards the bottom of the ThinCert, in order for cavitation to take place in proximity to the cell monolayer, Figure 4-16. The syringe driver was programmed to deliver the suspension for 1 sec, pause delivery for 3 sec and repeat the cycle until a button was pressed. The speed of delivery was 4 ml/min, delivering a total of 11 ml of suspension over the 11 min treatment period. This sequence enabled the suspension to be aspirated by a peristaltic pump quickly enough to avoid overflow into the basolateral chamber and made the experiment more cost-effective, given the high cost of MBs. During the insonation treatment, a TEER probe was inserted in the well and a value was recorded every minute. A thermometer probe (RS52 Thermometer Kit, RS, UK) was inserted just above the cell layer verifying that the temperature did not exceed 25°C at any point throughout the experiment.

Each sample was insonated for 11 min. TEER values were recorded for a further 9 min to assess TEER recovery towards the initial value. The decrease in barrier function was checked through TEER measurements and by quantifying the amount of FD4 that crossed the cell monolayer. Following treatment, once the ThinCert was removed from a well, the basolateral chamber was mixed with a P200 pipette 15 times and two 100 µl samples were taken. The 96 well plate was then read in a fluorescence plate reader (SpectraMax i3x, USA). Data were then analysed in MS Excel and graphs were drawn in GraphPad Prism 7.

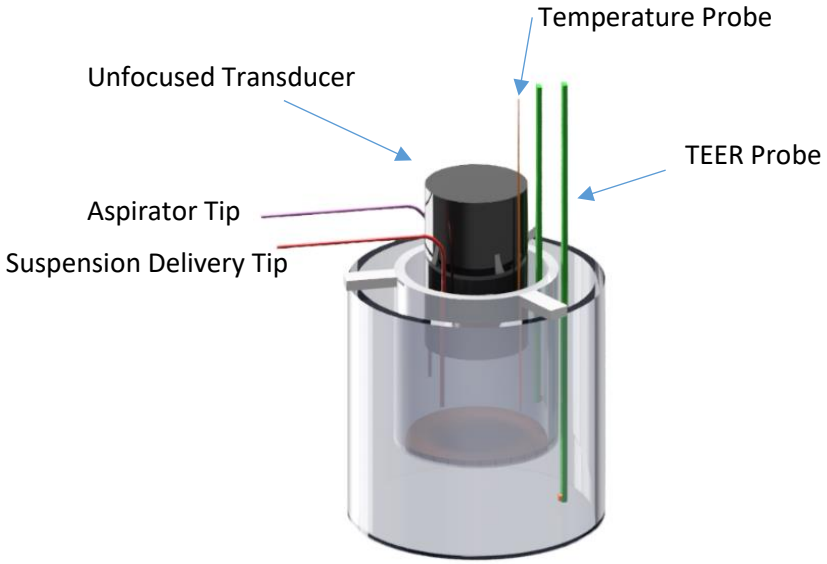

Figure 4-16 Setup for testing the unfocused single-element transducer *in vitro*. *A syringe driver facilitated suspension delivery to the ThinCert through the suspension delivery injection tip. The aspirator pump ensured no suspension overflowed in the basolateral chamber by aspiration through the aspirator tip. The temperature probe enabled the recording of the temperature of the suspension in proximity to the cells. The TEER probe allowed the change in barrier function to be recorded (Courtesy of Dr A Moldovan).*

4.3.4 Results

As seen in Figure 4-17, HBSS alone and HBSS + MBs did not decrease the TEER of the cell layer. HBSS + US, potentially partly because of the heat produced by the transducer (Figure 4-13), decreased the TEER by ~40%. Once the US was switched off, a slight increase in TEER was recorded. HBSS + MBs + US decreased the TEER by ~80%, with little or no recovery recorded over the following 9 min.

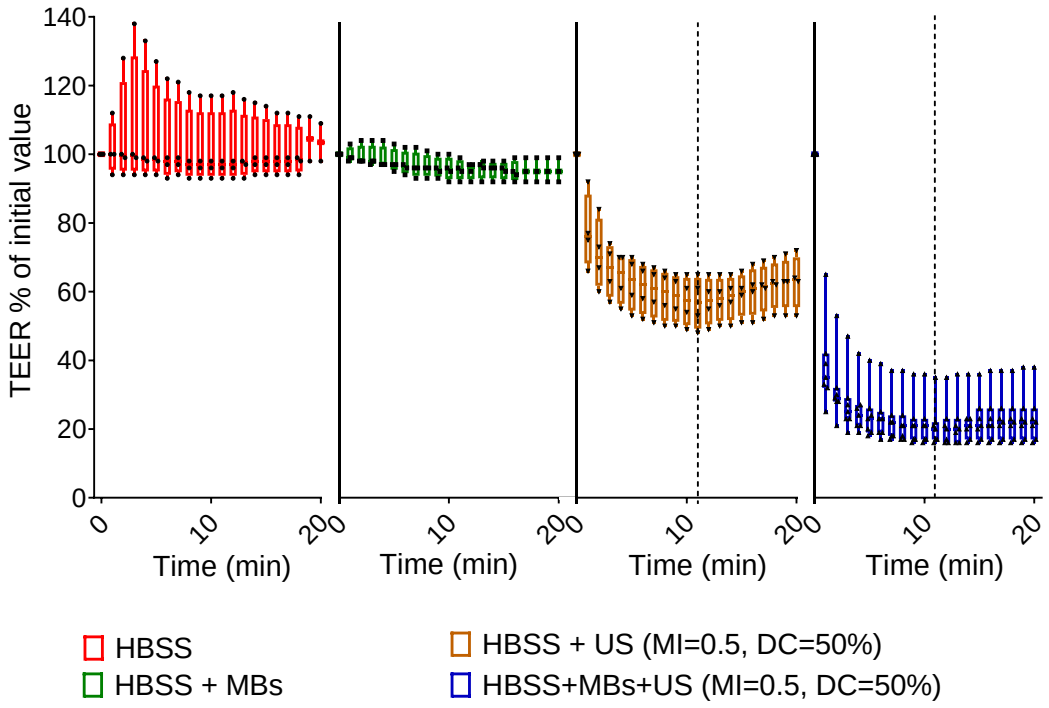

Figure 4-17 US and MBs can decrease the TEER of a Caco-2 monolayer. *TEER measurements were taken each minute to study the effect of the treatment on the barrier function of Caco-2 layers. The treatment consisted of either HBSS alone, HBSS + MBs, HBSS + US or HBSS +MBs +US. In the absence of US, the TEER dropped by up to 10% of the initial value. When US was delivered without MBs, the TEER decreased by ~40% of the initial value. In contrast, when US was delivered in the presence of MBs, the TEER decreased ~80% of the initial value. The abscissae show 20 time points (minutes) for each condition. Dashed line indicates the end of the 11 min treatment. $n \geq 2$.*

A DC increase from 1% to 5% promoted a TEER decrease from ~70% to ~55% after 11 min of treating the cell layer with US and MBs, Figure 4-18. There was no recovery observed over the 9 min following insonation.

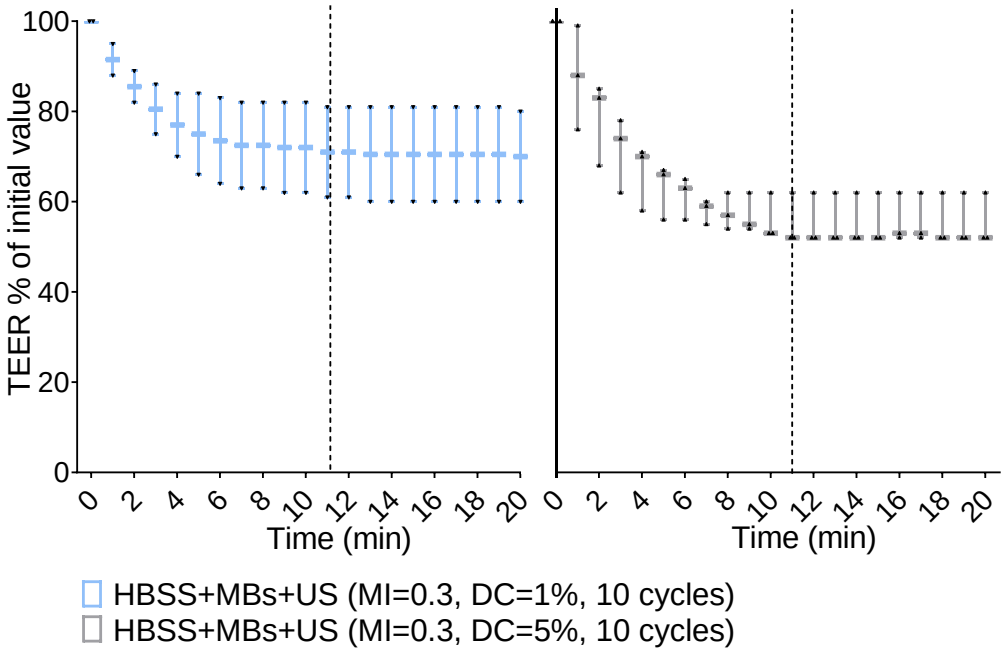

Figure 4-18 An increase in DC is associated with a drop in TEER. *The DC was increased from 1% to 5%, while all other parameters were kept constant. When DC = 1% the TEER decreased by ~30% of the initial value and when DC = 5% it decreased by ~50% of the initial value. There was no TEER recovery within the 9 min following treatment. Dashed line indicates the end of the 11 min treatment. $n \geq 2$*

An increase in MI from 0.25 to 0.5 resulted in a 20% larger decrease in TEER, suggesting a linear relationship between them, Figure 4-19. No recovery was recorded following the end of the insonation period.

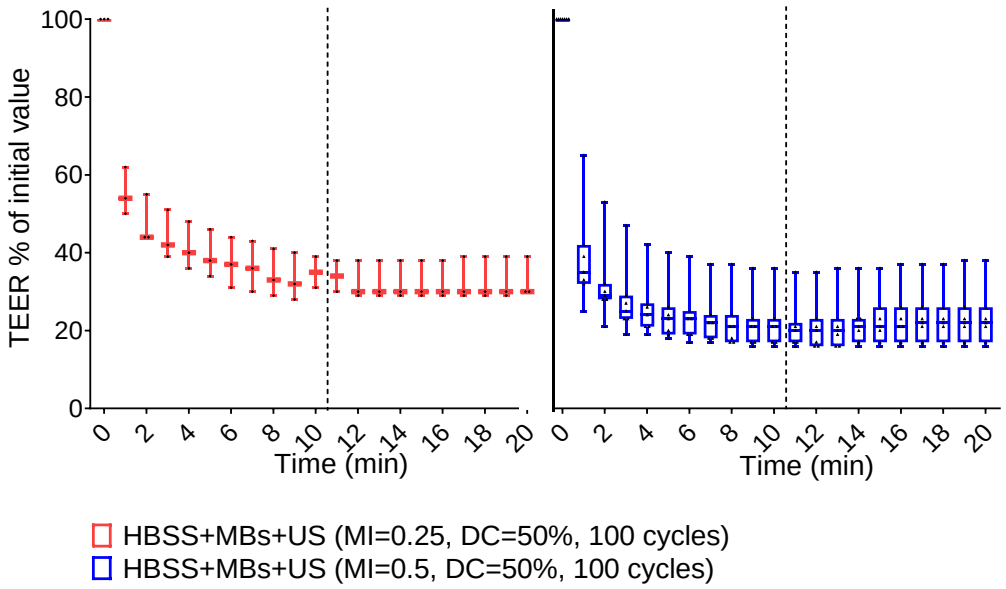

Figure 4-19 An increase in MI is associated with a drop in TEER. *The effect of increasing the MI from 0.25 to 0.5 was tested by recording the fluctuation in TEER. By minute 11 of treatment, MI = 0.25 decreased the TEER to 35% of the initial value. A larger MI, MI = 0.5, decreased the TEER to 20% of the initial value. Dashed line indicates the end of the 11 min treatment. $n \geq 3$.*

FD4 was not detected in the basolateral chamber without US exposure of the cell layer (control, cells alone), when the cells were treated only with MBs, when the cells were heated to 38°C, or when the cells were insonated in the absence of MBs and the medium in the apical chamber reached 38°C due to US treatment and transducer overheating (Figure 4-20). When the treatment included both US and MBs, different amounts of FD4 were detected in the basolateral chamber 20 min and 1 h post-treatment.

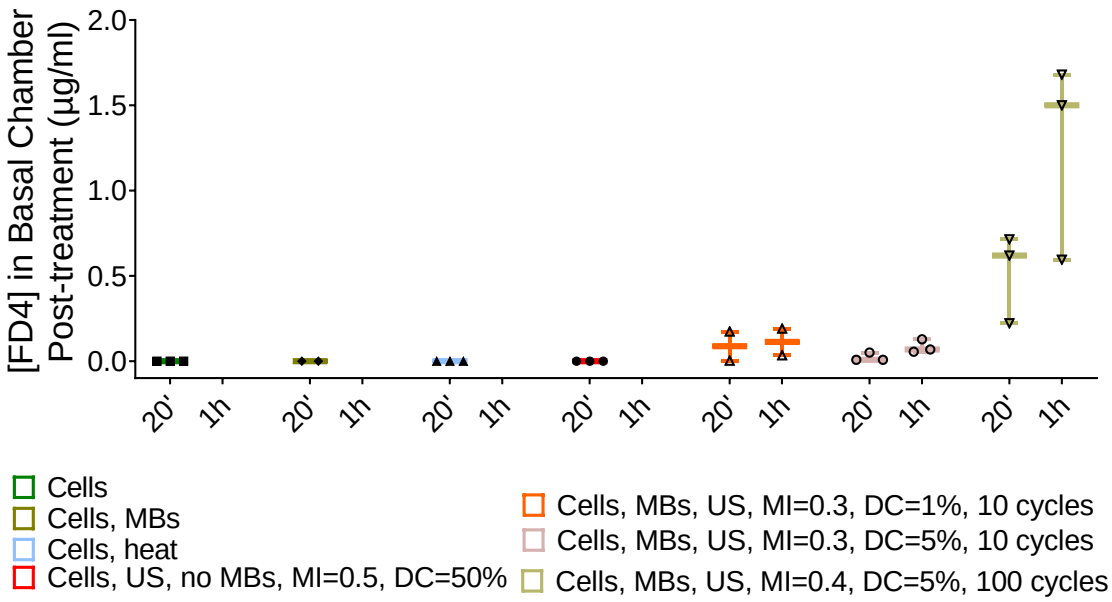

Figure 4-20 US and MBs can promote FD4 delivery across a Caco-2 monolayer. *The effect of different combinations of parameters on decreasing the barrier function was conducted by measuring the amount of FD4 that crossed from the apical chamber into the basolateral chamber within 20 min or 1 h. By themselves, heat, US and MBs do not promote FD4 delivery across the monolayer. When combined, US and MBs promoted the delivery of FD4 across the monolayer. The highest amount of FD4 was measured in the basolateral chamber when the insonation parameters were {MI =0.4, DC = 5%, cycles = 100} in the presence of MBs. $n \geq 2$.*

4.3.5 Section Conclusion

Background experiments enabled the following observations:

- 3 µm pore diameter filters were most suitable for experiments aiming to monitor movement of macromolecules through cell layers, Figure 4-5.
- US alone did not promote dextran diffusion across the filter alone, Figure 4-7 and Figure 4-8.
- FD4 adsorbed to the face of the transducer, Figure 4-9.
- The presence of the transducer in the well did not have deleterious effects on cells over a 30 minute period, Figure 4-10.
- Following exposure to US alone, the TEER of cells partially recovered over the subsequent 20 minutes, Figure 4-17 (condition in red, termed *HBSS*).

- The bioeffect of heating induced by US was weak and did not pose a danger to cells, Figure 4-12.

- The effect of US on TEER correlated with the effect of heat alone on TEER, Figure 4-13.

- US did not cause cellular detachment from the filter, Figure 4-15.

- US + MBs decreased the TEER by up to 80% of the initial value, Figure 4-17.

- The MI and the DC affected the decrease in barrier function, Figure 4-18 – 19.

- Following treatment, full recovery was recorded within 9 min only when the TEER decreased by no more than 10% of the initial value, Figure 4-17.

- US and MBs facilitated FD delivery across the monolayer only when used together, suggesting cavitation (oscillation, collapse, jetting or shockwaves) may be responsible for the drop in barrier function, Figure 4-20.

The present work allowed further technical observations: (1) the current setup with a syringe pump ensured MBs reach the bottom of the ThinCert where the monolayer is found and can be induced to cavitate; (2) the aspiration pump ensured media from the ThinCert did not overflow into the basolateral chamber, and (3) certain US parameters (low frequency, rapid short pulses (10 - 100 cycles), MI = [0.2-0.4]) were efficient at decreasing the barrier function.

Although the effects of heat alone and US alone on TEER appeared similar, in neither condition did FD4 move across the Caco-2 monolayer, Figure 4-20. Detectable amounts of FD4 moved across the Caco-2 monolayer only after exposure to a combination of US + MBs. Hence, it may reasonably be argued that MBs may facilitate cavitation, which may induce sonoporation. Sonoporation in epithelial layers has been recorded at an MI between 0.2 and 0.4 (Wang *et al.*, 2018). These values have been used in the present experiments as well, further suggesting sonoporation may be a reason for the effect noticed on the Caco-2 cell barrier.

The unfocused single-element transducer induced a larger decrease in barrier function compared to the focused transducer. To validate the results obtained in this section and to allow insonating a larger surface area, a phased array transducer was used. The following section presents preliminary experiments using this transducer.

4.4 Effect of Phased Array Transducers and MBs on the Barrier Function of Caco-2 Monolayers

4.4.1 Method

Two phased array transducers were fabricated from PZT-5H composite by Dr A Moldovan (Moldovan, 2021, Chapter 5, page 123) at the University of Strathclyde. A 3.0 MHz transducer comprised 32 elements, with a transducer length of 7.8 mm. It was used with an array controller (FI Toolbox, Diagnostic Sonar Ltd, Livingston, UK, no longer operating) to produce up to 13 beams (1.0 mm width x 2.4 mm elevation) at different angles with a focal distance of 7.0 mm. The second transducer operated at 1.5 MHz and comprised 24 elements, with a transducer length of 11.65 mm. It was used with the same array controller to produce up to the same number of beams as a focal distance of 9.0 mm. The array controller allowed the excitation voltage to be varied and the transducer input voltages were monitored with an oscilloscope (DS2102E 100 MHz Rigol, UK).

The same method described in Section 4.3.3, including the setup in Figure 4-16 was used again, the only difference being the use of the phased array transducers instead of the unfocused transducer, Figure 4-21.

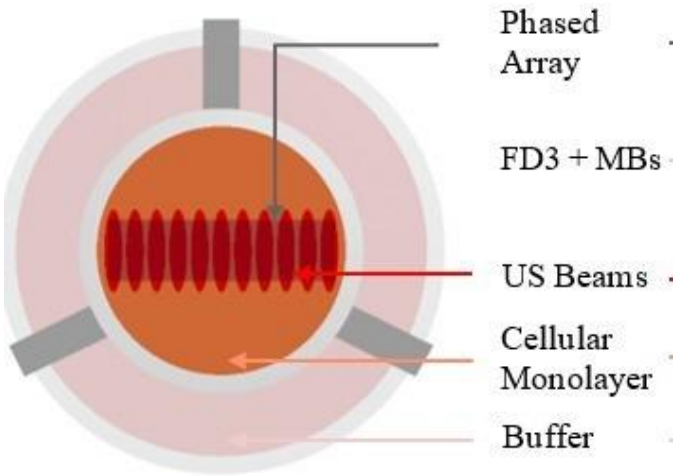

Figure 4-21 Top view of well with ThinCert insonated using a phased array transducer. *The transducer insonated several different regions of cellular layers grown on ThinCert filters. The oval shaped regions are termed US beams (Moldovan, 2021).*

Different combinations of parameters were tested to identify parameter combinations that effectively decreased the barrier function in a transient manner. The US parameters varied were frequency (1.5 MHz or 3.0 MHz, according to the transducer used), cycles in the pulse (5, 7 or 10), number of pulses (10 or 100), pulse repetition frequency (PRF, 22.8 – 57 kHz), DC (10 – 20.7%) and number of beam angles (3 – 13). Following good scientific practice, only one variable was modified at any one time. However, PRF was interdependent on the frequency, DC and number of pulses; hence, the PRF changed when other parameters were modified. Cycles were grouped into pulses, whereas pulses were grouped into bursts, Figure 4-22. Each beam caused insonation at a constant PNP, ensuring the MI was constant over the 13 beams.

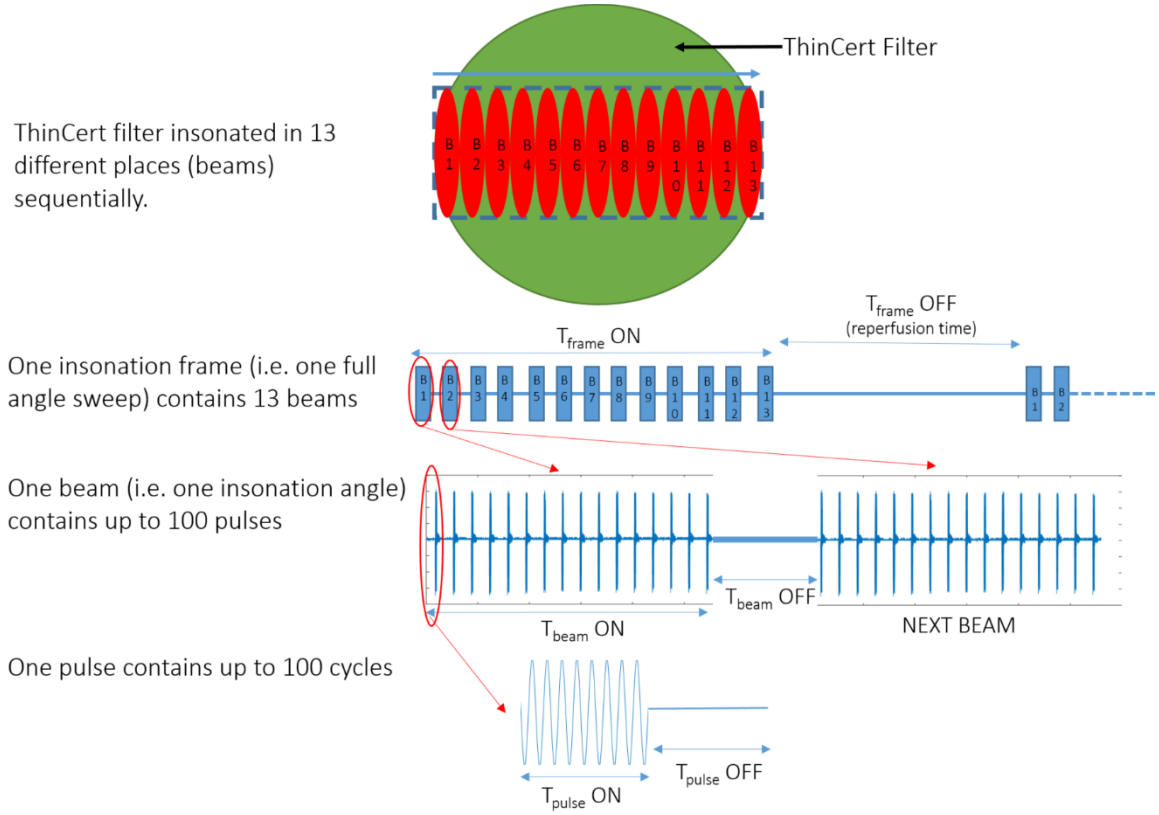

Figure 4-22 Timing of insonation. *Each ThinCert filter was insonated in 13 different regions (beams), as presented in Figure 4-22. Each beam consists of pulses and pauses; each pulse consists of cycles and pauses. The pause between beams enables insonated areas to be reperfused with MBs. The combinations of beams, pulses, cycles and pauses were varied in order to identify suitable parameters for decreasing the barrier function of cellular layers.*

4.4.2 Results

This section presents a series of results obtained with the phased array transducers. Conditions are described according to operating frequency of the transducer (1.5 MHz or 3.0 MHz), number of cycles, number of pulses, PRF, number of beams, MI, DC and fluorescent compound used (i.e. FD3 or FD4, as before). All samples were insonated for 11 min.

Effect of US, MBs or US + MBs on the barrier function

US + FD4 and MBs + FD4 showed weak effects on the barrier function, Figure 4-23. Only when US + MBs were combined did the barrier function decrease to 50% of the initial value by the end of the 11 min treatment period and to 45% of the initial value 9 min post-treatment. An outlier in the second condition in the concentration graph obstructs viewing of the pattern. 60 min post treatment there is a higher amount of FD delivered in the condition with US + MBs + FD4 compared to the other two conditions.

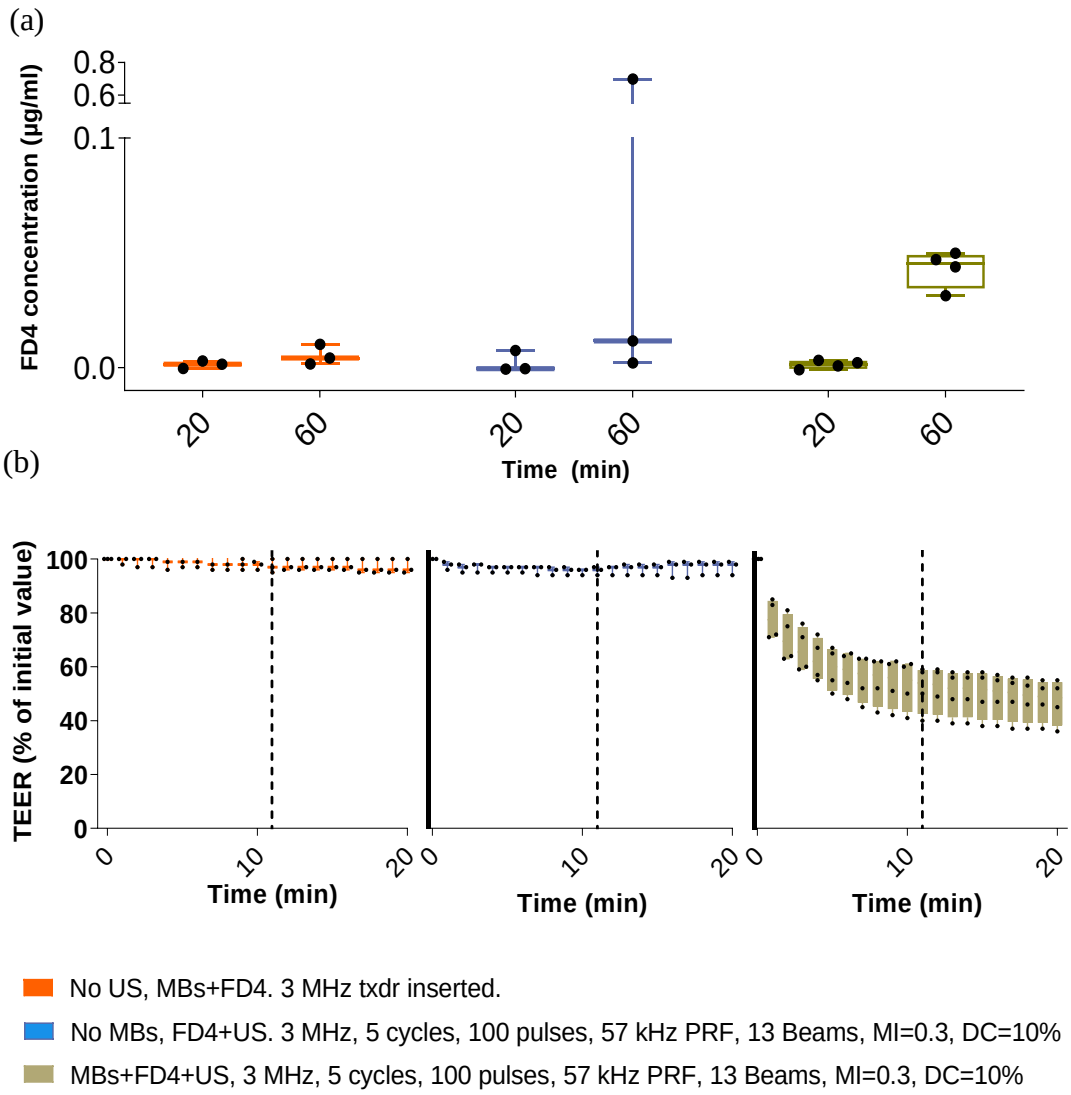

Figure 4-23 Effect of US, MBs and FD4 on barrier function. *(a) FD4 concentration in the basolateral chamber increased under the effect of MBs + FD4 + US compared to MBs + FD4. There is an outlier in the case of FD4 +US. (b) US + FD4 and MBs + FD4 do not show a decrease in TEER by more than 10% of the initial value. In contrast, US + MBs + FD4 shows a decrease in the barrier function by up to 50% of the initial value. $n \geq 3$.*

FD3 and FD4 delivery through the cell layer

FD3 and FD4 delivered together with MBs at the same US parameters showed a similar decrease in barrier function, Figure 4-24. FD3 is ~3 kDa in size and neutral and FD4 is ~4 kDa in size and negatively charged. The size and charge difference had no apparent effect on how much model drug moved to the basolateral chamber. Therefore, for subsequent figures, these two conditions were combined and called *FDx* as the insonation parameters were the same and the results were similar.

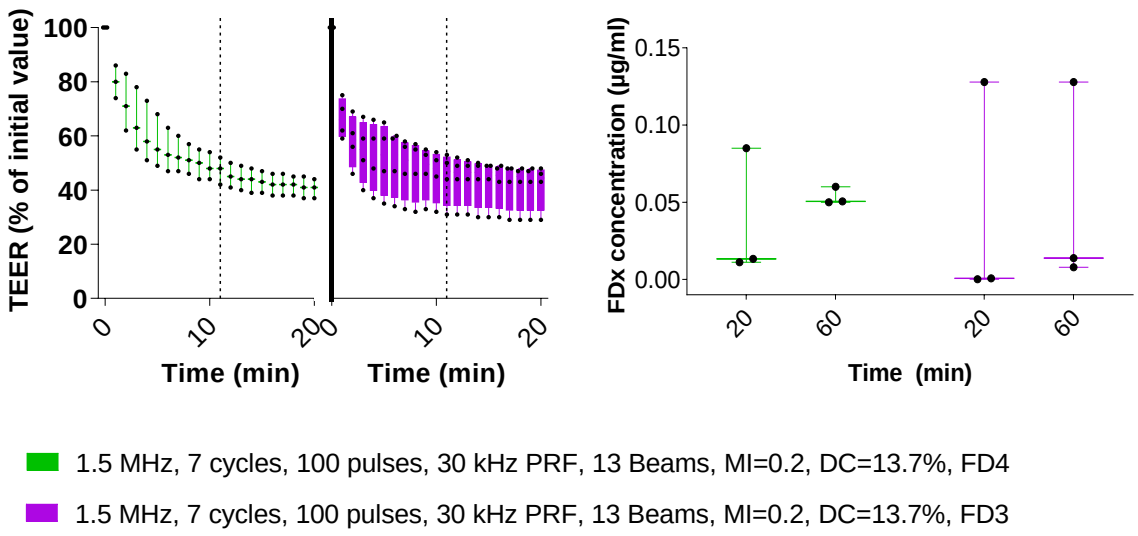

Figure 4-24 Effect of FD3 vs FD4 on barrier function and delivery across the cell monolayer. *Whether the model drug in the suspension was FD3 or FD4, the barrier function and amount of model drug delivered appeared to be similar at the 20 min time point. FDx delivery 60 min post treatment was higher in the case of FD4 compared to FD3. Dashed line indicates the end of the 11 min treatment. $n \geq 3$.*

Effect of frequency on barrier function

The 1.5 MHz and 3 MHz operating frequencies of the two transducers were used to allow the effects of frequency to be gauged, Figure 4-25. The TEER drops facilitated by the 1.5 MHz transducer were between 7% and 75%, whereas for the 3 MHz transducer the drops were between 2% and 55%. The FDx concentration graph also shows that under most conditions with the 1.5 MHz transducer more FDx was delivered to the basolateral chamber than with the 3 MHz transducer.

The MBs used, SonoVue, are resonant at 1.6 – 3.2 MHz, depending on the diameter of the MB insonated (4 – 2.6 µm) (Van der Meer, 2004). However, this applies if only one MB is present in the insonated area. In the current experiment, a multitude of MBs were delivered, complicating a potential simulation with finite element analysis software. However, Figure 4-25 clearly shows that a 1.5 MHz frequency produced a larger decrease in barrier function than a 3 MHz frequency. One reason for more sonoporation, i.e. more cavitation, to be produced with a 1.5 MHz than with a 3 MHz transducer is that the majority of SonoVue MBs were of the size that is resonant at frequencies around 1.5 MHz (4 µm diameter) and not 3 MHz (2.6 µm diameter) (Van der Meer, 2004).

(a)

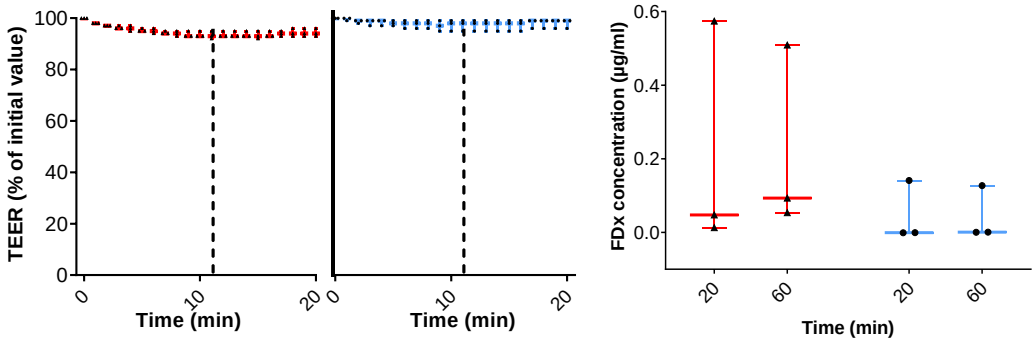

1.5 MHz, 5 cycles, 100 pulses, 30 kHz PRF, 13 Beams, MI=0.1, DC=10.6%
3 MHz, 5 cycles, 100 pulses, 57 kHz PRF, 13 Beams, MI=0.1, DC=10%

(b)

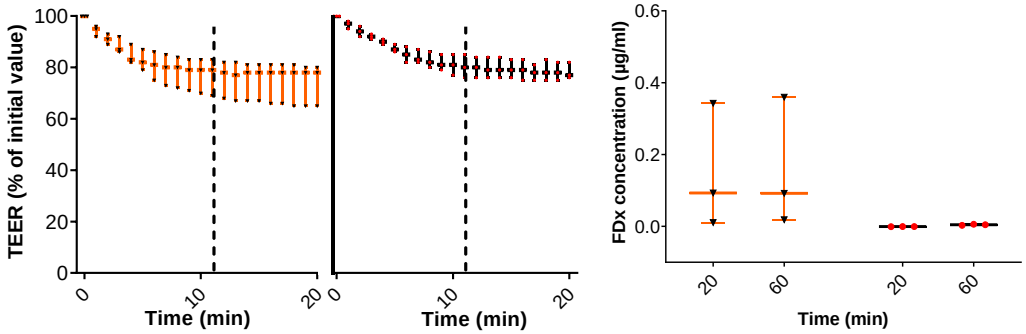

1.5 MHz, 5 cycles, 100 pulses, 30 kHz PRF, 13 Beams, MI=0.2, DC=10.6%
3 MHz, 5 cycles, 100 pulses, 57 kHz PRF, 13 Beams, MI=0.2, DC=10%

(c)

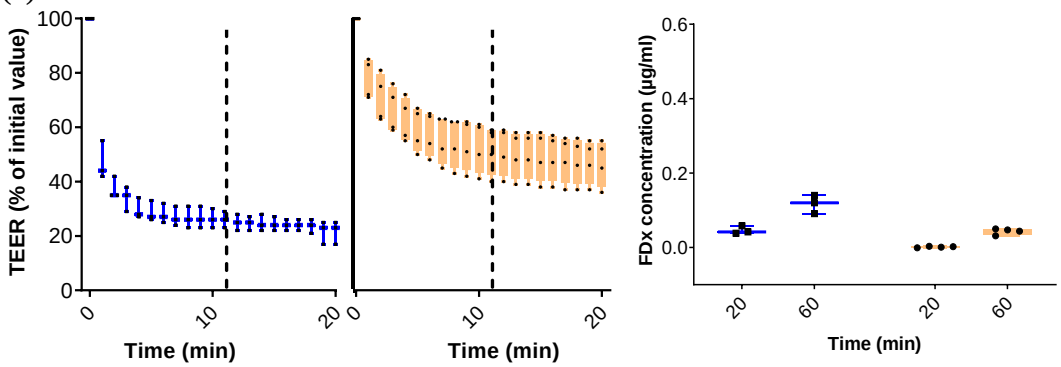

1.5 MHz, 5 cycles, 100 pulses, 30 kHz PRF, 13 Beams, MI=0.3, DC=10.6%
3 MHz, 5 cycles, 100 pulses, 57 kHz PRF, 13 Beams, MI=0.3, DC=10%

(d)

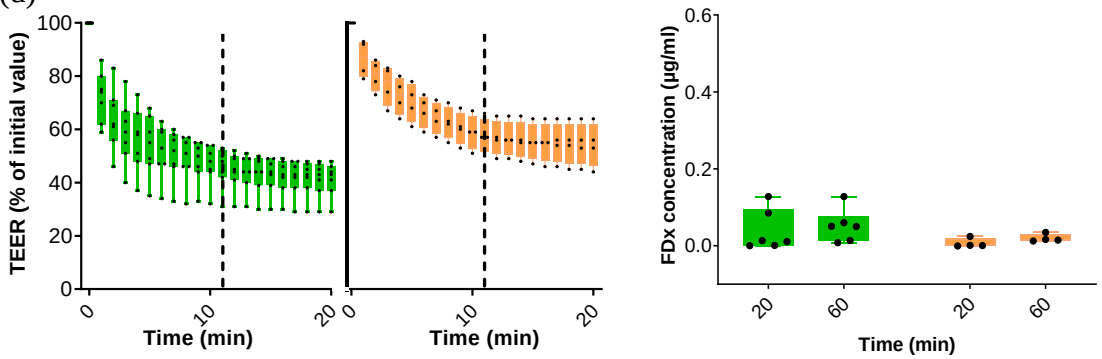

1.5 MHz, 7 cycles, 100 pulses, 30 kHz PRF, 13 Beams, MI=0.2, DC=13.7%

3 MHz, 7 cycles, 100 pulses, 57 kHz PRF, 13 Beams, MI=0.2, DC=13%

(e)

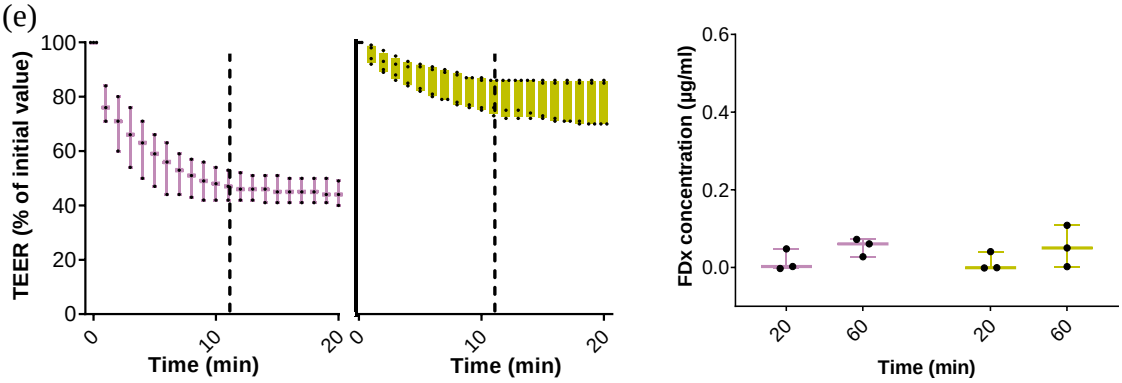

1.5 MHz, 7 cycles, 100 pulses, 30 kHz PRF, 9 Beams, MI=0.2, DC=14.4%

3 MHz, 7 cycles, 100 pulses, 57 kHz PRF, 9 Beams, MI=0.2, DC=13%

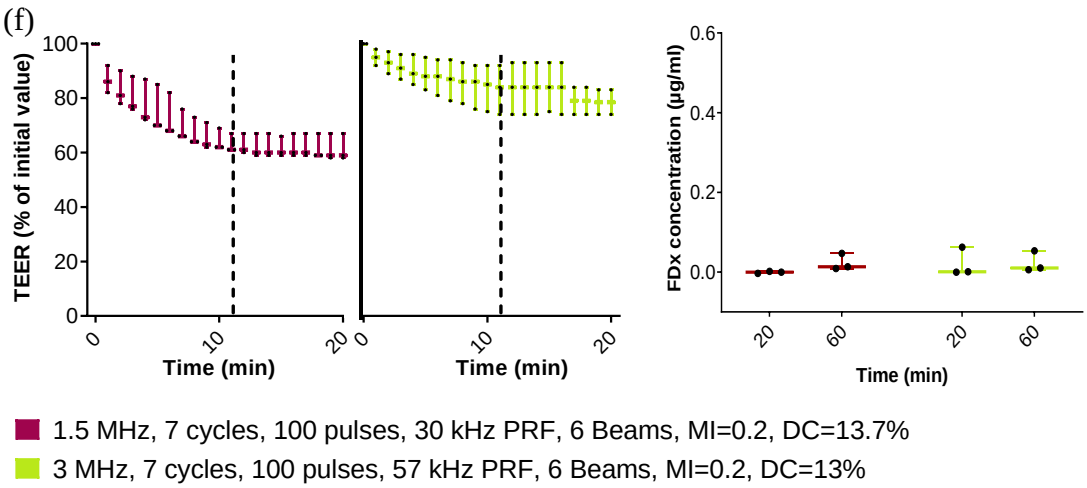

Figure 4-25 Effect of frequency on barrier function. *Each pair (a-f) presents the effect of frequency on barrier permeability when all parameters but the frequency and PRF were constant. PRF depends on frequency; hence, it was not possible to maintain the same PRF for the two frequencies studied. (a) The insonation parameters used do not seem to affect the TEER, but more FD4 was detected in the basolateral chamber at the 20 and 60 min time points. (b-f) The 1.5 MHz transducer shows more effect in decreasing the TEER than the 3 MHz transducer in the current setup. Graph to the left displays TTER and graph to the right displays FDx diffusion to the basolateral chamber. Dashed line indicates the end of the 11 min treatment. $n \geq 3$.*

Effect of MI on barrier function

MI values ranging between 0.1 and 0.3 were tested, Figure 4-26. At MI = 0.1, there was only ~10% decrease in TEER. The effect was more pronounced at MI = 0.2: a 10 – 70% drop, and stronger still at MI = 0.3: a 50 – 80 % drop from the initial value.

The 4th and 5th conditions investigated i.e. {1.5 MHz, 10 cycles, 100 pulses, 30 kHz PRF, 13 Beams, DC = 20.7%, MI = 0.2 or 0.3} showed similar drops in TEER, even though they had different MI values. This could be because the cycle number, pulse number and DC were high and the MI difference did not have a strong additional effect.

The FD diffusion into the basolateral chamber did not follow exactly the same pattern as TEER. However, the large variation in samples might obscure any pattern.

(a)

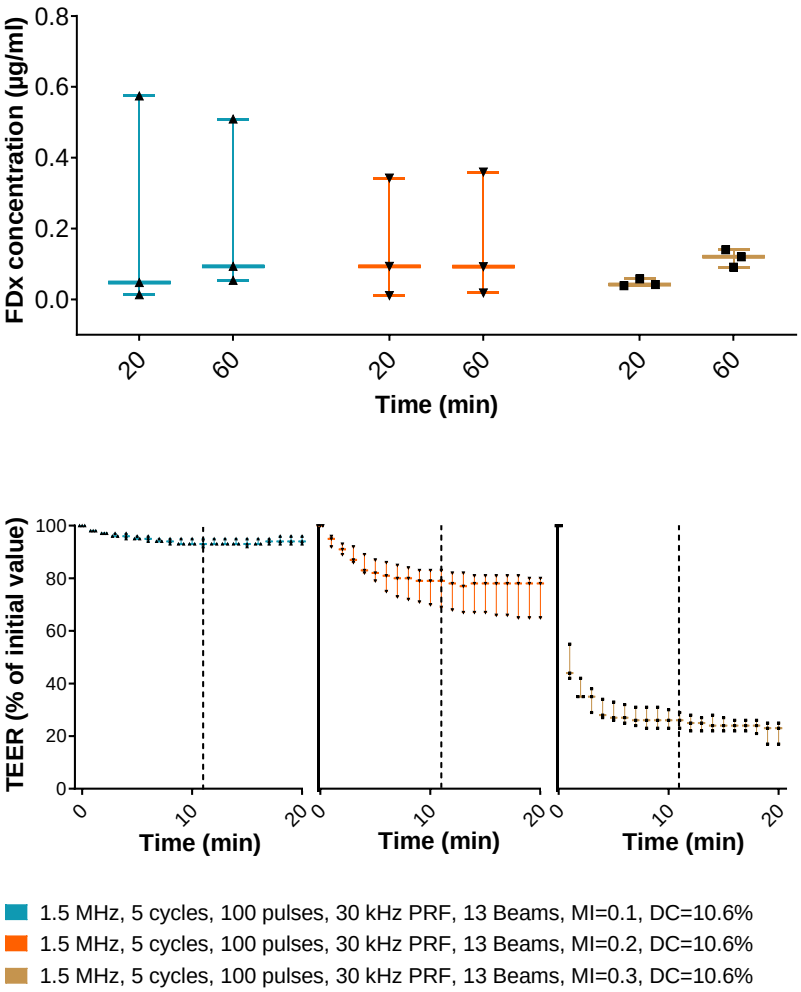
FDx concentration (μg/ml)
0.8
0.6
0.4
0.2
0.0
20
60
20
60
20
60
Time (min)
TEER (% of initial value)
100
80
60
40
20
0
0
10
20
Time (min)
Time (min)
Time (min)
1.5 MHz, 5 cycles, 100 pulses, 30 kHz PRF, 13 Beams, MI=0.1, DC=10.6%
1.5 MHz, 5 cycles, 100 pulses, 30 kHz PRF, 13 Beams, MI=0.2, DC=10.6%
1.5 MHz, 5 cycles, 100 pulses, 30 kHz PRF, 13 Beams, MI=0.3, DC=10.6%

(b)

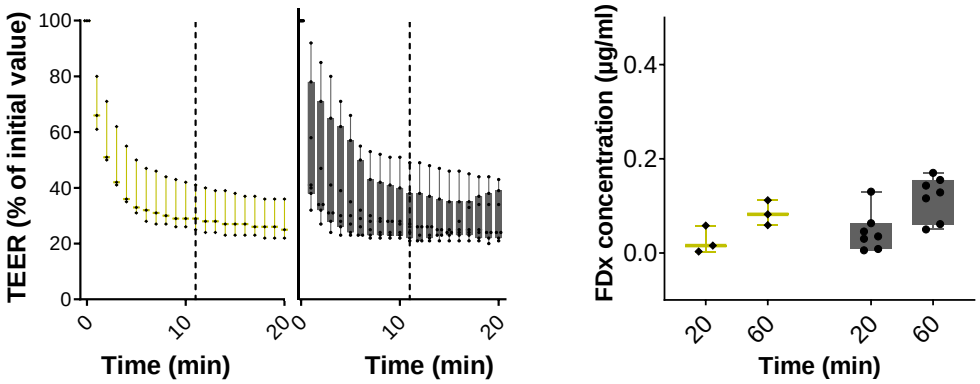

1.5 MHz, 10 cycles, 100 pulses, 30 kHz PRF, 13 Beams, MI=0.2, DC=20.7%
1.5 MHz, 10 cycles, 100 pulses, 30 kHz PRF, 13 Beams, MI=0.3, DC=20.7%

(c)

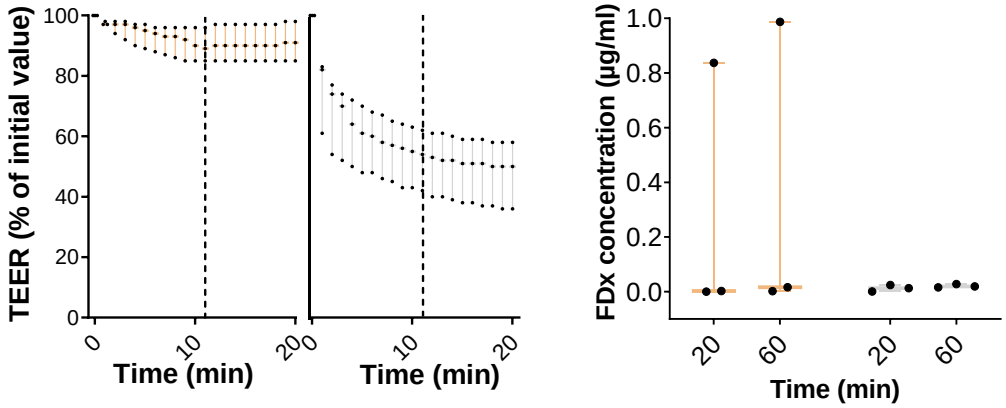

1.5 MHz, 7 cycles, 10 pulses, 30 kHz PRF, 13 Beams, MI=0.2, DC=13.5%
1.5 MHz, 7 cycles, 10 pulses, 30 kHz PRF, 13 Beams, MI=0.3, DC=13.5%

(d)

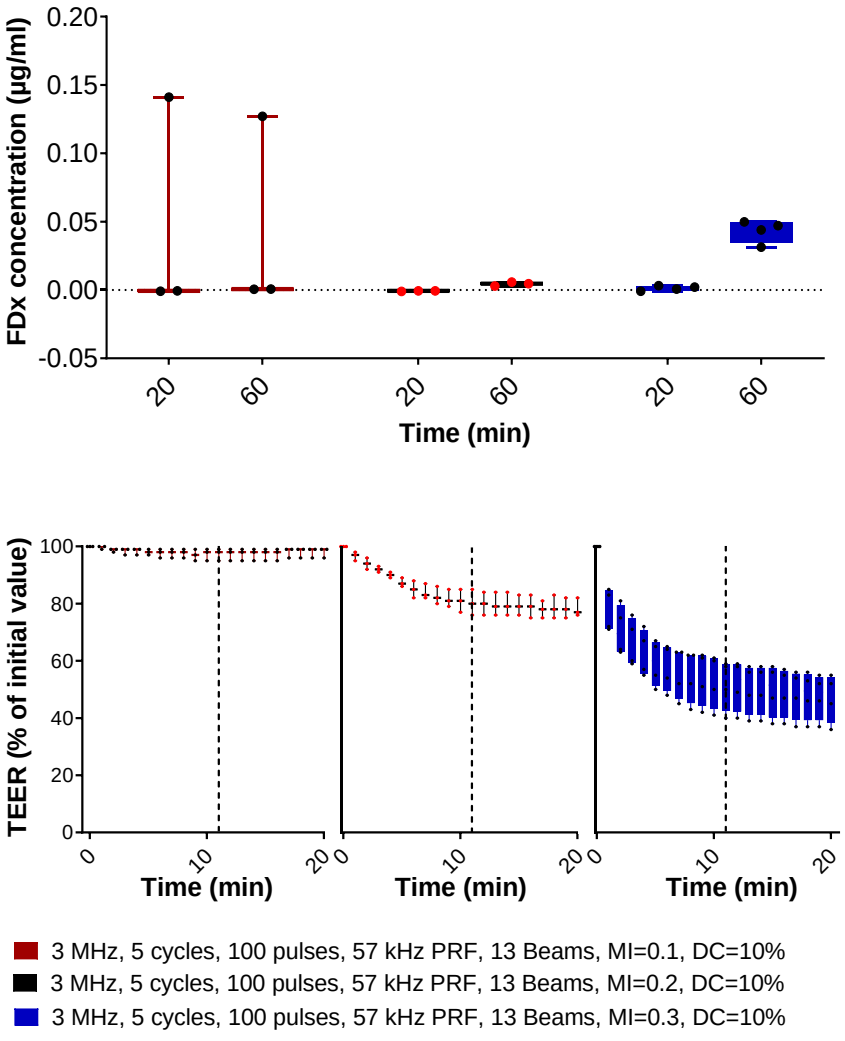

Figure 4-26 Effect of MI on barrier function. *Caco-2 cell layers were exposed to MI = 0.1, 0.2 or 0.3 to assess their effect on the barrier function. (a-d) represent data sets where parameters are consistent except for the MI, which is shown incrementally (from low MI to high MI). Where two conditions are shown (b-c), the TEER and FDx graphs are shown side-by-side. Where three conditions are shown (a,d), the FDx graph is above the TEER graph below. While small TEER drops were observed at MI = 0.1, larger drops were noticed at MI = 0.2 and 0.3. A larger MI correlated with a larger TEER decrease and a larger drop in barrier function. No TEER recovery was noticed over the 9 min following the 11 min treatment. For all samples, 13 beams were used. Dashed line indicates the end of the 11 min treatment. $n \geq 3$.*

Effect of number of cycles on barrier function

The numbers of cycles tested were 5, 7 and 10, Figure 4-27. At MI = 0.2, fewer cycles and a lower DC appeared to result in a lower TEER drop and hence a lower decrease in barrier function. However, at MI = 0.3, the TEER dropped so quickly that the increasing DC and number of cycles appeared to have no additional effect.

High FDx concentrations in the basolateral chamber were recorded in conditions with a high drop in TEER. The exception was for {1.5 MHz, 5 cycles, 30 kHz PRF, MI = 0.2, DC = 10.6%}, where one sample had a much higher value compared to the other samples. Overall, a larger number of cycles correlated with a larger TEER drop, i.e. a larger decrease in barrier function.

(a)

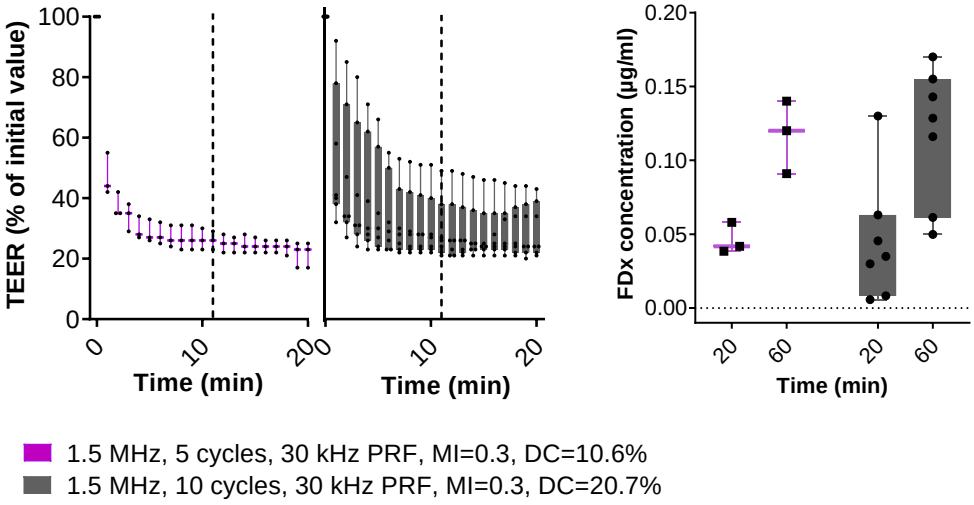

(b)

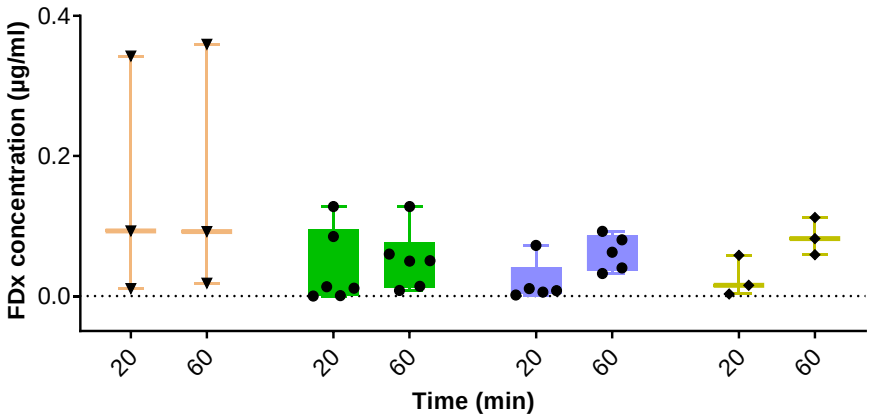

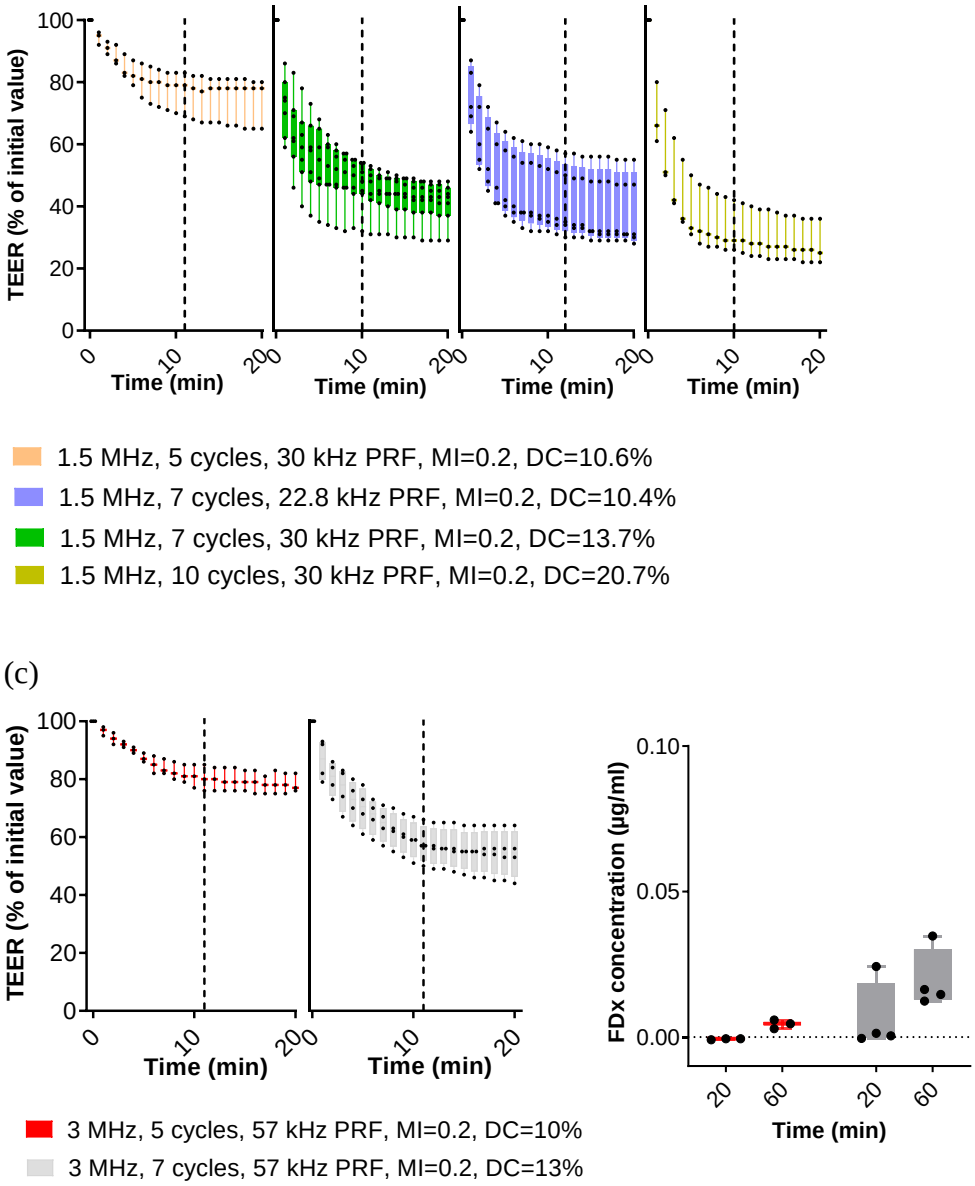

Figure 4-27 Effect of number of cycles on the barrier function. *Caco-2 cell layers were exposed to 5, 7 or 10 cycles to assess the effect of cycle number on the barrier function. In each graph (a-c), the number of cycles has been incremented sequentially. (a-c) each TEER graph indicates a correlation between increasing the number of cycles and decreasing the TEER. This is depicted by the FDx graphs in (a) and (c). The FDx graph in (b) suggests there might be an outlier in the first condition. The PRF and the DC could not be kept constant because the frequency and number of cycles depend on them. All experiments shown in this figure were conducted using 13 beams and 100 pulses. Dashed line indicates the end of the 11 min treatment. $n \geq 3$.*

Effect of pulse number on barrier function

The two pulse numbers tested were 10 and 100 pulses, Figure 4-28. 10 pulses decreased the barrier function to a minimum of 85% of its initial value, whereas 100 pulses decreased it to a minimum of 45% of its initial value. Although there is variation in the results with

10 pulses, it appears that more FD passed the barrier into the basolateral chamber when the layer was treated with 100 pulses rather than 10 pulses.

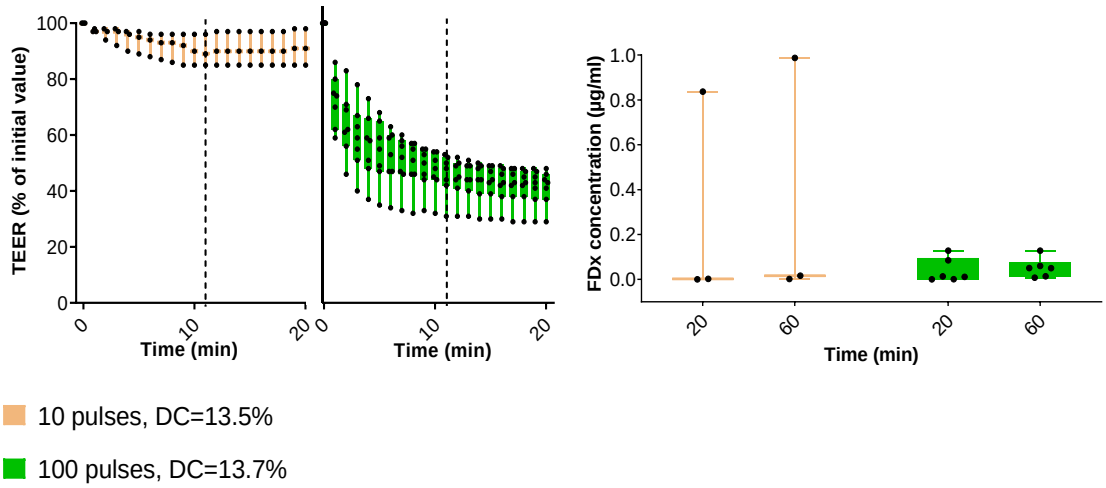

Figure 4-28. Effect of number of pulse on barrier function. *At the parameters studied, a tenfold increase in the number of pulses correlated with approximately a threefold decrease in TEER at the end of the 11 min insonation period. Both conditions were {1.5 MHz, 7 cycles, 30 kHz PRF, 13 Beams, MI = 0.2}. Dashed line indicates the end of the 11 min treatment. $n \geq 3$.*

Effect of number of beams on barrier function

An experiment was conducted to determine if a larger surface insonated correlates with a larger decrease in barrier function. The steering of the elements of the transducer can be controlled to produce a certain number of beams, Figure 4-29. The numbers of beams produced were 3, 6, 9 and 13. 3 beams decreased the TEER to ~80% of its initial value, 6 beams to ~60%, 9 beams to ~50% and 13 beams to ~35%, Figure 4-30. The graph of FDx concentration graph also suggests more FDx passed through the barrier into the basolateral chamber when more beams were produced, with the exception of the condition with 3 beams where the variation was very large.

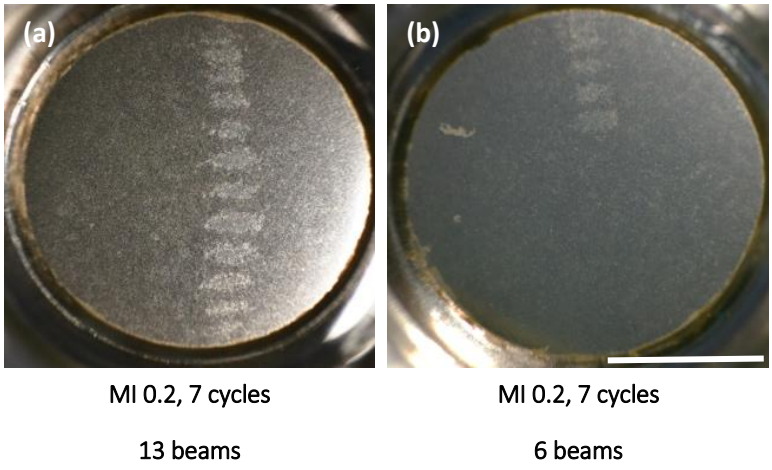

Figure 4-29 Top view of Caco-2 epithelium post-insonation *The Caco-2 cell layers were insonated with (a) 13 beams and (b) 6 beams. The effect on the epithelium could be observed with the naked eye. More oval-shaped insonation sites can be identified in (a) compared to (b). Scale bar = 6 mm.*

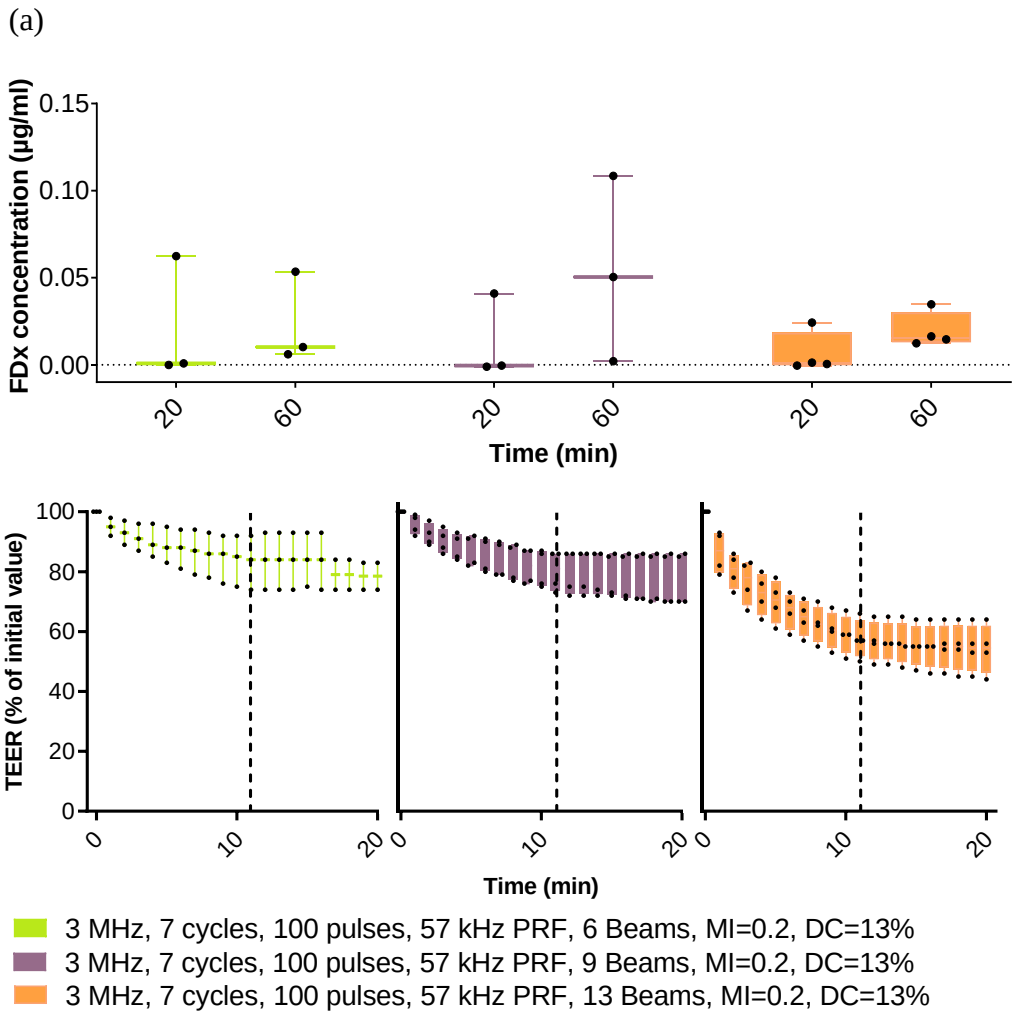

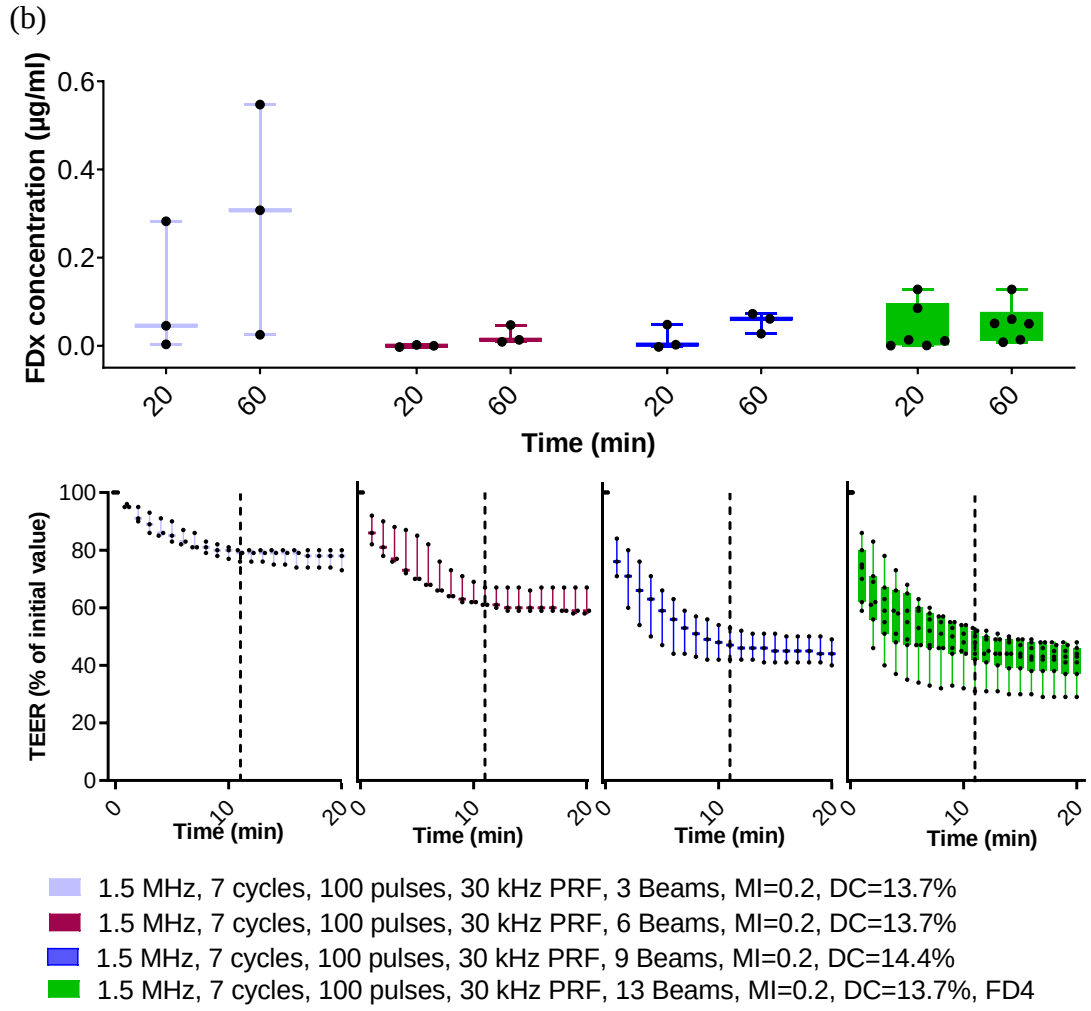

Figure 4-30 Effect of varying the number of beams. *Cell monolayers were exposed to 3, 6, 9 or 13 beams. (a-b) show the effect of increasing the number of beams sequentially. The TEER graphs show that a higher number of beams, correlating with a larger surface area treated, were associated with a larger decrease in TEER. FDx graph in (b) shows variation for the first condition, while the following three conditions depict a correlation between increasing the number of beams used and increasing the amount of FDx measured into the basolateral chamber. Dashed line indicates the end of the 11 min treatment. $n \geq 3$.*

Barrier function recovery

The recovery patterns of five samples were recorded for up to 12 h post-treatment. Following the experiment, the wells were returned to the incubator and were removed 3 h and 12 h later to record the TEER. When TEER dropped by 10%, it recovered within 3 h. However, when TEER dropped by ~50%, it did not recover within 12 h, Figure 4-31.

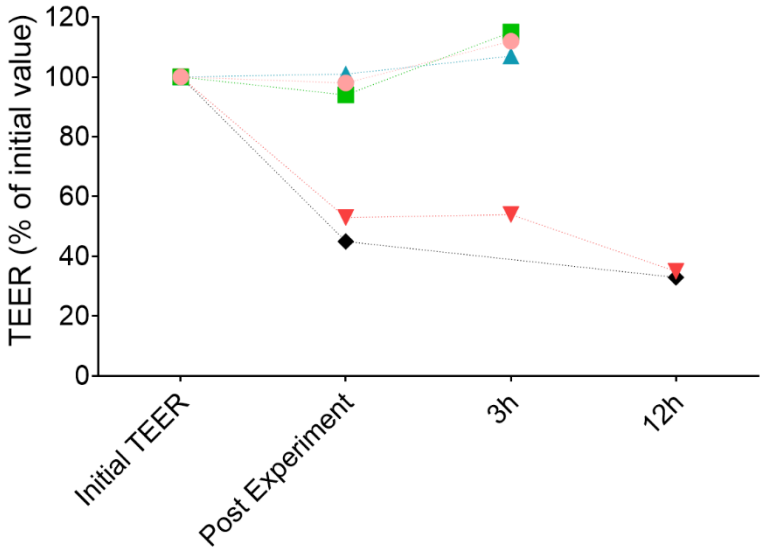

Figure 4-31 TEER recovery post insonation. *Following treatment, the TEER of cell layers was measured and they were returned to the incubator. They were retrieved either 3 h or 12 h later to measure the TEER of the cell layer. When the TEER dropped to half its initial TEER value, there was no recovery observed within 12 h.*

4.4.3 Section Discussion

Unfocused single-element transducer and phased array transducer experiments showed that a decrease in barrier function was associated with a lower transducer operating frequency, a higher MI, a higher number of cycles, a higher number of pulses and a higher number of beams.

Non-continuous insonation enables the MBs to diffuse to the central area when US is not delivered, and cavitate in that area once US is delivered (Choi *et al.*, 2011). This effect was used to open the blood-brain-barrier in a mouse model with an external focused transducer {f = 1.5 MHz, MI = 0.4, 3.45 cycles, PRF = 100 kHz, 1,000 pulses, 5 bursts/s, DC = 0.265%, burst repetition periods = 10, 1, 0.5, 0.2, 0.1 s, over 1 min treatment duration}. In the work described here, a different setup was used for a different application, but the focal area still needed to be replenished with MBs. Therefore, different combinations of cycle number, pulse number, reperfusion periods and burst numbers were used to identify the optimal parameters for decreasing the barrier function of the *in vitro* setup used.

Because of the multitude of variables in the process, they have not been unified into a single parameter, such as total delivered intensity for example. no published work was

found that correlates all of the aforementioned parameters in one, while also considering therapy effectiveness, which is the end goal. It may be that higher PNP administered continuously leads to more drug delivered, but it also may be that lower PNP, delivered intermittently to allow MB reperfusion could be equally effective (but take away the extra heating which is detrimental). Furthermore, it may be that a proportionally larger increase in DC would not correlate directly with a proportional decrease in PNP: i.e. {DC x 2, PNP x ½} may not be the same as {DC, PNP}.

The hardware used, the FI ToolBox and the two transducers, did not enable the investigation of the effect of frequencies other than 1.5 MHz and 3 MHz, a PRF > 57 kHz, a number of cycles > 100, DC > 30%. It cannot be suggested what the result on the tissue would be with other parameters and how this could be implemented into a unified measure.

In this work, frequency, cycles, PRF, DC were studied to make them as reproducible as possible.

Even in the absence of cells, FDx delivery to basal chamber can fluctuate by 10 µg/ml, Figure 4-7 (condition termed *No US, Transducer inserted*, depicted as a green square). When cells were added to the system, variation was still present. To compensate, several replicates were conducted for each condition. When data was analysed, the observed trend enabled conclusions to be drawn. Potential sources of variation inherent to the system included:

- ability to consistently work at focal length; when adjusting height of transducer, layers of plastic from well and insert obstructed visibility of fluid levels making precise adjustment difficult,

- difficult to detect air bubbles formed on the face of the transducer, which can obstruct US beams,

- variations were introduced by required assembly/disassembly of system and complexity of system, i.e. change ThinCerts and delivery tip, and

- because of capillary action, fluid could sometimes trickle up the suspension inlet while the pump was switched off; as a result, TEER sometimes increased towards the end of the 20 min recording time.

4.5 Cellular Effects of Sonoporation

The sections above report the effect of different US treatments on decreasing barrier function. This section describes some effects noticed at the cellular level to understand in more detail how different treatments decreased the barrier function and enabled FDx to move into the basolateral chamber. This section measured nuclei diameter and distribution as surrogate for the integrity of the cell layer and the distribution of cells within it.

Following insonation, cells were fixed in 4% PFA for 10 min. They were washed once in PBS, stained for 10 min with 1 µg/ml DAPI, then rinsed with PBS, and stained with 5 units/ml phalloidin (DyLight 550, catalogue no. 21835, Invitrogen, MA, USA). Following rinsing with PBS, the filters with cells were removed and mounted on microscope slides (Fisherbrand™ Frosted Microscope Slides, Thermo Fisher Scientific, Waltham, MA, USA) with mounting agent (ProLong™ Gold antifade mounting medium, Thermo Fisher Scientific, Waltham, MA, USA). Coverslips (no. 1.5, 22 x 22 mm2, Agar Scientific Ltd, Stansted, UK) were placed on top and nail varnish was used to seal them to the microscope slides. The slides were then imaged using a Zeiss LSM 710 or LSM 4 880 laser scanning confocal microscope (Carl Zeiss AG, Oberkochen, Germany).

4.5.1 Correlation between Presence of Pore and TEER Drop

The sample used for confocal microscopy was treated with US + MBs {f = 1.5 MHz, 10 cycles, 100 pulse, 13 beams, MI = 0.3, PRF = 30 kHz, DC = 20.7%}. It showed a TEER drop to 25% of the initial value (second condition, Figure 4-27 (a)). I used confocal microscopy to compare the appearance of insonated, edge-of-insonated and non-insonated areas, Figure 4-32. A hole with a diameter of 150 µm was detected in the sample. This suggests recovery did not take place because sealing such a pore might take longer than 12 h, Figure 4-31. Holes in Figure 4-32 generally correspond to the centre of the insonated areas.

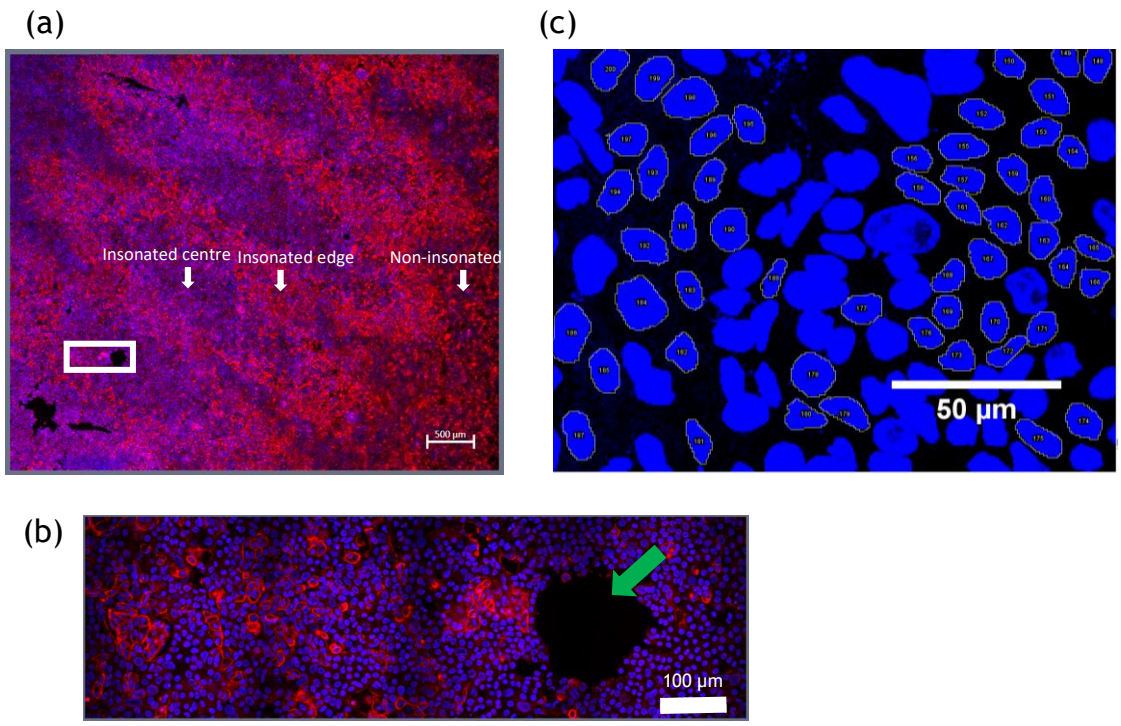

Figure 4-32 Effect of treatment on cell layer. *(a) Confocal microscope image of treated sample. The white rectangle shows the area magnified in (b); (b) The pore, green arrow, corresponds to the centre of the treated area. (c) Manually drawn nuclei to ensure exclusion of all overlapping nuclei and of those at overlapped junctions between two stitched images. Blue = DAPI, Red = Phalloidin.*

4.5.2 Effect of Insonation on Surface Area of Nuclei

To understand further the effect of the treatment on cells, the size, density and area covered by nuclei were calculated. Image analysis was performed using ImageJ (National Institute of Health, USA). Slices were overlapped and maximum intensity was selected. The contours of the nuclei were manually drawn, Figure 4-32 (c). Nuclei that were overlapped were not counted. Boundaries between two stitched images were avoided.

Three main observations were made. First, the average cross section of nuclei was significantly smaller in the centre of insonated and edge-of-insonated areas than in the non-insonated area, Figure 4-33 (a). It should be noted that cells are taken from a single biological replicate limiting the extent of this conclusion. The physical stress applied by the US + MBs + FDx treatment may have triggered the cells to slightly detach from the substrate, causing them to round up and become more spherical. This is expected to cause nuclei to become more spherical, too, resulting in a smaller cross section when viewed from the top. Second, there were 20% more nuclei per 1000 µm^2 on the edge-of-insonated area than in the insonated and non-insonated areas, Figure 4-33 (b). A possible reason is

that cells were pushed from the centre of the insonated areas towards the edge-of-insonated area. Third, in the centre of the insonated area, the surface area covered by nuclei was 10% smaller than in the non-insonated area and on the edge, Figure 4-33 (c).

A limitation of this experiment is that overlapped nuclei have not been accounted for because a top view is insufficient to distinguish reliably between many nuclei overlaid.

(a)

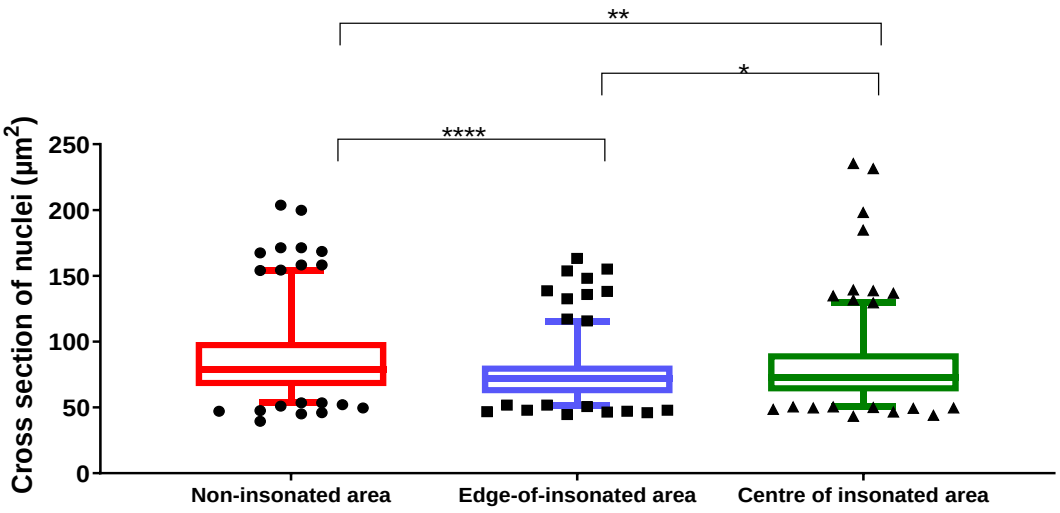

(b)

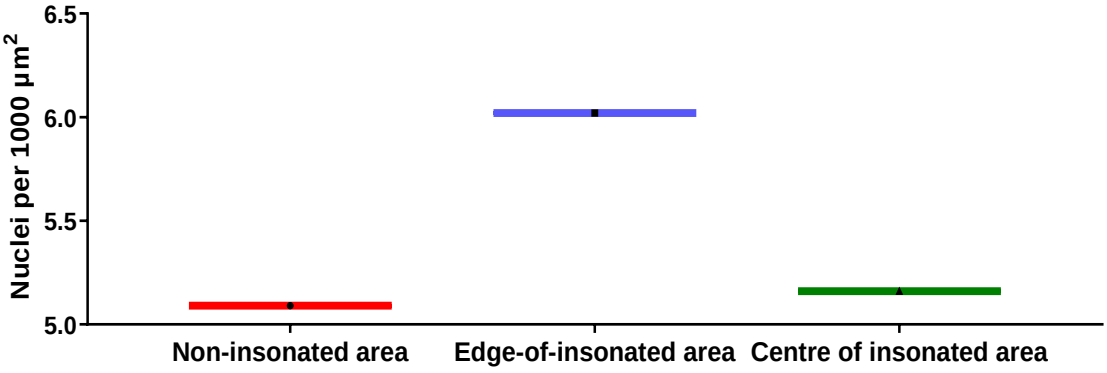

(c)

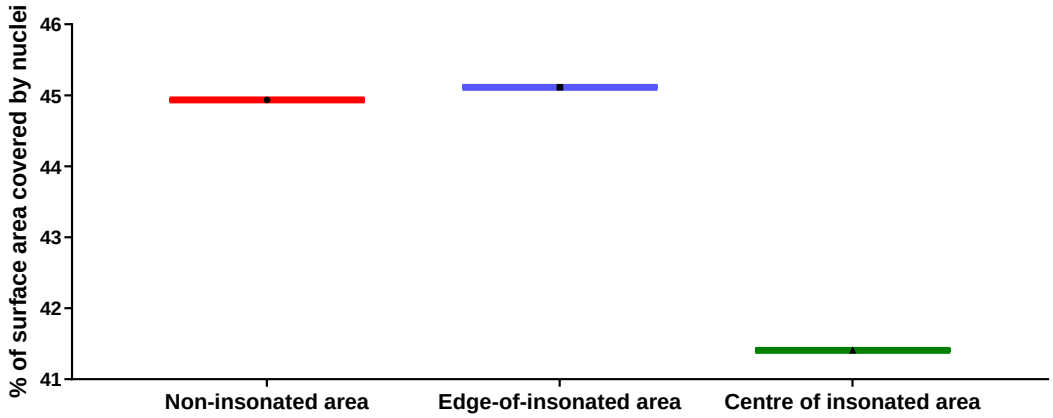

Figure 4-33 Effect of treatment on cells. *(a) Effect of treatment on the cross section of nuclei. The cross section of nuclei in non-insonated areas is significantly larger than on the edge and in the centre of insonated areas. Similarly, the cross section of nuclei on the edge-of-insonated areas was significantly larger than in the centre of insonated areas. n = 200 cells from a single biological sample, 5 – 95 percentile, Welch's Paired t-test. One-WAY ANOVA, p<0.0001. Points are extremums. (b) Effect of treatment on the density/number of nuclei. There were more nuclei on the edge-of-insonated areas compare to non-insonated and centre of insonated areas. Counted 380 – 450 nuclei per 250 x 300 μm^2 per condition. (c) Effect of treatment on the number and size of nuclei. The percentage of surface area covered by nuclei in the centre of insonated areas was smaller than on the edge and in non-insonated areas.*

4.5.3 Actin Distribution Across Insonated and non-Insonated Areas

This section further investigates the effects of the treatment on the cytoskeleton, specifically on actin filaments.

Actin is a cytoskeletal protein that forms microfilaments and is essential for cell shape, internal organisation, division and movement (Dominguez and Holmes, 2011). Actin exists as a globular monomer (G-actin) or as a filamentous polymer (F-actin), which is a chain of G-actin subunits. Phalloidin binds to F-actin, stabilises it and inhibits its depolymerisation, specifically at the junction between F-subunits, locking adjacent subunits together. At a molecular level, actin inhibits ATP hydrolysis by trapping ADP. Phalloidin has a higher specificity for F-actin than for G-actin.

In the present work, phalloidin staining appears more prominent on the edge of the insonated area, Figure 4-34 (b), than in the centre of the insonated area, Figure 4-34 (c). This suggests the treatment I applied to the cell layers, i.e. cavitation, may deplete cells of

F-actin. These observations are only qualitative as only one sample was stained with phalloidin.

The literature confirms this suggestion. According to Chen *et al.*, 2014, sonoporation leads to less F-actin and more G-actin. The actin cytoskeleton represents filaments physically interconnected with the plasma membrane. Hence, external physical stress (cavitation) will affect the cytoskeleton and the F-actin structure. Using a mathematical and statistical model, they have estimated that the required time for actin network disassembly was of the order of seconds. Viable sonoporated cells are more round in shape than sham control. Non-viable sonoporated cells showed irregular budding along the membrane, suggestive of apoptosis.

Filaments in the process of being dissembled might not be identified in the confocal images shown here. Phalloidin staining of F-actin can be hindered by cofilin, proteins that bind to F-actin and depolymerise it into G-actin (McGough *et al.*, 1997). Phalloidin needs to binds to seven actin subunits to stain successfully the filament (Kristó *et al.*, 2016). Hence, short F-actin polymers will not be stained.

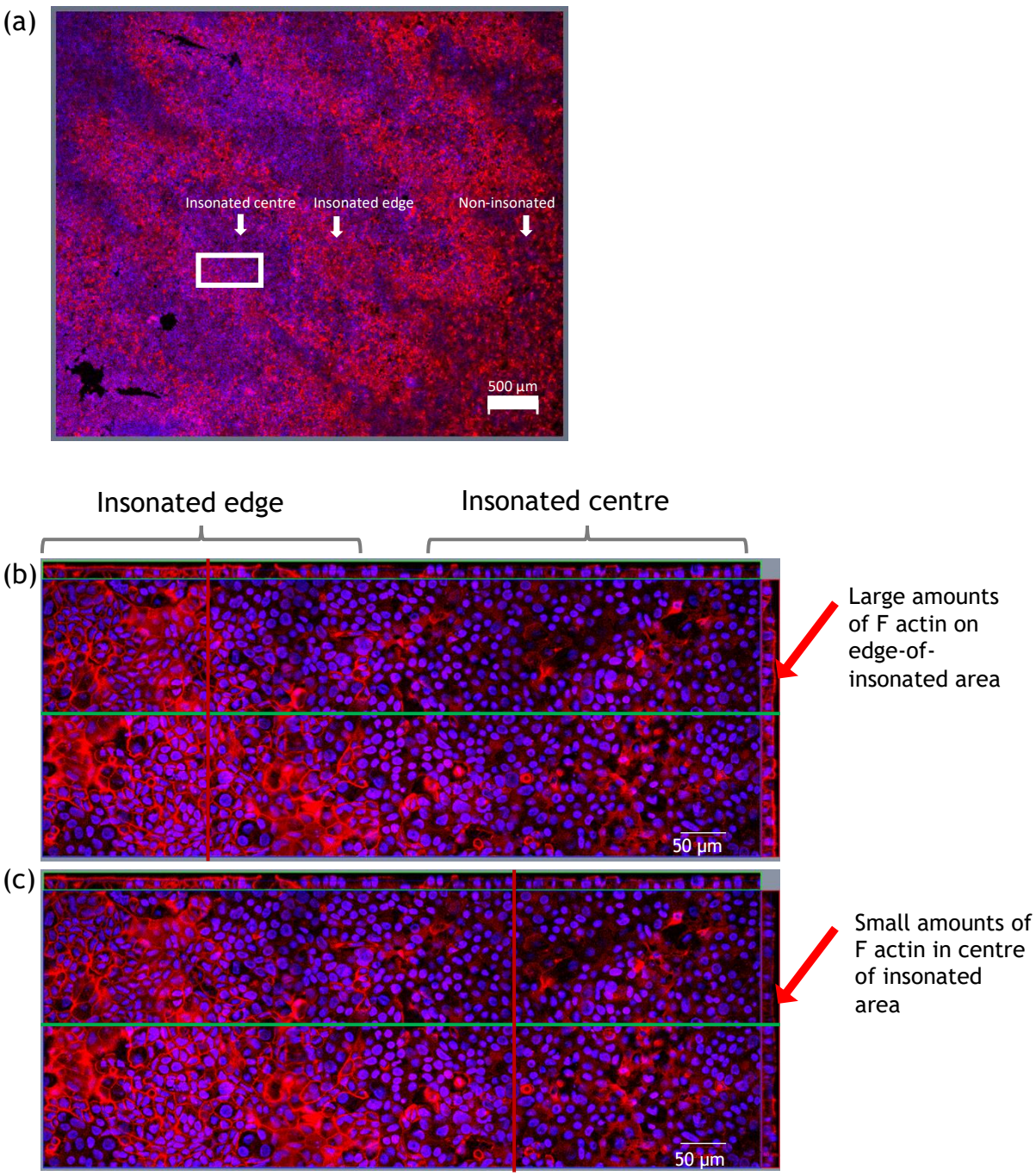

Figure 4-34 Effect of treatment on actin. *(a) White rectangle indicates the area magnified in (b) and (c). They are orthoviews of the sample: the top (green) panel shows the depth of the central green slice, while the (red) right panel shows the depth of the vertical red line. (b) Large amounts of F-actin appear on the edge-of-insonated sample. (c) Vertical panel through centre of insonated area shows small amounts of actin present. These observations are only qualitative as they are based on only one sample. Red = phalloidin, Blue= DAPI.*

4.6 Discussion

In this chapter, a ThinCert model was used to identify suitable US transducers and operating protocols to decrease the barrier function of intestinal cell layers *in vitro*.

While the setup was suitable for the focused single element transducer with a central delivery channel, it had to be adapted for the unfocused single-element and phased array transducers to deliver US + MBs in proximity to the cell layer. The decrease in barrier function was quantified by measuring the decrease in TEER and by the amount of FDx that crossed into the basolateral chamber.

Focused single-element transducers had a weak effect on promoting FD transfer across the monolayer, potentially due to the transducer's small focus area. Unfocused and phased array transducers had stronger effects, potentially due to the larger surface areas they treated.

Relying only on the TEER drop to assess the transducers is not reliable, because the formation of a single pore in the monolayer will result in a large drop in TEER, not accounting for its size or the potential presence of several pores. The amount of FDx crossing the cell barrier is a more suitable readout as passive diffusion is larger when the filter surface not covered by cells (i.e. the pore) is larger.

US did not facilitate movement of FDx into the basolateral chamber in the absence of cells Figure 4-7. Compound movement was facilitated by passive diffusion. US + MBs produced pores in the cell layer, Figure 4-32, which enabled passive diffusion to take place.

The unfocused transducer enabled more FD to cross the monolayer at MI = 0.4, Figure 4-20, compared to any phased array transducer condition at MI = 0.4, Figure 4-23 - Figure 4-30.

Unfocused single-element and phased array transducer experiments showed that decreased barrier function was associated with lower frequencies, a higher MI, more cycles, more pulses and more beams. Some conditions enabled the decrease in barrier function to as low as 20% of the initial value within seconds and created large pores, suggesting the technology is efficient. However, such parameters did not enable the tissue to seal the pore in a timely manner.

Rather than quickly creating large pores in a cell layer that cannot seal swiftly, it is better to create many small pores that are present sufficiently long (i.e. 11 min) to enable passive diffusion, but that still can recover swiftly. To achieve this, it is necessary to have better control over the beam produced. This was achieved by using 24-element phased array transducers. This allowed more control over the number of cycles, pulses, bursts, surface area insonated (beams) and pauses between transmission. The particular parameter set identified as optimal was {f = 1.5 MHz, PRF = 50 kHz, DC = 30%, MI = 0.2, 10 cycles, 100 pulses}. At a higher MI (MI = 0.3), pores formed and did not seal within 12 h. There should be less damage inflicted on the layer at MI = 0.2, while still allowing a considerable amount of model drug to cross the cell layer, as depicted by the 4^{th} to the 5^{th} condition in Figure 4-26 (b). The number of beams (1 to 13) correlates with the surface area insonated, so 13 beams should be chosen to maximise the area treated.

These parameters are suggested as a starting point for *in vivo* experiments. Phased array transducers were miniaturised and incorporated into capsules and tested *in vivo*, as described in Chapter 6.

A classical way to identify whether cavitation takes place in a well is to deliver a pulse and then use the transmitting transducer as a receiver. While this could have been done with the unfocused single-element transducer, it was not feasible with the phased array transducer because the FI ToolBox used software that did not enable the use of the transducer as a receiver. To do this in the future, different software would need to be developed.

4.7 Conclusions

This chapter showed how US + MBs can reduce the epithelial barrier and facilitate delivery of model drugs through a cell layer. The effect was stronger with US transducers with wide focal areas: phased array and unfocused transducers produced a larger drop in barrier function than focused transducers. The phased array transducers could even disrupt the monolayer and produce large pores.

In the next two chapters, investigations of *in vitro* models are described for studying USmTDD. Chapter 6 draws on the present chapter directly by implementing a phased array transducer in a capsule to deliver insulin to the porcine small intestine *in vivo*.

4.8 References

Ahn, G.Y., Eo, H.-S., Kim, D., Choi, S.-W., 2020. Transdermal delivery of FITC-Dextrans with different molecular weights using radiofrequency microporation. Biomater Res 24, 22. https://doi.org/10.1186/s40824-020-00201-7

CDER/FDA, 2015, Guidance for Industry, Waiver of in vivo bioavailability and bioequivalence studies for immediate release solid oral dosage forms based on a biopharmaceutics classification system, Center for Drug Evaluation and Research.

Chen, X., Leow, R.S., Hu, Y., Wan, J.M.F., Yu, A.C.H., 2014. Single-site sonoporation disrupts actin cytoskeleton organization. J. R. Soc. Interface. 11, 20140071. https://doi.org/10.1098/rsif.2014.0071

Choi, J.J., Selert, K., Vlachos, F., Wong, A., Konofagou, E.E., 2011. Noninvasive and localized neuronal delivery using short ultrasonic pulses and microbubbles. Proceedings of the National Academy of Sciences 108, 16539–16544. https://doi.org/10.1073/pnas.1105116108

Dahle, S., Meuthen, J., Viöl, W., Maus-Friedrichs, W., 2013. Adsorption of silver on glucose studied with MIES, UPS, XPS and AFM. Applied Surface Science 284, 514–522. https://doi.org/10.1016/j.apsusc.2013.07.126

Dominguez, R., Holmes, K.C., 2011. Actin Structure and Function. Annu. Rev. Biophys. 40, 169–186. https://doi.org/10.1146/annurev-biophys-042910-155359

Frost, T.S., Jiang, L., Lynch, R.M., Zohar, Y., 2019. Permeability of Epithelial/Endothelial Barriers in Transwells and Microfluidic Bilayer Devices. Micromachines (Basel) 10, E533. https://doi.org/10.3390/mi10080533

Guariguata, A., Pascall, M.A., Gilmer, M.W., Sum, A.K., Sloan, E.D., Koh, C.A., Wu, D.T., 2012. Jamming of particles in a two-dimensional fluid-driven flow. Phys. Rev. E 86, 061311. https://doi.org/10.1103/PhysRevE.86.061311

Guertin, D.A., Sabatini, D.M., 2006. Cell Size Control, in: John Wiley & Sons, Ltd (Ed.), Encyclopedia of Life Sciences. John Wiley & Sons, Ltd, Chichester, UK, p. a0003359. https://doi.org/10.1038/npg.els.0003359

Guo, S., Liang, Y., Liu, L., Yin, M., Wang, A., Sun, K., Li, Y., Shi, Y., 2021. Research on the fate of polymeric nanoparticles in the process of the intestinal absorption based on model nanoparticles with various characteristics: size, surface charge and pro-hydrophobics. J Nanobiotechnol 19, 32. https://doi.org/10.1186/s12951-021-00770-2

Kristó, I., Bajusz, I., Bajusz, C., Borkúti, P., Vilmos, P., 2016. Actin, actin-binding proteins, and actin-related proteins in the nucleus. Histochem Cell Biol 145, 373–388. https://doi.org/10.1007/s00418-015-1400-9

Leber, B., Mayrhauser, U., Leopold, B., Koestenbauer, S., Tscheliessnigg, K., Stadlbauer, V., Stiegler, P., 2012. Impact of temperature on cell death in a cell-culture model of hepatocellular carcinoma. Anticancer Res 32, 915–921.

Liu, M., Zhang, S., Cui, S., Chen, F., Jia, L., Wang, S., Gai, X., Li, P., Yang, F., Pan, W., Yang, X., 2017. Preparation and evaluation of Vinpocetine self-emulsifying pH gradient release pellets. Drug Deliv 24, 1598–1604. https://doi.org/10.1080/10717544.2017.1388453

Mannaris, C., Averkiou, M.A., 2012. Investigation of Microbubble Response to Long Pulses Used in Ultrasound-Enhanced Drug Delivery. Ultrasound in Medicine & Biology 38, 681–691. https://doi.org/10.1016/j.ultrasmedbio.2011.12.018

McGough, A., Pope, B., Chiu, W., Weeds, A., 1997. Cofilin Changes the Twist of F-Actin: Implications for Actin Filament Dynamics and Cellular Function. Journal of Cell Biology 138, 771–781. https://doi.org/10.1083/jcb.138.4.771

Meunier, V., Bourri, M., Berger, Y., Fabre, G., 1995. The human intestinal epithelial cell line Caco-2; pharmacological and pharmacokinetic applications. Cell Biol Toxicol 11, 187–194. https://doi.org/10.1007/BF00756522

Moldovan, A., 2021. Development of a 1D Phased Ultrasonic Array for Intravascular Sonoporation (Doctoral Thesis). University of Strathclyde, Glasgow.

Powell, D.W., 1981. Barrier function of epithelia. Am J Physiol 241, G275-288. https://doi.org/10.1152/ajpgi.1981.241.4.G275

Rappel, W.-J., Edelstein-Keshet, L., 2017. Mechanisms of Cell Polarization. Curr Opin Syst Biol 3, 43–53. https://doi.org/10.1016/j.coisb.2017.03.005

Shung, K.K., 2015. Diagnostic Ultrasound: Imaging and Blood Flow Measurements, Second Edition, 0 ed. CRC Press. https://doi.org/10.1201/b18323

Stewart, F., 2018. Capsule-based Ultrasound-mediated Targeted Drug Delivery (Doctoral Thesis). University of Dundee, Dundee.

Stewart, F., Qiu, Y., Lay, H., Newton, I., Cox, B., Al-Rawhani, M., Beeley, J., Liu, Y., Huang, Z., Cumming, D., Näthke, I., Cochran, S., 2017. Acoustic Sensing and Ultrasonic Drug Delivery in Multimodal Theranostic Capsule Endoscopy. Sensors 17, 1553. https://doi.org/10.3390/s17071553

van der Meer, S.M., Versluis, M., Lohse, D., Chin, C.T., Bouakaz, A., Jong, N. d., 2004. The resonance frequency of SonoVue as observed by high-speed optical imaging, in: IEEE Ultrasonics Symposium, 2004. Presented at the IEEE Ultrasonics Symposium, 2004, IEEE, Montreal, Canada, pp. 343–345. https://doi.org/10.1109/ULTSYM.2004.1417735

Wang, M., Zhang, Y., Cai, C., Tu, J., Guo, X., Zhang, D., 2018. Sonoporation-induced cell membrane permeabilization and cytoskeleton disassembly at varied acoustic and microbubble-cell parameters. Sci Rep 8, 3885. https://doi.org/10.1038/s41598-018-22056-8

Chapter 5
An Organoid-derived Cell Layer as an *in vitro* Model for Drug Delivery Studies

This chapter builds on the results obtained in Chapter 4 by testing the effect of the insonation treatment on an *in vitro* model physiologically more similar to the *in vivo* tissue than the Caco-2 monolayer used in Chapter 4. The work in this Chapter explored the feasibility of growing layers of cells derived from OGs grown from porcine small intestine and rectum, Figure 5-1. I compared the effect of US + MBs on the barrier function of a classic cell layer (Caco-2) and of an OG-derived cell layer. I then compared two different CAs in combination with US for decreasing the barrier function of a rectum OGs-derived cell layer and delivering insulin, as an example of a macromolecular drug, across the layer. I also assessed whether barrier function recovery takes place following insonation.

The response to therapeutic agents observed in in vitro systems and in animal models are not always consistent. Only ~12% of therapeutic agents are successful in preclinical testing and enter clinical trials (Van Norman, 2019). This suggests in vitro assays do not replicate in vivo conditions accurately. However, it is generally recommended that researchers should strive to replace animal studies with non-animal alternatives, reduce the number of animals used and refine methods by minimising animal suffering, collectively known as the three Rs (Goldberg *et al.*, 1996). One way of many to contribute to this is by developing more human-like *in vitro* systems for testing.

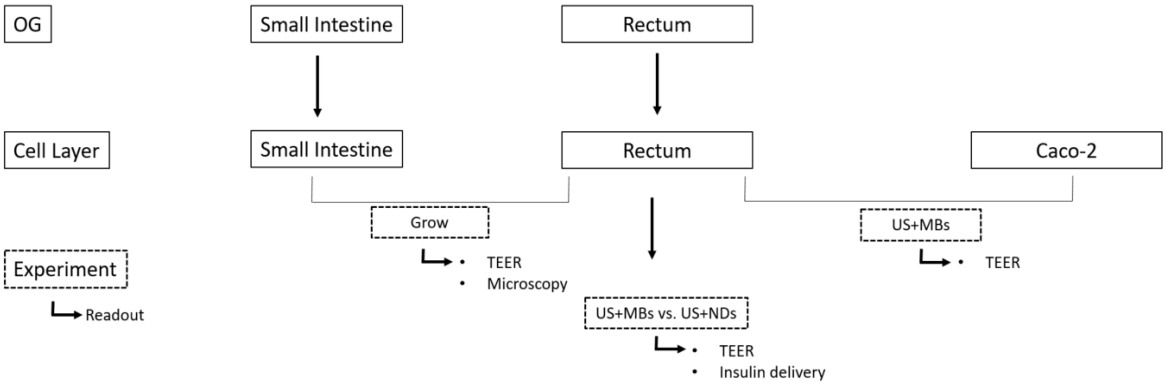

Figure 5-1 Overview of experiments presented in Chapter 5. *Where OG=organoid; ND=nanodroplets; MB=microbubbles. OGs were derived from small intestinal and rectal tissue. These were then plated as 2D cell layers and their barrier function was assessed using TEER measurements. The cell layers derived from rectal tissue were treated with US + MBs or US + NDs and the results were compared in terms of barrier function (TEER) and insulin delivery across the cell layer. The barrier functions of these cell layers were also compared to Caco-2 layers upon treatment with US + MBs.*

The areas of research that can be addressed by cell cultures include fundamental cell research, vaccine manufacture, regenerative medicine, drug discovery and disease and organ models. The global market for *in vitro* systems was valued at ~$2bn in 2020, with a CAGR of 16 – 24% (Manchester BioGel, 2020), further suggesting there is scope for developing more appropriate *in vitro* systems. A potentially more relevant cell culture system is described below.

5.1 Cells of the Intestinal Epithelium

As noted previously, the human epithelial colorectal adenocarcinoma (Caco-2) cell line is an FDA approved *in vitro* model for intestinal US-mediated drug delivery studies (CDER/FDA, 2015). As its name suggests, Caco-2 cells are isolated from tumorous colorectal tissue. However, *in vivo* small intestinal tissue contains stem cells, which can differentiate into cells responsible for compound absorption, mucus secretion and immunity. A heterogeneous *in vitro* model containing all the types of cells present *in vivo* would be more physiologically relevant and could therefore increase the probability of consistency between the observations made *in vitro* and *in vivo*. Thus, the drawback of the Caco-2 model could be addressed using cell layers derived from primary cells or intestinal OGs. The use of primary cells would require large areas of fresh human or animal intestinal tissue every time more cell layers are necessary. This would increase the number of animals sacrificed for research, while human intestinal biopsies are not available on

demand. Intestinal OGs are advantageous as they can be grown from small tissue biopsies, expanded and be readily available whenever more cell layers are necessary.

OGs are grown from crypts isolated from fresh intestinal tissue. Crypts are invaginations in the mucosa of the epithelium and are surrounded by many villi, finger-like protrusions in the mucosa (Lieberkühn, 1745), Figure 5-2 (a). The intestinal epithelium consists of millions of such crypt-villus structures. As outlined in Chapter 2, the villi increase the surface area of the intestine and thus increase the capacity to absorb nutrients. Capillaries and lymph vessels underneath the epithelium carry the nutrients via the hepatic portal circulation to the liver.

The following two paragraphs present details of the complex morphology and function of intestinal crypts to help the reader understand that Caco-2 cell layers do not represent the normal gut mucosa.

Crypts are invaginations and protected from the harsh environment necessary for digestion in the lumen, Figure 5-2 (c). They contain stem cells, crypt base columnar (CBC) cells and Paneth cells. CBC cells divide and become intestinal stem cells. Each CBC cell comes into contact with at least one Paneth cell (Sato, *et al.*, 2011). Paneth cells secrete antimicrobial products, which protect the crypt base and mix with the mucous to offer protection along the intestinal mucosa. Paneth cells also secrete growth factors for stem cells.

Stem cells divide and the resulting cells have equal chances to remain stem cells in the crypt or differentiate into lineage-committed progenitor cells and get pushed towards the villus by freshly divided cells, Figure 5-2 (c). The lineage-committed progenitor cells, also called transit amplifying cells, give rise to absorptive cells (enterocytes and M cells) or secretory cells (goblet, enteroendocrine or Tuft cells): enterocytes absorb ions, water, sugars, peptides and lipids; M cells transport antigens from the intestinal lumen to B cells, T cells and mononuclear cells; goblet cells secrete mucus, which protects the mucosa against pathogens and hazards of the digestive processes, Figure 5-2 (b); enteroendocrine cells control the metabolism, whereas Tuft cells regulate immunity against helminths (Gehart & Clevers, 2019). Mature cells can dedifferentiate if they re-enter the crypt; otherwise, they are shed after migrating upwards towards the villus tip usually within 4 – 5 days (Stange, *et al.*, 2013).

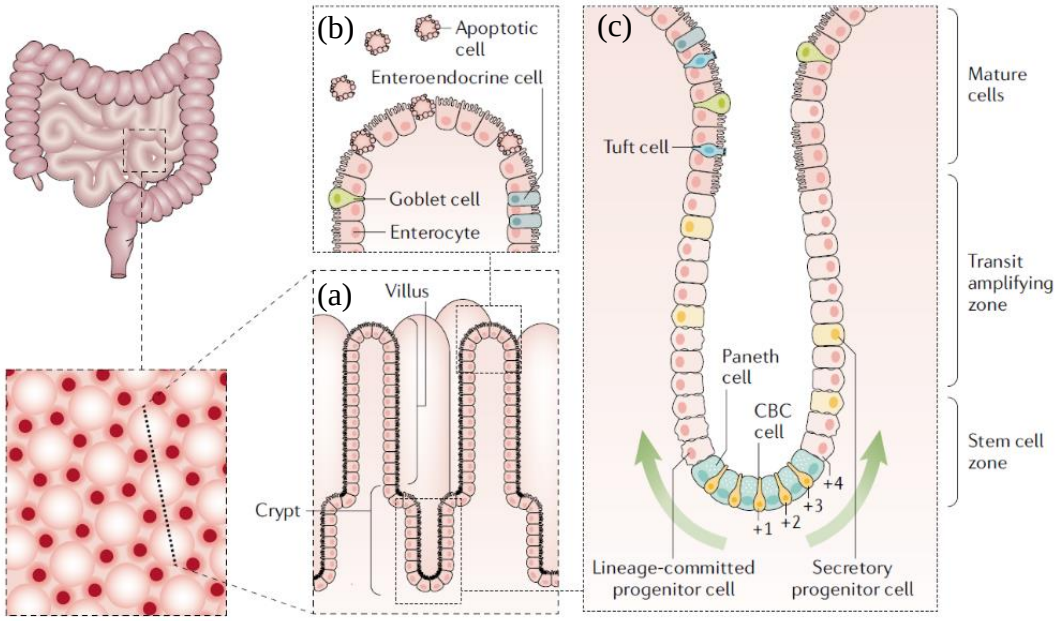

Figure 5-2 Morphology of intestinal crypts and villi. *(a) The lining of the intestine is organised in crypts and villi to increase the surface areas of the intestine. (b) Villi contain differentiated cells, such as enteroendocrine cells, goblet cells and enterocytes. (c) In contrast, crypts contain progenitor cells (CBC) and Paneth cells in the stem cell zone, or on the bottom of the crypt and Tuft cells in the area with mature cells (Adapted from Gehart and Clevers, 2018).*

5.2 Development of an Organoid-derived Cell Layer

This section presents how stem cells were harvested from porcine rectum and small intestine, cultured to grow into OGs, how these OGs were plated as a 2D layer of cells and how these layers developed over several weeks of culture. The work presented in this chapter was conducted while on placement at Curileum Discovery Ltd., The Griffin Institute, Harrow, UK.

5.2.1 Experimental Setup and Method

5.2.1.1 Isolation of Porcine Crypts

Porcine gut tissue from 4 – 6 month old Yorkshire pigs was kindly provided by The Griffin Institute (Harrow, UK). The mucosal tissue was cut with scissors into small pieces and rinsed three times with cold DPBS (D8537, ThermoFisher, UK) + 1% P/S (P0781, Sigma, UK) + 0.5% neomycin (N1142, Sigma, UK) in a Petri dish. The tissue was transferred to a 15 ml Falcon tube and washed vigorously five times. The washed tissue was transferred to a small cell culture dish with 10 ml of 1 mg/ml collagenase (C9407, Sigma, UK) in PBS and was incubated on a shaker at 38° C for 40 min. The collagenase was aspirated and the

tissue was resuspended in 10 ml of serum-free media (AIM V, 12055091, ThermoFisher, UK). The cell flask was tapped vigorously against the hand to release crypts from the tissue. The suspension was passed through a 250 µm filter to separate the released crypts from the rest of the tissue. A white-light inverted cell culture microscope (CKX53, Olympus, Essex, UK) was used to count the crypts in the media. This step enabled quality control and adjustment of crypt concentration per suspension volume for later stages.

The suspension with crypts was centrifuged at 150 G for 5 min at 4°C. The supernatant was removed and the crypts were resuspended into 200 µl media and 150 µl matrigel (MG, 354230, Corning, UK). 50 µl of the suspension was then plated in the middle of the wells of a warm non-adherent 24 - well plate (144530, Nunc, ThermoFisher, UK). The plate was incubated at 37°C for 30 min. 500 µl of warm full OG media (OGM) were then added to each well and the plate was returned to the incubator. Full OGM (OGMH) consisted of 98.9% IntestiCult Component A and B (06010, Stem Cell Technologies, Cambridge, UK) + 1% P/S (P0781, Sigma, UK) + 0.1% Y27632 (72304, Stem Cell Technologies, Cambridge, UK).

5.2.1.2 Passaging of Organoids

Isolated crypts were passaged approximately once a week. Media from each well was aspirated and 300 µl of cold AIM V was added to each well. The suspension was pipetted up and down until the MG dome detached from the well. The suspension was transferred to a Falcon tube and syringed up and down 10x with a P1000 pipette to disrupt the OGs. The suspension was made up to 10 ml with AIM V and centrifuged for 5 min at 300 G at 4°C. The supernatant was aspirated and cells were suspended into 50% MG + 50% pellet. 50 µl of the suspension were plated on each well of a warm non-adherent 24 - well plate. The plate was then incubated at 37 °C for 30 min. 500 µl of full OGM were then added to each well and returned to the incubator.

5.2.1.3 Plating of Organoids to Create Cell Layers

OGs were grown in MG domes for a week. Three MG domes were harvested for each ThinCert filter (200 – 250 OGs). The medium was removed and each MG dome was dissolved in cold PBS. The contents of the three wells were transferred to a 15 ml tube and topped up to 10 ml with cold PBS. The tube was centrifuged at 300 G for 5 min. The supernatant was discarded and the pellet was resuspended in 3 ml ice-cold DMEM/F-12 (11330032, Gibco, UK). The tube was centrifuged at 200 G for 5 min at 5°C. The

supernatant was removed and the pellet was resuspended in 1 ml TrypLE (12604013, Gibco, UK) at 37°C. The suspension was mixed thoroughly and incubated at 37°C for 5 - 10 min. The OGs were then disrupted by syringing them several times with a 1 ml syringe. 1 ml DMEM/F-12 was added to the suspension and the tube was centrifuged at 200 G for 5 min at 5°C. The supernatant was discarded and the pellet was resuspended in growth medium: 49% OGM + 49% DMEM/F-12 + 2% P/S. 0.5 ml of the suspension was then plated on ThinCert filters (665641, Greiner Bio-One, UK). The basolateral chamber received 1.5 ml of the same medium without cells, Figure 5-3. The TEER of the filter was recorded every 2 – 3 days from Day 8 onwards. Medium was replaced every 3 – 4 days. Images were acquired with a GXCAM HiChrome-MET camera (GT Vision, UK) connected to the white-light inverted cell culture microscope mentioned above.

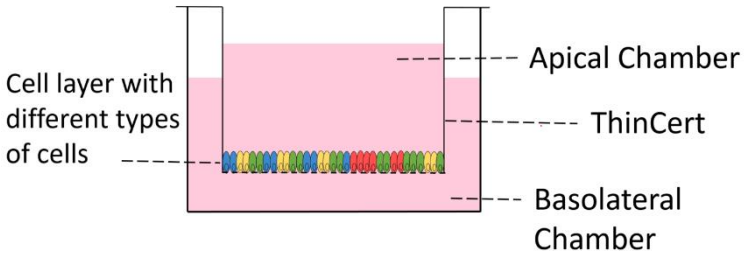

Figure 5-3 Well with cell monolayer of different cell types grown on a ThinCert.

5.2.2 Results

5.2.2.1 Porcine Rectum Organoid-derived Cell Layers Cycle between Confluent and Detached until Reaching a Plateau

Figure 5-4 presents the development of an OG-derived layer of cells over 14 days of culture. The layer was fully confluent by Day 7, it started to disintegrate at Day 12, was maximally disintegrated at Day 16 and became confluent again at Day 19. These observations are consistent with the observed fluctuations in TEER, Figure 5-5, suggesting the tissue layer went through periods of growth, cell death and cell re-growth. Between days 35 and 50 the TEER fluctuated less, suggesting a plateau was reached. Images acquired on Day 45 show areas where multilayers could have formed. Experiments were conducted around Day 50 of culture.

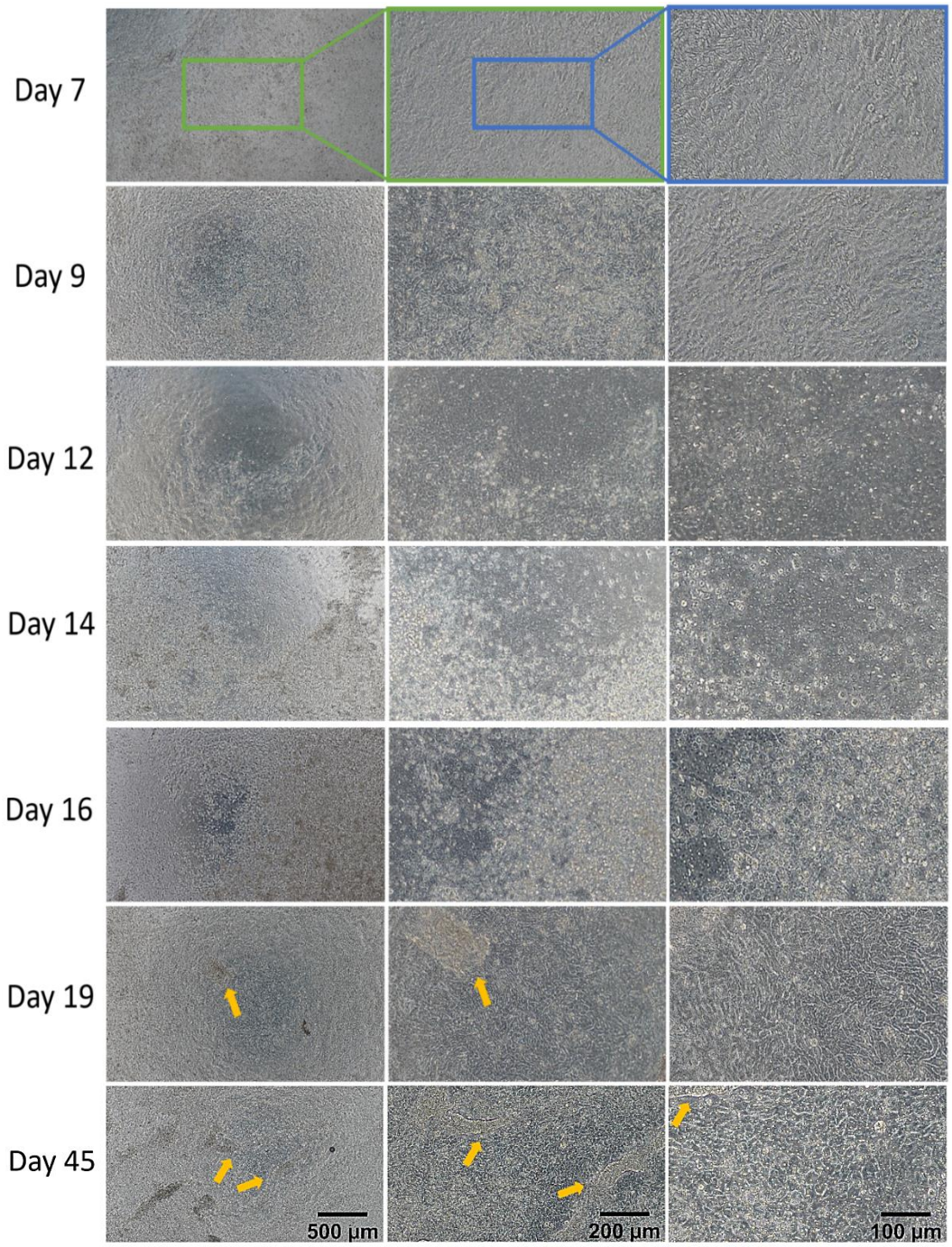

Figure 5-4 Bright-field images of a layer of cells derived from porcine rectal OGs. *Between Day 7 and Day 19 of culture, the layers underwent periods of confluency, detachment from the filter and confluency again. Yellow arrows point towards areas where a multilayer was visible. Central panels represent magnified images of the central regions of the left panel and right panels represent magnified images of the central regions of the central panels. The scale bar displayed on the bottom row applies for the entire column.*

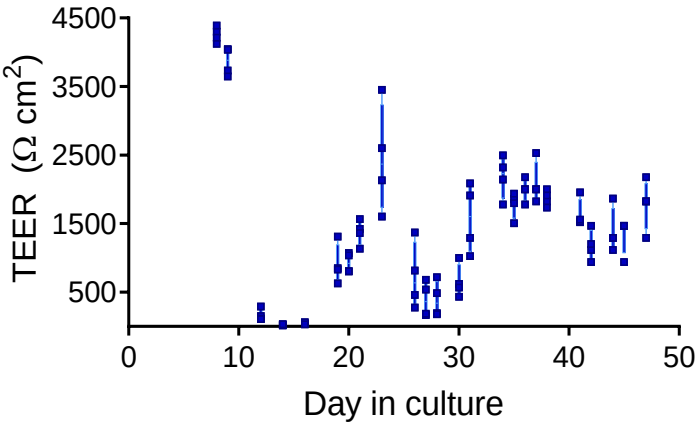

Figure 5-5 Fluctuation of barrier function of a cell layer derived from porcine rectal OGs. *TEER was measured on different days after plating crypts on four ThinCerts. One reading per well was taken each time. Between Day 8 and Day 47 of culture, the TEER fluctuated between 100 and 4400 Ω cm^2. A high TEER recorded on Day 8 was followed by low TEER on Day 15, high TEER around Day 23, low TEER on Day 28 and high TEER on Day 35, which then fluctuated less. n = 4.*

5.2.2.2 Porcine Small Intestine Organoid-derived Cell Layers did not Become Confluent

Cell layers derived from small intestine porcine OGs would have been a relevant tissue model for small intestine drug delivery studies. However, as seen in Figure 5-6, the TEER did not exceed 250 Ω/cm^2 even after 20 days in culture. The expected TEER value was around 800 Ω/cm^2 by Day 10 of culture (Speer, *et al.*, 2019). Given that the values obtained were lower and the layer of cells did not appear confluent even after 20 days, rectum derived cell layers were used for subsequent experiments.

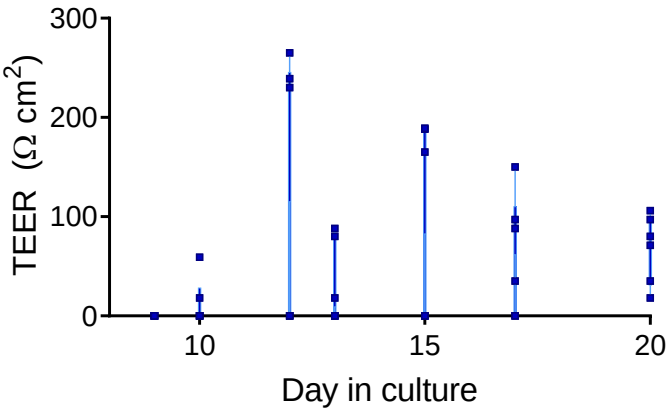

Figure 5-6 Fluctuation of barrier function of a cell layer derived from porcine small intestine OGs. *TEER was measured on different days after plating crypts on six ThinCerts. One reading per well was taken each time. Between Day 9 and 20 of culture, the TEER fluctuated between 0 and 230 Ω cm^2. Note difference in TEER scale between Figure 5-5 and Figure 5-6. TEER values recorded in Figure 5-5 are up to fifteen fold larger than those in this figure. n = 6.*

5.3 US + MBs can Decrease the Barrier Functions of Caco-2 and Rectum Organoid-derived Cell Layers

5.3.1 Experimental Setup and Method

Porcine rectal OGs were dissociated into single cells and seeded onto filters as described above. Caco-2 cells (ATCC, USA) were also seeded onto ThinCert filters and once they became confluent, they were grown for at least 3 weeks to differentiate and polarise (See full cell culture protocol in 3.1.1.5). On the day of the experiment, the medium was removed from the cells and the filters were rinsed once with HBSS (14170112, Gibco, UK) at RT to further remove phenol red. 0.9 ml HBSS at RT was added to each apical chamber and 1.5 ml HBSS to each basal chamber, Figure 5-3. The cells were allowed to acclimatize at RT for 20 min prior to the experiment.

Caco-2 and the OG-derived cell layers were insonated with the 1.0 MHz unfocused transducer (described in Section 4.4.1) {MI = 0.3, DC = 5%, 10 cycles} custom-built by Mr A. Moldovan. The cells were also exposed to 5% MBs (2 – 5 x 10^8 MBs/ml, 2 – 8 µm average diameter, SonoVue, Bracco, UK) in HBSS for 11 min. As described in Section 4.4.3, the suspension was delivered at a rate of 4 ml/min using a syringe pump through a pipette tip attached to the transducer, Figure 5-7. The chosen delivery rate enabled the projection of the MBs suspension towards the bottom of the ThinCert, to promote cavitation in proximity to the cell layer. The syringe driver was programmed to deliver the suspension for one second, pause delivery for three seconds and repeat the cycle for

11 min. During the insonation treatment, a TEER value was recorded every minute. A thermocouple inserted in the ThinCert indicated that the temperature did not exceed 22°C. After the 11 min of insonation and 9 min of follow-up TEER recording, the wells with cells had the HBSS replaced by growth medium and they were returned to the incubator. The TEER was recorded at the end of the experiment and 3, 12 and 24, 48 and 60 h later.

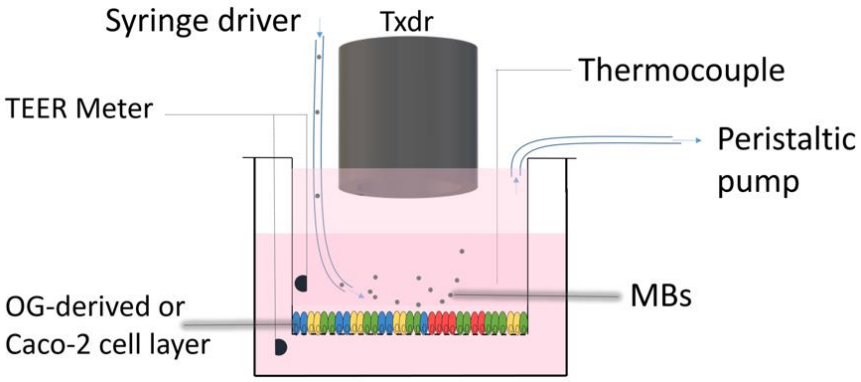

Figure 5-7 Experimental setup. *The epithelial layer was either a Caco-2 cell layer or an OG-derived cell layer. Fresh suspension of MBs in HBSS was delivered using a syringe driver. Barrier function was recorded with a TEER meter. The suspension was continually removed using a peristaltic pump to maintain a constant volume in the apical chamber. This ensured the transducer was always immersed in liquid and prevented overflow into the basolateral chamber, which would have caused incorrect TEER readings.*

5.3.2 Results

US + MBs application resulted in ~50% decrease in barrier function in both the Caco-2 and OG-derived layers, but the latter responded more variably, Figure 5-8 (a). According to Figure 5-8 (b), the barrier function of the treated Caco-2 cell layer continued to decrease for 12 h post-insonation. The TEER of the treated OG-derived condition decreased until 1 h post-insonation and then slowly recovered; one sample fully recovered within 12 h post-treatment, whereas the other two samples recovered to 70% of their initial value within 60 h post-treatment. The control sample displayed a decrease in barrier function to ~10% of its initial value 1 h post-treatment, but it returned to its initial value within 12 h.

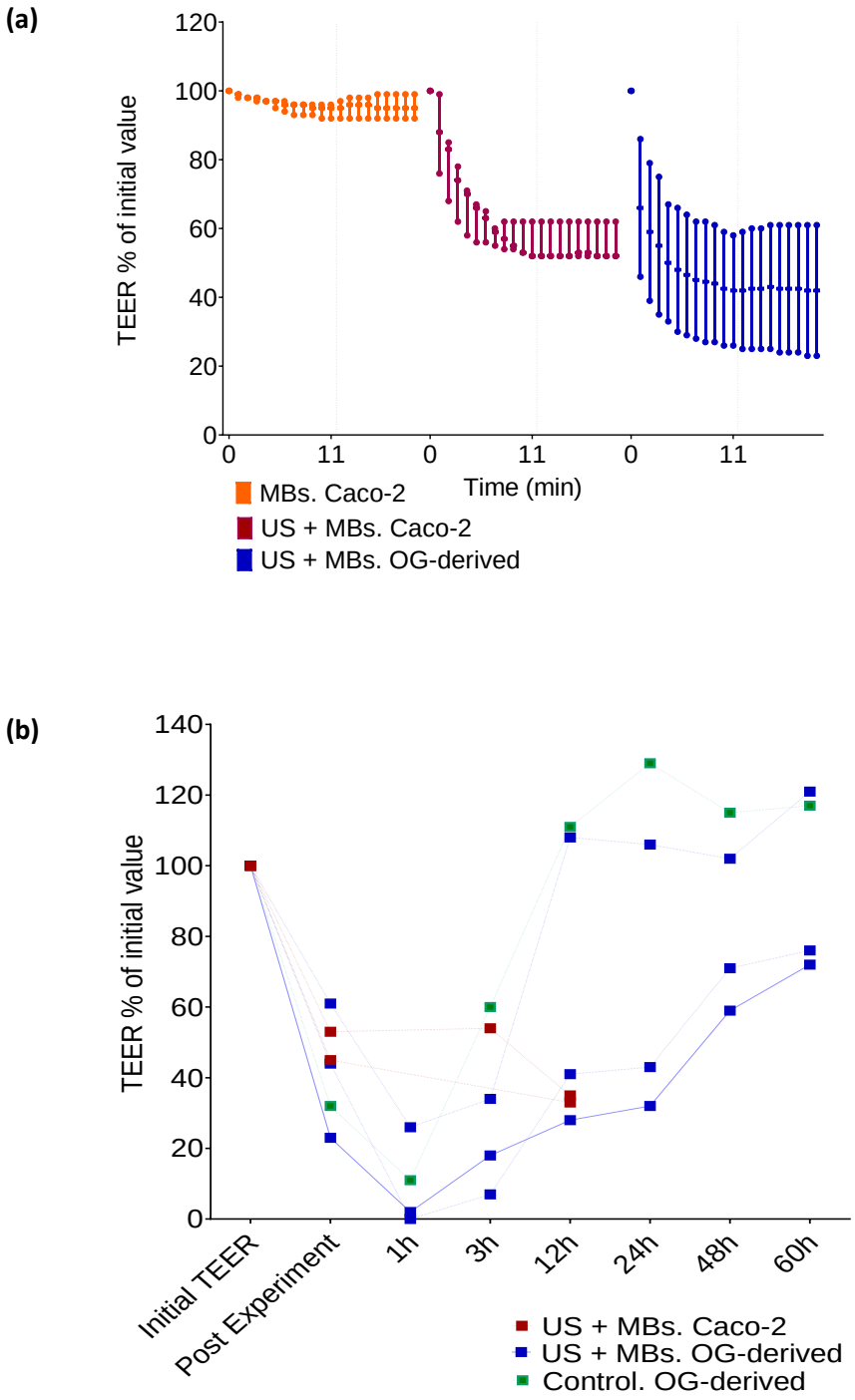

Figure 5-8 Effect of US + MBs on TEER of a Caco-2 monolayer and a rectum OG-derived layer. *(a) TEER fluctuation as a result of applying MBs or US + MBs to a Caco-2 or an OG-derived cell layer. US + MBs application resulted in ~50% decrease in TEER in both the Caco-2 and OG-derived layers; dashed line indicates end of treatment; n = 3 for Caco-2 conditions and n = 2 for OG-derived condition; (b) Recovery patterns of a Caco-2 and an OG-derived cell layer following delivery of US + MBs. Caco-2 and OG-derived cell layers show similar barrier function recovery patterns. Caco-2 samples were recorded only for 12 h post-treatment, whereas OG-derived cell layer values were recorded for up to 60 h post-treatment. Readings from samples in each condition were not averaged to enable the time course of each individual sample to be followed. (a) lacks the condition MBs. OG-derived due to lack of samples available.*

5.4 Effect of US + MBs and US + NDs on Decreasing the Barrier Function of a Rectum Organoid-derived Cell Layer and on Promoting Insulin Delivery

The following section describes experiments where US was delivered together with either MBs or NDs to produce cavitation and promote insulin transfer across the epithelial barrier. The main difference between this section and the previous one is that insulin was used (as a substance with large molecules) and that besides MBs, NDs were tested as an alternative cavitation-enhancement medium.

The use of MB's is complicated by a number of factors. The density of MBs is lower than that of the growth media, rendering them buoyant. By using a syringe driver to deliver MBs continuously in proximity to the cell layer on the ThinCert filter, sonoporation can be produced. However, the continuous delivery of MBs makes this method wasteful. NDs represent an alternative. They have the advantage that their overall density is higher than that of the growth media, enabling them to reside on the ThinCert filter. Once NDs are exposed to US of a resonant frequency, they can undergo acoustic droplet vaporisation and cavitation (Correas and Quay, 1996).

5.4.1 Experimental Setup and Methods

NDs were provided by M Thanou, Kings College London. They were stored in vials at a concentration of 15 mg/ml. Their mean diameter was 147.8±1.6 nm, PDI 0.229±0.023, lipid ratio 95:5 (1,2-Dipalmitoyl-snglycero-3-phosphocholine – DPPC : 1,2-distearoyl-snglycero-3-phosphoethanolamine-N-[methoxy(polyethylene glycol)-2000] – DSPE-PEG_{2000}) and 5% perfluoropentane.

The OG-derived cell layers were subjected to a treatment comprising US (f = 1.0 MHz, MI = 0.5, DC = 20%, 40 cycles) + 2 ml of 10% MBs or 10% NDs + 250 µg/ml Insulin-FITC (ThermoFisher, UK) in HBSS for 30 sec at a rate of 4 ml/min**,** Figure 5-9. Medium in the apical chamber was sampled prior to and 60 min post-treatment, whereas the medium in the basolateral chamber was sampled prior to the treatment and 4, 20 and 60 min post-treatment. For sampling, 100 µl of media were removed from the basolateral and/or the apical chambers and pipetted into a black 96 well plate (237108, ThermoFisher, UK). 100 µl fresh HBSS were then added back into the apical or basal chambers to maintain the same volume. The fluorescence of the samples was measured with a spectrophotometer plate reader (SpectroStar, BMG Labtech, Bucks, UK) at Ex

490 nm and Em 535 nm. A thermocouple inserted in the ThinCert indicated that temperature did not exceed 22°C.

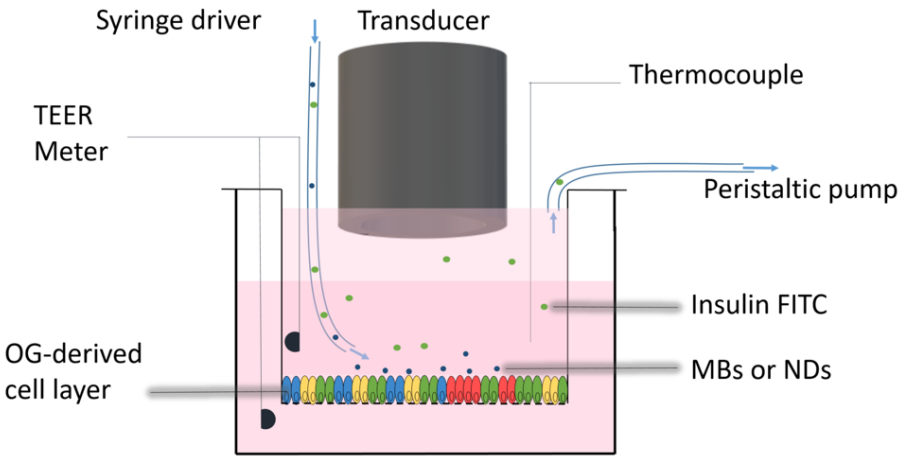

Figure 5-9 Assessment of effect of US + MBs vs US + NDs. *The peristaltic pump aspirated the excess suspension, as explained in the caption of Figure 5.7; MBs are gas filled and float towards the top of the fluid in the chamber; NDs are liquid filled and they mainly pool towards the bottom of the apical chamber. As indicated by glowing lines, insulin FITC is depicted as green dots, MBs and NDs as blue dots.*

5.4.2 Results

US + MBs and US + NDs decreased the barrier function of the cell layer to about half their original values. US + MBs was ~25% more efficient at decreasing the barrier function than US + NDs by the end of the treatment, Figure 5-10 (a). The barrier function of the control sample (i.e. insulin alone) remained constant during delivery of the insulin suspension, but 20 min post-treatment it decreased to 20% of the initial value, further decreasing to ~10% 1 h post-treatment. The barrier function of US + MBs and US + NDs also decreased to 10 - 30% of their initial value within 20 min post-treatment. Barrier function returned to the original value within 24 h for the control and US + ND conditions and within 48 h for the US + MBs condition.

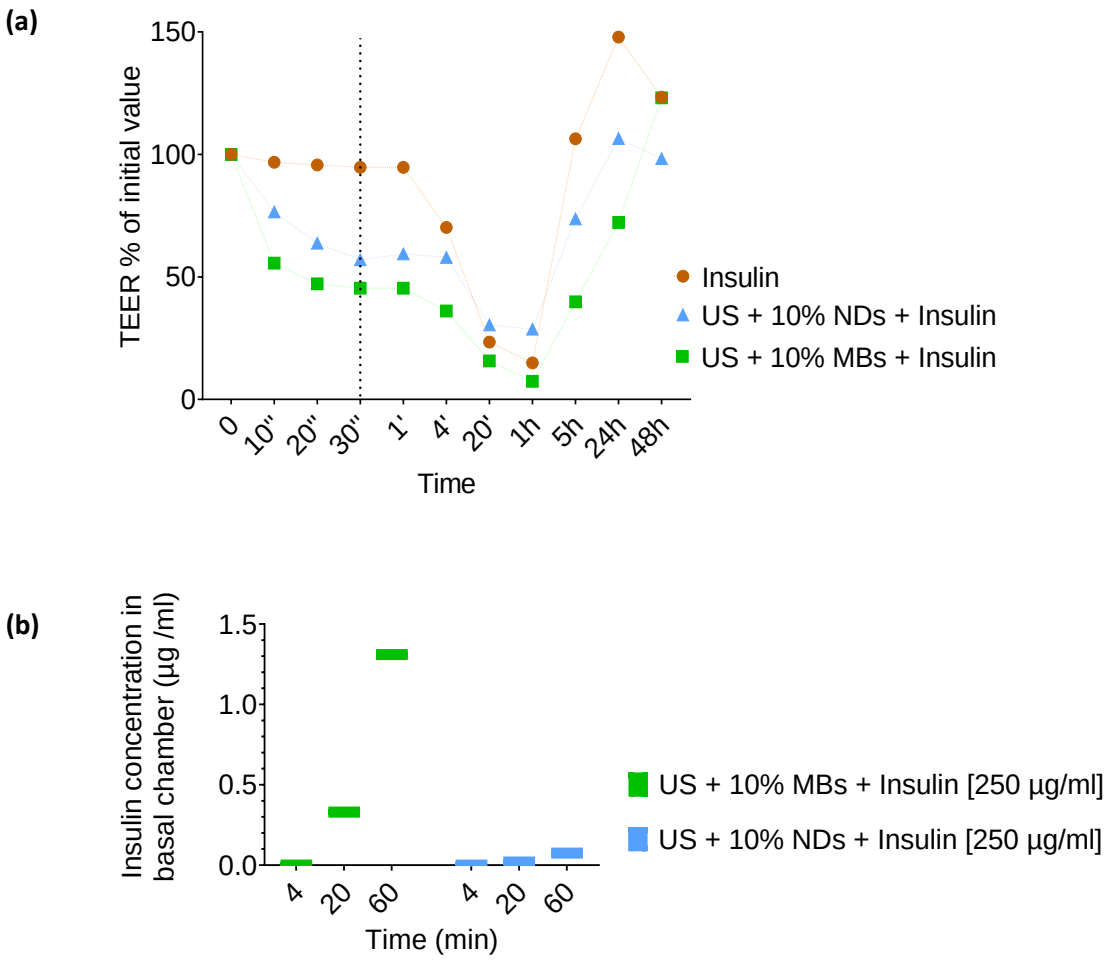

Figure 5-10 Effect of US + MBs and US + NDs on the barrier function and insulin delivery over an OG-derived cell layer. *(a) US + MBs and US + NDs may decrease the barrier function of an OG-derived layer within 10 s of treatment delivery. Dashed vertical line indicates end of treatment. By the end of the 30 s treatment period, US + NDs + Insulin decreased the TEER by 45% of the initial value. Similarly, US + MBs + insulin decreased the TEER to 55% of the initial value. The control sample, insulin alone, did not seem to affect the TEER within this period. (b) 20 and 60 min post treatment, under the effect of US + MBs + Insulin, the insulin concentration in the basolateral chamber was 0.05 and 0.1 µg/ml, respectively. In contrast, under the effect of US + NDs + Insulin, the concentration of insulin in the basolateral chamber was much higher, 0.3 and 1.3 µg/ml, respectively. US + MBs promoted more Insulin-FITC delivery over the cell layer compared to US + NDs. Within 4 min post treatment, the insulin concentration in the basolateral chamber was very small in both cases. n = 1.*

US + MBs promoted a 13-fold increase in insulin transport across the OG-derived cell layer compared to US + NDs, Figure 5-10 (b). However, this could be due to the pore US + MBs produced in the layer, Figure 5-11 (b). US + NDs did not produce any visible pore in the layer, Figure 5-11 (c). Figure 5-10 (b) lacks the control sample because the thermocouple touched the cell layer when it was removed from the ThinCert, punching pores in it, Figure 5-11 (a). As a result, the control sample was discarded. The pore should be responsible for the TEER drop recorded in the control sample 1 h post insulin treatment,

Figure 5-10 (a). Given that the results presented in this section are based on only one sample per condition, the conclusion should be considered with appropriate caution.

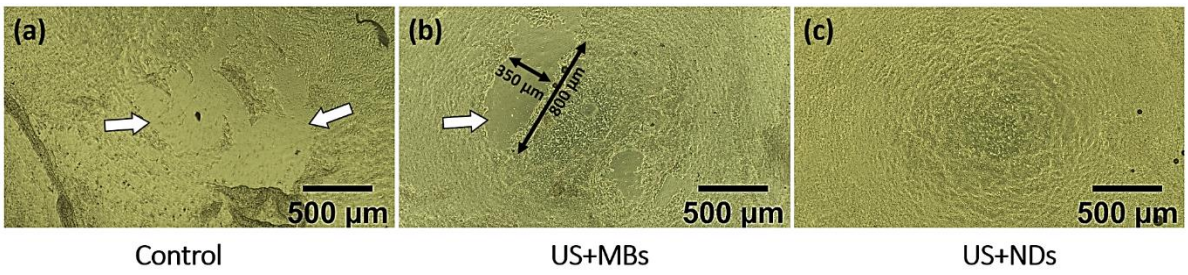

Figure 5-11 Effect of US + MBs and US + NDs on epithelial integrity. *Bright-field images of the epithelial layer post-treatment. White arrows point towards pores in the layer; (a) Control sample was damaged by the thermocouple; (b) US + MBs produced pores in the cell layer; (c) US + NDs did not produce visible pores in the cell layer.*

5.5 Discussion

The experiments described in this chapter aimed to (1) determine the feasibility of growing a cell layer from porcine rectal OGs and small intestine OGs, (2) compare the effect of US + MBs on a Caco-2 monolayer vs a porcine rectum OG-derived cell layer and (3) compare the effects of US + MBs and US + NDs on a porcine rectum OG-derived cell layer.

The cell layer derived from rectum OGs appeared to undergo stages of confluency and detachment from the filter (cell death), until it reached a plateau (Figure 5-4 and Figure 5-5). In the *in vivo* mucosal layer, mature cells are viable for 4 – 5 days and eventually undergo apoptosis and desquamation (Stange *et al.*, 2013). In the ThinCert model, where we have a flat layer of cells, cells which are shed would detach from the filter and would potentially loosen the barrier function, consistent with the low TEER value recorded at days 10 – 16 and 25 – 32 of culture. The stem cells and other progenitor cells that remained attached to the filter could expand the transit amplifying zones and rapidly rebuild a confluent layer.

Fully developed Caco-2 cell layers usually develop TEER in the range of 500 – 1500 Ω/cm^2 (See Section 4.4.1 and Meunier *et al.*, 1995). The TEER values recorded for the cell layer derived from porcine rectum OGs was much higher, up to 4000 Ω/cm^2, Figure 5-5. The mucosa of the rectum, similarly to the mucosa of the intestinal epithelium, consists of simple columnar cells. However, close to the anal transitional zone, the epithelium flattens and becomes stratified squamous non-keratinized epithelium (Fenger and Nielsen, 1982). A stratified epithelium would be expected to have

a higher barrier function, hence a higher TEER value. Having this form could also explain the barrier function plateau reached by Day 40 in Figure 5-5: even if many cells are shed, having more than one layer of cells would ensure the barrier function remains high. This observation is further supported by the multilayer formed by Day 45 in Figure 5-4.

Confluent cell layers could not be grown from porcine small intestine OGs, Figure 5-6**.** Other groups have grown them successfully after coating the substrate with MG (Speer, *et al.*, 2019) (Altay *et al.*, 2019). In the current experiments, the ThinCert filter represents an additional barrier insulin needs to cross; in order to avoid creating a further barrier, the filter was not pre-coated with MG. Further studies may test the extent to which the additional MG layer obstructs insulin diffusion in the basolateral chamber and identify a suitable thickness of the MG layer. They can also test whether frequent changes of medium, cell detachment and cell reattachment affect the thickness of the MG layer over weeks of culture. The layers would need to be studied over several cycles of detachment and confluency to predict the periods when the barrier function would be high so that experiments could be conducted on those days. Otherwise, if experiments took place while the cell layer was undergoing detachment, drug permeability might be falsely increased and the TEER value over the 48 hours recovery period would be falsely low.

Human large intestine familial adenomatous polyposis (FAP) OGs and porcine large intestine OGs were also grown and seeded as cell layers (data not shown), but they did not become confluent within three weeks. FAP OG-derived layers grew very slowly, potentially because they originated from diseased tissue. For drug delivery studies, it would be ideal to use cell layers derived from OGs originating from healthy human small intestine biopsies. Healthy humans do not undergo biopsies, but marginal tissue could be isolated from intestinal cancer resections. However, cancer of the small intestine is rare.

Speer *et al.*, 2019b grew colonic epithelial cells as a 2D monolayer on the surface of collagen gels. They compared growth on hydrogels with different ratios of MG (8.7 mg/ml) to collagen (2 mg/ml). When the MG concentration was less than 25% and collagen more than 75%, cells formed a 2D monolayer; when the MG concentration was higher than 50% and collagen lower than 50%, they formed 3D spheroids.

In response to US + MBs, Caco-2 and rectum OG-derived cell layers behaved similarly. However, given that it is unknown how an *in vivo* layer would have responded, it cannot be concluded which model was more relevant. Speer *et al.*, 2019 used primary cells to

develop a cell layer and compared it to the OG-derived layer. However, compared to any *in vitro* model, *in vivo* tissue is also subject to many other factors including commensal gut microbes, by products of gut digestive processes, interaction with the other cell layers and vascularisation. Although there are *in vitro* models that allow including these factors individually, none of them reproduce all features of *in vivo* tissue. Nevertheless, in contrast to Caco-2 layers, OG-derived layers secrete similar levels of intestinal metabolising enzymes similar to those secreted by *in vivo* tissue (Speer *et al.*, 2019), have a variety of cell types and recovered better post-treatment.

Barrier function recovery

The barrier function response pattern of OG-derived control samples in Figure 5-8 (b) showed drops to 10% of their initial TEER values 1 h post-treatment. This suggests it is possible that the layer was sensitive to the suspension delivery, the prolonged exposure to RT, low CO_2 levels, or the lack of nutrients in HBSS buffer compared to growth media. The insonated OG-derived samples also exhibited a decrease in barrier function until 1 h post-treatment, suggesting this drop was not caused by the US + MBs or US + NDs treatment.

Samples treated for only 30 s recovered to their initial barrier function faster than those treated for 11 min, Figure 5-10 (a)**.** When the insonation treatment lasted for 30 s, barrier function recovery to the initial value required 24 h post-treatment for control and US + NDs samples and 48 h for the US + MBs sample. This suggests the damage in the cell layer observed in the control and in the US + MBs samples were resolved within 24 and 48 h, respectively. On the contrary, in Figure 5-8 (b), when insonation treatment lasted for 11 min, the OG-derived control samples and one US + MBs samples recovered within 12 h, but two other US + MBs samples did not recover even within 60 h.

Given that the TEER of the Caco-2 samples was recorded for only 12 h post-treatment and did not recover within this timespan, whereas the OG-derived samples were recorded for 60 h post-treatment and some of them did recover, reliable comparisons cannot be drawn between their recovery patterns, Figure 5-8 (b). Further work is necessary to record the recovery patterns over longer periods and increase the number of replicates. The protocol designed initially expected recovery to occur within several hours; hence, the maximum recovery period was chosen to be 12 h. However, given that this was found inadequate, the

period was extended to 60 h. Given that the set-up is unique, data from other sources cannot be reliably used for comparison.

The barrier function recovery in the Caco-2 and the OG-derived cell layers show there is potential for the barrier function to recover within several days. A fully differentiated Caco-2 layer is no longer undergoing division, whereas an OG-derived layer continually contains transit amplifying cells, where cell division is rapid; this could explain the ability of the OG-derived cell layer to recover barrier function better than Caco-2. However, a recovery *in vivo* should ideally take seconds, to decrease chances for pathogens to penetrate the mucosa and gain access to the portal and systemic circulation and spread around the body. The pore produced by US + MBs in Figure 5-11 (b) (white arrow) has a diameter of roughly 280 000 μm^2 and resealed only within 12 – 24 h (Figure 5-10 (a), green box). This is consistent with observations by Hu *et al.*, 2013, who showed that sonoporation resulting in perforation sites < 30 μm^2 resealed within 1 min, but for pores > 100 μm^2 resealing failed even within 20 min. Pores with a long axis diameter between 11 and 30 µm did not reseal within 20 min, whereas those with a long axis dimeter between 1 and 7 µm resealed within 30 s.

NDs and MBs

US + MBs were more efficient than US + NDs at decreasing the barrier function and delivering insulin-FITC across the OG-derived cell layer, Figure 5-10 (b)**.** This could be because the MBs were more resonant than the NDs at the frequency and insonation parameters used.

5.6 Conclusions

A confluent monolayer on ThinCert filters could not be grown from small intestine OGs within 4 weeks of culture. However, such a layer could be grown from rectal OGs. The Caco-2 and OG-derived cell layers appeared similarly sensitive to US + MBs treatment. US + MBs induced a pore in the OG-derived layer, potentially through sonoporation, promoting more insulin delivery across the cell layer when compared to US + NDs. This also suggested the experimental parameters were more suitable for MB sonoporation than ND sonoporation. Full barrier function recovery in the rectum OG-derived layer was recorded within 48 h post-treatment when the treatment lasted for 30 s, but not when it lasted for 11 min.

Following the work described in this chapter, Chapter 6 describes the testing of the insonation treatment *in vivo*.

5.7 References

Altay, G., Larrañaga, E., Tosi, S., Barriga, F.M., Batlle, E., Fernández-Majada, V., Martínez, E., 2019. Self-organized intestinal epithelial monolayers in crypt and villus-like domains show effective barrier function. Sci Rep 9, 10140. https://doi.org/10.1038/s41598-019-46497-x

Correas, J.-M., Quay, S.D., 1996. EchoGen emulsion : A new ultrasound contrast agent based on phase shift colloids. Clin. radiol 51, 11–14.

Fenger, C., Nielsen, K., 1982. Stereomicroscopic Investigation of the Anal Canal Epithelium. Scandinavian Journal of Gastroenterology 17, 571–575. https://doi.org/10.3109/00365528209182252

Gehart, H., Clevers, H., 2019. Tales from the crypt: new insights into intestinal stem cells. Nat Rev Gastroenterol Hepatol 16, 19–34. https://doi.org/10.1038/s41575-018-0081-y

Goldberg, A.M., Zurlo, J., Rudacille, D., 1996. The three Rs and biomedical research. Science 272, 1403. https://doi.org/10.1126/science.272.5267.1403

Hu, Y., Wan, J.M.F., Yu, A.C.H., 2013. Membrane Perforation and Recovery Dynamics in Microbubble-Mediated Sonoporation. Ultrasound in Medicine & Biology 39, 2393–2405. https://doi.org/10.1016/j.ultrasmedbio.2013.08.003

Lieberkühn, J.N., 1745. Dissertatio anatomico-physiologica de fabrica et actione villorum intestinorum tenuium hominis. apud Conrad et. Georg. Jac. Wishof.

Meunier, V., Bourri, M., Berger, Y., Fabre, G., 1995. The human intestinal epithelial cell line Caco-2; pharmacological and pharmacokinetic applications. Cell Biol Toxicol 11, 187–194. https://doi.org/10.1007/BF00756522

Sato, T., van Es, J.H., Snippert, H.J., Stange, D.E., Vries, R.G., van den Born, M., Barker, N., Shroyer, N.F., van de Wetering, M., Clevers, H., 2011. Paneth cells constitute the niche

for Lgr5 stem cells in intestinal crypts. Nature 469, 415–418. https://doi.org/10.1038/nature09637

Speer, J.E., Gunasekara, D.B., Wang, Y., Fallon, J.K., Attayek, P.J., Smith, P.C., Sims, C.E., Allbritton, N.L., 2019a. Molecular transport through primary human small intestinal monolayers by culture on a collagen scaffold with a gradient of chemical cross-linking. J Biol Eng 13, 36. https://doi.org/10.1186/s13036-019-0165-4

Speer, J.E., Wang, Y., Fallon, J.K., Smith, P.C., Allbritton, N.L., 2019b. Evaluation of human primary intestinal monolayers for drug metabolizing capabilities. J Biol Eng 13, 82. https://doi.org/10.1186/s13036-019-0212-1

Stange, D.E., Koo, B.-K., Huch, M., Sibbel, G., Basak, O., Lyubimova, A., Kujala, P., Bartfeld, S., Koster, J., Geahlen, J.H., Peters, P.J., van Es, J.H., van de Wetering, M., Mills, J.C., Clevers, H., 2013. Differentiated Troy+ Chief Cells Act as Reserve Stem Cells to Generate All Lineages of the Stomach Epithelium. Cell 155, 357–368. https://doi.org/10.1016/j.cell.2013.09.008

Van Norman, G.A., 2019. Limitations of Animal Studies for Predicting Toxicity in Clinical Trials. JACC: Basic to Translational Science 4, 845–854. https://doi.org/10.1016/j.jacbts.2019.10.008

Chapter 6
Microbubbles and Ultrasound Delivery of Insulin and Quantum Dots to the Porcine Small Intestine *in vivo*

Chapter 5 demonstrated the use of a 1.5 MHz phased array transducer in *in vitro* applications and identification of parameters that promote compound delivery through a cell layer. This chapter takes the idea further to test whether a tethered capsule with a miniature 1.5 MHz phased array transducer and MBs can promote insulin delivery to the systemic circulation in a live animal, Figure 6-1. Three methods were used to detect blood glucose levels producing promising results that justify further exploration. Histology analysis further confirmed the effect of the intervention on the intestinal mucosa.

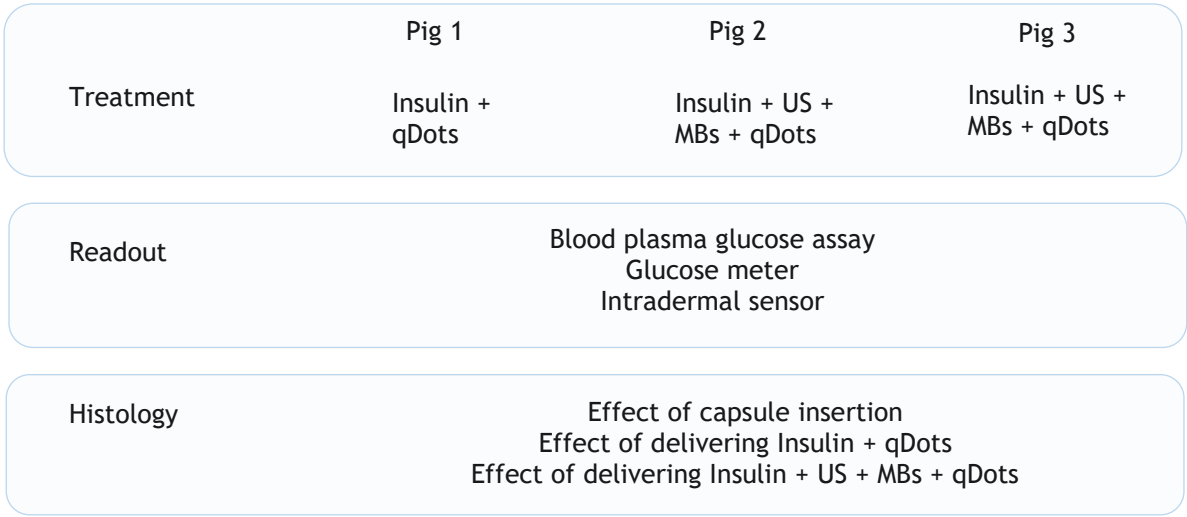

Figure 6-1 Overview of experiments presented in Chapter 6. *Three pigs were used to test the effect of the treatment, called Pigs 1- 3; one was a control pig and two were experimental pigs. The readout consisted of three methods. Once the pigs were culled, tissue was harvested for histological analysis. Where US = ultrasound, qDots = quantum dots, MBs = microbubbles.*

6.1 Capsule Motivation

The first report of oral delivery of insulin dates to almost a century ago (Harrison, 1923). However, despite the attraction and importance of the process, there is still no routine method to address it, suggesting that balancing insulin bioavailability and safety of delivery method are challenging.

As mentioned in Chapter 2, large molecules such as insulin cannot be absorbed easily from the intestinal lumen. Insulin is normally stable as a hexamer (Gast *et al.*, 2017), but its half-life decreases considerably as a dimer and monomer. Insulin normally elicits its effect as a monomer (Brange *et al.*, 1990). Once insulin is absorbed from the intestine, it is transported to the liver for metabolism and release in the systemic circulation. Insulin molecules signal to muscle, liver and fat cells to absorb glucose from blood (Nakrani *et al.*, 2021). Therefore, insulin increase in the blood correlates with a decrease in glucose levels. This mechanism underpins observations described in this chapter.

The work described in this chapter was conducted to explore the following hypotheses:

(1) A tethered capsule, SonoCAIT (insonation capsule for autonomous imaging and therapy), makes adequate (intimate) contact with the mucosa during peristalsis;

(2) Capsule insertion, including friction against the mucosa of the small intestine, does not damage the intestinal tissue;

(3) Transmucosal delivery of insulin using US + MBs can affect blood glucose levels to a measurable extent; and

(4) Insulin + US + MBs + quantum dot (qDot) treatment does not damage the intestinal tissue.

6.2 Capsule Development

The work presented in this chapter was conducted in collaboration with Dr Moldovan. I prototyped the capsule, devised and organised the *in vivo* trial, took a principal role in its execution and I analysed the data. I also assisted Dr Moldovan to manufacture the transducers, integrate them into capsules, test their safety and characterise their behaviour, as presented elsewhere (Dr Moldovan's Thesis, 2021). The protocol is briefly presented below.

6.2.1 Capsule Design and Fabrication

Three SonoCAIT capsules were developed and tested. Each capsule included a tether which housed individual signal cables to the array elements, a common ground connection and two suspension delivery tubes that ensured in situ transport of drugs, CAs and fluorescent compounds. The capsule was designed in SolidWorks, comprising three independent parts to facilitate integration of the array and other relevant components, Figure 6-2 (a). The parts were designed with a lip/groove locking system to decrease moisture ingress and improve the robustness of the device, Figure 6-2 (b). The lip/groove width was set to 0.525 mm. The external capsule dimensions were length, L = 44.6 mm, including the 4.6 mm tether connection port, and OD = 11 mm. The internal dimensions, excluding the rounded edges, were L = 30.0 mm and ID = 8.0 mm. The body of the capsule included a recess, called the active face, designed to ensure a separation of 4.5 mm between the face of the transducer and the tissue when the capsule is inserted in the intestine. FEA was conducted by Dr Moldovan to ensure beam steering was not obstructed by the walls of the recess. Prototypes were 3-D printed in VeroBlack with Gloss mode with an Objet Eden 350V (Stratasys, MN, USA).

The suspension was delivered in proximity to the array aperture through two orifices in the enclosure, Figure 6-2 (a, c), connected to two 3.2 m long suspension delivery tubes (Smiths Medical, MN, USA). These two tubes exited the capsule through a 3 m long tether. Besides the two suspension delivery tubes, the tether included 26 microcoax signal connections and one copper (Cu) wire for the ground connection. Out of the 26 microcoax cables, 24 cables were for the active elements, two cables were used to connect the ground layer of a flexi circuit and the Cu wire was used to connect the ground electrode of the transducer (the front electrode). The suspension delivery tubes were polyurethane with ID = 0.58 mm and OD = 0.96 mm.

These two tubes were attached with epoxy (Epofix, Struers, UK) to two sacrificial microcoax cables, and together with the 26 other microcoax cables were soldiered to the tip of a catheter stylet. The combination of microcoax cables, suspension delivery tubes and Cu ground wire was pulled through a 1 m long biocompatible nasogastric tube (Corflo, nasogastric/nasointestinal feeding tubes, 12 Fr 109 cm, Avanos, USA). The remaining length of bunched wires was then inserted into a 1.7 m long silicone tube (Cole Parmer, UK) with a wider diameter for easier insertion. The biocompatible nasogastric tube housed the part of the tether to be inserted in the pig's small bowel, while the silicone tube

provided protection for the fragile cables. The continuity of all 26 microcoax cables was checked with a multimeter.

After insertion through the tether, the distal ends of the microcoax cables were soldered to the flexi circuit of the array. The array was then attached to Part 1 of the capsule enclosure, Figure 6-2 (a), and the flexi circuit with the microcoax wire connections was placed in Part 2 of the enclosure. The first suspension delivery tube was then inserted through its channel in Part 1. Subsequently, the two parts were joined together and filled with a mixture of air filled microballoons (3M Company, Minnesota, USA) in epoxy (Epofix, Struers, UK) that sealed the joints between the two components, added robustness to the device and acted as a light backing material for the array. Then, the Cu ground wire and the second delivery tube were inserted through the appropriate channels in Part 3. The interconnect cover (Part 3) was joined with the previous assembly and the gaps were filled with a similar mixture of microballoons and epoxy (G3349, Agar Scientific, UK). The joints between the three parts were subsequently sealed with silicone (692-542, RS PRO, UK) and the front face of the array was insulated with varnish to increase waterproofness. A custom made PCB connector was soldered to the proximal end of the cable for interfacing with the FI ToolBox. The capsules were coated with an 8 µm thick layer of Parylene C to render them biocompatible.

A 3D US immersion scanning tank was used to create pressure maps of the US fields generated by the arrays. This allowed calculation of the voltage inputs required to generate the desired MI and verification that the arrays steered correctly.

For all *in vivo* experiments, the focus was set to 5 mm anterior to the transducer. FEA showed that this produced a maximum -3 dB beam width 4.5 mm anterior to the transducer, which was the height of the recess, hence the distance between the transducer and the tissue when the capsule was inserted in the intestine. The -3 dB profile was chosen as it was considered the interval relevant for therapy. In this region, the appropriate peak negative pressure for cavitation was to be produced.

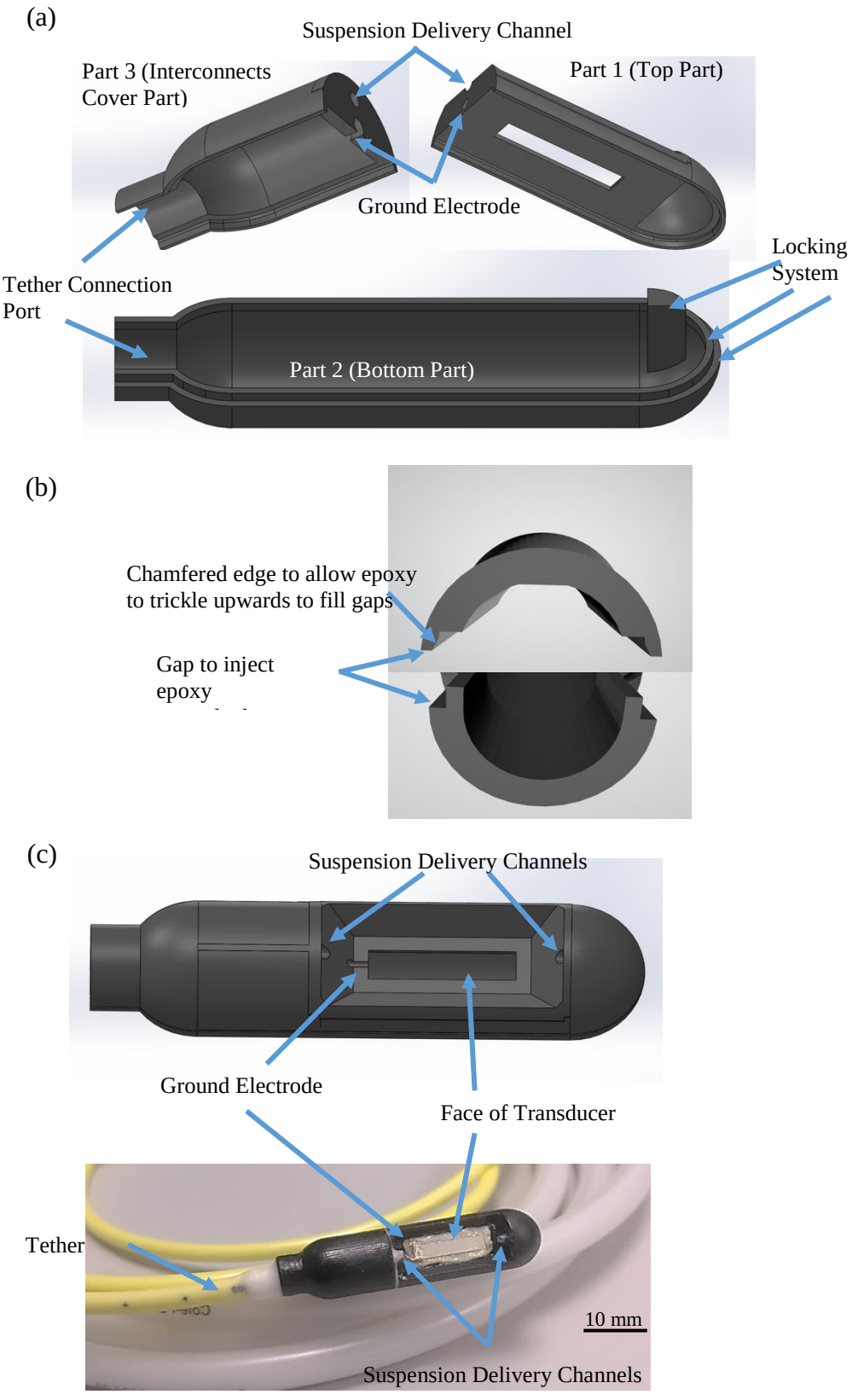

Figure 6-2 Capsule Design and Construction. *(a) The capsule was composed of three parts, termed Parts 1 – 3. Part 1 housed the face of the transducer and provided exit points for the suspension delivery channels, Part 2 housed the flexi and the transducer, and Part 3 which housed the interconnects and provided exit points for the ground electrode. (b) Chamfer edges and gaps enabled sealing of the capsule with epoxy. (c) Assembled capsule (top), final capsule (bottom). The external capsule dimensions were 44.6 x 11 mm.*

6.2.2 Safety Testing

6.2.2.1 Shear Strength of Tether and Bondage Joint

Once inserted in the small intestine, the capsule was expected to be subject to force from the tether during the pullback procedure. To ensure the capsule and tether did not separate and the tether remained intact in the lumen, the shear strength of the bonded joint and the tensile strength of the tether were investigated.

Nine mock capsules were fabricated. Five capsules were filled with Epofix and four capsules with Epofix with air-filled plastic MBs. The tether (nasogastric tube) and its joint in the capsule were filled with wires to mimic the real capsules. The shear strength of the bonded joint and the tensile strength were measured with a Material Testing System (Instron, MA, USA). The site of separation in all nine cases was the joint between the capsule and the tether, Figure 6-3 (a). The minimum breaking force for the joint was 90 N for capsules with Epofix + MBs and 125 N for capsules filled with Epofix only, Figure 6-3 (b).

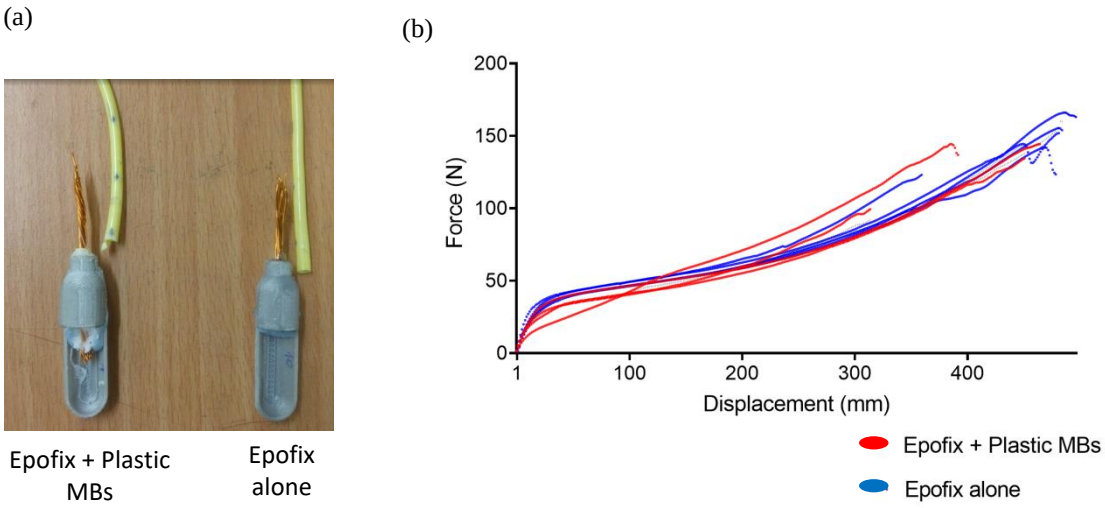

Figure 6-3 Tensile strength of tether and bondage joint of capsule. *The tether was attached to the capsule using either Epofix + plastic MBs, or Epofix alone. (a) All capsules separated at the joint between the tether and the capsule, regardless of how the tether was attached to the capsule. (b) Both types of capsules exhibited a large tensile strength, but the ones filled with Epofix alone exhibited a larger tensile strength.*

Wang and Meng (2010) measured the resistant friction of a capsule endoscope pulled though the lumen of the small intestine. The capsule endoscope measured 11 mm in diameter and 26 mm in length, similar to the capsule presented in this chapter. The

resistant force they identified was between 20 and 100 mN. This force is approximately 1 000 times smaller than the minimum breaking force for the present capsule / tether combination (measured above). Therefore, both configurations tested rendered the capsule suitable for the application. The adhesive comprising Epofix + plastic MBs was chosen due to its increased viscosity, which made assembly easier.

6.2.2.2 Heat Transfer between Capsule and Tissue

Given the relatively high MI generated by the capsule and the relatively lengthy procedure at a single position, it was necessary to check whether the capsule would cause overheating in the lumen. This was relevant to ensure (1) the capsule did not cause local overheating of the mucosa which promotes mucosal permeation (see Section 4.4.2.1), misattributing the result of the test, or (2) the capsule did not reach a temperature above 42°C, which could induce permanent tissue damage (Dewhirst *et al.*, 2003).

Treatment was therefore carried out in isolated *ex vivo* porcine small intestine sourced from Medical Meats (York, UK). Two thermocouples (RS, UK) recorded the temperature. One thermocouple was placed against the rear surface of the capsule and the other thermocouple was placed against the external wall surface of the intestine, Figure 6-4. Further intestinal tissue was placed around the experimental tissue to better mimic *in vivo* conditions and to minimize the influence of ambient conditions.

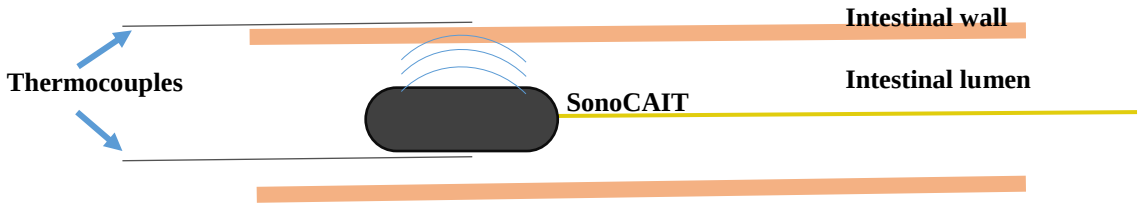

Figure 6-4 Thermocouples recorded temperature fluctuations caused by insonation treatment. *Once the capsule was inserted in the intestine, a thermocouple was placed in contact with the back of the capsule, which is the side of the capsule opposite the side with the face of the transducer. Another thermocouple was placed against the outer wall of the intestinal tissue in the area exposed to US.*

The tissue was allowed to acclimatise at RT for 60 min prior to insonation. Temperature fluctuations were recorded while delivering the treatment with two different capsules. The treatment protocol comprised delivery of a suspension of 10% MBs in PBS simultaneously with US parameters as in the *in vivo* experiments {f = 1.5 MHz, 10 cycles, 100 pulses,

PRF = 50 kHz, DC = 30%}. The four conditions tested were control (suspension only) and MBs delivered with US at MI = 0.2, MI = 0.3 and MI = 0.4. The tests were conducted with two SonoCAIT capsules used later *in vivo*, termed SonoCAIT 1 and 2.

The maximum temperature increase was about 1.5°C, Figure 6-5, which was recorded in the control sample. The initial tissue temperature was lower in this sample than in the other cases and potentially the suspension delivered was warmer than the tissue itself, thus generating the larger increase in temperature compared to the other cases. In the presence of US, the maximum temperature increase was up to 1°C for SonoCAIT 1, and 1.5°C for SonoCAIT 2. These results indicated that the capsule was unlikely to damage the mucosa when used at MI ≤ 0.4.

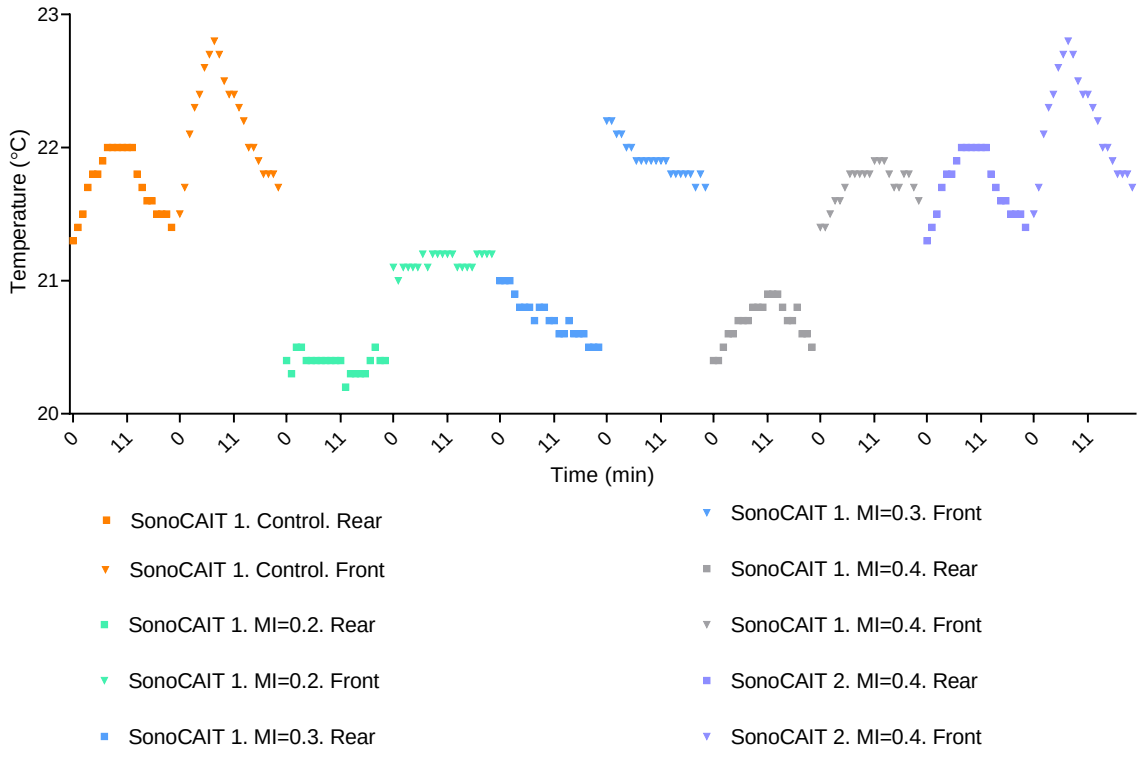

Figure 6-5 Temperature fluctuation in the *ex vivo* lumen during treatment. *The capsules tested were SonoCAIT 1 and SonoCAIT 2. The highest MI tested (MI = 0.4) was tested with both capsules. The temperature increase was up to 1.5°C for both capsules. SonoCAIT 2 was used only at the highest MI (MI = 0.4) as an additional test to ensure the capsule did not overheat either.*

6.2.2.3 Capsule Leakage Currents

A final test necessary to ensure capsule safety measured the electrical leakage current from the capsule towards the surrounding tissue (Hommelgaard, 1976). This was conducted together with Dr Moldovan, and showed that there was no current leakage and the capsule was thus deemed safe for use.

6.3 Ultrasound, Microbubbles and Insulin can Affect Blood Glucose Levels of Pigs *in vivo*

6.3.1 Protocol

The following protocol was approved by the UK Home Office under PPL PP9921057: three female pigs, Landrace X, 40 – 46 kg, underwent liquid diet for 48 h prior to the day of the experiment (Gregson *et al.*, 2021). The animals were anaesthetised. Pre-anaesthetic medication was based on midazolam, ketamine and alfaxalone. Anaesthesia was induced using isoflurane delivered by mask. The auricular vein was cannulated and induction completed with propofol. Anaesthesia was maintained with isoflurane. A stoma was created by the veterinary surgeon and a length of the small intestine of ~1 m was externalised.

A SonoCAIT capsule was cleaned with 70% EtOH and its suspension delivery line was primed prior to insertion to eliminate air in the tubes and to ensure fresh MBs were delivered to the target location. SonoCAIT was inserted 70 cm into the externalised small intestine by the surgeon. The mesentery adjacent to the site with the capsule was marked with a stitch to enable the detection of the treated area *ex vivo*. Subsequently, the small intestine was re-internalised and the stoma was closed with clamps. A wetted gauze pad was placed over it. Fluctuations in glucose levels were recorded for the next 45 min to assess whether capsule insertion affected glucose levels.

Glucose levels were recorded every 15 minutes with an intradermal sensor (FreeStyle Libre, Abbott, UK) and a glucometer (FreeStyle Lite, Abbott, UK). Because of its use of sampling sticks, the Glucometer is termed Glucostix hereafter. 2 ml blood samples were taken from the auricular artery every 30 min and stored in fluoride-oxalate tubes. These tubes were later analysed by the Pathology Unit at the Royal (Dick) School of Veterinary Studies, UofE. They conducted the Beckman Coulter AU Syste Glucose procedure with a Beckman Coulter AU480 Analyser (Beckman Coulter Inc., CA, USA). The assay relies on

the hexokinase G-6-PDH method to quantify the amount of glucose in fasted plasma (Bergmeyer and Stein, 2012; Bondar and Mead, 1974).

Of the three pigs in this proof-of-concept experiment, one was a control and two were experimental. The control pig was given 12 ml of 10 U/ml insulin + 2% qDots delivered over 12 min, Figure 6-1. qDots were delivered in order to enable the identification of the treated tissue section. The other two pigs were subject to US and 10 U/ml insulin + 10% MBs + 2% qDots delivered over 12 min. The suspension was delivered for 1 second, followed by a 3-second pause, at a rate of 4 ml/min, which ensured the suspension was projected towards the focal areas. US was applied for 11 min, starting 1 min after suspension delivery was initiated to allow for adequate coupling between the capsule and the tissue.

Certain insonation parameters optimal for *in vitro* experiments, identified in Section 4.6, were used as a starting point for *in vivo* experiments, {f = 1.5 MHz, 10 cycles, 100 pulses, PRF = 50 kHz}. However, a larger MI than what was tested *in vitro* was used as a starting point in the following *in vivo* experiments. The rationale was that once an effect would be observed at a high MI, it would be decreased in order to find the lowest MI that can induce the desired effect. This was an adequate approach, because as seen later on, porcine *in vivo* experiments required a higher MI than the *in vitro* experiments.

First treatment: small intestine. The first treatment was at MI = 0.4. The other US parameters were {f = 1.5 MHz, 10 cycles, 100 pulses, PRF = 50 kHz, DC = 30%}. Glucose levels were recorded for at least 150 min from the start of the procedure. Three SonoCAIT capsules were used in the trial, so one capsule per pig. This enabled the treatment to be delivered quasi-simultaneously.

Second treatment: small intestine. Subsequently, the intestine was re-externalised, the capsule was pulled back 20 cm, the mesentery was marked with a stitch, the intestine was re-internalised and the stoma was clamped. The treatment was delivered again, but at MI = 0.6. The decision to increase the MI was made because a decrease in glucose levels was not evident following insonation at MI = 0.4. Glucose levels were recorded again for at least 150 min from the start of the second treatment.

Third treatment: rectum. The small intestine was re-externalised, the capsule was retrieved, the intestine was re-internalised and the capsule was inserted 5 cm in the rectum.

As the rectum was not fully clean, the veterinarian removed all faecal material from the 5 cm of the anal canal prior to inserting the capsule. The treatment was then delivered in the rectum at MI = 0.6. Glucose levels were recorded for 85 min from the start of the third treatment.

Fourth treatment: systemic. All three pigs were administered insulin i.v. (Novorapid, Novo Nordisk, Denmark) to ensure they were insulin sensitive. 1 U of insulin/kg was administered in the auricular vein. Glucose levels were assessed for up to 50 min from the start of the fourth treatment.

The pigs were euthanised using an overdose of anaesthetic.

6.3.2 The Treatment Affected Glucose Readings

After the first treatment (MI = 0.4), glucose levels increased more in the pig treated with insulin + qDots (Pig 1) compared to the pigs treated with insulin + US + MBs + qDots (Pigs 2 and 3), Figure 6-6. After the second and third treatments, Pig 1 (insulin + qDots) continued to show higher glucose levels than the other two pigs.

To confirm the pigs were insulin sensitive, they were given 1 U/kg insulin i.v.. It was anticipated this intervention would induce hypoglycaemia swiftly. However, there was only a 30% decrease in glucose levels in Pig 1 within 20 min post administration. Therefore, the pig was administered a second dose of insulin i.v., but this time 2 U/kg. The glucose levels decreased further, suggesting the pig was insulin sensitive, but hypoglycaemia was not induced. Sequentially, Pigs 2 and 3 were administered i.v. insulin too, 1 U/kg, showing trends similar to that observed in Pig 1 after one dose of insulin. Pigs 2 and 3 were not administered a second dose, as they demonstrated insulin sensitivity similarly to Pig 1 after one dose, and were then euthanised. Overall, i.v. insulin administration was followed by a drop in glucose levels in all three pigs.

Pig 3 glucose levels were followed for only 150 minutes, not 225 minutes as the other pigs. The initial waiting time point was 120 min, but extra time was allowed to control for delayed delivery to systemic circulation. The pigs were anaesthetised successively, and Pig 3 was the last one to be anaesthetised. Because of this and the tight experimental time limit imposed by the Home Office, it was not possible to follow Pig 3 for 225 min between the two successive treatments.

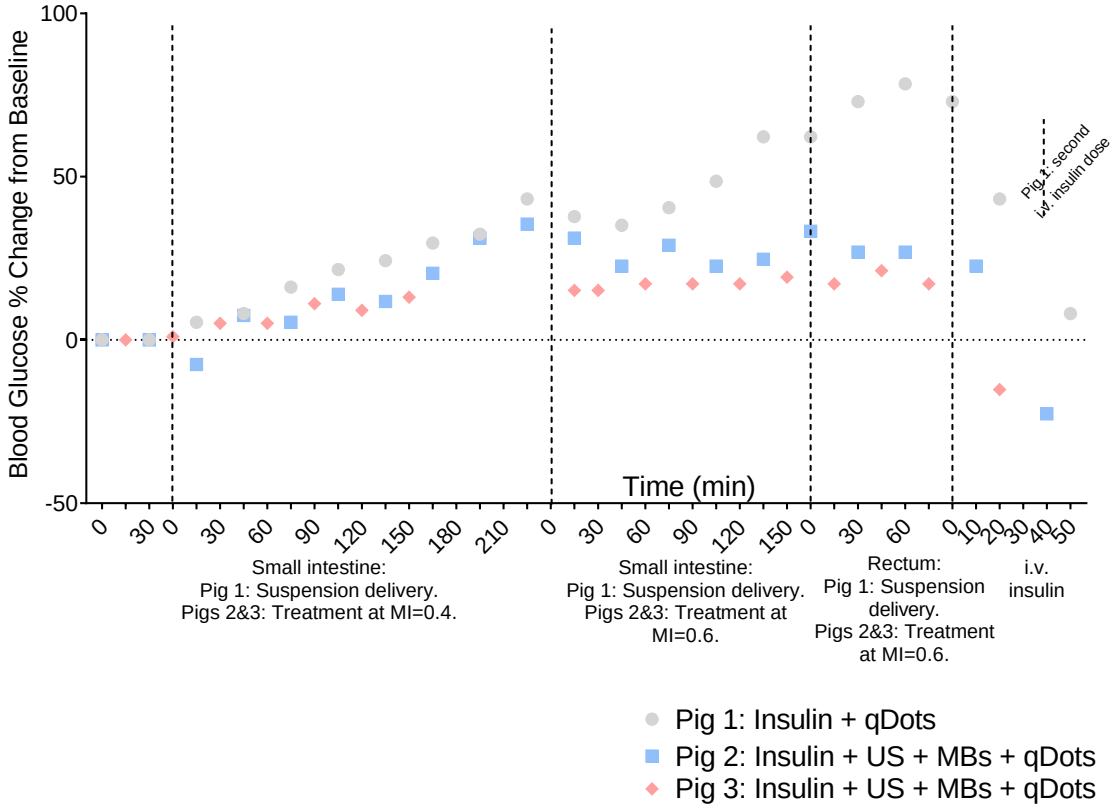

Figure 6-6 Blood glucose % change from baseline in Pigs 1-3. *Prior to i.v. administration of insulin, glucose levels of Pig 1 increased by 75% compared to baseline, whereas those of Pigs 2 and 3 increased by ~25% compared to baseline. Each of the first three capsule-based treatments delivered 3 U insulin/kg, whereas the i.v. administration consisted of 1 U insulin/kg. Data obtained from blood plasma glucose analysis. Values obtained over the first 30 min post anaesthesia were averaged and used to normalise subsequent values. Dashed lines indicate the end of each treatment. Each pig underwent four interventions. After each intervention, the time was reset to 0. After the first treatment (MI = 0.4 in the small intestine), the glucose levels of Pig 3 were followed for only 150 minutes, not 225 minutes as for the other pigs.*

Three methods were used to ensure the fluctuation in glucose levels was recorded as accurately as possible: intradermal measurements, Glucostix, and plasma measurements. Once the levels of glucose change in the blood, it can take 15 to 20 min for this to be reflected in the interstitial fluid and hence for the intradermal sensor to record this change (Dunn *et al.*, 2018). Therefore, the intradermal sensor provides a delayed recording.

Figure 6-7 presents the relative glucose measurements from all methods for all three pigs. Glucostix readings fluctuated more than Intradermal and plasma glucose readings. Plasma glucose analysis and intradermal readings were considered more reliable.

i.v. insulin administration was followed by a drop in glucose levels in all pigs for all three methods, Figure 6-7 (a-c). Blood tests (plasma glucose assay and Glucostix) showed a plateau or decrease in glucose levels after the second, third and fourth insulin treatments.

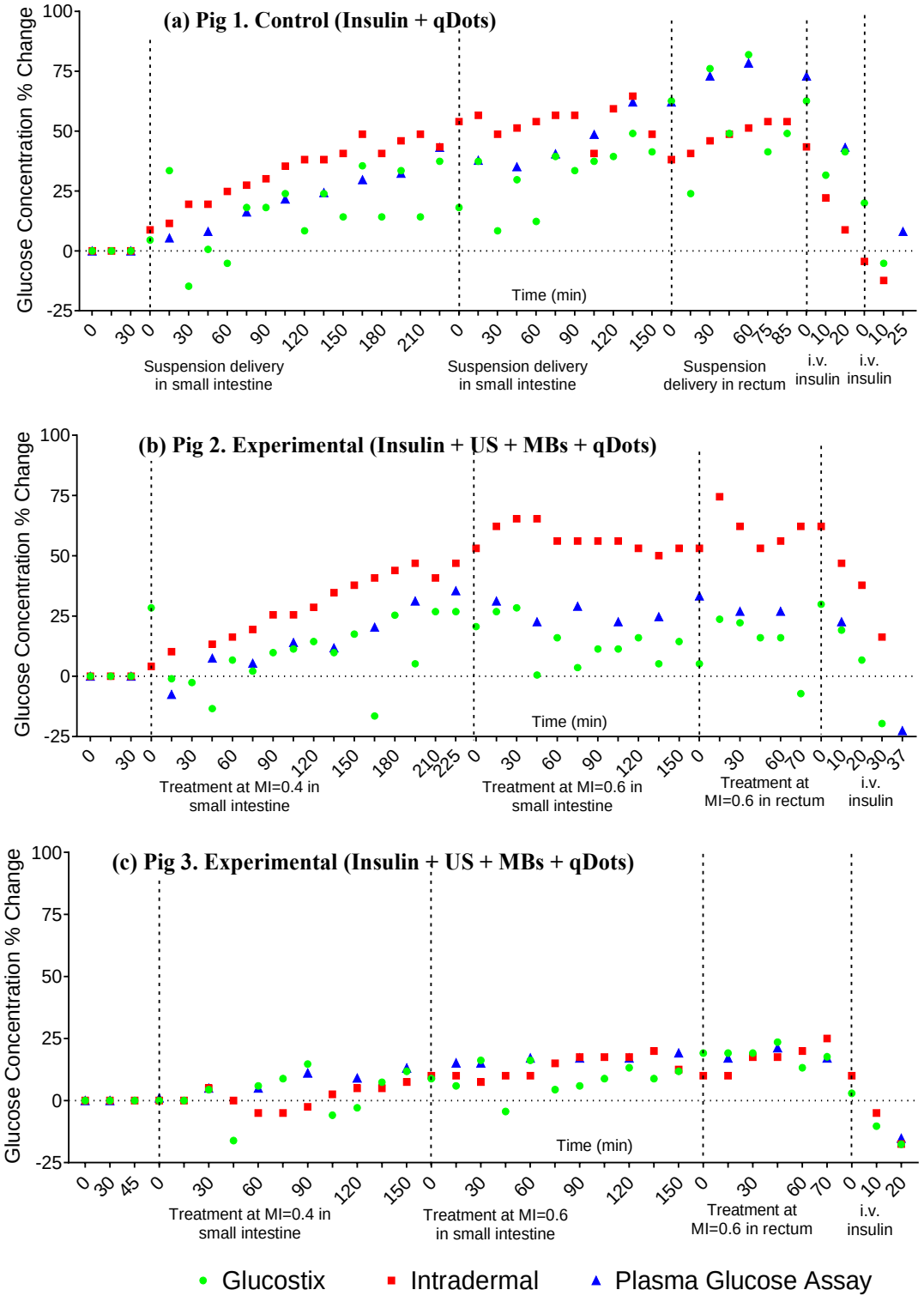

Figure 6-7 Comparison between three different methods of assessing glucose levels in three pigs. *(a) Pig 1 – control (insulin + qDots). (b) and (c) Pigs 2 and 3 - experimental pigs (Insulin + US + MBs + qDots). The key in (c) is the same for all three graphs.*

6.4 The Intestinal Mucosa was not Damaged as a Result of Capsule Insertion and Treatment

6.4.1 Protocol

Following terminal anaesthesia, the pigs were dissected, the small intestines were isolated and rinsed twice in PBS. The treated areas were identified with a UV lamp detecting the fluorescence of qDots, guided by the positions of the stitches in the mesentery. Photographs of the relevant areas were taken with the camera of a smartphone (OnePlus 7T, OnePlus Technology (Shenzhen) Co. Ltd, China). The relevant areas were fixed in 4% PFA and transported to DIF for embedding in wax, sectioning, staining with H&E and mounting on glass slides. They were then imaged at the Aberdeen University Microscopy & Histology Core Facility. Scoring of sections was assigned as follows:

- Score 0: Normal small intestinal mucosa with preservation of normal crypt architecture, Figure 6-8 (a).
- Score 1: Shortening of the villi or denuded of epithelium, Figure 6-8 (b).
- Score 2: Base of the mucosa effaced but residual surface epithelium and upper portion of the crypt preserved, Figure 6-8 (c).
- Score 3: Effacement of the mucosa and only residual surface epithelium present, Figure 6-8 (d).
- Score 4: Complete effacement and erosion of the mucosal surface, Figure 6-8 (e).

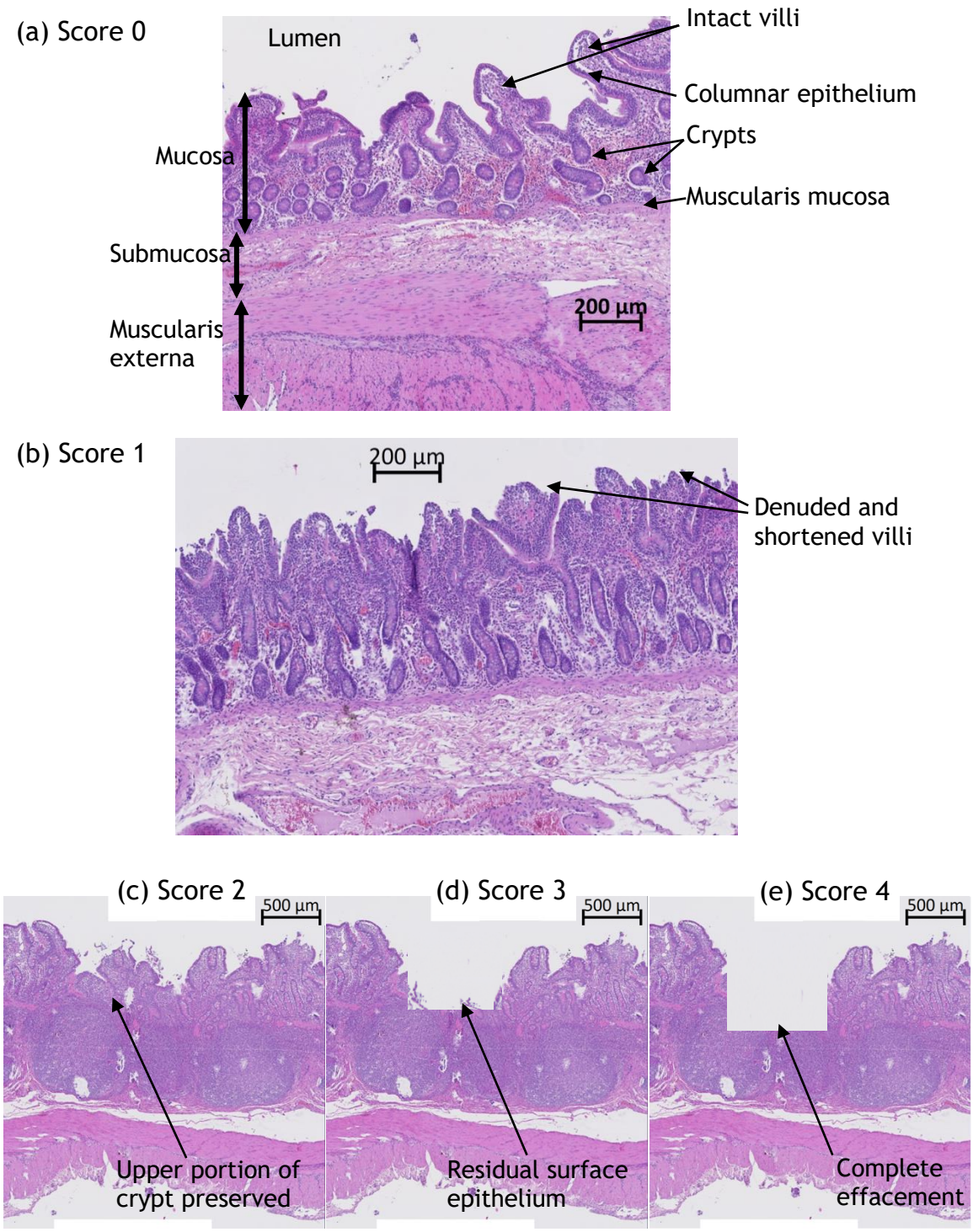

Figure 6-8 Examples of histology samples. *(a) Score 0, intact mucosa. The tissue section was exposed to treatment at MI = 0.6, Pig 3. For detailed morphology of the small intestine, see Section 2.1 and Figure 2-1. (b) Score 1, denuded and shortened villi. The tissue section was exposed to treatment at MI = 0.4, Pig 3. (c) Score 2, upper portion of crypts preserved. The tissue section was not exposed to any treatment or suspension delivery, no capsule introduced, Pig 1. (d) Score 3, residual surface of epithelium left. (e) Score 4, complete effacement of mucosa. No slide was assigned a score of 3 or 4; hence, (d) and (e) are manipulated versions of (c); while crypts are still visible in (c), they are eroded in (d) and absent in (e). These images were created to depict what the scoring refers to.*

Each tissue cross-section present on the microscope slide was scored individually between 0 and 4. The resulting score for each cross section examined for every condition was then averaged to determine the histology score for that condition. Histology scoring was adapted from Liu *et al.* (1998) and Schoellhammer *et al.* (2015). Scoring was conducted in a blinded fashion: the assessor did not know the treatment received by the tissue on each slide being scored.

6.4.2 Results

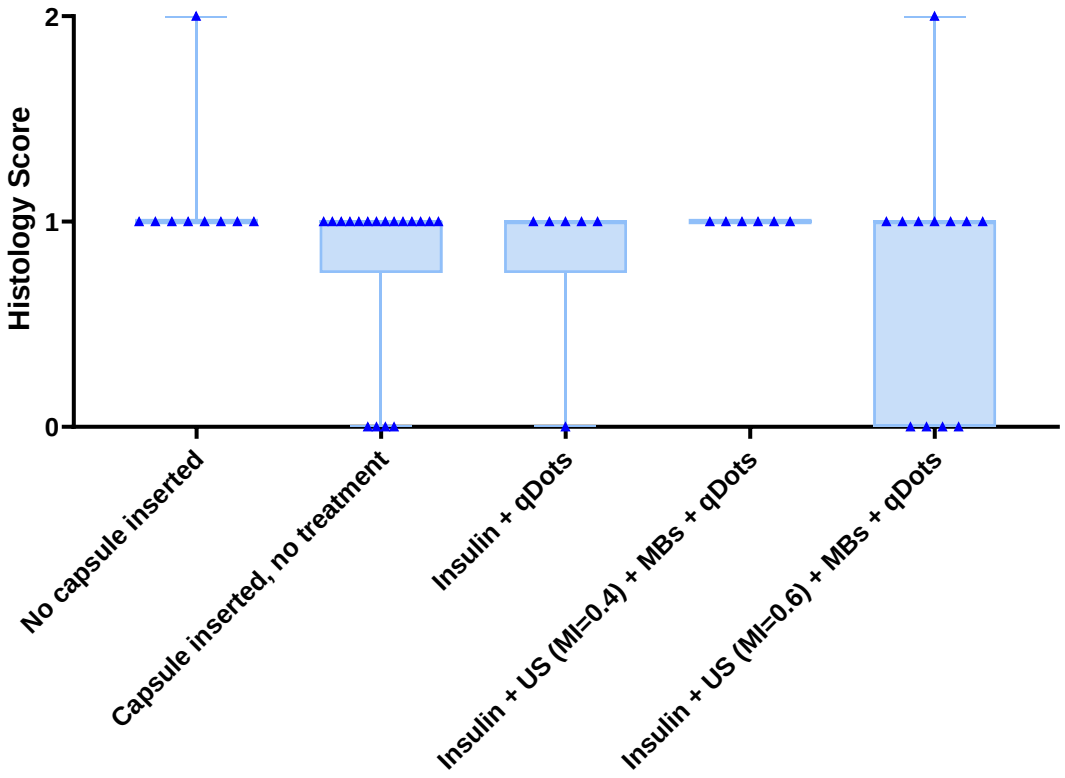

Figure 6-9 Effect of capsule insertion and treatment on tissue histology. *All study groups had most of their slides assigned a score of 1, meaning the villi were shortened or denuded. No sample was assigned a histology score above 2. Scoring was conducted in a single blinded fashion : the assessor was blinded to the treatment or lack of treatment applied to every tissue section prior to tissue harvesting.* $n \geq 6$.

Similar histology scores were assigned to tissue areas where the capsule was not inserted and where it was inserted, Figure 6-9. This suggests capsule insertion does not affect the histology of the intestinal tissue.

Furthermore, the sections of non-treated tissue had a similar histology score to sections of tissue where the suspension was delivered, suggesting suspension delivery does not affect the histology of the tissue either.

When the tissue was exposed to treatments at MI = 0.4 or MI = 0.6, all slides had a similar histology score to control samples, suggesting there was no tissue damage inflicted by the treatment either.

6.5 Discussion

This chapter tested the feasibility of using capsules with a miniature US transducer and MBs for delivering insulin to the intestine of live pigs. The readout of the experiment included three different methods of assessing blood glucose levels. Histology analysis revealed the effect of the intervention on the mucosa of the small intestine.

1 U/kg insulin delivered i.v. correlated with a 30% drop in glucose levels 10 – 20 min post treatment, Figure 6-6. Insulin delivery in the absence of US + MBs was followed by a ~70% increase in glucose levels. Prior to i.v. delivery, glucose levels of Pigs 2 and 3 were 50% lower than those of Pig 1. Based on the first figure in this paragraph and assuming the relationship is linear, to achieve this 50% drop in glucose levels, 1.6 U/kg should have reached the systemic circulation. Up until that point, 9 U/kg had been delivered from the capsule (each treatment delivered in the small intestine or rectum consisted of 3 U/kg). 1.6 U/kg represents ~17% of 9 U/kg. According to this approximate calculation, ~17% of insulin delivered reached the systemic circulation. This would assume that no insulin reached the systemic circulation in Pig 1. What has been suggested here requires further verification.

The recess in the capsule should have ensured that when the capsule was in contact with tissue, the distance between the face of the transducer and the tissue was 4.5 mm (approximately the focal length of the transducer). It is possible that pockets of fluid formed due to the relatively large volume delivered per treatment (12 ml). This could have increased the distance between the face of the transducer and the mucosa, not enabling the mucosa to be within the -3 dB range where cavitation was expected to take place.

Approximately 50% of drugs absorbed from the rectum bypass the hepatic portal circulation, hence they escape hepatic first pass metabolism (Brunton *et al.*, 2018; De Boer *et al.*, 1984). Therefore, rectal treatment was predicted to produce a relatively quick effect

on glucose levels. However, no drop in glucose levels was detected within 70 min post treatment, Figure 6-6 and Figure 6-7. This could be because of one or a combination of the following reasons:

- The treatment could not sonoporate the rectal mucosa. The rectum is lined by stratified epithelium, which is sturdier than the simple epithelium lining the small intestine.

- More than 70 min are necessary for glucose levels to fall. Due to time constraints, treatment four was investigated only for 70 min.

- Rectal mucus could be acoustically opaque, representing a barrier to US and MBs.

- Rectal faecal matter obstructed the interaction between the capsule and the rectum. The surgeon removed faecal matter prior to inserting the capsule, but more might have moved down the canal and obstructed the interaction.

- Contact between capsule and tissue was not adequate. There was no qDot staining detected in the rectum. However, it is also possible that the qDots used do not attach to the stratified epithelium of the rectal mucosa.

Ex vivo experiments showed the capsule did not overheat at MI = 0.4, Figure 6-5, suggesting the treatment should not cause damage due to local overheating. Histology scoring further corroborated this observation, also showing that capsule insertion and the treatment did not damage the intestinal mucosa, Figure 6-9.

Schoelhammer *et al.* (2015) used an axial US probe to deliver insulin through the rectum of six pigs. Within 45 min of treatment, the three control pigs displayed increased glucose levels, up to 12% from the initial values, whereas the three experimental pigs displayed 5%, 12% and 25% drops, respectively. The team delivered the treatment in the absence of MBs and their probe had a resonant frequency of 20 kHz, much lower than the frequency of 1.5 MHz used here, suggesting a completely different treatment regime. These differences makes it difficult to draw a direct comparison.

Abramson et al (2019) developed a device designed for oral administration that can attach itself to the mucosa of the small intestine and inject insulin. When the injected dose was

3 U/kg, the team recorded a 44 ± 5% decrease in glucose levels 25 min post treatment. Our capsule relies on creating pores via sonoporation and drug transfer facilitated by passive diffusion. Although we also delivered 3 U/kg per treatment, it is extremely unlikely that more than a small fraction of this material reached beyond the mucosa. Hence, the values we observed cannot be compared in terms of the delivery mechanism.

The present study investigated the effect of the treatment via an indirect method, fluctuations in glucose levels. Measuring the amount of insulin in the systemic circulation would have been a more suitable test. To differentiate between the amount of insulin secreted by the pig's pancreas and the insulin reaching systemic circulation because of our treatment, C-peptide protein levels could be investigated. Twenty veterinary haematology laboratories across the UK were contacted to enquire if they could conduct insulin and C-peptide blood analysis, but none of them offered the analysis for pigs.

Ideally, the present proof-of-concept study involved three pigs per condition and investigated the effect of delivering insulin and US in the absence of MBs. As the cost of facilities, personnel, pigs and consumables to study three pigs *in vivo* cost of the order of £10,000 (€11,700, US$13,800), the cost of such a study was prohibitive in the circumstances pertaining. Furthermore, time was not available.

6.6 Conclusions

This chapter considered whether US + MBs can facilitate insulin absorption from the intestinal lumen *in vivo* in a large animal model. Intradermal and plasma glucose readings showed that pigs treated with insulin + US + MBs + qDots displayed a lower increase in glucose levels than a pig treated with insulin + qDots. This suggests that insulin reached the systemic circulation. Glucostix readings showed high fluctuation and were deemed less reliable than intradermal and plasma glucose readings. As designed, SonoCAIT likely made adequate contact with the gut mucosa, at least temporarily. Capsule insertion and treatment did not damage the intestinal tissue. These encouraging results justify further exploration.

6.7 References

Abramson, A., Caffarel-Salvador, E., Khang, M., Dellal, D., Silverstein, D., Gao, Y., Frederiksen, M.R., Vegge, A., Hubálek, F., Water, J.J., Friderichsen, A.V., Fels, J., Kirk, R.K., Cleveland, C., Collins, J., Tamang, S., Hayward, A., Landh, T., Buckley, S.T., Roxhed, N., Rahbek, U., Langer, R., Traverso, G., 2019. An ingestible self-orienting system for oral delivery of macromolecules. Science 363, 611–615. https://doi.org/10.1126/science.aau2277

Bergmeyer, H.-Ui., Stein, 2012. Methods of Enzymatic Analysis. Elsevier Science.

Bondar, R.J., Mead, D.C., 1974. Evaluation of glucose-6-phosphate dehydrogenase from Leuconostoc mesenteroides in the hexokinase method for determining glucose in serum. Clin Chem 20, 586–590.

Brange, J., Owens, D.R., Kang, S., Vølund, A., 1990. Monomeric insulins and their experimental and clinical implications. Diabetes Care 13, 923–954. https://doi.org/10.2337/diacare.13.9.923

Brunton, L.L., Knollmann, B.C., Hilal-Dandan, R. (Eds.), 2018. Goodman & Gilman's the pharmacological basis of therapeutics, Thirteenth edition. ed. McGraw Hill Medical, New York.

De Boer, A.G., De Leede, L.G.J., Breimer, D.D., 1984. Drug absorption by sublingual and rectal routes. British Journal of Anaesthesia 56, 69–82. https://doi.org/10.1093/bja/56.1.69

Dewhirst, M.W., Viglianti, B.L., Lora-Michiels, M., Hoopes, P.J., Hanson, M., 2003. Thermal Dose Requirement for Tissue Effect: Experimental and Clinical Findings. Proc SPIE Int Soc Opt Eng 4954, 37. https://doi.org/10.1117/12.476637

Dunn, T.C., Xu, Y., Hayter, G., Ajjan, R.A., 2018. Real-world flash glucose monitoring patterns and associations between self-monitoring frequency and glycaemic measures: A European analysis of over 60 million glucose tests. Diabetes Research and Clinical Practice 137, 37–46. https://doi.org/10.1016/j.diabres.2017.12.015

Gast, K., Schüler, A., Wolff, M., Thalhammer, A., Berchtold, H., Nagel, N., Lenherr, G., Hauck, G., Seckler, R., 2017. Rapid-Acting and Human Insulins: Hexamer Dissociation

Kinetics upon Dilution of the Pharmaceutical Formulation. Pharm Res 34, 2270–2286. https://doi.org/10.1007/s11095-017-2233-0

Gregson, R., Greenhalgh, S., Cox, B., Cochrane, S., Clutton, R.E., 2021. Feeding management before gastrointestinal studies in pigs. Lab Anim 55, 177–180. https://doi.org/10.1177/0023677220960509

Harrison, G.A., 1923. Insulin in Alcoholic Solution by the Mouth. BMJ 2, 1204–1205. https://doi.org/10.1136/bmj.2.3286.1204

Hommelgaard, P., 1976. Risks involved in the use of electromedical equipment. I. A review. Ugeskr Laeger 138, 845–848.

Liu, J., Lewis, T.N., Prausnitz, M.R., 1998. Non-invasive assessment and control of ultrasound-mediated membrane permeabilization. Pharm Res 15, 918–924. https://doi.org/10.1023/a:1011984817567

Moldovan, A., 2021. Development of a 1D Phased Ultrasonic Array for Intravascular Sonoporation (Doctoral Thesis). University of Strathclyde, Glasgow.

Nakrani, M.N., Wineland, R.H., Anjum, F., 2021. Physiology, Glucose Metabolism, in: StatPearls. StatPearls Publishing, Treasure Island (FL).

Schoellhammer, C.M., Schroeder, A., Maa, R., Lauwers, G.Y., Swiston, A., Zervas, M., Barman, R., DiCiccio, A.M., Brugge, W.R., Anderson, D.G., Blankschtein, D., Langer, R., Traverso, G., 2015. Ultrasound-mediated gastrointestinal drug delivery. Sci. Transl. Med. 7, 310ra168-310ra168. https://doi.org/10.1126/scitranslmed.aaa5937

Wang, X., Meng, M.Q.-H., 2010. An experimental study of resistant properties of the small intestine for an active capsule endoscope. Proc Inst Mech Eng H 224, 107–118. https://doi.org/10.1243/09544119JEIM540

Chapter 7
Conclusions and Future Work

The present thesis considered issues relating to future potential developments of a platform for oral delivery of medication in the form of USmTDD. The first topic covered was the nature of intestinal mucus, particularly its rheology, and an artificial mucus recipe was proposed to aid future mucus studies. An advanced *in vitro* system for USmTDD was proposed that should increase the relevance of *in vitro* studies. Suitable US parameters for *in vitro* decrease of barrier function were identified. Finally, a proof of concept study was described that showed that US, MBs and insulin delivered from a capsule in the small intestine of live pigs decreased glucose levels compared to a control pig. This chapter briefly presents the main findings from each chapter, draws them together, and suggests future directions.

7.1 Conclusions

Beginning with the first layer with which drug delivery must content, Chapter 3 focused on characterising intestinal mucus to understand whether it represents a barrier to USmTDD. The chapter investigated mucus' pH, dry substance content and rheology. In order to avoid culling pigs for further experiments, an artificial recipe with similar rheology was developed. Artificial mucus was relatively acoustically transparent; it caused an attenuation between 0.1 % and 0.6 % of the US pressure at the studied parameters when controlling for the thickness of the layer in the small intestine *in vivo*. Nevertheless, qDots lodged in a mucus layer rather than in the mucosa when delivered with US + MBs to the *ex vivo* mouse small intestine. It is likely that this was an area adjacent to the focal zone, because the treatment was able to dislodge tissue from the mucosal surface in the focal area.

Moving on to intestinal tissue itself, Chapter 4 showed how US + MBs can overcome the epithelial barrier and facilitate delivery of model drugs through a cell layer. It was shown that the effect is stronger with transducers with wide application areas: single-element unfocused and phased array transducers produced a larger drop in barrier function compared to focused transducers. The phased array transducers even produced large pores. This chapter also showed that a larger decrease in barrier function is associated with a lower frequency, a larger MI, a larger PRF, a higher DC and a higher number of cycles of US. It was further shown that treated cells were depleted of F actin and their nuclei covered a smaller surface area than non-treated cells.

Monocultured cell monolayers are a conventional model for intestinal epithelia, but have clear shortcomings. Chapter 5 described the development and testing of an *in vitro* system more similar to the *in vivo* mucosa than the existing gold-standard Caco-2 cell layers. This was in the form of a confluent monolayer grown from rectal OGs on ThinCert filters. Caco-2 and OG-derived cell layers appeared similarly sensitive to US + MB treatment. NDs were also considered in this chapter and it was shown that US + MBs induced holes in the OG-derived layer, whereas US + NDs did not. Full barrier function recovery in this model was observed within 48 h post-treatment when the treatment lasted for 30 s, but not when it lasted for 11 min, respecting the time previously found to be required.

Finally, a proof of concept test was carried out on three pigs *in vivo*. This is described in Chapter 6, where the work tested whether the glucose levels of live pigs were affected by delivering a treatment of insulin + US + MBs + qDots in their small intestine. To carry out the test, capsules containing miniature phased array transducers identical to those used *in vitro* were inserted in the small intestines of the pigs. US was delivered based on parameters identified in Chapter 4. The two test pigs treated with insulin + US + MBs + qDots displayed lower increases in glucose levels than the control pig that was treated with insulin + qDots. This suggested US and MBs overcame both the mucus and mucosal barrier and that treatment facilitated insulin delivery to the systemic circulation.

The hypothesis of this project was proven true: US and CAs can be employed to successfully deliver drugs through the mucosa of the small intestine *in vitro* and *in vivo*. Overall, this thesis represents a proof of concept study for therapeutic US delivered to the small intestine using an intracorporeal capsule. This drug delivery tool should be acceptable to patients, leading to increased drug uptake with less side effects. This could

translate into improved treatment, a higher quality of life for patients, and reduced treatment costs.

7.2 Future Studies

Ideally, the work would be continued with pig studies, but the cost is prohibitive, they are time consuming and one should strive to reduce the number of animals used in research. Hence, developing better *in vitro* models, OG-based and testing different drugs should be prioritised. Further understanding how NDs can be manipulated for this purpose should be completed prior to conducting more porcine experiments *in vivo*. The sections below explore advanced *in vitro* models.

7.2.1 Dual-Chamber System

CliniCELL (Mabio, France) and Opticell^{TM} (VWR, PA, USA) are cell culture single cassettes with gas permeable films, access ports and ventilation ports. They can be used to study the effect of insonation on cell layers, but not for drug delivery across the cell layer. To address this drawback, I considered developing a dual-chamber cassette, where a polycarbonate filter, similar to the ThinCert filter, divides two chambers bordered by acoustically transparent and gas permeable films, Figure 7-1 (a). The films could be mylar sheets, rigid enough to hold the cell culture medium and the cells. Access ports would enable the insertion of cells in the apical chamber. The cells would attach to the polycarbonate filter on the bottom of the chamber and develop a confluent layer.

For positively buoyant CAs, such as MBs, on the day of the experiment, the construct would be rotated 180°, so that the cells are in the bottom chamber, attached to the filter, Figure 7-1 (b). The suspension of MBs and model drug would be injected into this chamber. MBs will float and come into contact with the cells. The construct would be inserted in a water bath and US would be applied from underneath. Cavitation would take place in proximity to the cells with the shockwaves decreasing the barrier function. The model drug would passively diffuse to the apical chamber. At different time intervals, the apical chamber would be sampled and the amount of model drug would be quantified.

For negatively buoyant CAs, such as NDs, the construct does not need to be rotated. The suspension of NDs and model drug would be injected in the top chamber, Figure 7-1 (c). The NDs would pool to the bottom of the chamber, coming into contact with cells. The construct would be immersed in a water bath and insonation would be applied from the

top. Following the experiment, the basal chamber was sampled at different intervals to quantify the amount of drug which diffused in the basal chamber. The prototype in Figure 7-1 (d) was fabricated by Mr Zutuo (MSc student). The software used was SolidWorks.

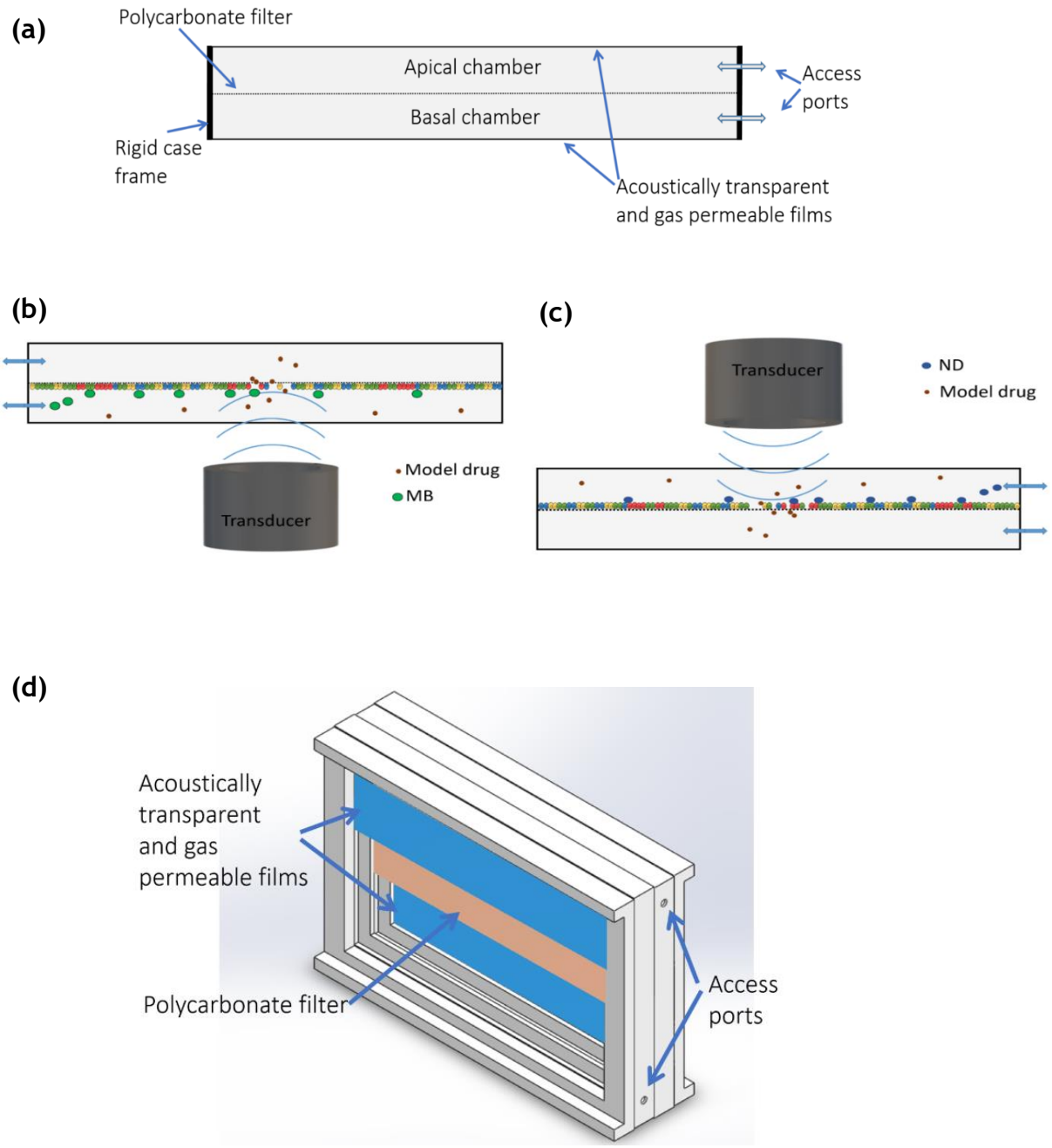

Figure 7-1 Dual chamber system for quantitative drug delivery studies. *(a) The apical and basal chambers are separated by a polycarbonate filter on which cells can grow. The outer border of the chambers is an acoustically transparent and gas permeable film, such as Mylar. The cells and media would be injected through the access ports. The cells would be seeded in the apical chamber. (b) MBs float, so the construct would be rotated to enable the MB to come into contact with the cell layer. US would be applied from underneath. (c) NDs pool to the bottom of the well, so the chamber would not need to be rotated. NDs would be injected in the apical chamber and US would be applied from above. (d) Rapid prototype of dual-chamber system. The polycarbonate filter separates the two chambers.*

7.2.2 ThinCert with Crypts

Intestinal metabolising enzymes can influence the intestinal absorption of drugs. Caco-2 cell layers have been shown not to secrete enzymes of the cytochrome P450 CYP3A subfamily. These enzymes might regulate the bioavailability of certain orally administered drugs (Breeman and Li, 2005) and are abundantly expressed by mature cells found in the villi of the small intestine (Peters and Kremers, 1989). Speer *et al.*, 2019a, have shown that intestinal OG-derived monolayers cultured on a gradient cross-linked scaffold expressed similar levels of CYP3A and other drug metabolising enzymes compared to those found in fresh villi. Employing OG-derived cell layers in US-mediated drug delivery experiments might further improve the probability of *in vitro* studies to be replicated *in vivo*.

Instead of a flat 2D monolayer, a crypt-like monolayer would be more representative. Speer *et al.*, 2019 have developed such a crypt. It could be used (1) to study the effect of insonation + MBs/NDs on the barrier function of such a layer, (2) to compare this to the effect of the treatment on a flat monolayer and on *in vivo* tissue, (3) to conduct fluorescence-activated cell sorting (FACS) analysis of such layer and *in vivo* tissue to check if the types of cells and their ratios are similar.

7.2.3 Microinjection of Organoids

In the small intestine, the apical surface of mucosal cells is the first to interact with drugs administered orally and which reach the intestinal lumen. In intestinal OGs, the apical surface faces towards the inside of the lumen. In order to mimic the *in vivo* condition, to enable the drug to interact with the apical surface of the mucosal cell layer, the drug needs to act from the inside of the OG. Although bright microscopy renders OGs as rings, they are actually sphere-shaped (Sachs at al., 2019). Therefore, microinjection was explored as a way to deliver drugs to the lumen of the OG.

7.2.3.1 Method Developed

Several chambers of a detachable chamber 8-well plate (Sarstedt AG & Co) were evenly coated with 150 µl MG to create a cushioning layer between the bottom of the well and OGs. The chamber was then incubated for 3 h. Porcine small intestine OGs were grown as described in Section 5.2.1. Selected large cystic OGs were then transferred to the wells of the plate. To transfer, each MG dome (50 µl) was dissolved in 70 µl PBS. 130 µl MG were added to the well. This was mixed and 50 µl were plated on each chamber well. The

chamber was then incubated for at least 2 h to ensure the MG hardened. If the experiment was conducted only the following day, once the MG hardened, 150 µl OGM (+1% AA, +0.1% Y27) were added to each well. Prior to the experiment, OGM was discarded and a scalpel was used to cut around the edges of the inner wells. This ensured the OGs did not stick to the wells when the frame was detached. Following frame detachment, the chamber was placed on the stage of a cell culture inverted bright light microscope (CKX53, Olympus, UK). The OGs that were the targets for injection were brought to the middle of the camera plane.

In order to pierce and inject the OGs, a pre-pulled glass capillary (ID = 5 µm, OD = 1 mm, product code TIP5TW1, WPI, UK) was filled with 1 mg/ml FD4 in HBSS (14170112, Gibco, UK). The microneedle was attached to a microstage to ensure accurate positional control. It was connected through a feeder tube to a 1 ml syringe, both filled with mineral oil (R21237, ThermoFisher, UK). Mineral oil has a higher density than 1 mg/ml FD4 in HBSS, thus ensuring the FD4 suspension was pushed out through the 5 µm microneedle tip. The syringe was placed in a syringe driver (New Era Pump, NE-1000) set to deliver the suspension at a rate of 2 ml/h.

In order to ensure the tip of the microneedle was not broken through touching other surfaces, it was run across the top of the MG dome to identify its shadow and observe its position in relation to the dome. Once the shadow was visible, the microneedle was lowered close to the dome, as seen in Figure 7-2 (a). The fine focus adjustment was then used to check whether the OG and the tip were in the same plane, see Figure 7-2 (b) The OG was pierced and FD4 was delivered, Figure 7-2 (c). Images were acquired with a GXCAM HiChrome-MET camera (GT Vision, UK).

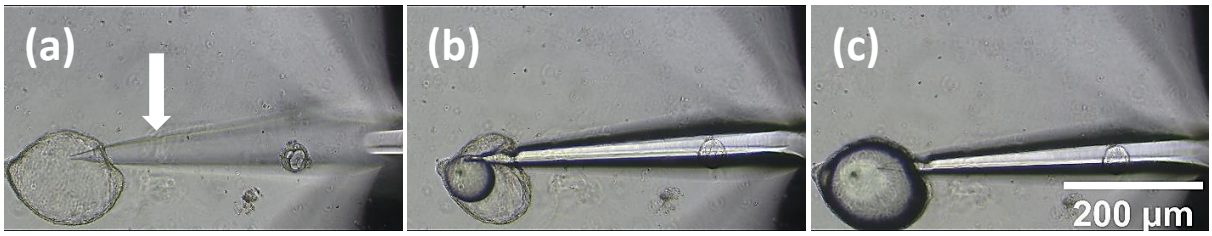

Figure 7-2 OG pierced (a) and injected (b-c) with mineral oil using a microneedle with a 5 µm tip diameter. *Mineral oil was used for this mock experiment as it can be visualised using bright field microscopy. FD4 injection could have been visualised with a bright field microscope only indirectly, by OG diameter expansion. White arrow in (a) points towards microneedle. Scale bar in (c) applies for (a-b) too.*

7.2.3.2 Considerations

Basal-out OGs have a very elastic outer wall, Figure 7-3 (b-d), rendering them difficult to pierce and inject. A microneedle tip with an ID of 2 µm is sharp enough to pierce the OG, but too narrow to allow the suspension to exit through it (data not shown). Conversely, a microneedle tip with an ID of 10 µm is too blunt to pierce the OG (Figure 7-3), but can reliably eject the suspension. A microneedle tip with an ID of 5 µm was found to both pierce the OG and reliably eject the suspension, Figure 7-3.

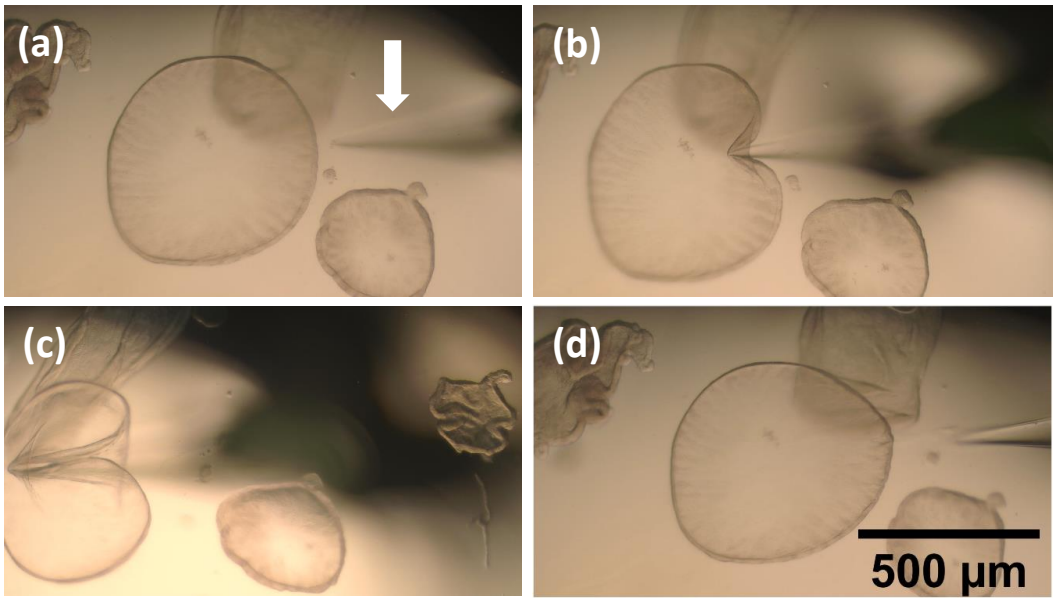

Figure 7-3 Large OGs are elastic and not pierced by a microneedle with a 10 µm tip ID. *(a) OG before tampering with it; white arrow points towards the microneedle; (b-c) The microneedle is pushed against the OG, but without piercing it; (d) Upon removal, the OG looks slightly deformed compared to (a), but not damaged or pierced. Scale bar in (d) applies for (a-c) too.*

The orifice of the needle is too narrow to reliably eject suspension immediately upon the syringe driver pushing the plunger of the syringe. Suspension is ejected only once enough positive pressure forms in the needle. This also means that even after the pump stops pushing the plunger, suspension will be ejected until there is insufficient positive pressure in the needle. Hence, following injection of an OG, once the needle is removed from the OG and from the MG dome, a trace of suspension may be left behind. If the compound is fluorescent and fluorescence is the assay readout, the background may be too high for accurate reporting.

It is unknown how long it takes for a pore made in an OG to seal, with dependence potentially on the size of the pore. This relates to how much of the needle was inserted in

the OG. Fluorescent probes are sensitive to duration of exposure to light, so the fact that an experiment can be started only once a pore has sealed may affect the signal strength and accuracy of the results obtained.

Metal microneedles were considered because of their reusability. 30 Gauge (0.3 mm OD) stainless steel needles, the smallest available, were glued to glass capillaries to build needles suitable for injecting OGs. However, the glue was found to trickle up the capillary, enter the needle, and obturate it. A 90 s epoxy might be more suitable. As an alternative, bespoke stainless steel needles with a bevelled sharper end (33 Gauge, 0.2 mm OD) to pierce the OG and a 1 mm opposite end to mate with the suspension delivery channel were sought. Such metal needles could not be manufactured by any company contacted.

Successful delivery with a glass / metal combination would require not just the tip of the microneedle, but the entire bevel to be inserted in the OG. This would result in a hole of 0.3 mm diameter in the OG, which would be very large. OG diameter is between 0.1 and 0.5 mm (Figure 7-2 and Figure 7-3). All considerations are summarised in Table 7-1.

The fine adjustments required for microinjection call for a steady hand and patience on the part of the operator, increasing the stress of the method compared to many other procedures required in cell culture. A solution could be offered by an US-actuated needle, which would reduce the force that needs to be applied (Jiang *et al.*, 2016).

Table 7-1. Risk assessment for microinjection into OGs.

Problem	*Mitigation*
MG and OGs move	Increase MG concentration. Allow MG dome to harden in incubator for longer. Use pump withdrawal function to stabilise OG.
Microneedles break easily	Coat bottom of well with MG to act as a cushion. Use a stainless steel microneedle.
Control of agent delivery quantity	Use syringe pump instead of a hand-held syringe. Identify suitable delivery rate and volume.
OG wall hard to pierce	Use microneedle with a smaller tip diameter
Suspension not ejected through needle	Use microneedle with a larger tip diameter Use suspension with compounds of smaller diameter.

7.2.3.3 Implications and Applications

The 5 µm microneedle tip was found to reliably eject the suspension used in this experiment. However, if the suspension required for injection is more viscous, or the compounds are of higher molecular weight (MW), or certain compounds aggregate, then the opening may require further optimisation.

The microinjection method was developed, but time constraints did not enable the testing of its suitability for insonation experiments. A potential experiment is detailed below. Large OGs would be microinjected with FD4-FITC, the gap would be allowed to heal, OGs would be transferred to six fresh wells without any background FITC. Three of the wells would then be insonated in the presence of CAs with a transducer as presented in Chapter 5, whereas the other three wells, the control ones, would not be insonated. More FD4-FITC would be expected to be released from insonated samples after a certain period if cavitation has sonoporated the OGs. Hence, the fluorescence intensity should be higher in insonated samples. This could be checked with a fluorescent microscope at different time intervals, or by sampling the well periodically and reading the samples with a plate reader. It was noticed that the FD4 used photobleached within 25 seconds under 492 nm light. Fluorescent microscopes usually have low resolution and cannot identify small fluorescence intensity differences. A confocal microscope might be more suitable, but access is required immediately due to photobleaching.

An alternative experiment, excluding microinjection, would require the seeding of crypts in the presence of high concentrations of a fluorescent compound (i.e. FD4). The fluorescent compound would then be incorporated in the OG. The OGs would be rinsed and transferred to a well free of fluorescent compounds. CAs and US could be applied to decrease the barrier function and enable the fluorescent compounds to exit the OG. The amount of fluorescent compounds measured would correlate to the extent of the decrease in barrier function of the OG.

7.2.4 Apical-out Organoids

In the small intestine, the apical surface of mucosal cells interacts with luminal contents and enables nutrient absorption, pathogen detection and secretion of antimicrobial compounds (Gehart and Clevers, 2019; Sachs *et al.*, 2019; Sato *et al.*, 2011). In contrast, the basal surface of mucosal cells anchors the tissue layer into the basement membrane, which is a thin and fibrous layer of extracellular matrix (ECM). The basal surface enables

the delivery of nutrients from the lumen to the hepatic portal circulation and the interaction between mucosal cells and their neighbours.

OGs are usually cultured embedded in MG, which has a similar composition to the ECM. The basal surface of OG cells faces the MG and their apical surface faces the interior of the OG. Hence, these OGs are called basal-out. The apical surface of these OGs cannot be accessed straight from the MG. However, removal of ECM proteins can reverse the polarity of OGs, leading to an apical-out configuration and rendering them useful for certain applications.

7.2.4.1 Method to Reverse Polarity

For the work described here, a protocol was used based on Co *et al.*, 2019. Porcine small intestine OGs were grown as described in Section 5.2.1. OGs were grown at 37°C with 5% CO_2 for 7 – 20 days. The media was removed and the MG was solubilized in 5 mM sterile EDTA in PBS for 1 h at 4°C on a rotating platform. OGs were centrifuged at 200 G for 3 min at 4°C and the supernatant was removed. The pellet was re-suspended in growth media in ultra-low attachment 24-well tissue culture plates. OGs were incubated at 37°C with 5% CO_2 for 3 days. For comparison, basal-out OGs from the same culture were transferred to a fresh well plate on Day 1.

EDTA is a chelating agent that disrupts cell-cell adhesion. EDTA selectively binds metal ions such as Mg^{2+} and Ca^{2+}. The latter is required for normal cell-cell adhesion. The addition of EDTA to cell media depletes cells of Ca^{2+}, which renders them unable to bind to other cells. This effect, combined with the fact that the cells are in suspension and do not interact with MG, which mimics the basement membrane, results in polarity eversion. Once this process is complete, the OGs are inside-out. According to Co *et al.*, 2019, this happens through tissue eversion in a B1 integrin-dependent manner.

From Day 2 to Day 4, basal-out OGs appeared more transparent than apical-out OGs. In the high magnification images, the outer layer of cells appears more visible in apical-out than basal-out OGs. By days 3 and 4, basal-out OGs are larger than apical-out OGs. At Day 4, some apical-out OGs appear to be surrounded by debris, suggestive of OG disintegration.

Co *et al.*, (2019) do not present data for the fourth day onwards. Figure 7-4 shows that after four days of culture, apical-out OGs started to disintegrate. The number of viable apical-out OGs at Day 5 were not studied because the OGs were used for flow cytometry on Day 4.

Day 2

Apical-out OG

Basal-out OG

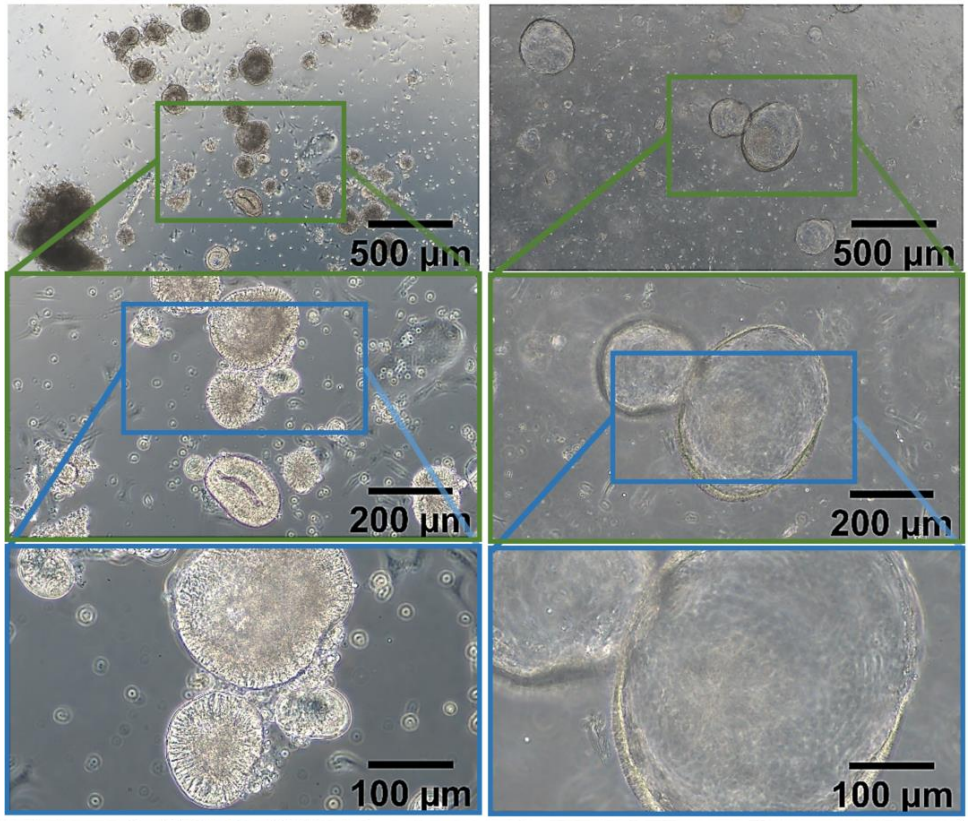

Day 3

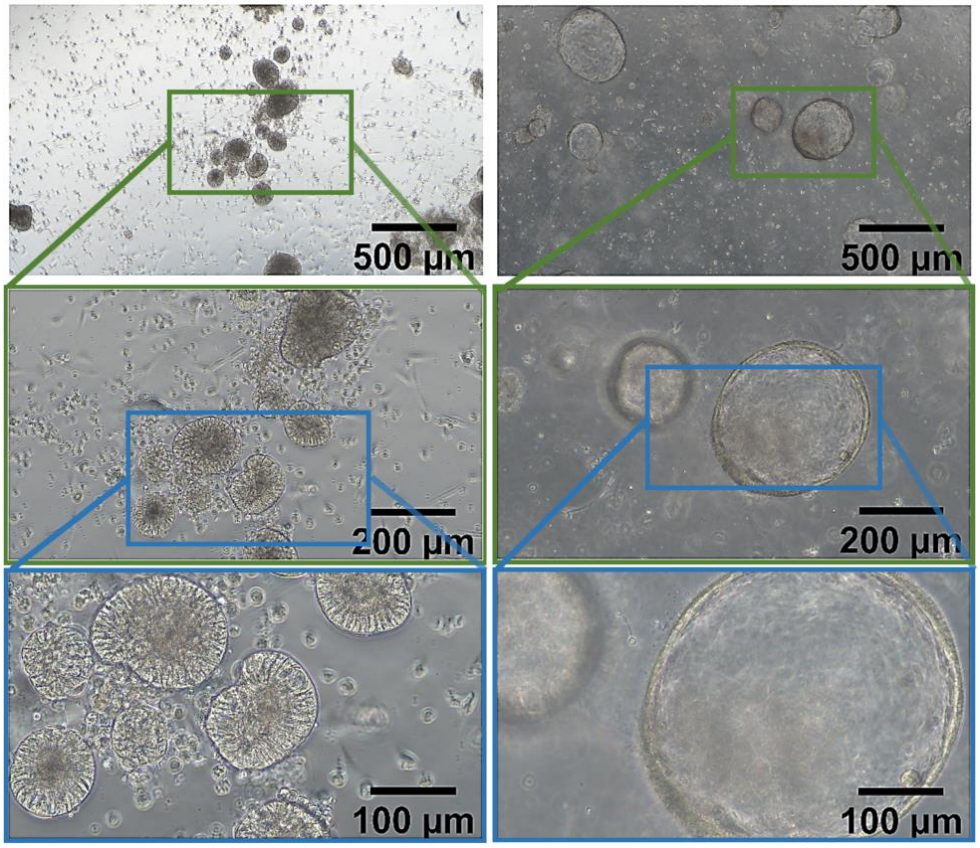

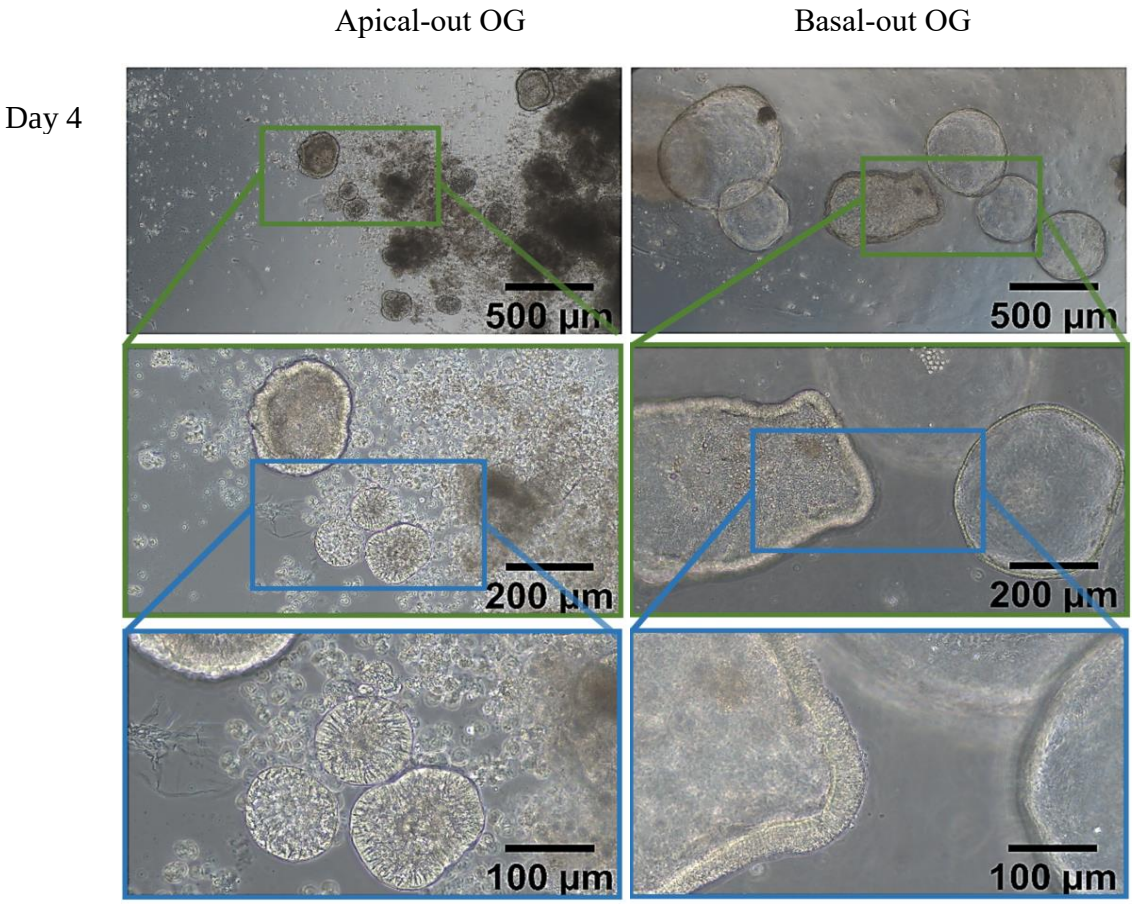

Figure 7-4 Development of apical-out OGs and comparison with basal-out OGs. *From Day 2 to Day 4, basal-out OGs appear more transparent than apical-out OGs. In the high magnification images, the outer layer of cells appears more visible in apical-out than basal-out OGs. By Days 3 and 4, basal-out OGs are larger than apical-out OGs. At Day 4, some apical-out OGs appear to be surrounded by debris, suggestive of OG disintegration. The dark OGs are in the process of disintegrating.*

7.2.4.2 Apical-out and Basal-out OGs Expression of Cellular Markers

Fluorescence-activated Cell Sorting

The apical-out and basal-out OGs were developed as described in Section 5.2.1. Once they reached Day 4 of culture, they were characterised with FACS. The supernatant was aspirated and the OGs were washed in PBS and incubated with trypsin at 37°C for 10 – 15 min. The content was made up to 10 ml with AIMV (1% FBS), centrifuged at 200 rpm for 5 min and the supernatant was removed. The cell suspension was prepared to a concentration of 3 x 10^6 cells/ml in cold PBS. The antibodies used stained cells against Leucine Rich Repeat Containing G Protein-Coupled Receptor 5 (LGR5), MUC2, KI-67 and villin. Their details are displayed in Table 7-2. LGR5 is an extracellular marker, whereas MUC2, KI-67 and villin are intracellular markers. To quantify the number of cells

positive for an intracellular marker, the cells required permeabilisation. To achieve this, they were blocked with 3% FBS, permeabilized in BD permeabilisation and fixation solution (554714, BD, USA) for 20 min at 4°C, then washed with BD wash buffer (554714, BD, USA) twice, for 10 min each time.

The LGR5 antibody used was directly labelled so secondary antibody staining was not necessary for it. The other three primary antibodies were not directly labelled, so the relevant samples required incubation with a labelled secondary antibody to detect the signal. For primary antibody staining, 100 µl cell suspension was added to each Eppendorf tube. The recommended quantity of primary antibody was added and incubated at 4°C for 30 min. The cells were washed three times by centrifugation at 400 g for 5 min and were then resuspended in ice cold PBS. For secondary antibody staining, the secondary antibody was diluted according to the manufacturer's recommendations, Table 7-3. The cells were incubated in the dark at 4°C for at least 30 min, then washed three times in PBS by centrifugation at 400G for 5 min. The cells were resuspended in cold PBS, 3% Bovine Serum Albumin (BSA) and 1% sodium azide then analysed with an ACCURI C6 Flow Cytometer (BD, USA) using CFLOW PLUS software (BD, USA). Between analyses of successive samples, the metal rod of the flow cytometer was rinsed with PBS. Each Eppendorf tube was flicked and tapped against the bench before analysis. The laser used was 488 nm for both FITC and PE. For LGR5-PE, the control used was immunoglobulin G1 (IgG1) - phycoerythrin (PE) and the one for the FITC antibodies was IgG1-FITC. For each sample, the entire 100 µl sample was analysed, each sample consisting of at least 12,000 events. The experiment was conducted only once, so the presented results are preliminary.

Table 7-2 List of primary antibodies.

Antibody	*Source*	*Cat. No.*	*Clonality*	*Species*	*Application*	*Dilution*
MUC2	DAKO Omnis	M7313	Monoclonal	Mouse	Flow Cyt	1:1000
KI-67	DAKO Omnis	GA626	Monoclonal	Mouse	Flow Cyt	1:1000
Villin	Abcam	ab130751	Monoclonal	Rabbit	Flow Cyt	1:100
LGR5	Miltenyi Biotec	130-112-437	Monoclonal	(cell line)	Flow Cyt	1:50

Table 7-3 List of secondary antibodies.

Secondaries	*Source*	*Cat. No.*	*Excitation/Emission*	*Label*	*Dilution*
Mouse IgG1 k Isotype	BD Pharmingen	555909	494 / 520 nm	FITC	Pre-diluted
Mouse IgG1 k Isotype	BD Pharmingen	555749	496 / 578 nm	PE	Pre-diluted

MUC2 protein is a marker specific for mature intestinal goblet cells. It is important to check whether this type of cell is present in OGs to ensure apical-out OGs have the capacity to secrete mucus. A mucus layer surrounding the OG would make insonation studies more relevant by further mimicking the human intestinal lumen. Both apical-out and basal-out OGs cells expressed similar levels of this protein, as seen in Figure 7-5 and Table 7-4.

KI-67 protein is a marker strictly associated with cell proliferation. Basal-out OGs express slightly more KI-67-positive cell (Table 7-4), which is consistent with the fact that basal-out OGs appear to be larger in diameter than apical-out OGs (Figure 7-4).

Villin is a cytoskeleton protein found in the brush border of the intestine. It is used in FACS as a tissue-specific marker for intestinal cells. Apical-out OGs have slightly more villin-positive cells, Table 7-4. This might be because basal-out OGs do not have villi exposed to the surrounding environment, and so their mucosal cells are not exposed to the surrounding nutrients, growth factors, media and so do not mimic the lumen conditions. Apical-out OGs enable the villi to be exposed to the surrounding environment, promoting cells to behave as if they were in the intestine. Ideally, this could be compared to the quantity of villin-positive cells in the tissue of origin.

LGR5 protein is associated with progenitor cells, the CBC mentioned in Section 5.1. They are adult intestinal stem cells that generate a range of functional cells in the intestinal tissue. Both types of OG appear to have similar levels of LGR5-positive cells, just under 1%, Table 7-4. This contrasts with information from Liu *et al.* (2018), who showed that basal-out OGs are 10.3% LGR5. The different protocols for culturing OGs and conducting FACS may be responsible for this.

The available antibodies were anti-human and the tissue was porcine. Some off-targeted binding might have occurred.

Table 7-4 Four markers similarly expressed in apical-out and basal-out OG. *The values were obtained from the FACS.*

Marker	*Apical-out OG*	*Basal-out OG*
MUC2	60%	62%
KI-67	52%	68%
Villin	93%	78%
LGR5	0.9%	0.7%

Confocal Microscopy

Inside-out and basal-out OGs were fixed and stained with DAPI and MUC2-FITC, as described in Table 7-2 and Table 7-3. The samples were imaged with a confocal microscope (A1R, Nikon, Tokyo, Japan). MUC2-FITC stained goblet cells in green, whereas DAPI stained the nuclei in blue. In the apical-out OG, Figure 7-5 (a), large quantities of goblet cells appear to be on the apical side, as it would be expected. In the basal-out OG, Figure 7-5 (b), goblet cells appear as honeycomb-like structures predominantly in the centre of the OG. The large green patch at the top of the basal-out OG (white arrow) might be internal content that has become externalised. Dead goblet cells from the apical side inside the OG can contain MUC2 proteins and they might be the reason for the fluorescence seen. The blue trace could be nuclei of cells externalised from the OG.

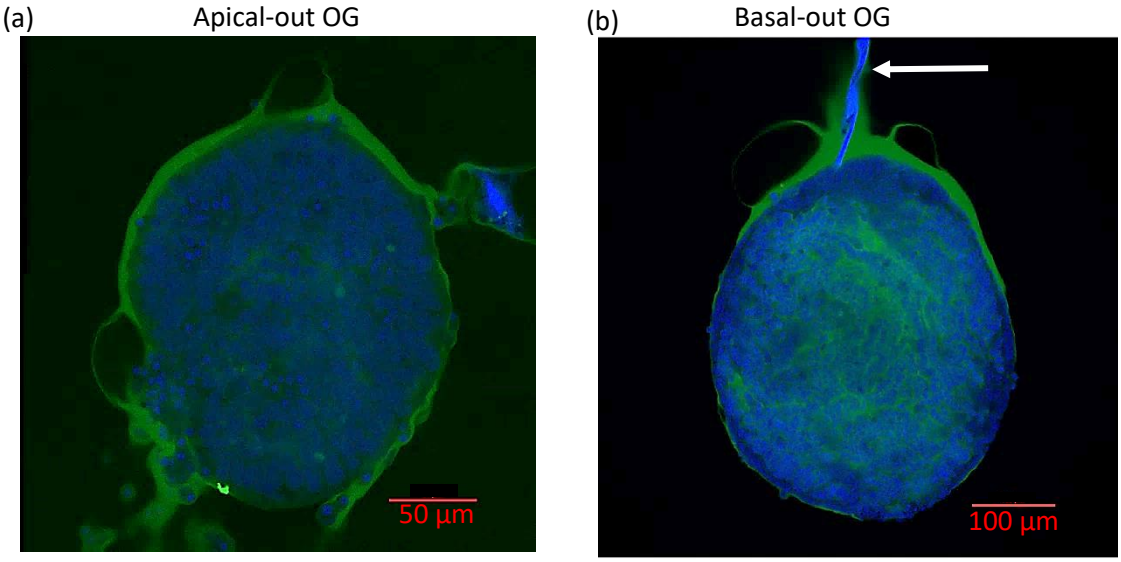

Figure 7-5 Confocal microscopy of OG. *(a) Apical-out OG displays high levels of goblet cells on the periphery. (b) Basal-out OG displays high levels of goblet cells in the centre. White arrow indicates dead content that might have been externalised. Green = goblet cells. Blue = nuclei. Note different scale bar.*

7.2.4.3 Implications and Applications

Apical-out OGs may be more suitable for studying the interaction of drugs with the mucosa than microinjected basal-out OGs. Apical-out OGs express similar amounts of MUC-2, villin, KI-67 and LGR5, making them equally suitable for studies where these proteins are important.

A disadvantage of apical-out OGs developed as above is that they start to disintegrate by culture Day 4. Hence, it is compulsory to use them at Day 3. If the assays that are employed are for drugs that act for longer than 24 hours, or the recovery of the external cell layer needs to be followed for several days, then apical-out OGs are likely to be inappropriate.

Apical-out OGs could be used for barrier integrity, nutrient uptake and infection studies (Co *et al.*, 2019). Apical-out epithelial barrier integrity could be assessed with a fluorescent dextran diffusion assay. US, CAs and fluorescent dextran could be applied to these OGs and to understand the extent of decrease in barrier function. The positive control could be EDTA-treated OGs, where the EDTA should have disrupted the barrier and made it leaky. The negative control would be non-insonated OGs. As mentioned in Section 7.2.3, fluorescent microscopy was insensitive to the dextran inside OG. Confocal microscopy would be necessary to ensure visualization of the fluorescent compound is possible.

Apical-out and basal-out OGs could be used to study whether drugs or pathogens interact with receptors on the apical or basal side of cells. The same drug or pathogen would be applied to both apical-out and basal-out OGs grown in separate wells and check which OG type is more sensitive. If drugs interact with receptors on the basal side of the mucosal cell layer, they should be administered systemically. If they interact with receptors on the apical side, ideally the drug reaches them from the lumen side.

7.2.4.4 Drawbacks of Cell Culture Systems

The drawbacks of cell culture systems compared to *in vivo* tissue include the cell layers' lack of vascularisation, lack of symbiosis between cells and commensal microbes and protocol inconsistencies (Saeidnia *et al.*, 2015). For example, protocols for OG cultures are not uniform across laboratories, with most teams following their own protocols. Variations in the growth medium can lead to signalling pathways being activated differently, resulting in different cell responses to drugs and stress. This can lead to different results according to the method adopted. Successful *in vitro* experiments can often be irrelevant if not replicable *in vivo*. However, OGs, acoustically transparent materials and structures similar to the *in vivo* anatomical structures presented in this section can be used to create more adequate *in vitro* assays and reduce the number of animals used in research.

A suitable system needs to replicate *in vivo* conditions well enough to conclude which treatment parameter combinations are safe; membrane resealing should ideally take milliseconds to decrease the possibility for pathogens to penetrate the mucosa and gain access to the portal and systemic circulation and spread around the body. To prevent this, the treatment should facilitate only the passage of therapeutic agents across the epithelium. One way to achieve this could be to deliver CAs labelled with the drug of interest to the cell layer and produce inertial cavitation and microjets which "inject" the CA's drug load across the cell layer.

7.3 References

Co, J.Y., Margalef-Català, M., Li, X., Mah, A.T., Kuo, C.J., Monack, D.M., Amieva, M.R., 2019. Controlling Epithelial Polarity: A Human Enteroid Model for Host-Pathogen Interactions. Cell Reports 26, 2509-2520.e4. https://doi.org/10.1016/j.celrep.2019.01.108

Gehart, H., Clevers, H., 2019. Tales from the crypt: new insights into intestinal stem cells. Nat Rev Gastroenterol Hepatol 16, 19–34. https://doi.org/10.1038/s41575-018-0081-y

Jiang, Y., Qiu, Z., McPhillips, R., Meggs, C., Mahboob, S.O., Wang, H., Duncan, R., Rodriguez-Sanmartin, D., Zhang, Y., Schiavone, G., Eisma, R., Desmulliez, M.P.Y., Eljamel, S., Cochran, S., Button, T.W., Demore, C.E.M., 2016. Dual Orientation 16-MHz Single-Element Ultrasound Needle Transducers for Image-Guided Neurosurgical Intervention. IEEE Trans Ultrason Ferroelectr Freq Control 63, 233–244. https://doi.org/10.1109/TUFFC.2015.2506611

Liu, Y., Qi, Z., Li, X., Du, Y., Chen, Y.-G., 2018. Monolayer culture of intestinal epithelium sustains Lgr5+ intestinal stem cells. Cell Discov 4, 32. https://doi.org/10.1038/s41421-018-0036-z

Peters, W.H.M., Kremers, P.G., 1989. Cytochromes P-450 in the intestinal mucosa of man. Biochemical Pharmacology 38, 1535–1538. https://doi.org/10.1016/0006-2952(89)90194-9

Sachs, N., Papaspyropoulos, A., Zomer-van Ommen, D.D., Heo, I., Böttinger, L., Klay, D., Weeber, F., Huelsz-Prince, G., Iakobachvili, N., Amatngalim, G.D., Ligt, J., Hoeck, A., Proost, N., Viveen, M.C., Lyubimova, A., Teeven, L., Derakhshan, S., Korving, J., Begthel, H., Dekkers, J.F., Kumawat, K., Ramos, E., Oosterhout, M.F., Offerhaus, G.J., Wiener, D.J., Olimpio, E.P., Dijkstra, K.K., Smit, E.F., Linden, M., Jaksani, S., Ven, M., Jonkers, J., Rios, A.C., Voest, E.E., Moorsel, C.H., Ent, C.K., Cuppen, E., Oudenaarden, A., Coenjaerts, F.E., Meyaard, L., Bont, L.J., Peters, P.J., Tans, S.J., Zon, J.S., Boj, S.F., Vries, R.G., Beekman, J.M., Clevers, H., 2019. Long-term expanding human airway organoids for disease modeling. EMBO J 38. https://doi.org/10.15252/embj.2018100300

Saeidnia, S., Manayi, A., Abdollahi, M., 2015. From in vitro Experiments to in vivo and Clinical Studies; Pros and Cons. Curr Drug Discov Technol 12, 218–224. https://doi.org/10.2174/1570163813666160114093140

Sato, T., Stange, D.E., Ferrante, M., Vries, R.G.J., van Es, J.H., van den Brink, S., van Houdt, W.J., Pronk, A., van Gorp, J., Siersema, P.D., Clevers, H., 2011. Long-term Expansion of Epithelial Organoids From Human Colon, Adenoma, Adenocarcinoma, and Barrett's Epithelium. Gastroenterology 141, 1762–1772. https://doi.org/10.1053/j.gastro.2011.07.050

Speer, J.E., Gunasekara, D.B., Wang, Y., Fallon, J.K., Attayek, P.J., Smith, P.C., Sims, C.E., Allbritton, N.L., 2019a. Molecular transport through primary human small intestinal

monolayers by culture on a collagen scaffold with a gradient of chemical cross-linking. J Biol Eng 13. https://doi.org/10.1186/s13036-019-0165-4

Speer, J.E., Wang, Y., Fallon, J.K., Smith, P.C., Allbritton, N.L., 2019b. Evaluation of human primary intestinal monolayers for drug metabolizing capabilities. J Biol Eng 13, 82. https://doi.org/10.1186/s13036-019-0212-1

van Breemen, R.B., Li, Y., 2005. Caco-2 cell permeability assays to measure drug absorption. Expert Opinion on Drug Metabolism & Toxicology 1, 175–185. https://doi.org/10.1517/17425255.1.2.175